UNIVERSITY OF SOUTHAMPTON

Faculty of Natural and Environmental Sciences:
Ocean and Earth Sciences

Investigations of the variability of tidal mixing fronts and their importance for shelf-sea ecosystems across multiple trophic levels

by

Lavinia A. Suberg

Thesis for the degree of Doctor of Philosophy

August 2015

UNIVERSITY OF SOUTHAMPTON

ABSTRACT

FACULTY OF NATURAL AND ENVIRONMENTAL SCIENCES
Ocean and Earth Sciences

Doctor of Philosophy

INVESTIGATIONS OF THE VARIABILITY OF TIDAL MIXING FRONTS AND THEIR IMPORTANCE FOR SHELF-SEA ECOSYSTEMS ACROSS MULTIPLE TROPHIC LEVELS

By Lavinia A. Suberg

Tidal mixing fronts establish during the summer months over shelf-seas, and separate tidally-mixed from stratified water masses. They play an important part in shelf-sea bio-physical processes, including volume transport and facilitation of primary productivity. Frontal hydrodynamics provide the physical necessities for prey aggregations to develop, holding the potential for biodiversity hotspots. However, there is limited knowledge on long-term variability of tidal mixing fronts and its effect on associated ecosystems, due to a lack of adequate datasets. Such information would greatly benefit spatial conservation efforts and improve our understanding of ecosystem dynamics on the continental shelf.

Satellite-derived frontal maps and extensive biological datasets (from 1990-2010) are employed here to investigate spatio-temporal variability of tidal mixing fronts and their significance for shelf-sea biology from zooplankton tomegavertebrates in the Celtic Sea. In addition, this study assesses the suitability and limitations of satellite-derived frontal metrics for quantitative analyses and employs innovative technology (submarine gliders) to fill data gaps in species-environment interactions.

This research provides guidance on the use of frontal metrics in quantitative analysis, such as the need to account for data variability over the years and the careful consideration of the employed frontal metric. This thesis furthermore, represents the first description of long-term temporal variability of tidal mixing fronts on the European shelf and highlights a potential sensitivity to climate change due to positive correlations with rising temperatures. Consequences could include extension of the frontal season and intensification of the frontal density gradient with knock-on effects on associated biota.

The density gradient of tidal mixing fronts was shown to act as a direct distribution boundary for plankton between different shelf-sea domains. Climate-change-driven shifts in the seasonality of these fronts may have a direct impact on dispersal of passive floating organisms, habitat connectivity and adult populations of species with planktonic larvae, including commercially important fish and the benthos. Apart from a barrier function, fronts were also found to be important foraging areas for specialist megavertebrates, which were strongly associated with persistent frontal areas, whereas generalist feeders were not. Tidal mixing fronts represent suitable conservation areas for sensitive species in shelf-seas. The underlying mechanisms leading to bio-aggregations at these sites require more research. High-resolution data, simultaneously collected across multiple trophic levels can be obtained by autonomous robotic fleets in the near future.

TABLE OF CONTENTS

1 GENERAL INTRODUCTION 1
1.1 Rationale 1
1.2 Occurrence of tidal mixing fronts 4
1.3 Hydrodynamics at tidal mixing fronts 5
1.4 The Ushant and Celtic Sea Front 7
1.5 Mechanisms of primary productivity enhancement at tidal mixing fronts 9
1.6 Zooplankton abundance at tidal mixing fronts 10
1.7 Apex predator associations with tidal mixing fronts 12
1.8 The use of frontal composite maps in marine ecology 15
1.9 Aims and hypotheses 16
1.10 List of collaborator contributions 20

2 Time series analyses of thermal fronts based on satellite-derived frotnal maps: Results depend on data availability and the choice of a metric 25
2.1 INTRODUCTION 26
2.2 METHODS 30
2.2.1 Processing of frontal maps 31
2.2.2 Frontal metrics used in this research 33
2.2.3 Spatial downscaling 36
2.2.4 Expression of frontal metrics in digital values 37
2.2.5 Data processing 39
2.2.6 Statistical analyses 43
2.3 RESULTS 46
2.3.1 Comparison between *Fmean* and *Fprob* based on differences in their temporal variability 46
2.3.2 Effect of *Fclear* on temporal variability of *Fmean* and *Fprob* 49
2.4 DISCUSSION 55
2.4.1 Differences in temporal variability pattern between *Fmean* and *Fprob* 55
2.4.2 Effect of *Fclear* on temporal variability of *Fmean* and *Fprob* 57
2.4.3 Comparison between other commonly frontal metrics and their use in spatial analyses 60
2.4.4 Other notable points 62
2.4.5 Limitations and recommendations 64
2.4.6 Conclusions 65
2.5 Supplementary material 67

3 Physical drivers of inter-and intraannual variability of two tidal mixing fronts on the northwest European shelf 77
3.1 INTRODUCTION 78
3.2 METHODS 81
3.2.1 Explanatory variables used in the analyses 81
3.2.2 Creation of time series of meteorological variables 84
3.2.3 Statistical modelling of meteorological drivers of frontal variability 87

3.3 RESULTS 89
3.3.1 Meteorological drivers of intraannual variability of *Fmean* and *Fprob* 89
3.3.2 Meteorological drivers of interannual variability of *Fmean* and *Fprob* 98
3.4 DISCUSSION 106
3.4.1 Meteorological drivers of inter- and intraannual variability of *Fmean* and *Fprob* 106
3.4.2 Limitations and recommendations 110
3.4.3 Conclusion 111
3.5 Supplementary material 113

4 Fronts as boundaries: Frontal density gradients restrict dispersal of passive floating organisms on shelf-seas 121
4.1 INTRODUCTION 122
4.2 METHODS 126
4.2.1 Plankton collection 126
4.2.2 Statistical analysis of the effect of spatial variations of the Ushant Front on abundance of *Calanus helgolandicus* and echinoderm larvae 126
4.3 RESULTS 132
4.4 DISCUSSION 135
4.4.1 Influence of small-scale spatial variability of the Ushant Front on *Calanus helgolandicus and* echinoderm larvae abundance 135
4.4.2 Limitations and recommendations 137
4.4.3 Conclusion 138

5 Shelf-sea fronts as conservation sites for marine megavertebrates with specialist foraging ecology 139
5.1 INTRODUCTION 140
5.2 METHODS 143
5.2.1 Data collection 143
5.2.2 Data processing 146
5.2.3 Explanatory variables 146
5.2.4 Statistical analysis 150
5.3 RESULTS 152
5.3.1 Survey summary 152
5.3.2 Effect of the Ushant tidal mixing front on species distribution 154
5.3.3 Importance of frontal metrics in relation to other environmental variable 156
5.4 DISCUSSION 161
5.4.1 Effect of the Ushant tidal mixing front on species distribution 162
5.4.2 Importance of frontal metrics in relation to other environmental variable 165
5.4.3 Limitations and recommendations 166
5.4.4 Conclusion 167
5.5 Supplementary material 168

6 Assessing the potential of autonomous submarine gliders for ecosystem monitoring across multiple trophic levels (plankton to cetaceans) and pollutants in shallow shelf-seas 171
6.1 INTRODUCTION 172
6.1.1 Survey area 174
6.2 METHODS 176
6.2.1 Gliders 176
6.2.2 Glider sensors 178
6.2.3 Glider mission 181
6.3 RESULTS 182
6.3.1 Mission summary 182
6.3.2 Physical environment 184
6.3.3 Echosounder 188
6.3.4 Passive acoustic monitoring 190
6.3.5 Passive sampling devices 192
6.4 DISCUSSION 194
6.4.1 Glider operations 194
6.4.2 Sensors 196
6.4.3 Conclusions and recommendations 198
6.5 Supplementary Material 200

7 GENERAL DISCUSSION 203
7.1 A guide to frontal metrics 204
7.2 Meteorological drivers of inter-and intraannual variability of frontal strength and persistence: potential implication of the effect of climate change on tidal mixing fronts and associated ecosystems 205
7.3 Tidal mixing acting as boundaries for zooplankton distribution and dispersal 207
7.4 Tidal mixing fronts as important foraging sites for species with specialist foraging ecology 208
7.5 Assessing new technologies to improve data sampling of frontal characteristics and associated biota 208

8 REFFERENCES 211

9 APPENDIX 243
9.1 Peer-reviewed publications: 243

LIST OF FIGURES

Figure 1.1: Schematic diagram of the hydrodynamics occurring a tidal mixing front. ……7

Figure 1.2: Frontal map showing the predominant fronts over the SW shelf. 9

Figure 2.1: Histogram of a sharp front illustrating the principles of the SIED-algorithm. 32

Figure 2.2: Monthly composites for Fvalid, Fprob, Fmean, Fpers, Fcomp and Fdens from June 2009. 38

Figure 2.3: Fcomp maps for spring (March-May), summer (June-August), autumn (September-November) and winter (December-February), showing different sized sampling subsets. 41

Figure 2.4: Boxplots of bootstrap-resampled mean for Fprob and Fmean at Celtic Sea and Ushant Front 42

Figure 2.5: Yearly anomalies of Fmean, Fprob, Flcear and Fvalid at the Celtic Sea and Ushant Front from 1990 to 2010 48

Figure 2.6: Monthly anomalies for of Fmean, Fprob, Flcear and Fvalid at the Celtic Sea and Ushant Front.. 49

Figure 2.7: Results of GAMM with AR1 structure for a seasonal subset of Fmean at the Celtic Sea Front as a function of year, month and Fclear..... 52

Figure 2.8: Results of GAMM with AR1 structure for a seasonal subset of Fmean at the Ushant Front as a function of year, month and Fclear..... 53

Figure 2.9: Results of GAMM with AR1 structure for a seasonal subset of Fprob at the Celtic Sea Front as a function of year, month and Fclear. 54

Figure 2.10: Results of GAMM with AR1 structure for a seasonal subset of Fprob at the Ushant Front as a function of month and Fclear. 54

Sup.Figure 2.1: Yearly anomalies for metrics not included in the analysis: Fpers, Fcomp and Fdens at the Celtic Sea and Ushant Front from 1990 to 2010..... 67

Sup.Figure 2.2: Seasonal anomalies for metrics not included in the analysis: Fpers, Fcomp and Fdens at the Celtic Sea and Ushant Front. 68

Sup.Figure 2.3: Autocorrelation functions for Fmean and Fprob at the Celtic Sea and Ushant Front. 69

Sup.Figure 2.4:Histograms, Pearson correlation coefficients and scatter plots showing the relationship between the frontal metrics Fprob and Fmean and explanatory variables Fclear, year and month at the Celtic Sea Front. 70

Sup.Figure 2.5:Histograms, Pearson correlation coefficients and scatter plots showing the relationship between the frontal metrics Fprob and Fmean and explanatory variables Fclear, year and month at the Ushant Front. 71

Sup.Figure 2.6: Model validation plots of residual analysis for Fmean at the Celtic Sea Front.. 72

Sup.Figure 2.7: Model validation plots of residual analysis for Fmean at the Ushant Front. 73

Sup.Figure 2.8: Model validation plots of residual analysis for Fprob at the Celtic Sea Front.. 74

Sup.Figure 2.9: Model validation plots of residual analysis for Fprob at the Ushant Front.. 75

Figure 3.1: Map of NCAR grid cells showing SST for each grid averaged from March to November 1990 – 2010.. 86

Figure 3.2: Monthly anomalies of net heat flux, SST, wind stress, precipitation and Fclear at the Celtic Sea and Ushant Front. 91

Figure 3.3: Wind roses for Celtic Sea Front and Ushant Front. 92

Figure 3.4: Results of GAMM with AR1 structure for a seasonal subset of Fmean at the Celtic Sea Front as a function of heat flux (at lag1), Fclear and precipitation. 95

Figure 3.5: Results of GAMM with AR1 structure for a seasonal subset of Fprob at the Celtic Sea Front as a function of Fclear, heat flux (at lag2) and wind stress (at lag1).. 96

Figure 3.6: Results of GAMM with AR1 structure for a seasonal subset of Fmean at the Ushant Front as a function of Fclear, heat flux (at lag2), precipitation and year. 97

Figure 3.7: Results of GAMM with AR1 structure for a seasonal subset of Fprob at the Ushant Front as a function of SST, Fclear and year. 98

Figure 3.8: Time series of anomalies of net heat flux, SST, precipitation, wind stress, Fclear and the NAO at the Celtic Sea Front.. 100

Figure 3.9: Time series of anomalies of net heat flux (Flux), SST (Temp), precipitation (Precip), wind stress, Fclear and the NAO at the Ushant Front. 101

Figure 3.10: Results of GAMM with AR1 structure for a seasonal subset of Fmean at the Celtic Sea Front as a function of month, Fclear and SST..... 103

Figure 3.11: Results of GAMM with AR1 structure for a seasonal subset of Fprob at the Celtic Sea Front as a function of Fclear, month and heat flux.... 104

Figure 3.12: Results of GAMM with AR1 structure for a seasonal subset of Fmean at the Ushant Front as a function of Fclear, month, precipitation and SST, precipitation and year. 105

Figure 3.13: Results of GAMM with AR1 structure for a seasonal subset of Fprob at the Ushant Front as a function of SST, Fclear and wind stress. 106

Sup.Figure 3.1: Model validation plots of residual analysis for meteorological drivers of intraannual variability of Fmean at the Celtic Sea Front. 113

Sup.Figure 3.2: Model validation plots of residual analysis for meteorological drivers of intraannual variability of Fprob at the Celtic Sea Front. 114

Sup.Figure 3.3: Model validation plots of residual analysis for meteorological drivers of intraannual variability of Fmean at the Ushant Front. 115

Sup.Figure 3.4: Model validation plots of residual analysis for meteorological drivers of intraannual variability of Fprob at the Ushant Front. 116

Sup.Figure 3.5: Model validation plots of residual analysis for meteorological drivers of interannual variability of Fmean at the Celtic Sea Front. 117

Sup.Figure 3.6: Model validation plots of residual analysis for meteorological drivers of interannual variability of Fprob at the Celtic Sea Front. 118

Sup.Figure 3.7: Model validation plots of residual analysis for meteorological drivers of interannual variability of Fmean at the Ushant Front. 119

Sup.Figure 3.8: Model validation plots of residual analysis for meteorological drivers of interannual variability of Fprob at the Ushant Front. 120

Figure 4.1: Selected Synoptic and frontal density maps to demonstrate the different classification scenarios and locations of PR-route samples 131

Figure 4.2: LMM predictions of Calanus helgolandicus and echinoderm larvae abundances for each scenario: 133

Figure 5.1: Frontal frequency and effort map of the survey area.. 144

Figure 5.2: Effort corrected abundance per 100km^2 of study species 155

Figure 5.3: Partial fits of GAM-GEE results, showing the relationship between significant covariates and the probability of harbour porpoise sightings 158

Figure 5.4: Partial fits of GAM-GEE results, showing the relationship between significant covariates and the probability of kittiwake sightings.. 159

Figure 5.5: Partial fits of GAM-GEE results, showing the relationship between significant covariates and the probability of storm petrel sightings 160

Figure 5.6: Partial fits of GAM-GEE results, showing the relationship between significant covariates and the probability of gannet sightings. 161

Sup.Figure 5.1: Boxplots showing effort in kilometres 168

Sup.Figure 5.2: GAM-GEE results, showing the relationship between significant temporal/survey covariates and the P/A of a given species.. 169

Sup.Figure 5.3: GAM-GEE results, showing the relationship between significant covariates and the P/A of a given species. 170

Figure 6.1: Map of survey area and glider positions. 175

Figure 6.2: Picture of U194 showing ES853 echosounder and picture of Zephyr showing the d-tag hydrophone and silicone rubber passive sampling sheets attached to the glider body..... 177

Figure 6.3: Timeline glider deployments……...183

Figure 6.4: **:** Comparison between ship and glider derived temperature and chlorophyll for *Zephyr* and *U194*……...185

Figure 6.5: Time series plots of temperature and chlorophyll concentration of both gliders against depth……187

Figure 6.6: Echograms of glider-integrated ES853 at 120 kHz and equivalent vessel based EK60 120 kHz……190

Figure 6.7: Waveforms and power spectra of detected dolphin and porpoise clicks using the d-tag hydrophone on Zephyr. 191

Figure 6.8: Spectrum-level noise measurements at third octave intervals for times when the Zephyr pump was on and when the pump was off.. 192

Sup.Figure 6.1: Composite satellite-derived front map of the survey area off southwest UK, based on data from 12 September- 17 October 2013.. 200

Sup.Figure 6.2 Calibration profiles between ship and U194 showing uncorrected chlorophyll a data. 201

Sup.Figure 6.3: Temperature of surface waters and deeper waters as a function of time and longitude and latitude 202

Sup.Figure 6.4: Map showing the area where the d-tag hydrophone on Zephyr was active. 202

LIST OF TABLES

Table 1.1: List of types of fronts occurring worldwide 3

Table 2.1: List of metrics of metrics used in this research 36

Table 2.2: Maximum, minimum and mean sampling sizes for zeros excluded and included in the analysis 43

Table 2.3: Correlation coefficients for all metrics combinations.. 44

Table 2.4: Summary of GAMMs with AR1 structure for Fmean and Fprob for both fronts modeled as a function of year, month and Fclear. 51

Table 2.5: Summary of the significance of Fclear on temporal variability of Fmean and Fprob at both fronts Celtic Sea and Ushant Front. 55

Sup.Table 2.1: Spatial similarities between all metric combinations……84

Table 3.1: Summary of explanatory variables used in the analysis and their spatio-temporal resolution. 88

Table 3.2: Summary of lagged dataset that were created for each metric and meteorological variable at the Celtic Sea and Ushant Front. 94

Table 3.3: Summary of GAMMs for Fmean and Fprob at both fronts, testing for meteorological drivers of intraannual variability of Fmean and Fprob. 94

Table 3.4: Summary of GAMMs for Fmean and Fprob at both fronts, testing for meteorological drivers of interannual variability of Fmean and Fprob. 102

Table 4.1: Summary of explanatory variables used in the analysis 130

Table 4.2: Summary of LMM of log-transformed abundances of Calanus helgolandicus and echinoderm larvae 133

Table 5.1: Information on spatial and temporal scale and numerical values of explanatory variables used in the analysis.. 150

Table 5.2: Summary effort and survey statistics. 153

Table 5.3: Summary statistics for cetacean and seabird species 154

Table 5.4: Results of GAM-GEEs of P/A of selected shelf species 157

Table 6.1: Key events in chronological order……183

Table 6.2: Mission statistics. ……...184

Table 6.3: Passive sampling rates, typical exposure times, and limits of detection for various passive sampler deployment modes……..……..194

DECLARATION OF AUTHORSHIP

I, Lavinia A. Suberg, declare that this thesis entitled '*Investigations of the variability of tidal mixing fronts and their importance for shelf-sea ecosystems across multiple trophic levels'* and the work presented in it are my own and have been generated by me as the result of my own original research. I confirm that:

1. This work was done wholly or mainly while in candidature for a research degree at this University;
2. Where any part of this thesis has previously been submitted for a degree or any other qualification at this University or any other institution, this has been clearly stated;
3. Where I have consulted the published work of others, this is always clearly attributed;
4. Where I have quoted from the work of others, the source is always given. With the exception of such quotations, this thesis is entirely my own work;
5. I have acknowledged all main sources of help;
6. Where the thesis is based on work done by myself jointly with others, I have made clear exactly what was done by others and what I have contributed myself;
7. [Delete as appropriate] None of this work has been published before submission [or] Parts of this work have been published as: [please list references below]:

Signed:.....

Date:

ACKNOWLEDGEMENTS

I am very grateful to my primary supervisor Dr. Russell Wynn for providing me with all sorts of opportunities over the last few years. Many thanks for creating this PhD particularly for me, for getting me involved in the Shearwater work and pretty much every single other research project out there during that time and especially, for letting me play with gliders. You have a talent for pushing your students to the edge of sanity, which does not make a PhD easier, but you also always had an open door for us and a solution to any problem. Thank you for that, too.

I am greatly thankful to my supervisor Simon Ingram and Clare Embling for their detailed, honest and constructive comments on my work. I am also extremely grateful to David Johns for providing his expertise, but especially his encouragements and guidance throughout difficult times. Finally, Peter Miller for fulfilling never-ending data requests and his help in the resolving the mysterious Fcomp problem.

This project would not have been possible without all those people that were involved in the collection of the very large datasets used in this research, but who I have never met. I am extremely grateful to volunteers, members and staff of MarineLife, in particular Tom Brereton, and SAHFOS. There are many other people, who have supported me at some point and I would like to thank, including Jeroen van der Kooij, Simon Josey, my local supervisor Ken Collins, my panel chair Adrian Martin, everyone involved in the Shearwater work (Tim, Lou, Ana, Miguel) and my fellow PhD colleagues and friends for their help: Sam Cox, Kylie Scales and Ally Jones.

A special thanks to my office mates Matt, Sophia, Rhi and Lizzy, for cake times, mental support and mostly for a lot of good laughs. You made work bearable during the hard times of this PhD. Extra much love to Jessy and Rhi for a great friendship. On that note, thank you to all the many people I have met along the way in Southampton, who made my stay fun and the city a bit more entertaining, especially the Alma road occupants, Melanie, Rosie and Zuzanna.

Also, thank you Paul for your kindness, patience and for making it work for so long.

Most importantly, I would like to thank the people closest to me: My parents and sister, who (once again) have been the greatest support despite being on the other side of the Channel. This thesis is dedicated to my grandparents, who very sadly never got to see it in the end. The most heartfelt thank you is to Jonathan for always having my back.

1 GENERAL INTRODUCTION

1.1 Rationale

Our oceans and their inhabitants are facing increasing pressure due to anthropogenic impacts, including climate change, pollution and overfishing. In order to counteract some of the consequences, such as degradation of habitat and loss of biodiversity, improved management of the marine environment and conservation measures are being implemented in many areas. Spatial protection efforts, such as the establishment of Marine Protected Area (MPA) networks, aim to provide sanctuary and recovery areas for vulnerable species and preserve habitats of ecological significance (Gilman, 2002; Jameson et al., 2002). However, the manner in which marine organisms are influenced by their bio-physical environment and in turn, use the seascape is complex and greatly variable (Block et al., 2011; Young et al., 2015). In order to identify sites of effective conservation potential, information on multiple trophic levels over adequate spatio-temporal scales is required.

Understanding ecosystem dynamics, bio-physical coupling and drivers of species distribution can significantly improve marine conservation planning (Hobday et al., 2014). Identifying biodiversity hotspots and the mechanisms leading to such have therefore become a key topic in marine ecology. It is now understood that heterogeneous hydrodynamic features, such as eddies (e.g. Jaquemet et al., 2014), upwelling areas (e.g. Hazen et al., 2011) and frontal zones (e.g. Bailey et al., 2010), represent sites of conservation interest (Hazen et al., 2013; Hyrenbach et al., 2006). They provide the physical necessities for food webs to develop, resulting in elevated biomass of animals across multiple trophic levels and consistently re-occurring feeding events (Bost et al., 2009; Weeks et al., 2015). Hence, they provide the potential to simultaneously protect a range of taxonomic groups and elevated biomass.

Frontal zones in particular have been the subject of a considerable research effort in this context. The term ‘fronts’ concerns a class of oceanographic features, which are defined as transition zones between water masses of

different physical properties (LeFevre, 1986). They can develop from a variety of mechanisms and occur at a multitude of spatio-temporal scales, ranging from the large-scale Polar Current to small, temporally variable, tidal intrusion fronts (**Table 1.1**) (Owen, 1981). Their importance for the ecosystem is manifold, including climate regulation, serving as biodiversity hotspots and dispersal highways and acting as barriers between distinct eco-regions (Bakun, 2006; Nihoul, 1981; Sournia, 1994).

Shelf-seas are particularly productive and diverse domains of the oceans, but subject to severe anthropogenic pressures (directly and indirectly) due to extensive shipping traffic, commercial fisheries, recreational activities and high population densities along the coast and hence, in need of effective marine management (Dauvin, 2012; Holt et al., 2010). During the summer, tidal mixing fronts, which separate seasonally stratified from tidally-mixed waters, establish on the shelf (Bowers et al., 1987). They are known to enhance primary productivity and provide the physical necessities for the creation of biodiversity hotspots (Franks et al., 1996; Gomez-Gutierrez et al., 2007; Wishner et al., 2006). Tidal mixing fronts are seasonally persistent, far ranging (typically >100km in length) and closer to shore than other known hotspots (e.g. the shelf break), which potentially facilitates their management as conservation sites within a heavily used marine domain.

Previous studies have provided evidence for shelf-sea fronts to act as accumulation and dispersal zones for zooplankton (Robins et al., 2013; Sabatini et al., 2002) and larval stages of commercially important fish (Lough et al., 2001; Munk, 2014; Munk et al., 2009; Woodson et al., 2015), and to serve as foraging grounds for a variety of apex predators, including sharks (Miller et al., 2015; Queiroz et al., 2012), common dolphins (Goold, 1998) and seabirds (Begg et al., 1997; Durazo et al., 1998). However, most of these studies are fine-scale, which makes them suitable to resolve the underlying mechanisms of species-environment interactions, but lack the spatio-temporal extent necessary to identify fronts as hotspots within wider shelf-sea habitat.

Table 1.1: List of types of fronts occurring worldwide, their definition, spatio-temporal scales of occurrence and a description of their development and maintenance mechanisms. Classification based on Acha et al. (2015)

Frontal type	Definition	Example	Spatial extend	Temporal scale	Mechanisms
Planetary Fronts/Open Ocean Convergences	Convergences or divergences of two current systems	The Antarctic Polar Front	Ocean basin scale; 1000s km	Permanent	Divergences and convergence in the Ekman Layer
Eastern & Western Boundary Systems; Coastal Upwelling	Area, where cold, deep water is transported to the surface	Benguela Current Front, Kuroshio Current	Up to 1000s of kilometres	Permanent	Surface water movements caused by wind are deflected by the earth's rotation (Coriolis effect) until perpendicular to the wind direction (Ekman Transport). When the wind blows parallel to the coast, water is transported offshore and cannot be replaced by horizontal flows due to the coastal boundary. Instead, it is replaced by upwelled water from the deeper layers
Shelf break fronts	Transition zone between cold shelf waters and saline, warm ocean waters	Celtic Sea Shelf Break Front	A few 100 kilometres	Mostly permanent	An interaction of an abrupt change in topography at the continental slope and other factors (wind, Ekman transport, eddies, internal waves) results in upwelling of oceanic bottom water
Tidal mixing fronts	Transition zone between tidally-mixed coastal & stratified shelf waters	Ushant tidal mixing front	Up to a few 100 kilometres	Seasonal, during stratification season	During the summer, the majority of the shelf seas are stratified. However, at a certain depth the turbulence created by tides and winds is strong enough to break the watercolumn stability and the water becomes well mixed. This point marks the front
a) Plume fronts b) Estuarine fronts	Transition between riverine freshwater and saline seawater	a) Mississippi River Plume Front b) Rio de la Plate Estuarine Front	Up to 100s of meters	Mostly permanent	Form at the mouth of an estuary or along its banks, where less dense fresh water is transported seawards, resulting in a) a steeply sloping pycnocline in the mixing zone or b) a vertical layering of fresh and salt water
Topographically controlled fronts	Turbulences around topographies		Varies, up to few 100 meters	Periodically changing with the tidal flow	Interactions between headlands, islands, reefs (topography) and tidal flows resulting in complex turbulences

Tidal mixing fronts themselves are indirectly affected by anthropogenic pressures, because they are directly linked to meteorological forcing and water temperature. Climate-change-related alterations in these parameters will lead to changes in stratification intensity and duration and, in turn, affect frontal occurrence (Holt et al., 2010). Understanding long-term variability of these fronts and the effect on species distribution provides information necessary to identify ecological hotspots and predict consequences of climate change. Unfortunately, spatio-temporally extensive datasets on both biological and physical parameters at tidal mixing front are extremely rare.

This thesis uses large-scale datasets from the shelf-seas around the UK. These data are unique in their spatio-temporal extent and coverage of a variety of trophic levels. The research aims to improve our understanding of temporal variability of shelf-sea fronts and its broad-scale influence on organisms from the bottom and top of the food chain by means of the Continuous Plankton Recorder (CPR), long term monitoring datasets of marine megavertebrates (MarineLife) and recently developed frontal metrics derived from satellite imagery, covering a 20-year period (1990-2010).

1.2 Occurrence of tidal mixing fronts

Tidal mixing fronts only occur in tidally-driven shelf-seas, where they separate mixed coastal from seasonally stratified waters. The coastal (inshore) side is characterized by a homogenous and cool water layer with moderate nutrient levels (Mann et al., 2005). The oceanic (offshore) side consists of a thermocline separating a cold, salty and nutrient-rich bottom layer from warm, nutrient-depleted surface waters. The homogeneity of the coastal part is maintained by tidal mixing along the seabed and by atmospheric forcing on the upper part of the water column (LeFevre, 1986). At a critical depth, the turbulence created by tides is insufficient to counteract water column stabilization generated by solar heating, and stratification will develop during the summer. The point of stratification essentially describes the position of a tidal mixing front, which is defined by the Simpson-Hunter index as = h/U^3 where ‘h’ is the water depth and ‘U’ the tidal amplitude (Simpson et al., 1974). The mean position of a tidal front changes with the advance of the thermocline over the seasonal cycle and can

be temporally altered by the spring-neap tidal adjustment, which leads to further advance of the front into the mixed side during neaps and vice versa during springs (Holt et al., 2008b).

Tidal mixing fronts display a lifecycle in accordance with shelf-sea stratification. During winter, the shelf-seas are homogenous due to the mixing effects of wind and tides. In early summer, persistent solar heating leads to development of a thermocline. On the coastal side, heat is distributed throughout the entire water column, whereas on the stratified side, it is primarily stored in the upper surface layer, while the bottom part remains mixed by tides. When temperature and solar radiance decrease in autumn, convection and turbulent kinetic energy causes destabilization of the layering system until mixed scenarios are fully established in early winter (Hill et al., 2008; Schumacher et al., 1979). Wind speed, direction, and other kinetic energy affect fronts, particularly during periods of frontogenesis (frontal establishment) and frontolysis (frontal breakdown). The timing of frontogenesis and frontolysis depends on an interaction of a variety of factors, e.g. depth, wind velocity, tides, solar energy uptake, and heat loss (Bowers et al., 1987; Dooley, 1981; Elliott et al., 1991; Holt et al., 2010).

Because tidal mixing fronts are driven by meteorological forcing, strong inter-annual variability caused by climatic variation has been observed (Young et al., 2004). As a consequence, it is expected that changes in meteorological variables due to climate change will directly affect timing and intensity of stratification, and potentially affect the occurrence of tidal mixing fronts in the future. Model predictions suggest an elongation of the frontal season by 10-15 days within the next 100 years (Holt et al., 2010). How this will impact upon density currents on the shelf, primary productivity, and the food chain, still remains largely unknown.

1.3 Hydrodynamics at tidal mixing fronts

Figure 1.1 shows a simplified schematic of the hydrodynamics occurring at a tidal mixing front, which influence establishment of biodiversity hotspots.

Baroclinic circulation on the stratified side directs residual flows towards the mixed domain along the seabed and in the surface layer (Pedersen, 1994). In both layers, residual flows move away from the mixed side along the thermocline, creating a strong frontal jet, which is responsible for a considerable amount of volume transport over the shelf during the summer. On the mixed side, residual flows are directed away from the stratified side, along the seabed and towards the front in the surface layer. These processes result in convergence near the outcropping thermocline and divergence on the mixed side (Drinkwater et al., 2001; Luyten et al., 2003). Tidal and wind driven turbulence occurs along the seabed and on the surface respectively (Flament et al., 2000; Ryan et al., 2010).

During the spring-neap adjustment the front moves further into the coastal domain at neaps, whereby the additional intrusion of bottom and surface water is compensated by an enhanced offshore-directed flow in the thermocline (Pedersen, 1994). Vertical and horizontal movement of the thermocline, as well as eddy diffusion along the front, lead to nutrient exchange between the different frontal domains and refuel depleted areas (Badin et al., 2009; Garrett et al., 1981; Loder et al., 1985; Sharples, 2008). Frontal hydrodynamics are key for enhancement of primary productivity, the passive accumulation of floating particles, e.g. zooplankton, and the accessibility of these items near the surface (LeFevre, 1986), which will be discussed in sections 1.6 and 1.7.

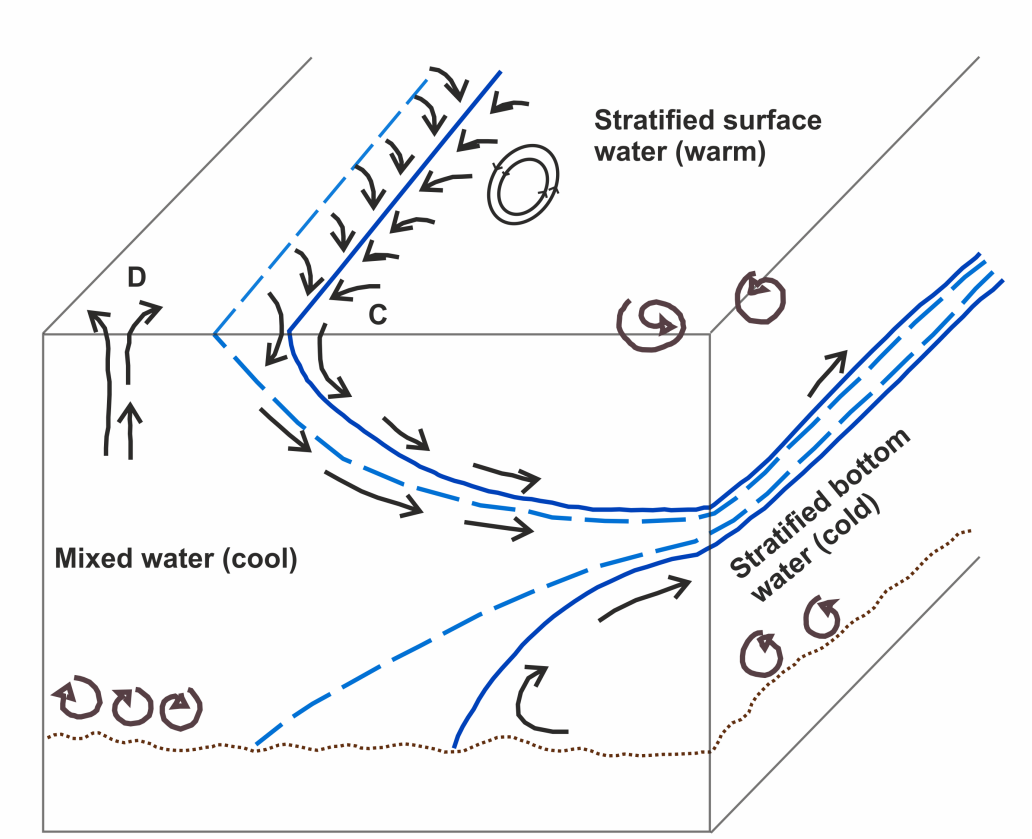

Figure 1.1: Schematic diagram of the hydrodynamics occurring a tidal mixing front. The blue lines represent the pycnocline, a strong density gradient (dashed: position of the front at neap tide). Black arrows show the direction of the main frontal flows as described in the text (note: size of arrow is not associated with strength of flow). The circled grey arrows represent turbulent mixing by wind or tides. 'C' indicates convergence zones, 'D'= divergence zones. Eclipse represents eddies.

1.4 The Ushant and Celtic Sea Front

Within the study area of the wider Celtic Sea, a large variety of fronts exist, such as short-lived ephemeral segments, thermohaline coastal currents, tidal-topographically-driven fronts and the shelf-break front. The predominant tidal mixing fronts are Ushant and Celtic Sea Front, which are the subjects of this research (Figure 1.2). The Ushant Front runs from the Mer d'Iroise northwards, curving into the Western English Channel and then northwards where it meets with coastal thermohaline fronts off the south of Britain (LeFevre, 1986; Sournia et al., 1988). In contrast to the stable southern part of the Ushant Front, the

section covering the Channel is spatially extremely variable and very responsive to the spring-neap adjustment and meteorological forcing. This concerns in particular the surface front, whereas the bottom section is considered more stable (Sournia, 1994). The Ushant Front has played a significant role in shelf-sea oceanography, as initial research describing the occurrence of these features and their importance for primary productivity was largely conducted here (e.g. Pingree et al., 1977; Pingree et al., 1979; Pingree et al., 1976; Pingree et al., 1975; Simpson, 1977;1981; Simpson et al., 1981).

The Celtic Sea Front marks the boundary between the stratified Celtic Sea and the mixed waters of the Bristol Channel and the Southern Irish Sea. The front runs from southwest Wales to southeast Ireland with a characteristic curve that follows the bottom topography around the Celtic Deep (Brown et al., 2003; Horsburgh et al., 1998) (Figure 1.2). In contrast to the Ushant Front, this front is less affected by tides and is spatially very stable once fully established (Simpson et al., 1974).

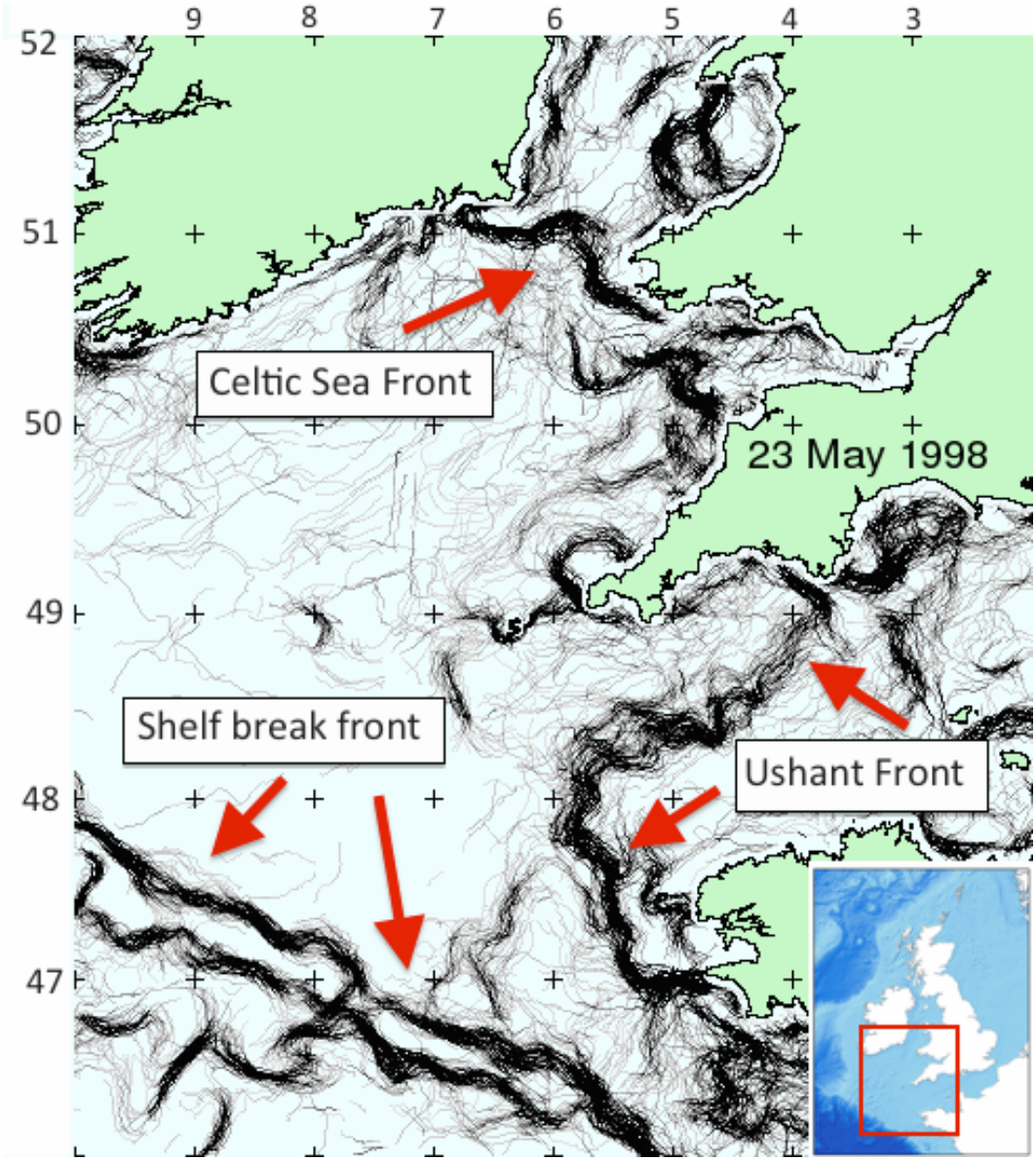

Figure 1.2: Frontal map showing the predominant fronts over the SW shelf (the shelf break front as well as the two tidal mixing fronts that are the focus of this study: the Celtic Sea and Ushant Front). The dark lines show frontal segments. The thicker and darker the lines, the more persistent the front.

1.5 Mechanisms of primary productivity enhancement at tidal mixing fronts

A considerable amount of evidence shows increased primary productivity and phytoplankton standing stocks at tidal mixing fronts, including the Ushant Front (Bargeron et al., 2006; Le Boyer et al., 2009; Pingree, 1975), Celtic Sea Front (Pemberton et al., 2004; Savidge, 1976; Savidge et al., 1978) and at features

elsewhere (e.g. Georges Bank, US East Coast) (Franks et al., 1996). Maxima are usually encountered in the outcropping thermocline on the stratified side. This has been attributed to a combination of stratification providing stability to retain phytoplankton in the photozone and a constant refueling of nutrients from beneath the thermocline and the adjacent mixed domain (Franks, 1992a). Where the thermocline shallows to break the surface, phytoplankton is exposed to enhanced levels of light and able to increase their growth rate (Holligan et al., 1984). Nutrients, which tend to become depleted in the surface layer above the seasonal thermocline elsewhere in stratified seas, are re-fuelled in the frontal zone by cross-frontal exchange mechanisms as described in section 1.4.

Consistently elevated levels of primary productivity at fronts are believed to be the starting point of a cascading effect up the trophic chain, because it provides foraging grounds for the basis of the food web, the zooplankton (Bakun, 2006; Bonnet et al., 2005; LeFevre, 1986). However, primary productivity in the Celtic Sea during the summer is generally high and frontal systems are not the only place where increased phytoplankton standing stocks can be found (McGinty et al., 2014).

1.6 Zooplankton abundance at tidal mixing fronts

The association between zooplankton distribution and the occurrence of tidal mixing fronts is more complex. Results vary between location (e.g. European Shelf, Georges Bank), even along a single feature and between species (Franks et al., 1996; Holligan, 1981; Robinson et al., 1986; Wishner et al., 2006). Theoretically, it is expected to find increased zooplankton biomass due to passive and active accumulation mechanisms. Convergence zones and current flows associated with the front represent physical aggregation processes that retain floating organisms (Franks, 1992b). Zooplankton actively approaching a front in response to elevated food availability or increased dispersal potential has also been put forward (McGinty et al., 2014). However, these arguments are contradicted by increased predation pressure at the front and phytoplankton occurring in sufficient concentrations elsewhere on the shelf (McGinty et al., 2014).

In the only available study conducted at the Celtic Sea Front, McGinty et al. (2014) showed that zooplankton community structure differed between each side of the front, but did not find evidence for enhanced zooplankton biomass at the feature itself. Changes in species composition are reported from most other studies concerning front-zooplankton association, which has been attributed to changes in the hydrodynamic regime and species-specific environmental niches (Sabatini et al., 2002; Sabatini et al., 2012; Schultes et al., 2013).

Zooplankton distribution patterns at the Ushant Front vary between studies, depending on sampling methodology and location. Similar to the Celtic Sea Front, changes in community composition have been observed crossing the frontal boundary (e.g. Schultes et al., 2013). Some studies report the occurrence of particular frontal species, which are predominantly found in the transition zone (Robinson et al., 1986) and increased biodiversity in this domain compared to the stratified or mixed side (Schultes et al., 2013). Others suggest increased abundance in the frontal zone only (Grall et al., 1980; Perry et al., 1993). However, various studies conducted at the Ushant Front and elsewhere, showed highest abundances of especially copepods in the stratified side (Kiorboe, 1993; Sabatini et al., 2002). In addition, multi-year surveys found clear inter-annual differences in zooplankton assemblages (Robinson et al., 1986) and recent fine-scale research suggests that abundance also differs significantly between spring and neap tides (Schultes et al., 2013; Wishner et al., 2006). Therefore, observed differences between these studies are due to a great amount of natural variability caused by a variety of environmental factors and differences in sampling methodology, resolution, location and time.

However, a couple of findings appear to be consistent. Firstly, there is a positive relationship between tidal mixing fronts and mero- and ichtyo-plankton, the larval stages of benthic organisms and fish. Increased biomass of these has been reported from fronts in the North Sea (Munk, 2007; 2014), Georges Bank (Lough et al., 2001), off California (Ryan et al., 2014) and the Patagonian shelf (Derisio et al., 2014; Sabatini et al., 2002). Larval aggregation at fronts is due to reliable and greater foraging opportunities (Hidalgo et al., 2014), improved aggregation and dispersal potential along the frontal jet (Lough et al., 2001) and

increased spawning activity of adult fish near fronts (Munk et al., 2009; Temperoni et al., 2014).

Secondly, most studies observe differences in zooplankton community structure over the front. A barrier and blender effect has been mentioned in this regard. Frontal systems represent boundaries between different types of water masses and separate seas into distinct eco-regions (Nihoul, 1981; Sournia, 1994). Many zooplankter are physiologically incapable to deal with the abrupt changes in the bio-physical setting over the transition zone, such as a drastic decrease in temperature, salinity or differences in phytoplankton composition (Franks et al., 1996; Sournia, 1994; Wishner et al., 2006). The frontal transition itself tends to hosts species from both sides and is considered a mixing zone (Schultes et al., 2013).

Fronts are potential biodiversity hotspots as they provide the physical prerequisites for food webs to develop (Bost et al., 2009; Weeks et al., 2015). Consistently increased primary productivity and passive accumulation mechanisms are thought to enhance zooplankton abundance at fronts and in particular copepod numbers, which serve many prey fish as primary food source (Bakun, 2006; Bonnet et al., 2005; LeFevre, 1986). However, recent research suggests that copepods maxima do not occur directly in the frontal zone, but in the stratified side (Sabatini et al., 2002). This partially invalidates the theory of a simple cascading effect up the food chain. It also suggests that the interactions across different trophic levels at a front are more complex than a simple bottom-up controlled ‘more will lead to more’ relationship (Bertrand et al., 2008). The importance of tidal mixing fronts on zooplankton distribution appears variable and certainly deserves more attention.

1.7 Associations between megavertebrates and tidal mixing fronts

A significant body of published research is available focused on species-environment interactions and megavertebrate distribution at fronts (reviewed in e.g. Ballance et al., 2006; Bost et al., 2009; Palacios et al., 2006; Scales et al.,

2014b). Evidence for a significant association between marine top predators and frontal features has been described across all oceans and for a large variety of frontal types, including vast persistent features like the Antarctic Circumpolar Current (Bost et al., 2009), major upwelling systems (Nur et al., 2011), shelf break fronts (Azzellino et al., 2008) and estuarine plumes (Zamon et al., 2014). Likewise, increased abundances of animals at fronts have been observed for a range of taxonomic groups, such as pinnipeds (Cotte et al., 2015), turtles (Pikesley et al., 2013; Scales et al., 2015), sharks (Miller et al., 2015; Queiroz et al., 2012) and various cetacean (Doniol-Valcroze et al., 2007; Joiris, 2011; Kai et al., 2009) and seabird species (Ainley et al., 2009; Force et al., 2015; Haney et al., 1985; Ribic et al., 2011).

The affiliation between higher trophic levels and fronts is based on improved foraging opportunities due to greater predictability, density, and accessibility of prey. Large pelagic fish as well as smaller bait fish not only aggregate along frontal features, but also show faster growth rates at these locations, providing a rich food source for top predators (Chassot et al., 2011; Klemas, 2013; Woodson et al., 2015). Upwelling and convergence zones at fronts make prey readily available at the surface, which is of particular benefit to seabirds. For instance, gannets have been shown to switch to Area Restricted Search (ARS) near frontal zones (Scales et al., 2014a) and change their diving behaviour from U-shaped to V-shaped (Cox et al., unpublished data), indicating increased prey availability and accessibility. Recurring feeding events at fronts and subsequent bio-aggregation lead to increased biodiversity. However, the strength and nature of predator-front associations are variable due to complex interactions with other biological and environmental factors driving species distribution, and need to be assessed on a feature specific basis (Scales et al., 2014b).

At tidal mixing fronts, bio-aggregation mechanisms are expected to be similar to those of hydrodynamic features elsewhere. However there is no published evidence for increased prey availability at the tidal fronts analysed in this study. For instance, vessel monitoring system (VMS) data from the Western Channel do not show elevated levels of fishing activity around the Ushant Front (Campbell et al., 2014; Martinez et al., 2013). However, this does not directly

suggest there are less available fish at the fronts, as other factors such as increased shipping traffic and controls may be influential, e.g. a traffic separation scheme in the Channel. Further afield, the commercial hake fishery on the Patagonian shelf is concentrated over a tidal mixing front during the summer season (Ocampo et al., 2013) and areas of intensified spawning and elevated larval biomass (including cod, haddock and sandeel), spatially coincide with tidal mixing fronts in the North Sea (Munk, 2014; Munk et al., 2009), the eastern US shelf (Lough et al., 2001) and elsewhere (Woodson et al., 2015).

Tidal mixing fronts represent the most persistent and predominant type of front during the summer months on shelf-seas. Due to their close proximity to shore and consistency over the summer season, shelf-sea fronts could be of particular importance for central-place foraging breeding seabirds and animals with higher energy constraints that rely on predictable food sources near the centre of distribution, such as breeding grounds. Hence, tidal mixing fronts have the potential to become protected zones for pelagic species in a region of our oceans intensively used by humans. Research investigating the importance of these fronts on megavertebrate distribution is limited. Isolated studies suggest that top predators indeed use tidal mixing fronts as foraging areas. Increased abundance, encounter probabilities and direct exploration have been reported for ocean sunfish (Sims et al., 2002), blue and basking sharks (Miller et al., 2015; Priede et al., 2009; Queiroz et al., 2012), common dolphins (Goold, 1998) and a variety of seabirds with different feeding ecologies (Begg et al., 1997; Durazo et al., 1998). However, most of these studies are conducted at a small scale, focusing on processes at the fronts themselves rather than investigating a general influence on species distribution. In addition, the datasets are often limited as they are based on few tagged individuals or temporally-restricted vessel surveys.

Large spatio-temporal datasets on cetacean occurrence are available for the northeast European continental shelf, which have been used to map cetacean distribution (Reid et al., 2003) and investigate temporal variability of selected species (Macleod et al., 2009; McClellan et al., 2014), but no analytical

attempts have been made to relate their distribution pattern to environmental variables other than depth in this region (Kiszka et al., 2007). General distribution maps suggest enhanced presence near frontal features for species such as harbour porpoise, minke whale and bottlenose dolphin (McClellan et al., 2014). On the other hand, there are a range of cetaceans that do not appear to aggregate in frontal areas, including common, white beaked and Rissos dolphins (Reid et al., 2003). Large datasets on megavertebrate distribution are extremely limited, but offer the unique opportunity to investigate the influence of shelf-sea fronts on their distribution and the potential for fronts as conservation foci.

1.8 The use of frontal composite maps in marine ecology

The availability of satellite remote sensing data has significantly improved our understanding of the oceans, including physical and biological components. Remotely measured variables, such as SST and chlorophyll *a* often explain a great deal of the spatial variation in species abundance across multiple trophic levels (Stegmann et al., 2004; Suryan et al., 2012; Tremblay et al., 2009). Over the past two decades, algorithms have been introduced that translate some of the remotely sensed variables into metrics that measure hydrodynamic features or events, such as upwelling zones, eddy formation and fronts. It allows for cost-effective mapping of frontal systems almost anywhere in the oceans, the retrospective analysis of frontal variability over recent decades and quantitative analysis in combination with biological datasets (Miller, 2004; 2009; Miller et al., 2014). Frontal maps can be used to investigate environment-species associations at the point where the physical setting leads to the establishment of productivity hotspots and refine locations of bio-aggregation. Frontal mapping has already been implemented in the process of MPA network establishment in the UK and provides potential for dynamic ocean management (Maxwell et al., 2015; Miller et al., 2014).

Different frontal metrics have been successfully employed to identify habitat use over a range of taxa, including gannets (Sabarros et al., 2014; Scales et al., 2014a), basking sharks (Miller et al., 2015; Priede et al., 2009), turtles (Pikesley

et al., 2013; Scales et al., 2015), and fish (Chassot et al., 2011; Reese et al., 2011) all over the world. The applied metrics capture various frontal characteristics, such as presence/absence of the front, frontal strength, frequency, probability, or the distance to the nearest frontal feature. Although frontal metrics are increasingly used in ecology, not much attention has been paid to exploring the suitability of each metric for a given research question. It is not clear if available metrics are equally effective for a range of diverse approaches, such as time series analysis, identifying biodiversity hotspots or habitat use of single species.

1.9 Aims and hypotheses

1.9.1 Chapter two: Time series analyses of thermal fronts based on satellite-derived frontal maps: Results depend on data availability and the choice of a metric

Chapter two provides a comparison between commonly used frontal metrics, which will be used throughout this thesis and illustrates some of the limitations of the use of frontal metrics in quantitative analyses. Frontal metrics are based on complex algorithms and there are hidden caveats, which need to be considered during data processing and statistical analysis of frontal maps, such as variations in data availability throughout the season and over long time scales. Although the incorrect application of frontal metrics in quantitative analyses can lead to wrong estimates, not much guidance is available on how to handle them appropriately. An analysis of inter-and intraannual variability of Celtic Sea and Ushant tidal mixing fronts from 1990 to 2010 serves as a case study to a) explain commonly used frontal metrics (so-called *Fmean*, *Fprob*, *Fpers*, *Fcomp* and *Fdens*) in more detail and demonstrate the differences between them in order to aid scientists in their choice of frontal metrics, b) demonstrate the different effect of *Fclear* on temporal variability of *Fmean* and *Fprob* and c) provide some general advice on use of frontal metrics in quantitative analyses.

Hypotheses:

A) *H1*= There are differences in inter- and intraannual patterns of commonly used frontal metrics (*Fprob, Fmean, Fpers, Fcomp, Fdens*) based on monthly composites between January 1990 and December 2010 for the Celtic Sea and Ushant tidal mixing fronts.

B) *H1*= The increase of available data (monthly composites of *Fclear*) from January 1990 to December 2010 affects inter-and intraannual variability pattern based on monthly composites of commonly used frontal metrics (*Fprob, Fmean, Fpers, Fcomp, Fdens*).

1.9.2 Chapter three: Physical drivers of inter-and intraannual variability of two tidal mixing fronts on the northwest European shelf

Chapter three builds on chapter two by investigating the key meteorological drivers of inter-and intraannual variability pattern revealed in chapter two, based on monthly frontal composites between 1990 and 2010. Revealing the key meteorological causes of long-term frontal variability provides useful information for predictions of potential impacts of changing weather pattern on tidal mixing fronts in the future. Meteorological parameters considered in the analysis are net heat flux, wind stress, wind direction, precipitation, SST and NAO. The analysis focuses on temporal variability of the frontal metrics *Fmean* and *Fprob*, which provide information on different frontal characteristics, namely frontal gradient strength (*Fmean*) and frontal persistence (*Fprob*).

Hypotheses:

A) *H1*= One or more selected meteorological parameters (net heat flux, wind stress, wind direction, precipitation, SST and NAO) explain the intraannual variability in *Fmean* and *Fprob* between 1990 and 2010.

B) *H1*= One or more of selected meteorological parameters (net heat flux, wind stress, wind direction, precipitation, SST and NAO) explain the interannual variability in *Fmean* and *Fprob* between 1990 and 2010.

C) *H1*= The key meteorological drivers of temporal variability between *Fmean* and *Fprob* are different.

1.9.3 Chapter four: Fronts as boundaries: Frontal density gradients restrict dispersal of passive floating organisms on shelf-seas

Chapter four is the first of three studies that look at the influence of tidal mixing fronts on marine biota in the Celtic Sea. This chapter investigates a potential boundary effect of tidal mixing fronts on zooplankton distribution in the English Chanel and Celtic Sea. Distribution and abundance of zooplankton directly affects dependent predator species (e.g. commercially important fish) and populations dynamics of organisms with planktonic life cycle (e.g. the benthos). A barrier effect of the Ushant Front is expected to be expressed in changes in plankton abundance in response to the movement of the front. The influence of local movements of the Ushant Front on abundance of *Calanus helgolandicus* and echinoderm larvae is investigated using monthly satellite-derived frontal maps and Continuous Plankton Recorder (CPR) data from a fixed route between 1990 and 2009.

Hypotheses:

A) *H1*= The Ushant Front acts as a dispersal boundary by limiting the distribution of *Calanus helgolandicus* and echinoderm larvae, which is manifested in abundance changes of the two plankter in relation to spatial movements of the front.

1.9.4 Chapter five: Shelf-sea fronts as conservation sites for marine megavertebrates with specialist foraging ecology

Chapter five investigates the influence of tidal mixing fronts on higher trophic levels. This study tests if the Ushant tidal mixing front area is associated with higher sightings of megavetebrates species with different foraging ecologies: a) surface feeding kittiwakes and storm petrels, which benefit from food sources made available near the water surface, b) harbour porpoises, which need to feed frequently to refuel energy deposits and therefore, benefit from predictable and persistent foraging areas; and c) for comparison purposes a generalist feeder, the gannet. 16 years of Presence/Absence data (1996- 2010), a range

of satellite-derived frontal metrics (strength, persistence, frequency and distance to nearest front) and other habitat variables (depth, chlorophyll, SST) at various lags, covering the English Channel and Celtic Sea are used to identify the key environmental drivers of spatial variability of the four study species.

Hypotheses:

A) *H1*= sightings probability of the three specialist species is positively associated with one or more of the frontal metrics

B) *H1*= frontal metrics describe more of the variations in sightings probability for specialist species than other environmental variables

C) *H1*= frontal metrics are not important descriptors of the variations in sightings probability for gannets

1.9.5 Chapter six: Assessing the potential of autonomous submarine gliders for ecosystem monitoring across multiple trophic levels (plankton to cetaceans) and pollutants in shallow shelf-seas

Chapters two to five demonstrated the usefulness of extensive spatio-temporal datasets for investigation of large-scale variability of tidal mixing fronts and its effect on zooplankton and megavertebrates. However, this research also highlighted a range of limitations of satellite-derived frontal metrics and long-term biological time series. Usually there is a trade-off between spatio-temporal extent of a dataset versus resolution and quality. This last chapter explores new ways to overcome some of the shortcomings of current methodologies in order to fill the knowledge gaps in front-biota interactions. This chapter represents a methods study and is less driven by hypothesis. **Research objectives** included:

1. Simultaneously collect data on the physical properties of the water column (temperature, salinity, density, chlorophyll *a*) and the biological environment across multiple trophic levels (zooplankton, fish and cetaceans- focus on harbour porpoises)

2. Identify possible associations between the physical and biological variables, e.g. a cascading effect of increased productivity up the food-chain
3. Investigate differences in the physical and biological variables between frontal and non-frontal zones
4. Asses the future potential of gliders for long-term simultaneous monitoring of physical and biological parameters of the water column.

1.10 List of collaborator contributions

1.10.1 Chapter two: Time series analyses of thermal fronts based on satellite-derived frontal maps: Results depend on data availability and the choice of a metric

Contributors: Lavinia Suberg (National Oceanography Centre Southampton), Dr. Peter Miller (Plymouth Marine Laboratories), Prof. Russell Wynn (National Oceanography Centre Southampton)

Monthly level-4 composites of the various frontal metrics used in the analysis were provided by Peter Miller as 8bit raster files. Data processing and analysis was carried out independently. Comments on the final document were provided by Peter Miller and Russell Wynn.

1.10.2 Chapter three: Physical drivers of inter-and intraannual variability of two tidal mixing fronts on the northwest European shelf

Contributors: Lavinia Suberg (National Oceanography Centre Southampton), Dr. Peter Miller (Plymouth Marine Laboratories), Prof. Russell Wynn (National Oceanography Centre Southampton), Prof. Simon Josey (National Oceanography Centre Southampton)

Monthly level-4 composites of the various frontal metrics used in the analysis were provided by Peter Miller as 8bit raster files. Suitable datasets of meteorological variables for the analysis and data processing were discussed with Simon Josey. Data processing and analysis was carried out independently.

Comments on the final document were provided by Peter Miller and Russell Wynn.

1.10.3 Chapter four: Fronts as boundaries: Frontal density gradients restrict dispersal of passive floating organisms on shelf-seas

Contributors: Lavinia Suberg (National Oceanography Centre Southampton), Dr. David Johns (Sir Alister Hardy Foundation for Ocean Science), Dr. Pierre Hélaouët (Sir Alister Hardy Foundation for Ocean Science), Dr. Peter Miller (Plymouth Marine Laboratories), Prof. Russell Wynn (National Oceanography Centre Southampton)

Monthly level-4 composites of the various frontal metrics used in the analysis were provided by Peter Miller as 8bit raster files. The CPR zooplankton data was provided by David Johns. Research aims and analytical approach were discussed with Pierre Hélaouët. Data processing and analysis was carried out independently. Comments on the final document were provided by David Johns and Russell Wynn.

1.10.4 Chapter five: Shelf-sea fronts as conservation sites for marine megavertebrates with specialist foraging ecology

Contributors: Lavinia Suberg (National Oceanography Centre Southampton), Dr. Simon Ingram (University of Plymouth), Dr. Clare Embling (University of Plymouth), Dr. Tom Brereton (MarineLife), Dr. Peter Miller (Plymouth Marine Laboratories)

Monthly level-4 composites of the various frontal metrics used in the analysis were provided by Peter Miller as 8bit raster files. Megavetebrate sightings data was provided by Tom Brereton. Research aims and analytical approach were discussed with Simon Ingram and Clare Embling. Data processing and analysis was carried out independently. Comments on the final document were provided by Simon Ingram and Clare Embling.

1.10.5 Chapter six: Assessing the potential of autonomous submarine gliders for ecosystem monitoring across multiple trophic levels (plankton to cetaceans) and pollutants in shallow shelf-seas

Contributors: Lavinia Suberg (National Oceanography Centre Southampton), Prof. Russell Wynn (National Oceanography Centre Southampton), Dr. Jeroen van der Kooij (Centre for Environment, Fisheries and Aquaculture Science), Dr. Liam Fernand (Centre for Environment, Fisheries and Aquaculture Science), Dr. Sophie Fielding (British Antarctic Survey), Dr. Damien Guihen (British Antarctic Survey), Dr. Douglas Gillespie (University of St. Andrews), Dr. Mark Johnson (University of St. Andrews), Kalliopi C. Gkikopoulou (University of St. Andrews), Dr. Allan (Norwegian Institute of Water Research), Branislav Vrana (Research Centre for Toxic Compounds in the Environment
), Dr. Peter Miller (Plymouth Marine Laboratories), Dr. David Smeed (National Oceanography Centre Southampton), Dr. Alice R. Jones (University of Adelaide)

Data collection was a big collaborative effort from scientists and institutions listed below as well as glider technicians and research vessel crew. Data processing and analysis were largely performed independently but with contributions from the following people: Liam Fernand gave advice on sampling design and survey set up. He also provided temperature and chlorophyll *a* data from *in situ* water samples collected on the CEFAS Endeavour for comparison purposes with glider-collected data. Liam Fernand furthermore, provided advice on oceanographically data analysis. Advise and discussion on sampling scheme of the echosounder was provided by Sophie Fielding, Damien Guihen and Jeroen van der Kooij. Processing, analysis and visualisation of echosounder data was largely conducted by Damien Guihen. Data from vessel-based echosounder for comparison purposes with data from glider-based echosounder was provided by Jeroen van der Kooij. Written contribution to echosounder related methods, results and discussion sections were made Sophie Fielding, Damien Guihen and Jeroen van der Kooij. Development, integration and discussion on the sampling scheme of the D-TAG came from Mark Johnson and Douglas Gillespie. Processing and visualisation of D-TAG data was conducted by Mark Johnson, Douglas Gillespie and Kalliopi

Gkikopoulou. Written contributions to D-TAG related methods, results and discussion sections were made by Douglas Gillespie and Kalliopi Gkikopoulou. Passive pollutant samplers and analysis of pollutants were provided by Ian Allan and Branislav Vrana. Written contributions to passive pollutant samplers related methods and result sections were made by Ian Allan and Branislav Vrana. Peter Miller provided satellite-derived frontal maps during the glider survey and for the manuscript. David Smeed provided code for glider navigational data processing and contributed to glider data processing. All co-authors made suggestions to improve manuscript drafts.

2 Time series analyses of thermal fronts based on satellite-derived frontal maps: Results depend on data availability and the choice of a metric

Satellite-derived frontal metrics describe characteristics of thermal fronts, such as their strength or persistence. They are increasingly used in marine science to investigate spatio-temporal variability of thermal fronts or in ecological studies to explain species distribution. However, most metrics are based on complex algorithms, which can make it difficult to fully understand their meaning. Although the incorrect application of frontal metrics in quantitative analyses can lead to wrong estimates, not much guidance is available on how to handle them appropriately. Therefore, this research aims to a) explain commonly used frontal metrics (so-called *Fmean*, *Fprob*, *Fpers*, *Fcomp* and *Fdens*) and the differences between them b) give guidance on their use in quantitative analyses and c) provide some general advise on processing frontal metrics for statistical analyses. As a case study serves an investigation of inter-and intraannual variability of two tidal mixing fronts in the Celtic Sea. Generalized Additive Mixed Models (GAMMs) with an Autoregressive Correlation Structure (AR1) were applied on monthly frontal maps from 1990 to 2010. Metrics of the group *Fprob*, *Fpers* and *Fcomp* (Pearson correlation: r=0.8-1.0; p<0.001); and *Fmean* and *Fdens* were almost identical (r=0.8-0.9; p<0.001). Therefore, analyses were continued on the simpler metrics *Fprob* and *Fmean* representatively. Inter-and intraannual variability of *Fmean* and *Fprob* were significantly different. *Fmean* showed an oscillating pattern between 1990 and 2010 whereas there were no changes in *Fprob* over time. In addition, there has been a >2-fold increase of available satellite imagery from 1990 to 2010 due to more active satellites, which significantly affected *Fprob* (negatively) and *Fmean* (positively). When using frontal maps for quantitative analyses, the choice of metric should be carefully considered and data availability needs to be accounted for as it can produce variable results otherwise. The production of a coherent guide on the use of frontal metrics would be helpful to minimize mistakes and potentially wrong estimates in statistical analyses.

2.1 INTRODUCTION

Fronts are defined as transition zones between different water masses, where steep gradients in physical (e.g. temperature, density), chemical (e.g. nitrogen and iron) and/or biological (e.g. plankton) parameters can be found (LeFevre, 1986). The types of fronts, their spatio-temporal extent and formation mechanisms are as divers as the parts they play within the oceans and for our climate. Fronts can be permanent (e.g. The Antarctic Polar Front), seasonally re-occurring (e.g. tidal mixing fronts) or short-lived (e.g. upwelling events) (**Table 1.1**) (Owen, 1981). Reasons for the establishment of fronts vary depending on the type of front. Some common factors are bathymetry (shelf break fronts), freshwater input (river plumes), tides (tidal-topographic fronts), meteorological forcing such as wind or solar radiation (upwelling events, tidal mixing fronts) or a combination of these (Acha et al., 2015).

Fronts have many functions within the marine and atmospheric system. Sea-air interactions along the major fronts significantly impact the regulation of our climate (Diakhate et al., 2016; Nakamura et al., 2015). Large frontal currents are responsible for the transportation of considerable volumes of water and organic matter across several thousands of kilometres (Thompson, 2008). Some fronts act as boundaries between ecosystems and serve migratory species as ‘marine highways’. Foraging events and high diversity across multiple trophic levels caused by passive and active bio-accumulation are frequently observed along fronts (Bost et al., 2009; Hyrenbach et al., 2000). Subsequently, they are of interest to the commercial fishing industry and conservationist alike (Hyrenbach et al., 2000; Podesta et al., 1993). Fronts are important and continuing research aims to improve our understanding of fronts, their sensibility to climate change and potential knock-on effects on ecosystems, hydrodynamic regimes and world climate.

Satellite-derived frontal metrics describe characteristics of thermal fronts, such as their strength or frequency, in the area of interest and for a desired period. They come in form of images, so called ‘frontal maps’. These maps are usually a composite of multiple satellite images, because single images are often cloud-covered (Miller, 2009). Combining multiple images into one map creates

(ideally) a cloud free view on the ocean surface. The resulting frontal maps are a mosaic of pixels containing values describing a front (frontal values) or not (cloud free pixel that are cloud free and cover an area of sea without fronts). They provide information on the surface signal of thermal fronts over large spatio-temporal scales at low cost, which makes them very popular for scientist from a variety of backgrounds, including oceanographers and ecologists.

Frontal maps are particularly useful to study large-scale processes, because of their spatio-temporal coverage (time series begin in the 80's and cover the entire globe). For example, they have been used to create detailed maps of surface fronts all over the world, e.g. Southern Ocean (Dong et al., 2006), Bering Sea (Belkin et al., 2009), Patagonian Shelf (Rivas et al., 2010) and California Current System (Armstrong et al., 2012) and to describe their spatio-temporal variability. Research on spatial variability of fronts usually focuses on selected, persistent features (e.g. Bisagni et al., 2006; Lee et al., 2015; Yu et al., 1996), whereas temporal variability studies tend to summarize frontal activity over an entire ecosystem (e.g. Belkin et al., 2009). Despite interest in the impact of climate change on frontal structures, only limited research utilises frontal metrics to investigate long-term trends of fronts. (e.g. Belkin et al., 2009).

Satellite-derived frontal metrics are not just of interest to oceanographers, but have become popular in recent years amongst marine ecologists to explain and predict species distributions, particularly for marine apex predators. The potential for fronts to act as biodiversity hotspots has also received attention from policymakers involved in development of spatial conservation measures such as Marine Protected Areas, and future monitoring of mobile species as part of the Marine Strategy Framework Directive (MSFD) (Defra, 2009; 2012; European Union, 2008). Initially, frontal maps were used only descriptively and compared to tracks or distribution maps of marine biota (Doniol-Valcroze et al., 2007; Edwards et al., 2013; Pemberton et al., 2004; Priede et al., 2009; Schabetsberger et al., 2013). However, they are increasingly being used in statistical models to investigate bio-physical coupling and ecosystem dynamics (Oppel et al., 2012; Pirotta et al., 2014). Despite interest in the impact of

climate change on frontal structures, only limited research utilises frontal metrics to investigate long-term trends of fronts. (e.g. Belkin et al., 2009).

A range of frontal metrics is available by now and new ones are still being developed. Some metrics are comparably simple, such as probability of observing a front. Other metrics are based on complex algorithms. Each metric has been developed for a particular purpose and provides information about a specific frontal characteristic, e.g. one metric describes frontal strength and another one provides information on the persistence of a front. Some metrics are more popular than others in specific scientific studies. For example, a metric describing the probability of observing a front has been used frequently in the past by remote sensing scientists to analyse spatio-temporal variability of fronts and to map fronts all over the world (Bisagni et al., 2006; Bisagni et al., 2001; Cyr et al., 2015; Mavor et al., 2001; Rivas et al., 2010). So called frontal 'composite' and 'density' maps have been particularly popular with marine ecologists to investigate spatial association between species distribution and frontal activity, particularly top predator species and megafauna, such as sharks, turtles, marine mammals and seabirds (e.g. Doniol-Valcroze et al., 2007; Edwards et al., 2013; Miller et al., 2015; Oppel et al., 2012; Pemberton et al., 2004; Pirotta et al., 2014; Priede et al., 2009; Scales et al., 2015).

Most metrics represent highly processed data based on, sometimes complex, algorithms that can make it difficult for the user to understand the actual meaning of the provided values and the behaviour of metrics when applying statistical measures. For example, each metric describes a particular frontal characteristic and therefore, different metrics display particular spatial and temporal variability pattern and the results of quantitative analyses can be variable, depending on the metric employed. Still, not much guidance for researchers is available in the scientific literature on the use of frontal metrics, the differences between them and factors to consider during their statistical processing.

There is also a lack of information concerning factors influencing the metrics directly, such as the quantity of data used to create a frontal map or the method

by which frontal values are spatially averaged. However, these factors need to be considered when working with frontal metrics in order to avoid incorrect estimates of a front. For example, there has been a steep and continuous increase in satellite passes over the past 20 years, which resulted in an increased number of satellite images per day and therefore, more data availability. In addition, data available is usually higher during summer months, because of less cloud cover. However, varying sampling size can affect the results of statistical analyses. Still, many studies looking at long-term trends of satellite-derived frontal metrics often do not account for a continuous rise in data availability (e.g. Belkin et al., 2005; Kahru et al., 2012; Ullman et al., 2007). More information how data availability affects statistical analyses of frontal metrics would be desirable.

In this study, inter- and intrannual variability of two shelf-sea fronts from January 1990 to December 2010 is examined using monthly composites of frequently used frontal metrics (details in the method section 2.2.2). The temporal analysis serves as a case study to demonstrate differences between frequently employed frontal metrics and the factors that need to be considered when using these metrics in temporal analyses, such as variations in data availability. This research aims to provide guidance on understanding frontal metrics and their limitations and to give advice on the choice of metric and their analyses.

Study objects are the Celtic Sea and Ushant tidal mixing fronts, which separate the Celtic Sea from the Irish Sea and Western English Channel respectively (Figure 1.1, General Introduction section 1.4). Tidal mixing fronts are transition zones between tidally-mixed coastal and seasonally-stratified shelf waters. Tidal mixing fronts depend on the onset of stratification and have therefore, a distinct seasonal cycle (Holt et al., 2008b). The spatial and intra-annual variability of the Celtic Sea and Ushant Front is well documented from four decades of *in-situ* and modelling studies, which provide a solid comparison background for the results of this research. The fronts are present from approximately April to November and absent during winter due to the lack of stratification (Elliott et al., 1991; Holt et al., 2010; Pingree et al., 1978; Young et al., 2004). In addition, the seasonal nature of the two fronts allows for the demonstration of the

introduction of unwanted noise by other frontal types during winter and the advantages of studying single fronts in isolation. Furthermore, both fronts are in close proximity to each other, which allows for a comparison between individual fronts of the same type.

Tidal mixing fronts are critical in shaping oceanographic and biological processes during the summer months. They significantly contribution to the shelf-sea circulation, greatly increase primary productivity and are foraging areas for various development stages of commercially important fish (Hickox et al., 2000), sharks (Alemany et al., 2009; Munk et al., 2009), marine mammals (Miller et al., 2015; Priede et al., 2009; Queiroz et al., 2012) and seabirds (Goold, 1998). Despite their importance, not much information is available on long-term variability of tidal mixing fronts in the Celtic Sea. In addition to providing guidance for the analyses of frontal metric, this research represents the first data based long-term investigation of the temporal variability of the Celtic Sea and Ushant Front.

2.2 METHODS

This section is divided into two parts:

- The first part describes the processing of frontal maps and provides a description of the frontal metrics used in the analysis, including their underlying algorithms. This section also explains how the spatial extend of the sampling area for each front was determined, e.g. how large does the area need to be in order to capture spatial deviations from the core position of the front and at the same time, minimize the inclusion of frontal segments from neighbouring fronts in the vicinity. Finally, the construction of the time series for each front is described, which involves the spatial averaging of frontal values over the sampling area.
- The second part concerns the statistical analysis: Calculation of anomalies of frontal metrics, data exploration, detailed description of the statistical model used and the factors included in the analyses and model validation.

2.2.1 Processing of frontal maps

Frontal maps in this research were based on 'monthly composites', which means that all satellite images obtained during a given month are combined into a single map. Although higher temporal resolution would have been more desirable, weekly and fortnightly frontal maps were still highly affected by cloud cover (even during the summer months) and were unsuitable for the analysis. Particularly at the beginning of the 21 years time period in this research (the early 90's), there were only few satellite passes and hence, few images per day. Consequently, satellite images collected over weeks were required to obtain a fairly cloud-free view on the sampling area, particularly during the wintertime. Nowadays, higher resolution composites (e.g. fortnightly) can be sufficient, because the number of satellites and subsequently, satellite passes, have consistently increased over the past 20 years, providing multiple images per day.

Frontal maps used in this research are based on Advanced Very High-resolution Radiometer (AVHRR) data from National Oceanic and Atmospheric Administration (NOAA) satellites, which were received at the Dundee Satellite Receiving Station, Scotland, by the NERC Observation Data Acquisition and Analysis Service (NEODAAS). These raw data are translated into SST values, geo-corrected, cloud masked, and mapped by the Remote Sensing Group (RSG) of Plymouth Marine Laboratory (PML) at 1.1km^2 resolution. Thereafter, fronts are detected on each satellite image by application of the Single Image Edge Detection algorithm (SIED) developed by Cayula and Cornillon (1992). In this approach, a histogram of the SST frequency distribution is created, based on a user-defined array of pixels, but usually 32x32 pixel (also used in this research). If the histogram has a bimodal form, it suggests the presence of two different water masses (Figure 2.1). In order to qualify as two separate water masses, the temperature difference between the two populations has to be at least 0.4°C (in this research). The SIED then marks the transitional values between the two modes of in the histogram as 'valid pixels' = frontal (*Fvalid*).

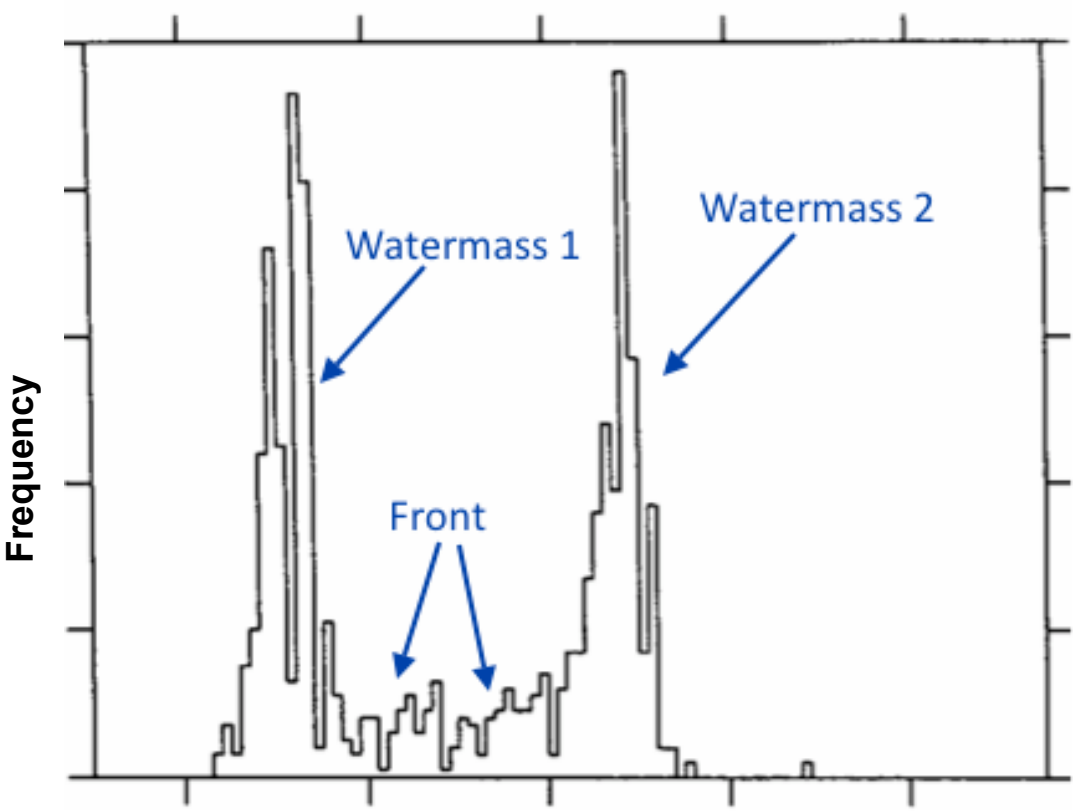

Figure 2.1: Histogram of a sharp front. The histogram has a bimodal shape and shows temperature distribution of two distinct water masses. The temperate difference between the two water masses has to be at least 0.4°C in order to be classified as distinct by the SIED. The transitional values between the two modes are classified as frontal. Figure modified from Cayula and Cornillon (1992), Figure 7.

A SIED-derived frontal map from a single satellite image is unsuitable for the description of meso-scale features due to their variable nature and the frequency of cloud cover in the study region, which disguises dynamic processes (Miller, 2009). Therefore, all images obtained each month were used to obtain a clear frontal picture. Rather than averaging over the images, they are accumulated into a single map, which highlights stable frontal features. Further steps of data processing depend on the metric chosen and are explained in detail below.

2.2.2 Frontal metrics used in this research

Fprob (Figure 2.2, **Table 2.1**) represents the probability of observing a front in a given pixel over the sequence of images used (Miller, 2009). For example, 40 images were obtained over the period of one month. Of these 40 images, only 30 images had clear views on a given pixel (example pixel), in the other ten images the example pixel was obscured by clouds. In this sequence of 30 clear views, the example pixel was identified as valid pixel (frontal) 20 times by the SIED-algorithm. The *Fprob* value for this pixel would be:

$$Fprob = \frac{valid\ pixels}{clear\ pixels} = \frac{20}{30} = 0.67.$$

The higher the *Fprob* value, the more often a front was detected in the pixel. Therefore, clusters of pixels with high *Fprob* on a frontal map represent areas of higher frontal occurrences. The advantage of *Fprob* is that it is simple and easy to understand. However, there are two apparent disadvantages. Firstly, it is a proportion and can easily biased when the relationship between the numerator and denominator is not linear or if both change in the same direction, but at different rates. Secondly, *Fprob* does not provide information on the strength of a front.

Fmean (Figure 2.2, **Table 2.1**) provides information on the temperature gradient (temperature change per pixel) and hence, an indication of the strength of a front (Miller, 2009). After applying the SIED-algorithm to a single image, the temperature gradients between a valid pixel (example pixel) and its neighbouring valid pixels are calculated. The value of the greatest gradient found is assigned to the example pixel. This is done for all valid pixels on a map and all images going into a composite. For the final map, the mean of all values (greatest temperature gradient) for the example pixel, obtained over the sequence of images for one month, is taken. However, the mean is only based on valid pixels in the sequence and not on pixels that were cloud free, but non-frontal. For example, 40 images were obtained over the period of one month. Of these 40 images, only 30 images had clear views on the example pixel. In the other ten images the example pixel was obscured by clouds. In this sequence of 30 clear views, the example pixel was identified as valid pixel (frontal) 20 times by the SIED-algorithm. Because *Fmean* is based on valid pixels only, 20 times

the greatest temperature gradient found was calculated for the example pixel. For the final map, the 20 gradient values were added and divided by the number of times the example pixel was valid, which is 20 in this case.

$$Fmean = \frac{sum\ of\ max.gradient\ values\ (20\ different\ values)}{number\ of\ times\ the\ pixel\ was\ identified\ f\square ontal} = (e.g.)\ \frac{21.4}{20} = 1.7$$

A disadvantage of *Fmean* (Figure 2.2, **Table 2.1**) is the disregard of clear pixels. For instance, the example pixel was identified as frontal 20 times in the sequence of 30 clear images and had a final *Fmean* of 1.7. Another pixel, example pixel 2, has been identified as frontal twice in the sequence of 30 clear images, but also had a temperature gradient of 1.7 each time. Example pixel 2 will receive the same value on the map as example pixel 1 although its frontal frequency was very small. This results in maps containing many transient frontal segments that are displayed with the same strength than the persistent ones. This is not desirable for visualisation purposes as it introduced noise to a map and complicates the detection of stable fronts.

Fpers (Figure 2.2, **Table 2.1**) is the product of multiplying the final monthly composite of *Fmean* by the final composite of *Fprob*:

$$Fpers_{final} = Fmean_{final} \times Fprob_{final}$$

By weighting *Fmean* by a measure of persistence (*Fprob*), areas of frequently occurring fronts are highlighted and noise introduced by short-lived frontal segments is reduced (Miller, 2009). While the multiplication of *Fprob* and *Fmean* aids visualisation of more consistent features, it complicates an interpretation of the metric itself, because it is comprised of two entities that have different meanings. A change in *Fpers* cannot be directly attributed to either changes in *Fprob* or *Fmean* (or both). However, in certain cases it might be crucial to know which metric is more affected, e.g. if interested in the meteorological drivers of the observed variability.

In ***Fcomp*** maps (Figure 2.2, **Table 2.1**) an additional weighting factor (*Fprox*) is applied to the final *Fpers* maps, which considers the spatial proximity of valid pixels (Miller, 2009).

$$Fcomp_{final} = Fpers_{final} \times Fprox$$

Pixels near or in clusters of valid pixels, will receive an additional 'boost'. The closer the pixel is to a frontal cluster, the more it will be boosted. This process will ignore pixels located beyond a certain distance from any frontal clusters. The resulting maps further emphasise persistent features and further reduce the occurrence of noise. Like *Fpers*, *Fcomp* obscures the influences of each of the components for the final product and it is not possible to identify the most variable component.

Fdens (Figure 2.2, **Table 2.1**) is basically an *Fcomp* map plus the application of an additional spatial smoother (Scales et al., 2014a). *Fdens* is particular useful for visualisation of persistent, spatially stable features as it removes nearly all transient frontal segments.

$$Fdens_{final} = Fcomp_{final} + spatial\ smoother$$

Fclear and ***Fvalid:*** For each pixel in a final composite map, ***Fclear*** and ***Fvalid*** (Figure 2.2, **Table 2.1**) simply provide the total amount of clear and valid pixels. Valid pixels are pixels that have been identified by the SIED-algorithm as frontal (described in section 2.2.1). Clear pixels are pixels that were not cloud covered and had a free satellite view on the ocean. These can be frontal or non-frontal. As in the example above, 40 images were obtained over the period of one month. Of these 40 images, only 30 images had clear views on a given pixel (example pixel), in the other ten images that pixel was obscured by clouds. The example pixel would have an *Fclear* value of 30, while it was covered by clouds the on the other ten occasions. The pixel's *Fvalid* would be 20, because in the 30 clear views on that pixel, the SIED-algorithm classified it as frontal only 20 times.

Table 2.1: List of metrics of metrics used in this research and their abbreviations, common names, quantitative derivation, value range and spatio-temporal resolution. Temp.= Temperature

Metric	Common name	Definition	Value range	Spatio-temporal res.
Fvalid	Valid pixels	Total of valid (frontal) pixels in a sequence of images	Any positive integer	Monthly 4.8km^2
Fclear	Clear pixels	Total of clear pixels in a sequence of images	Any positive integer	Monthly 4.8km^2
Fprob	Frontal probability	$\frac{Fvalid}{Fclear}$	0-1	Monthly 4.8km^2
Fmean	Temp. gradient	$\frac{Temperature\ gradient}{Fvalid}$	0-2.54	Monthly 4.8km^2
Fpers	Frontal persistence	$Fprob\ x\ Fmean$	0-0.254	Monthly 4.8km^2
Fcomp	Frontal composite	$Fpers\ x\ Fprox$ *Fprox*= additional 'boost', when other frontal clusters in the neighbourhood	0-0.254	Monthly 4.8km^2
Fdens	Frontal density	$Fcomp + spatial\ smoother$	0-0.254	Monthly 4.8km^2

2.2.3 Spatial downscaling

The final composites of each metric initially had a spatial resolution of 1.1km^2. For this research, the resolution was reduced to 4.8km^2 by taking the mean of a four by four pixel array on the final monthly composites. Spatial downscaling was performed to reduce variability around the frontal contours, which facilitated the determination of the sampling area (see section 2.2.5.1). It is important to consider the observed movement of dynamic fronts through the sequence, as this can affect the interpretation of front metrics, particularly if they are spatially averaged or smoothed. For example, a strong static front would give a thin line of high *Fmean* values, whereas a weaker dynamic front would result in a wider ribbon of lower *Fmean* values. Even a weaker static front causes greater variability in the detected location of the frontal boundary. The greater number of frontal pixels covered by a weak front may cause the spatial averaging to

give higher metric values than for a strong front. This contributes a small, unavoidable uncertainty, which affect all front detection techniques similarly.

2.2.4 Expression of frontal metrics in digital values

The metrics *Fpers*, *Fcomp* and *Fdens* are in so-called 'digital values' and range between 0 and 255. The software used to process the frontal maps produces values in the range of 0-255 to conserve memory and to run more efficiently. In order to achieve some distinction between the metrics, a specific conversion factor is applied to each one, resulting in a different value range for most metrics (usually one or more decimal degrees from the base value). However, the converted metrics still do not relate to real-life values and spatio-temporal differences of a given metric can only be described as relative change. Exceptions are *Fvalid* and *Fclear*, which represent the actual number of pixels that were valid and clear respectively. *Fmean* values also represented the actual temperature gradient, which is the change in temperature per pixel. *Fprob* is a proportion of *Fvalid* and *Fclear* that ranges between 0–1.

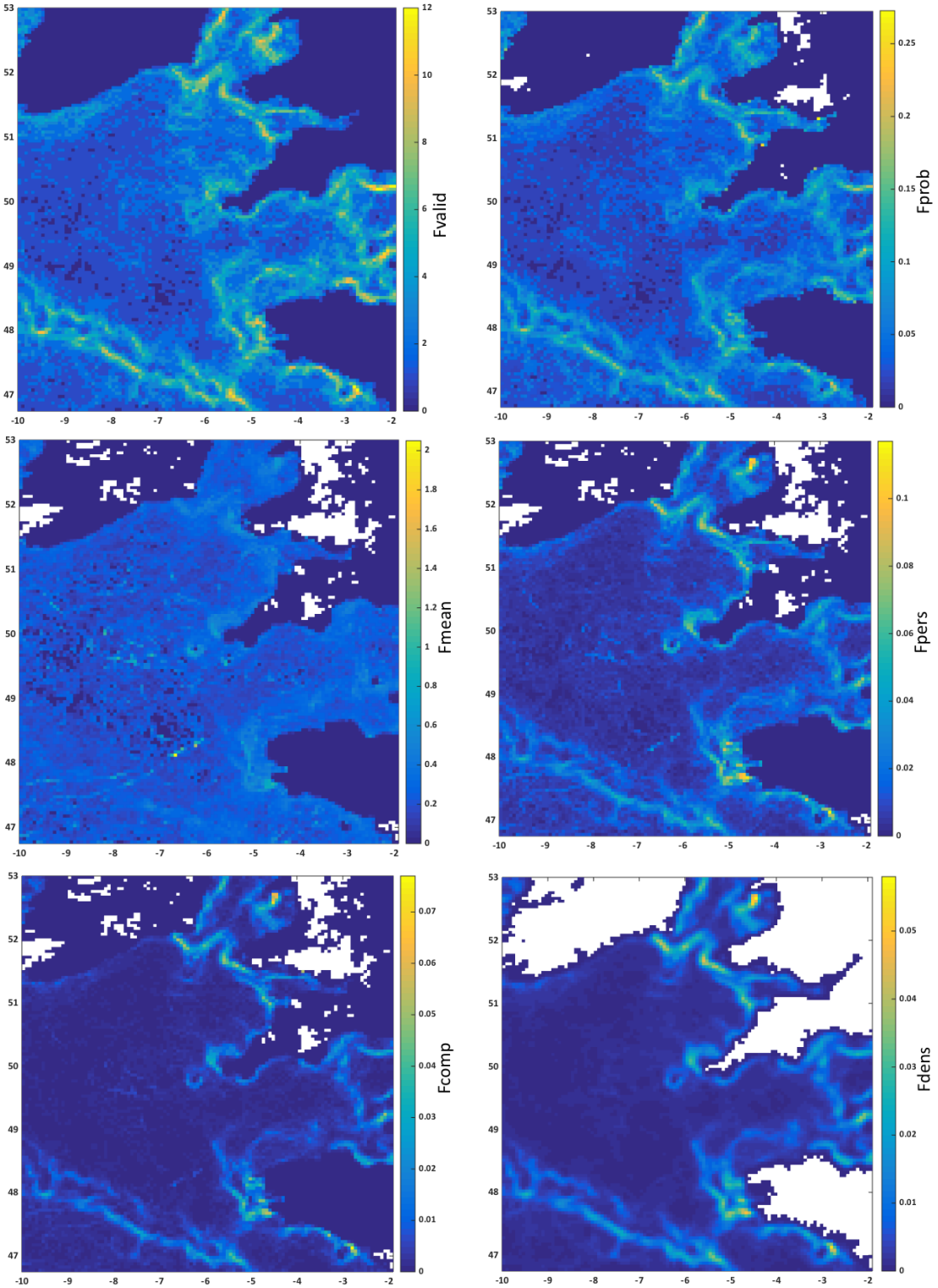

Figure 2.2: Monthly composites for *Fvalid*, *Fprob*, *Fmean*, *Fpers*, *Fcomp* and *Fdens* from June 2009. Blue colours indicate lower and yellow higher values of a given metric. Pixels covering land are no-value pixels and therefore, come up as white or zero.

2.2.5 Data processing

All statistical analysis was performed in 'R', figures and geographic maps were created in either 'R', Matlab or ArcMap10.1 (ArcMap, 2012; Matlab, 2009; R Core Team, 2013),.

2.2.5.1 Determination of sampling areas for Celtic Sea and Ushant Front

To investigate inter- and intraannual variability of the selected frontal metrics for each front (Ushant and Celtic Sea Front), time series for each metric had to be created, which encompasses the spatial averaging of pixels to obtain a single value per front and monthly composite. The position of tidal mixing fronts varies seasonally, in response to tidal movements, storm events and other factors. Therefore, the sampling area for each front needed to be large enough to capture the spatial variability of the fronts, but small enough to exclude unwanted features in the vicinity as much as possible, which would add noise (e.g. other fronts such as river plumes or coastal currents). In order to identify the spatial variations of each front over the yearly cycle, seasonal maps of *Fcomp* were created by averaging monthly composited of *Fcomp* from 1990 to 2010 according to season (Spring: March-May; Summer: June-August; Autumn: September-November; Winter: December-February). Each maps showed the average spatial extent (from 1990 to 2010) of the Celtic Sea and Ushant Front in each season, which provided a first indication of a suitable sampling area for each front.

Based on the visually identified core areas for the Celtic Sea and Ushant Front, different sized subsets were created (Figure 2.3). Subsets were limited to ≥12km away from the coast to avoid the influence of coastal factors, such as coastal currents and freshwater plumes. Resampling on the different subsets was conducted to a) refine the sampling area and b) ensure no bias caused by an 'area size effect' was introduced. By resampling different sized subsets the minimum sampling area required can be refined, ensuring no significantly large segments of the Celtic Sea or Ushant Front are left out and at the same time, keeping the subsets small enough to reduce noise from unwanted other fronts in the vicinity. For example, spatial averages for each subset are expected to

increase with decreasing subset size, because less non-frontal pixels are included in the averaging.

Resampling was conducted in 'R' using the *one.boot* function in the 'simpleboot' package (Peng, 2008). Bootstrapping with 999 permutations on the mean was performed on the entire data set and a seasonal subset (March-November), which only considers the frontal season. For the Celtic Sea Front three subsets of different size were resampled and for the Ushant Front four subsets (Figure 2.3). Boxplots of the resampled mean of *Fprob* and *Fmean* for the Celtic Sea Front show no signs of a 'sampling area effect' (Figure 2.4, showing *Fprob* and *Fmean* only, representative of other metrics). Values declined as expected when increasing the spatial extent of the subsets. At the Ushant Front, the seasonal subset did not show any signs of an area effect. However, the differences of the bootstrapped mean between subset 1 and 2 of the entire dataset were small (Figure 2.4) and indicated that the larger subset still captured new frontal pixels. Since this was only the case for the full data set and not the seasonal one, it suggests that the additional frontal pixels belong to wintertime fronts. Wintertime fronts are not of interest in this research and considered noise. Therefore, final analyses were performed on subsets 1 for both fronts.

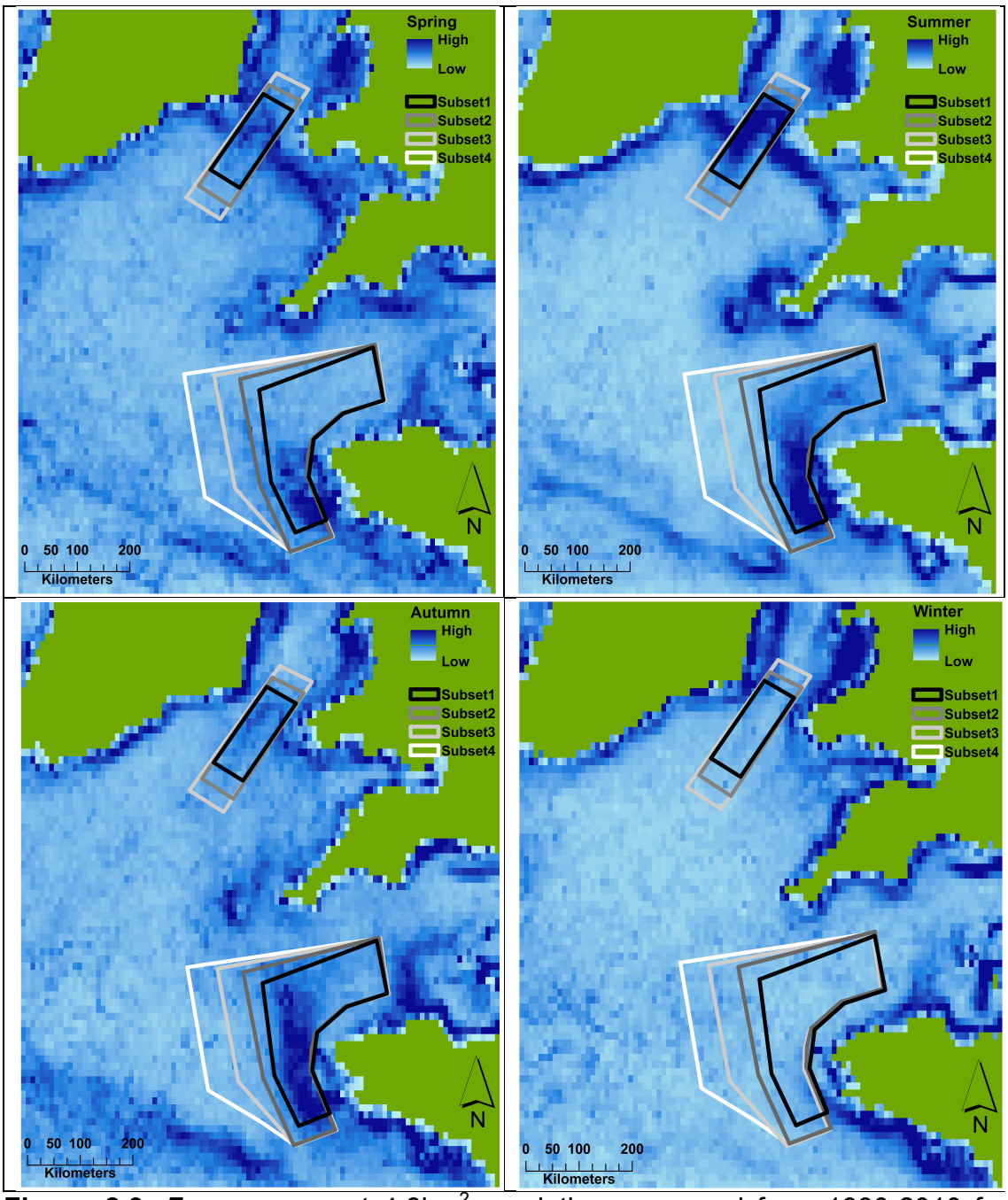

Figure 2.3: *Fcomp* maps at 4.8km^2 resolution, averaged from 1990-2010 for spring (March-May), summer (June-August), autumn (September-November) and winter (December-February), showing areas of low (light blue) and high (dark blue) *Fcomp*. Green indicates land; coloured polygons show different sized sampling subsets considered for analysis and used during resampling.

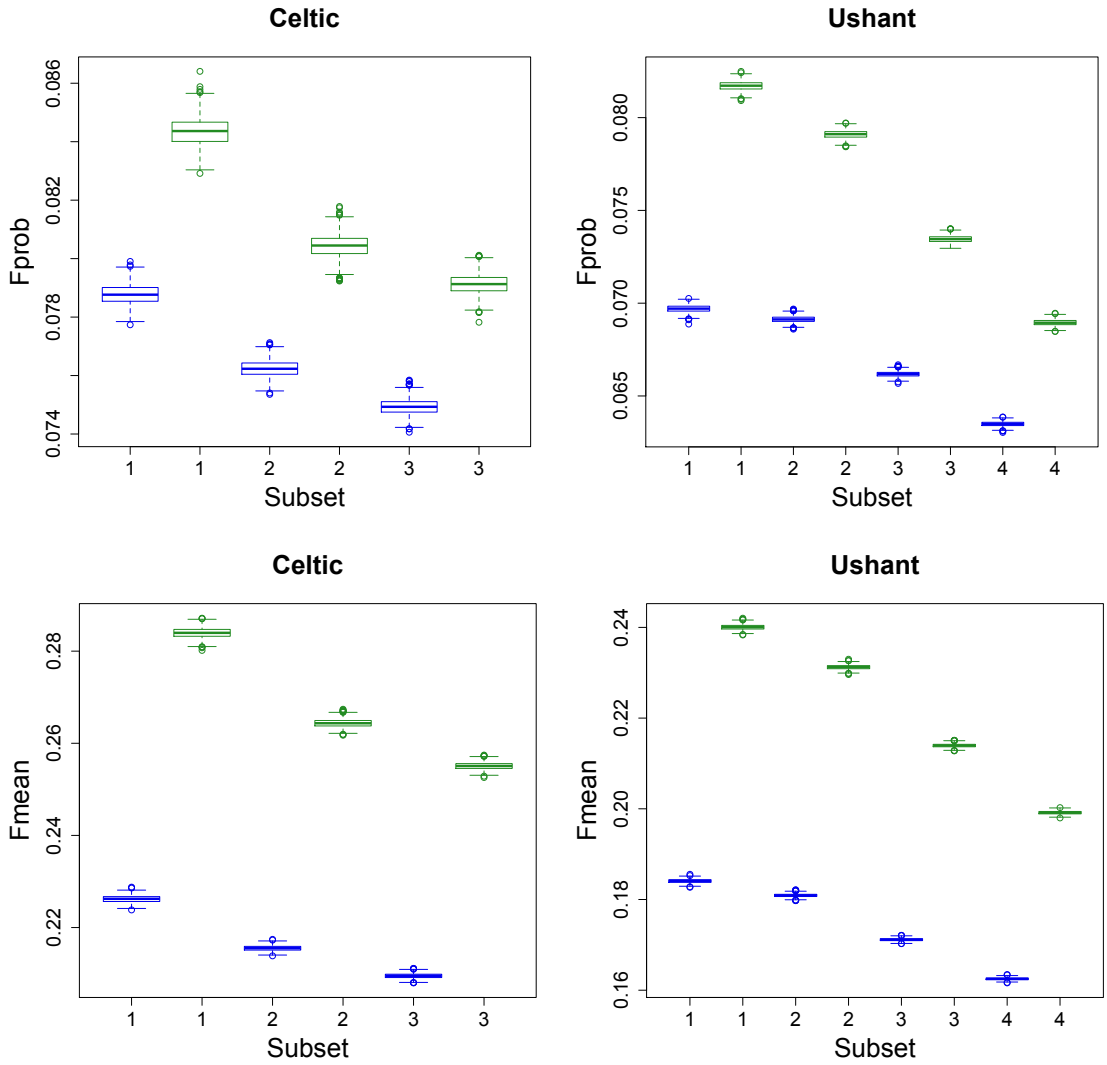

Figure 2.4: Boxplots of bootstrap-resampled mean (999 permutations) for *Fprob* (top panel) and *Fmean* (bottom panel) at Celtic Sea and Ushant Front, based on the entire dataset (blue) and a seasonal subset (green), including months March- November only. Subsets are labelled as in **Figure 2.3**

2.2.5.2 Spatial averaging of frontal pixels over the sampling area

To obtain time series for each frontal metric at the Celtic Sea and Ushant Front, pixels within the two subsets 1 were averaged for each monthly composite and metric, using the arithmetic mean. The spatial averaging can either include all pixels (including non-frontal, but clear) or frontal pixels only. Since the subjects of interests are fronts, one might consider using frontal pixels only, and hence, extract merely information on the fronts. However, using only frontal pixels would result in highly variable sampling sizes for the spatial averaging (**Table**

2.2), because there will be fewer frontal pixels during winter months in the sampling area and more during the summer (tidal mixing fronts are absent during the wintertime). In addition, there will be more frontal pixels during periods of higher *Fclear* (e.g. the summer months or good weather periods). Sampling size can affect the results of statistical analyses. In order to avoid a sample size effect, spatial averaging in this research was performed using all pixels within subset 1 for both fronts, including non-frontal ones.

Table 2.2: Maximum, minimum and mean sampling sizes (pixels included in spatial averaging of subset 1 for each front) if zeros were excluded and when they are included

Front	**Celtic Sea Front**			**Ushant Front**		
	Max	**Min**	**Mean**	**Max**	**Min**	**Mean**
Excl. zeros	213	19	180	837	37	628
Incl. zeros	213	210	213	837	833	837

2.2.6 Statistical analyses

2.2.6.1 Correlations between frontal metrics used in this research

Data exploration revealed very high correlations between the metrics *Fprob*, *Fpers, Fcomp* as well as between *Fdens*, *Fpers, Fcomp* and between *Fdens* and *Fmean* (**Table 2.3**). Therefore, analyses in this research were conducted on *Fprob* and *Fmean* only, each representative for a metric group of similar metrics. *Fcomp* and *Fdens* are probably two of the most frequently used frontal metrics in ecology at the moment. However, *Fprob* was selected instead of *Fcomp* or *Fdens*, because it is a) more comprehensible compared to *Fcomp, Fpers* and *Fdens*, b) frequently used in remote sensing research and c) the dominant component in *Fcomp* and *Fpers* (most of the variability in *Fcomp* and *Fpers* is caused by the variability in *Fprob*). Surprisingly, *Fmean* has not been used much in ecological or oceanographic research. It is included in this research instead of *Fdens*, because a) it is more comprehensible compared to *Fdens* and b*)* it provides useful information on the strength of the front (different frontal characteristic than *Fprob*). Time series plots of metrics not included in the analysis (*Fpers*, *Fcomp* and *Fdens)* can be found in the appendix (Sup.Figure 2.1 and Sup.Figure 2.2).

Table 2.3: Pearson Product Moment correlation coefficients (*r*) for all metrics combinations. Green shading refers to Celtic Sea Front and blue shading to Ushant Front correlations. Coefficients above 0.7 are in *italic* and bold numbers are coefficients of correlation analyses with *p-values* <0.05.

Metric/*r*	*Fprob*	*Fpers*	*Fcomp*	*Fmean*	*Fdens*
Fprob	**1.0**	***0.9***	***0.9***	**0.3**	**0.5**
Fpers	***0.8***	**1.0**	***1.0***	**0.5**	***0.7***
Fcomp	***0.8***	***1.0***	**1.0**	**0.5**	***0.8***
Fmean	0.006	**0.5**	**0.5**	**1.0**	***0.8***
Fdens	**0.4**	***0.8***	***0.8***	***0.9***	**1.0**

2.2.6.2 Statistical analysis of inter-and intraannual variability of *Fprob* and *Fmean* and the effect of *Fclear* on temporal variability pattern on both metrics

Inter- and intraannual variability of *Fprob* and *Fmean* and the effect of *Fclear* on temporal variability pattern of both metrics were investigated using monthly anomalies of *Fprob* and *Fmean*. Anomalies were created by subtracting the overall mean of the time series from each data point of the time series. For example, the overall mean of all 252 data points of *Fprob* was calculated and then subtracted from each single of the 252 *Fprob* data points (168 data points for the seasonal subset used in the analysis below). In order to avoid noise introduced by frontal segments in the sampling area during wintertime when tidal mixing fronts are absent, only months March to November were considered for statistical analysis. Temporal explanatory variables were 'year' to account for interannual variability, 'month' to account for seasonal variability and '*Fclear*' to account for the increase in data availability over the course of the time series and to account for variability of *Fclear* throughout the yearly cycle (e.g. more data availability during the summer due to less cloud cover). Before the modelling process, all covariates were examined for collinearity using Pearson-correlation and Variance Inflation Factors (VIF) (*corvif* function in 'HighstadLibV4' by Zuur et al. (2009)). A Pearson-correlation coefficient ≥0.6 and/or VIF-values ≥3.0 indicate collinearity (Zuur et al., 2009), but collinearity was not the case for any of the explanatory variables. Autocorrelation plots

based on monthly anomalies of *Fprob* and *Fmean*, generated using the *acf* function in 'R', indicated temporal autocorrelation and seasonality (Sup.Figure 2.3). In addition, data exploration suggested non-linear relationships between the two response variables (monthly anomalies of *Fprob* and *Fmean*) and all three explanatory variables (Sup.Figure 2.4 and Sup.Figure 2.5). Generalized Additive Mixed Models (GAMMs) with an autoregressive correlation structure of order one (AR(1)) were used in order to account for temporal autocorrelation and the non-linear relationship between the response and explanatory variables. Different correlation AR and Autoregressive moving average (ARMA) structures were tested before deciding on an AR(1) structure, but it was the simplest structure that resulted in the lowest Akaike Information Criterion (AIC) (Pan, 2001a). The GAMMs take the structure as specified by Hastie and Tibshirani (1987) and were fitted using the *gamm* function in the 'mgcv' package (Wood, 2006) In this package, the degree of smoothness of each parameter is automatically estimated as part of the fitting process, using penalized regression splines. However, after an initial model run, smoothed terms were fitted as regression splines with fixed maximum degrees of freedom ($k=6$) for the covariate 'month' and '*Fclear'* in order to avoid overfitting. The variable 'month' was modelled using cyclic cubic regression splines, setting knots manually between 3 (March) and 11 (November) in order to account for the circular nature of this term. If a term was smoothed with 1 degree of freedom, the model was refitted with that covariate modelled as a linear term. Model selection was conducted using manual stepwise-backwards selection. In this approach, the model is run with all covariates. If a covariate is insignificant (*p-value* > 0.05), the term is excluded from the model if the exclusion results in a AIC-decrease of at least 2.0. This process is repeated until a) the model includes only significant terms and/or b) no decrease in AIC is achieved by dropping another insignificant term and/or c) the R^2 does not increase by more than ≥0.1. Model fit was examined by means of residual analysis (Sup.Figure 2.6 to Sup.Figure 2.9). Residual analysis displayed a few single outliers in the *Fprob* model. The outliers were excluded to improve model fit and the models re-run.

2.3 RESULTS

2.3.1 Comparison between *Fmean* and *Fprob* based on differences in their temporal variability

The correlation between *Fmean* and *Fprob* at the Celtic Sea Front was insignificant. At the Ushant Front, the correlation between *Fprob* and *Fmean* was significant, but weak (r=0.5, p<0.001). The differences between the two metrics were also mirrored in distinct interannual variability pattern for both metrics. There was a decrease in *Fmean* at the beginning of the time series from 1990 to 1996 at both fronts, followed by a general increase from 1996 to 2010 (Figure 2.5). From 2003 onwards anomalies of *Fmean* were consistently positive at both fronts. Prior to 2003, *Fmean* anomalies were negative apart from four isolated years, which differed for each front. A notable low occurred in 1996 at both fronts. Overall, the temporal pattern for *Fmean* were alike at the Celtic Sea and Ushant Front and only minor differences were evident, particularly in the first ten years of the time series. *Fmean* values were slightly higher at the Celtic Front (0.22±0.09) compared to the Ushant Front (0.19±0.08). In contrast to *Fmean*, anomalies for *Fprob* were positive until 1996 and dropped profoundly thereafter at both fronts. Apart from minor variations, temporal variability was consistent for the remainder of the time series. Notable highs in *Fprob* occurred in 1990 and 1996 at the Celtic Sea Front, which were not as profound at the Ushant Front. Overall, higher *Fprob* values were observed at the Celtic Sea Front compared to the Ushant Front (Celtic: 0.078±0.03, Ushant: 0.072±0.03). Essentially, *Fprob* and *Fmean* displayed a very metric-specific interannual variability.

The differences in intraannual variability between *Fmean* and *Fprob* were not as profound compared to the interannual pattern of both metrics (Figure 2.6). Anomalies for *Fmean* became positive in May at both fronts, displayed a typical seasonal curve with an initial increase in values in the summer, and followed by a decrease during autumn until anomalies became negative again in October at the Celtic Sea Front and November at the Ushant Front. Intraannual pattern of *Fprob* differed between the two fronts. At the Ushant Front, seasonal variability of *Fprob* was similar to *Fmean*, but shifted by one month (later). *Fprob*

anomalies did not become positive until June and remained so until November. At the Celtic Sea Front on the other hand, temporal pattern of *Fprob* were more variable. Anomalies were positive during the summer from June to September and negative between March and May as well as in October and November. Furthermore, positive *Fprob* anomalies were found from December to February. Tidal mixing fronts are absent during this time of the year and the high *Fprob* during the wintertime indicate the inclusion of fronts that are not focus of this study, such as coastal currents or thermohaline fronts.

In summary, the two metrics displayed profound differences in their interannual pattern. *Fmean* showed a sinusoidal pattern with a short decrease in the beginning of the time series and a consistent increase since 1996. In contrast, *Fprob* values were high until 1996 and then dropped notable. After 1996, no profound fluctuations occurred in *Fprob*. The differences in seasonal variability were not as extreme, but varied between the two fronts. In addition, *Fprob* at the Celtic Sea Front only indicated the inclusion of noise during the winter months.

Fclear and *Fvalid* exhibited a typical seasonal cycle, similar to the one seen for *Fmean* (Figure 2.6). Anomalies of *Fclear* were positive between March and September at both fronts. Intraannual variability of *Fvalid* was consistent with intraannual variability pattern of *Fmean*. Positive anomalies of *Fvalid* occurred from May to September at the Celtic Sea Front and May to October at the Ushant Front. There was a fairly consistent increase in *Fclear* and *Fvalid* from 1990 to 2010. Anomalies of both entities became positive at both fronts in the middle of the time series, around 2001. However, since 2005 the trend stagnated and there was even a slight decrease in *Fclear* and *Fvalid* in the last couple of years of the time series. Notable lows in *Fclear* and *Fvalid* coincided with the low *Fmean* and high *Fprob* years of 1990 and 1996. A potential correlation between the observed increase in *Fclear* and interannual variability of *Fprob* and *Fmean* is discussed in the following section.

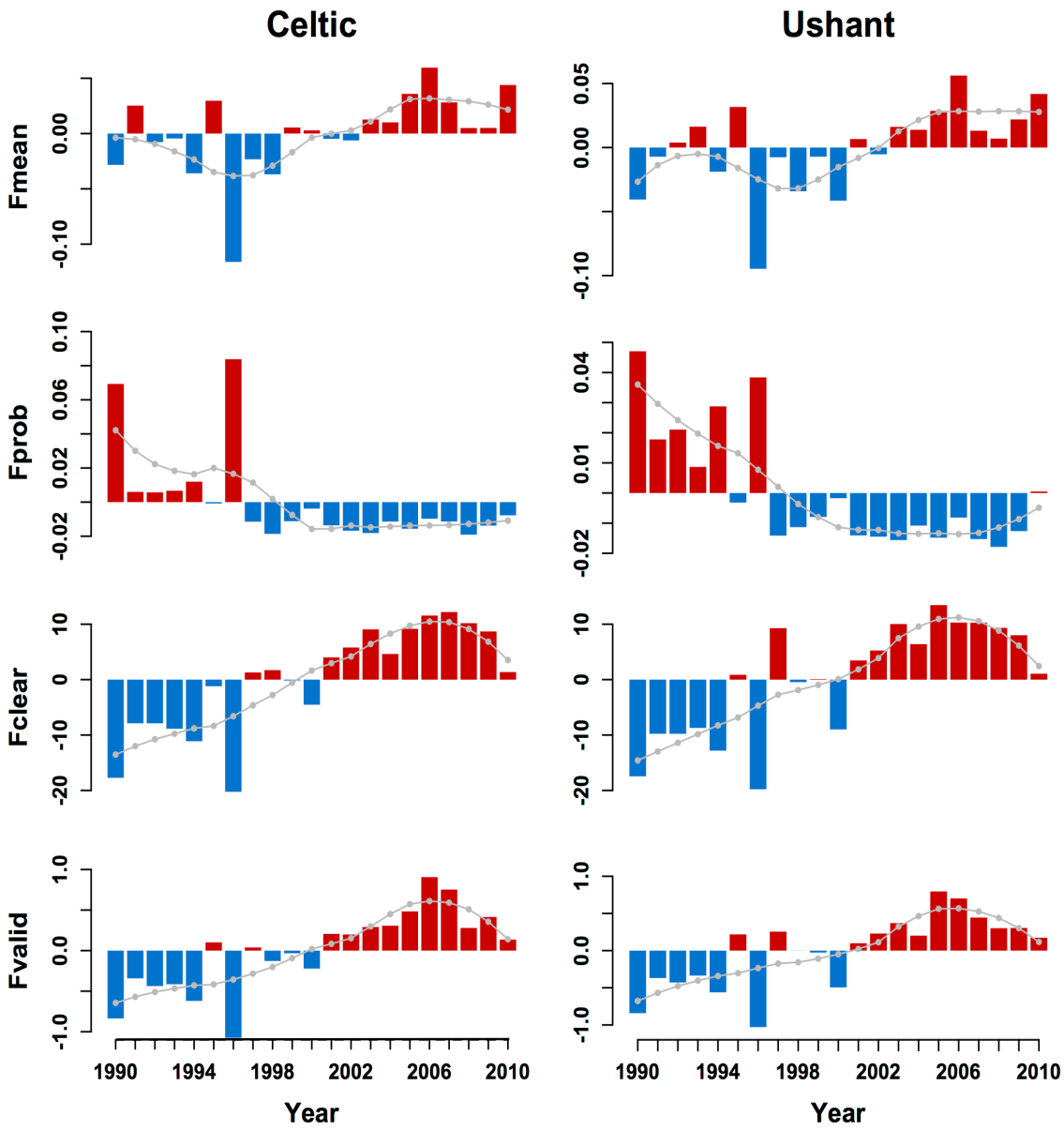

Figure 2.5: Yearly anomalies with loess smoother (α= 0.6, grey line) of *Fmean*, *Fprob*, *Flcear* and *Fvalid* at the Celtic Sea and Ushant Front from 1990 to 2010, based on a seasonal subset (March to November). Blue bars represent negative anomalies and red positive anomalies.

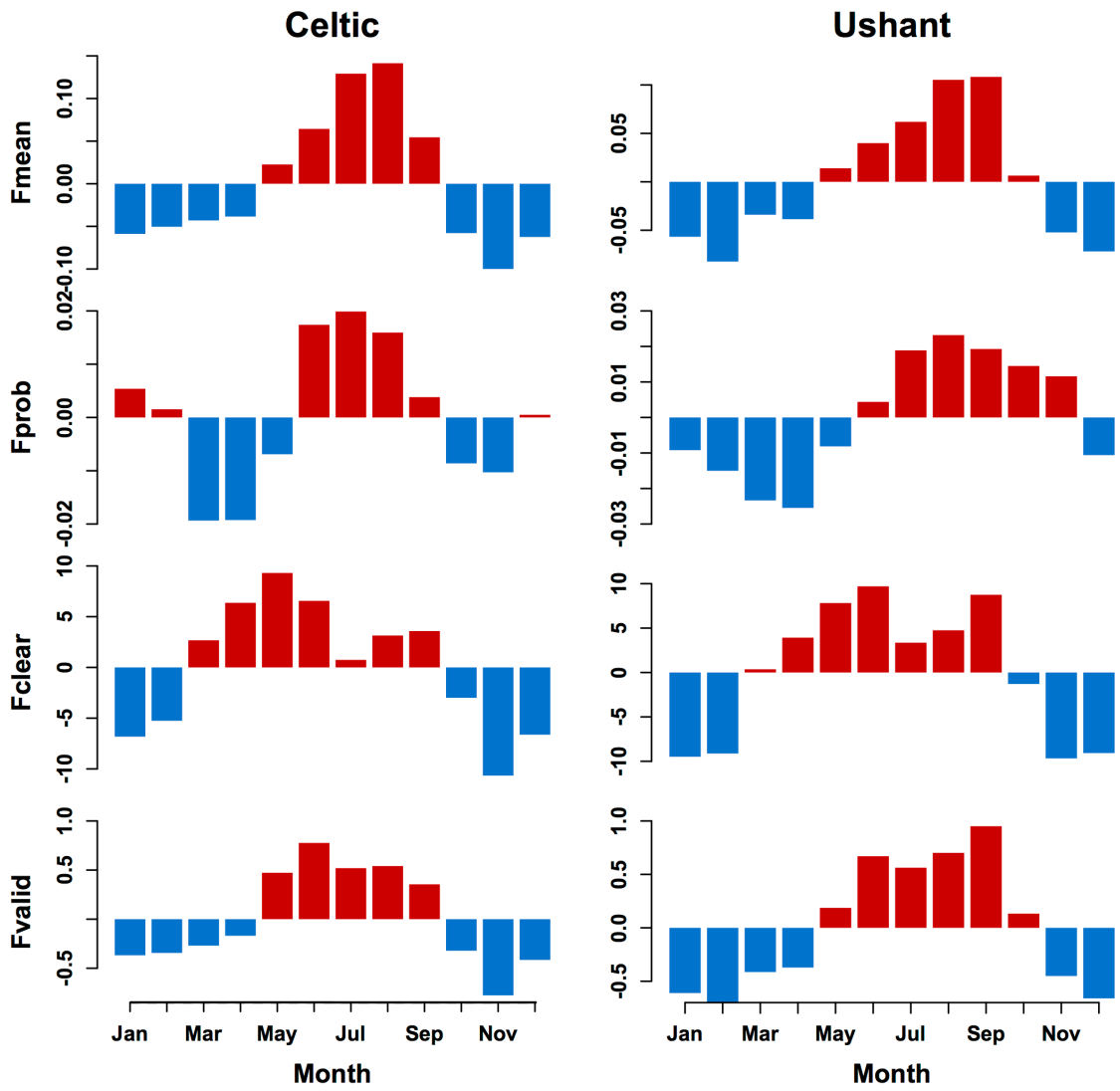

Figure 2.6: Monthly anomalies for of *Fmean*, *Fprob*, *Flcear* and *Fvalid* at the Celtic Sea and Ushant Front. Blue bars represent negative anomalies and red positive anomalies.

2.3.2 Effect of *Fclear* on temporal variability of *Fmean* and *Fprob*

Preliminary analyses indicated some correlation between *Fclear* and the two metrics *Fprob* and *Fmean* (Sup.Figure 2.4 and Sup.Figure 2.5). Therefore, the temporal pattern seen for *Fprob* and *Fmean* might not purely be a result of changes in meteorological forcing over time, but caused to a certain degree by variations in available data. To investigate an effect of *Fclear* on temporal variability of *Fmean* and *Fprob*, inter- and intraannual variability of *both metrics* were modelled including *Fclear* as an explanatory variable. *Fclear* significantly affected the temporal pattern of *Fprob* and *Fmean* (**Table 2.4**). Again, the

results were similar for both fronts, but there were profound differences in the relationship between *Fclear* and each of the frontal metrics.

There was a strong, generally positive, relation between *Fclear* and *Fmean* at both fronts (Figure 2.7 and Figure 2.8). The relationship was stronger at the lower value range of *Fclear* and levelled off with increasing number of clear pixels. In consequence, accounting for *Fclear* resulted in changes in the temporal pattern of *Fmean*. The decrease at the beginning of the time series was stronger and the increase in the second half was less steep compared to the pattern seen in Figure 2.5. Intraannual variability was less affected by *Flcear* and still displayed a seasonal cycle, beginning around April and lasting until October at the Celtic Sea Front and November at the Ushant Front. While *Fclear* and 'months' explained considerable amount of the variability, 'year' only lead to a 0.03/0.05 (Celtic Sea/Ushant) increase in the model R^2.

There was also a significant effect of *Fclear* on *Fprob* (**Table 2.4**). In contrast to *Fmean*, the relationship was negative and levelled off at higher *Fclear* values (Figure 2.9 and Figure 2.10). The inclusion of *Fclear* caused a notable modification of the temporal pattern of *Fprob*. The model accounting for *Fclear* did not suggest significant interannual variability in *Fprob* at the Celtic Sea and Ushant Front. In addition, the seasonal curve of *Fprob* was more distinct when accounting for *Fclear* and showed the expected pattern with higher *Fprob* values during the summer months. A summary of the effect of *Fclear* on temporal variability of *Fprob* and *Fmean* is given in **Table 2.5**.

Table 2.4: Summary of GAMMs with AR1 structure for a seasonal subset of *Fmean* and *Fprob* (March to November) for Celtic Sea and Ushant Front modeled as a function of year, month and *Fclear*. Only significant covariates are listed, including their estimated degrees of freedom (edf), F-values, p-values and reduction in AIC. The adjusted R^2 is given for the final model (Adj.R^2).

Front	Metric	Covariate (edf)	F-value	*p-value*	Δ-AIC	Adj. R^2
Celtic Front	*Fmean*	Year (2.77)	4.85	0.004	4.33	
		Month (3.85)	99.96	<0.001	167.0	
		Fclear (4.21)	24.67	<0.001	67.16	**0.82**
	Fprob	Month (3.82)	36.1	<0.001	108.93	
		Fclear (6.82)	33.65	<0.001	156.98	**0.81**
Ushant Front	*Fmean*	Year (4.27)	4.27	<0.001	17.54	
		Month (3.66)	67.5	<0.001	103.82	
		Fclear (4.26)	47.09	<0.001	111.9	**0.78**
	Fprob	Month (3.54)	26.03	<0.001	48.72	
		Fclear (4.47)	27.58	<0.001	60.05	**0.59**

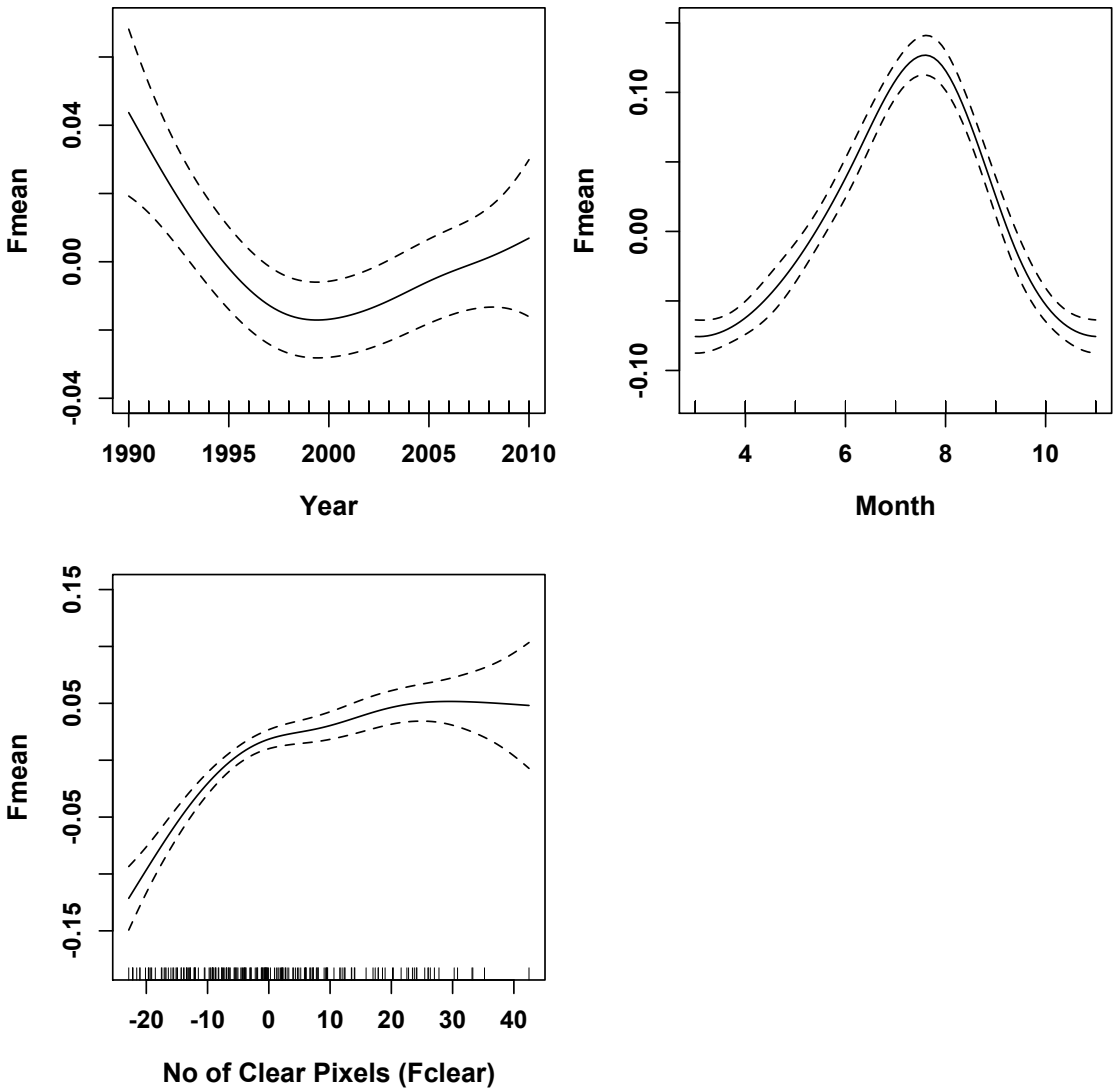

Figure 2.7: Results of GAMM with AR1 structure for a seasonal subset of *Fmean* (March to November, *N*=189) at the Celtic Sea Front as a function of year, month and *Fclear*. Solid black line represents fitted values, dotted lines 95% confidence intervals.

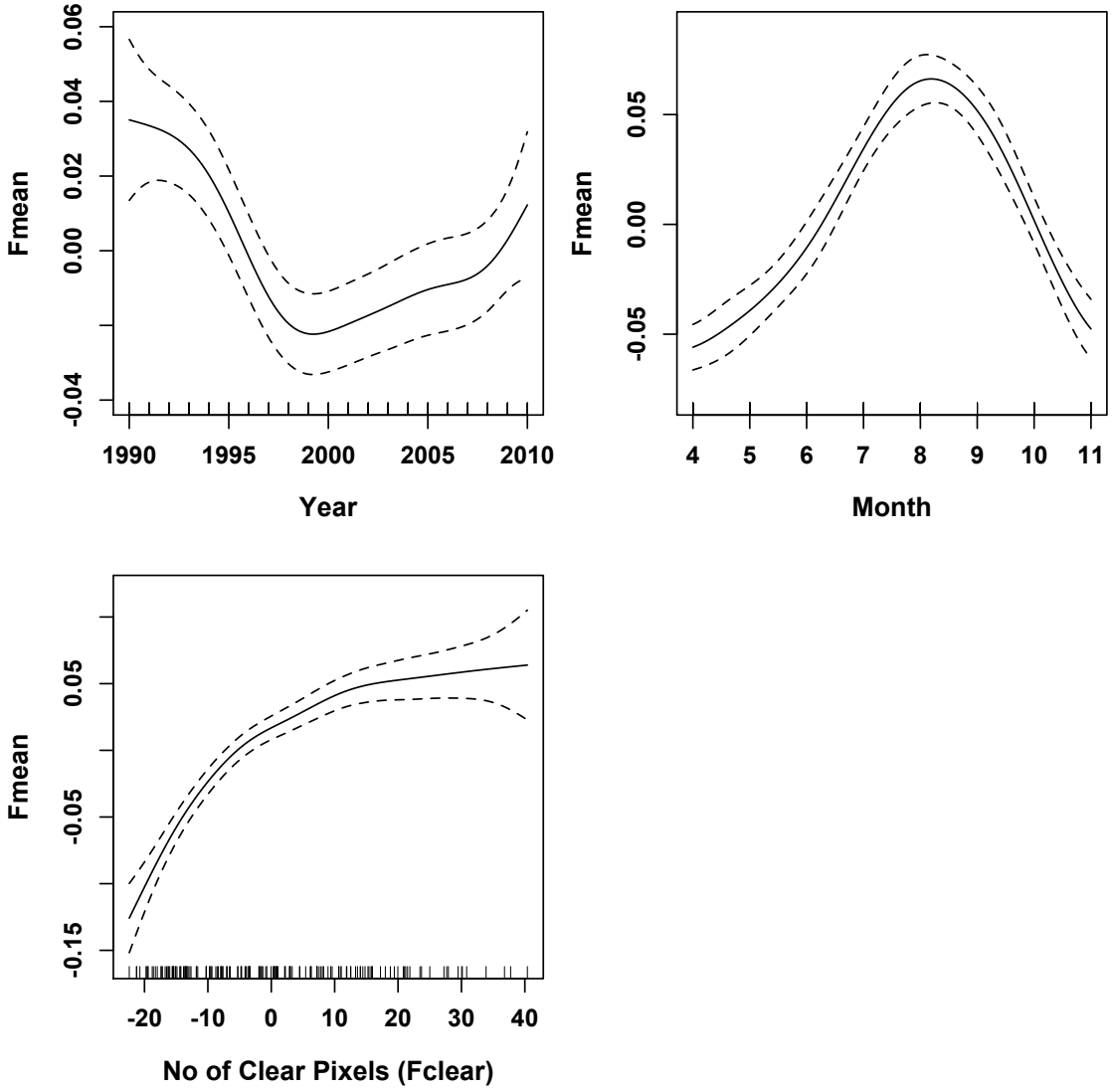

Figure 2.8: Results of GAMM with AR1 structure for a seasonal subset of *Fmean* (March to November, *N*=189) at the Ushant Front as a function of year, month and *Fclear*. Solid black line represents fitted values, dotted lines 95% confidence intervals.

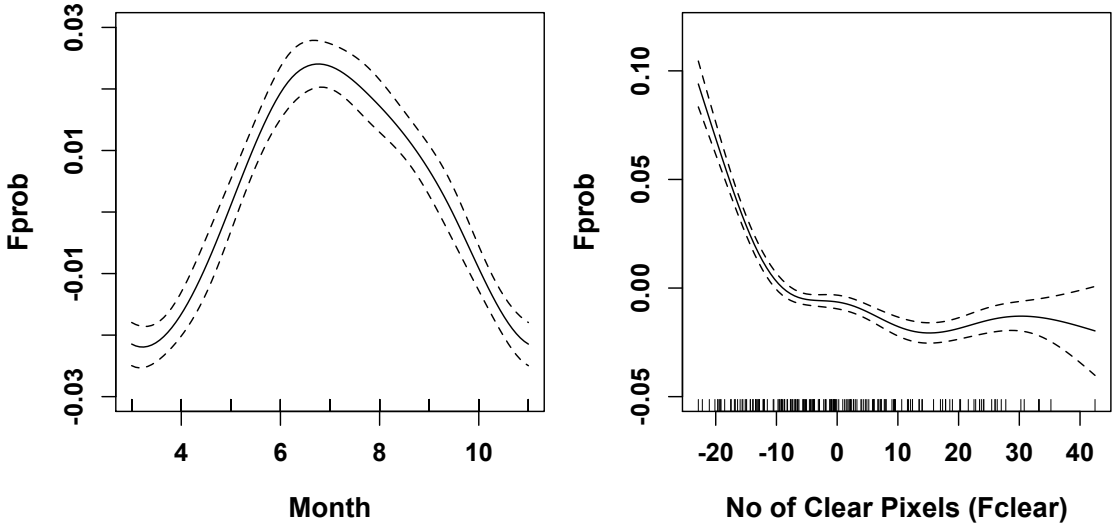

Figure 2.9: Results of GAMM with AR1 structure for a seasonal subset of *Fprob* (March to November, *N*=184) at the Celtic Sea Front as a function of year, month and *Fclear*. Solid black line represents fitted values, dotted lines 95% confidence intervals.

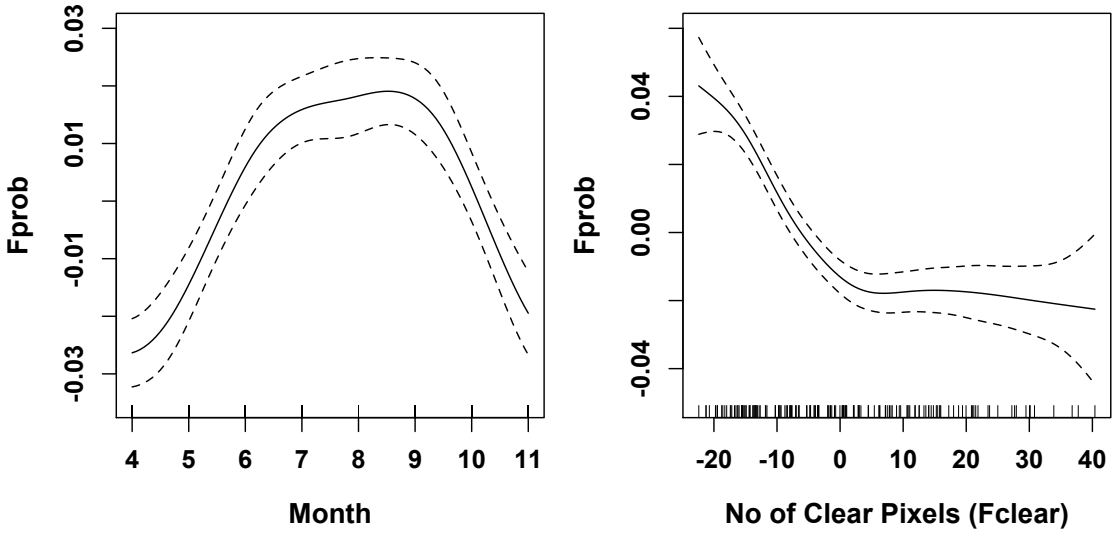

Figure 2.10: Results of GAMM with AR1 structure for a seasonal subset of *Fprob* (March to November, *N*=189) at the Ushant Front as a function of month and *Fclear*. Solid black line represents fitted values, dotted lines 95% confidence intervals.

Table 2.5: Summary table of the significance of the number of clear pixels and its effect on inter- and intrannual variability of *Fmean* and *Fprob* at both fronts Celtic Sea and Ushant Front.

Front	Metric	Effect of *Fclear*
Celtic Sea Front	*Fmean*	Significance: **Yes** (positive correlation) Inter-annual variability: **Strong effect** Intra-annual variability: **No effect**
	Fprob	Significance: **Yes** (positive correlation) Inter-annual variability: **Strong effect** Intra-annual variability: **Weak effect**
Ushant Front	*Fmean*	Significance: **Yes** (negative correlation) Inter-annual variability: **Strong effect** Intra-annual variability: **No effect**
	Fprob	Significance: **Yes** (negative correlation) Inter-annual variability: **Strong effect** Intra-annual variability: **Weak effect**

2.4 DISCUSSION

This research provides a comparison between frequently used frontal metrics, highlights some of their limitations and emphasizes factors to consider before using these metrics for quantitative analysis. In addition, this study represents the first long-term statistical analysis of temporal variability of tidal mixing fronts in the Celtic Sea, based on satellite-derived frontal maps.

2.4.1 Differences in temporal variability pattern between *Fmean* and *Fprob*

There were clear differences in intra-and interannual variability of *Fmean* and *Fprob*. All metrics are derived from the same data and all show the occurrence of surface thermal fronts. Therefore, some of the differences between *Fmean* and *Fprob* might appear surprisingly profound, such as the contrasting pattern in interannual variability. However, the meaning of each metric and their underlying algorithms are very distinct. *Fmean* represents the temperature gradient between two pixels and provides an indication of the strength of a front, but it does not provide information on the persistence of a front. In contrast, *Fprob* provides information on frontal persistence, but not directly on frontal

strength. However, persistent fronts usually have a stronger gradient than short-lived ones and vice versa.

The results of this research suggest, that the strength of the frontal temperature gradient oscillated between 1990 and 2010 at both fronts, displaying period of increasing and decreasing frontal strength. The meteorological causes of this variability will be investigated in the following chapter. In contrast, no notable changes in frontal persistent were observed between 1990 and 2010.

The differences in intraanual variability between *Fmean* and *Fprob* were much smaller compared to the interannual differences. Months of high frontal persistence coincided with months of stronger frontal gradients at the Celtic Sea and Ushant Front. Hence, the degree of change over the season was similar between the two metrics. Notable however, were high *Fprob* values during the winter months at the Celtic Sea Front, which were not seen in *Fmean*. Tidal mixing fronts are absent during the winter and the high *Fprob* indicate the inclusion of noise from wintertime fronts. The noise was probably caused by parts of a coastal current that runs along the East coast of Ireland. By restricting the sampling subset 12km away from the coasts, it was anticipated to exclude coastal influences, but they were unfortunately not completely excluded. In addition, wintertime *Fprob* was likely to be increased, because of the *Fclear* effect, which will be discussed in more detail in section 2.4.2. The increase in *Fmean* during the winter was not as strong as seen for *Fprob*. This is probably because only the edges of the coastal currents were included and the temperature gradients at the edges are a lot lower in relation to gradients encountered over the tidal mixing fronts during the summer. The issues of the unwanted inclusion of noise will be discussed in 2.4.4.1.

In summary, there were significant differences in temporal variability between *Fmean* and *Fprob* at both fronts. The discrepancies arise from the underlying algorithms and the distinct meanings of both metrics: frontal strength versus frontal persistence. Therefore, it is essential to be clear about the research objectives before analyses and chose the metric accordingly as the results can vary significantly.

2.4.2 Effect of *Fclear* on temporal variability of *Fmean* and *Fprob*

Fclear had significant, but contrasting effects on the temporal pattern of *Fmean* and *Fprob*. Overall, the relationship between *Fclear* and *Fmean* was positive, but levelled out at high numbers of clear pixels. A positive relationship was expected, because more clear pixels will lead to more cloud free scenes and subsequently, a higher detection rate of frontal segments. In addition, indirect factors increase the relationship between *Fmean* and *Fclear*. For example, stronger temperature gradients across a tidal mixing fronts are likely to be correlated with summer months or good weather periods with less cloud, more sun and higher temperatures. Under these conditions, tidal mixing fronts will strengthen or develop quicker (Holt et al., 2010; Young et al., 2004). At the same time, summer months and decreased cloud cover are also linked to higher *Fclear*. Although *Fmean* provides valuable information on the strength of a front, it is not a commonly used frontal metric. Therefore, no comparative information is available concerning temporal variability of *Fmean* or the effect of available data.

For the same reasons as for *Fmean*, a positive relationship between *Fprob* and *Fclear* was expected. In contrast to *Fmean*, the relationship between *Fclear* and *Fprob* showed an entirely opposite pattern. *Fprob* decreased with increasing *Fclear*, but also levelled out at higher numbers of *Fclear*. The reason for the negative correlation is that *Fprob* is a simple proportion between valid and clear pixels (*Fvalid* and *Fclear*). To recall, *Fprob* is simply the quotient of valid pixels divided by clear pixels. There was a strong positive correlation between *Fvalid* and *Fclear* (r=0.8) and a notable increase over time for both. Intuitively, one would expect a similar increase in *Fprob*, but that was not the case. In addition, years with notably low *Fclear,* and for that matter low *Fvalid* (e.g. 1990 and 1996), showed disproportionally high *Fprob* values. This contradictive pattern is due to a 'divisor' effect. Over the time frame of this research, the number of clear pixels has increased by much more than the number of valid pixels. For example, from the first five years of the time series (1990-1994) valid pixels have increased from 0.97±0.42 to 1.91 ±0.86 in the last five years (1996-2010) at the Celtic Sea Front (Ushant: from 0.88 ±0.45 to 1.56 ±09), whereas clear pixels have risen from 11.62 ±6.15 to 30.75 ±13.38 (Ushant: from 10.7 ±6.55 to

27.28 ±15.22). This means a 2.65-fold increase in clear pixels (Ushant: 2.55), but only a 1.97-fold increase in valid pixels (Ushant: 1.77). Therefore, the number of valid pixels is divided by an increasingly higher number of clear pixels over time, which results in a decrease of *Fprob*. The average *Fprob* between 1990-1994 was 0.08 compared to 0.06 between 2006 and 2010 at both fronts. According to this, frontal probability has decreased by 25% from the first to the last quarter of the time series, which is unlikely and not supported by any other studies concerning interannual variably of *Fprob* (e.g. Belkin et al., 2005; Kahru et al., 2012). The *Fclear* effect also adds to the high *Fprob* observed during winter. Due to more cloud cover, fewer clear pixels are available. Hence, *Fvalid* divided by a smaller number of *Fclear*, which results in a higher *Fprob*.

Generally, the relationship between *Fprob* and *Fclear* has been ignored in the majority of research that uses satellite imagery to investigate temporal variability of fronts (e.g. Belkin et al., 2005; Kahru et al., 2012) and only been mentioned in a couple of studies (Obenour, 2013; Ullman et al., 2007). Ullman et al. (2007) suggested that the non-linear relationship between clear and valid pixels is caused by the failure of the SIED-algorithm to identify all frontal pixels as such, particularly in partially cloud-covered scenes. The clouds block the contour-following part of the SIED algorithm, resulting in *Fprob* being underestimated. Obenour (2013) suggests the SIED-window to be at least 90% cloud free during image processing in order to avoid exactly this problem and subsequently, avoid temporal variability of *Fprob* caused by the fraction of clear pixels. The Obenour approach is slightly different to the one used in this study. Obenour (2013) addresses the *Fclear* effect by increasing data quality and only considers frontal composites with a high *Fclear* rate. This research on the other hand, accounts for the amount of clear pixels during the statistical analysis stage, regardless of the data quality of the composite. In the end, both approaches relate to the same problem: effect of the amount of clear pixels.

Most temporal variability studies focus on seasonal variability and did not report any discontinuities of *Fprob* caused by *Fclear* (e.g. Castelao et al., 2014; Hickox et al., 2000; Mavor et al., 2001; Rivas et al., 2010). However, the *Fclear* effect

appears to be less obvious when investigating intra-annual variability, as seen in this study. Less research focused on interannual pattern and mostly reported an increase in *Fprob* over time. For example, Belkin and Cornillon (2005) found a 50% rise in the annual mean of *Fprob* between 1985-96, averaged for the entire Bering Sea, which is an impressive increase in frontal segments. Similarly, Kahru et al. (2012) showed a significant increase in *Fprob* in the California Current System over 29 years (1981-2009). However, both studies did not consider the changes in available data. Ullman et al. (2007) used frontal maps from 1985 to 2001 to investigate temporal and spatial variability of *Fprob* in four regions of the North Atlantic. They mentioned the dependency between *Fclear* and *Fprob*, which could lead to an underestimation of *Fprob*. However, they concluded that it did not influence their results, because seasonal peaks of *Fclear* did not coincide with peaks in *Fprob*. In this research intra-annual pattern between *Fprob* and *Flcear* were not identical either, with different seasonal peaks and the relationship between the two entities became clear only during the modelling process. Therefore, Ullman might have underestimated the relationship between *Fclear* and *Fprob*. An unpublished research by Obenour (2013) is the only one to our knowledge that accounts for the clear pixel issue in their analyses, using the method described above (SIED-window >90% cloud free). Despite accounting for *Fprob*, Obenour (2013) still found an overall increase in global *Fprob* from 1981 to 2011, which varied between different regions of the world.

Although most studies did not account for *Fclear*, they generally report a rise in *Fprob* over time. According to this research, a decrease or no trend would have been expected. However, direct comparisons between this study and previous research are difficult, because of different study locations (e.g. California Current System, Bering Sea), study periods (length and years) and the fact that these studies combine distinct fronts by spatially averaging over large areas. Subsequently, winter and summer time fronts, which may have different long-term trend pattern, are merged. Belkin and Cornillon (2005) use frontal maps from pre-mid 90's and the increase in satellite imagery was not as profound during this period. It is possible that a 'divisor' effect in other parts of the world is not as significant because of different weather pattern and cloud cover

throughout the year. It is also possible that in this research the effect of *Fclear* has been overestimated by the model and subsequently, annulled genuine temporal variability. In short, this study cannot confirm an increase in *Fprob* as seen in most other studies investigating interannual variability of *Fprob*.

In summary, the effect of *Flcear* on both metrics is strong and the amount of available data should be considered in any analysis. It clearly requires more investigations on how to best account for an *Fclear* effect. In this research, *Fclear* was included as a factor in the statistical model to demonstrate its effect on variability of *Fmean* and *Fprob*. However, it is possible that the model overestimated the correlation between *Fclear* and the two frontal metrics and resulted in a reduction of genuine temporal variability. It is not advised to included *Fclear* as an offset to account for data availability. An offset term assumes a correlation coefficient of 1 and a linear relationship. However, the relationship between frontal metrics and *Fclear* levels out at high *Fclear* and an offset would cause an unrealistic reduction in *Fmean* or *Fprob* during high *Fclear* periods (e.g. the summer). A different approach is proposed by Obenour, who accounts for *Fclear* during the map processing stage. A combination of both approaches could be useful. However, how to best account for a *Fclear* effect requires more research.

2.4.3 Comparison between other commonly frontal metrics and their use in spatial analyses

Fcomp and *Fpers* were not analysed in detail due to nearly identical temporal pattern and high correlations with *Fprob* (Sup.Figure 2.1 and Sup.Figure 2.2). In addition, the use of *Fprob* is recommended for temporal analyses instead of the use of *Fcomp* and *Fpers*, mainly due to the simplicity of *Fprob* and its ease of interpretation. *Fdens* showed high correlations with *Fprob* and its derivatives as well as with *Fmean*. Although temporal variability pattern of *Fdens* were more similar to *Fmean* than to *Fprob*, *Fdens* still appears to be influenced strongly by both metrics. The combined effect of *Fmean* and *Fprob* on *Fdens* makes it difficult to explain what the temporal variations in *Fdens* relate to. At the same time, *Fdens* does not provide additional information to what has already been obtained by *Fprob* and *Fmean*. Again, it is advised to stick with the simpler

metrics (*Fmean* and *Fprob*) and avoid a complex one that does not provide further details, but is much more difficult to interpret.

It is important to note that the here-described differences between the fontal metrics only relate to their temporal variability. Spatially, the relationship between the metrics is different. Spatial correlations between the complex metrics (*Fcomp*, *Fdens*) are higher compared to correlations between complex and simple metrics (*Fmean*, *Fprob)* (Sup.Table 2.1). The complex metrics are cleared off temporally short-lived frontal segments as much as possible and focus on more persistent fronts. In contrast to temporal analyses, complex metrics are often preferred over the simple ones in spatial analyses, because there is a clearer distinction between low frontal frequency areas and high frontal frequency areas. Spatial similarities between the metrics can be seen in Figure 2.2. As mentioned earlier, the choice of metric needs to be well thought through and might be quite different depending on the type of analyses or on the research questions.

Frontal maps and metrics were initially developed to visualise fronts. Image processing focused on how to detect, identify and potentially enhance certain frontal features, such as persistent fronts. The use of frontal maps in quantitative analyses was not necessarily considered when frontal metrics were first developed. Still, frontal maps are clearly very useful for a variety of research interests, including oceanography and ecology. However, this study highlights some of the weaknesses of frontal maps in statistical analyses. There is a range of confounding factors that need to be considered when using frontal metrics quantitatively in order to produce meaningful results. Therefore, the choice and processing of frontal metrics need to be well thought through and ideally in collaboration with remote sensing scientists and statisticians to ensure potentially biases are accounted for as much as possible. It might also be useful to include multiple metrics in the analysis to cover different characteristics of the front.

2.4.4 Other notable points

2.4.4.1 Advantages of studying distinct types of fronts in isolation to avoid noise

The analysis of seasonal variability of *Fprob* showed the inclusion of noise, in this case, wintertime fronts at the Celtic Sea Front. Wintertime fronts display a different seasonal variability than tidal mixing fronts. Therefore, their inclusion can influence the outcomes of temporal analyses, because it adds variability not belonging to the front of interest. Different types of fronts respond to atmospheric and hydrodynamic forcing in specific ways and subsequently, display a distinct spatio-temporal variability (Hickox et al., 2000). When summarising frontal activity over large areas, e.g. ecosystem scale, fronts with different temporal variability pattern will be combined and their individual temporal signals blurred. Therefore, it is difficult to draw meaningful conclusions about frontal activity from a cumulative temporal signal obtained over large areas. Still, the majority of research concerning temporal variability of fronts merge all fronts over the sampling area.

The majority of fronts occur on the continental shelf, sometimes in close proximity to each other and with quite distinct underlying physical drivers (Acha et al., 2015)(**Table 1.1**). It would make sense for any type of temporal analyses, seasonal or trend, to separate distinct types of fronts in order to avoid individual temporal signals cancelling each other out. In addition, individual fronts or particular types often play a specific role in oceanographic or biological processes and their effect of the ecosystem can vary (Scales et al., 2014b). It is, therefore, of interest for ecologists and oceanographers alike to be able to distinguish between individual features and study them in isolation in certain cases rather than assuming all fronts are the same.

Isolating features of interest is difficult, particularly in areas with high frontal activity, such as continental shelves, where various fronts exist in close proximity and often merge. In this research, a coarse study area was defined by examining seasonal frontal maps and then refined by resampling different sized subsets. Although the process was parameterized as much as possible, there is some arbitrariness and the possibility of unwanted features entering the study region.

A newly developed frontal metric, called synoptic frontal maps (*Fsyn*) could prove to be useful in the future to isolate fronts of interest. It is based on a novel line-clustering algorithm, which first involves smoothing the *Fmean* map with a Gaussian filter of eight pixels width. Then the most prominent frontal observations and directions are identified and followed to generate contiguous contours. The fronts appear as lines of varying thickness, according to the strength of the front. In addition, the maps indicate the cold and warm water side of a front in red (warm) and blue (cold). The colour coding aids identification of the fronts of interest. For example, tidal mixing fronts will have the cold side facing mixed waters and the warm side facing the stratified waters. If knowledge on the core location of a front is available, frontal lines belonging to the front of interest can be isolated and used for research. The lines will have values according to their thickness or rather frontal strength. This front simplification algorithm is in preparation for publication (Miller, in preperation) and the details are proprietary to Plymouth Marine Laboratories.

2.4.4.2 Differences between the Celtic Sea Front and Ushant Front compared to previous research

The result of inter-and intraannual variability of the Celtic Sea and Ushant Front were remarkably similar. Only minor differences occurred, which can be attributed to location-specific parameters, such as the amount of riverine input or topographic influences, which will not be discussed in detail here. It highlights again the usefulness of studying fronts in isolation, because individual features are subject to location-specific forcing and can respond to meteorological and climatic changes in distinct ways. *Fprob* and *Fmean* displayed a sharp increase in April, had a peak in July and decrease in October. Seasonal pattern for both metrics at the Ushant Front are similar, but delayed by one month. The variability described by both metrics after adjustment of *Fclear* is in agreement with previous research of tidal mixing fronts in the Celtic Sea. Model simulations of stratification in the Celtic Sea predict the thermocline to establish around the Celtic Deep first (near the Celtic Sea Front) around April, advancing over the shelf and reaching the Western English Channel (location Ushant Front) within a month (Pingree, 1975; Young et al., 2004). Breakdown of stratification occurs

in autumn and can last as long as November (Horsburgh et al., 1998; Neil et al., 2012). Intraannual variability of the Celtic Sea and Ushant Front revealed by satellite-derived frontal maps are in good agreement with past research and are capable of picking up even small differences between individual features. Therefore, they are useful and fairly accurate tools to study temporal pattern of thermal surface fronts.

2.4.5 Limitations and recommendations

Satellite-derived frontal maps only consider the surface signal of thermal fronts. In the case of a fully three-dimensional structure like a tidal mixing front, this means a large part of the front is not accounted for. Considering a substantial amount of front-biota interactions and take place near the thermocline, an important component of the front is not covered by satellite data. In addition, the bottom part of tidal mixing fronts (bottom front) has been shown to display quite different behaviour to the surface component (Brown et al., 2003; Le Boyer et al., 2009). For example, the bottom fronts are less subject to atmospheric forcing and hence, much more stable in time and space. Because the bottom front is primarily driven by tides, bathymetry and the differences between winter and summer temperatures, its spatial and long-term variably could be very different to that of a surface front.

Due to the frequent cloud cover in the study region, the frontal maps used in this research were based on monthly composites. However, tidal mixing fronts are spatially and temporally dynamic features, which are influenced by processes working on timescales of a few days, such as the spring-neap adjustment (Sharples, 2008; Sharples et al., 2006; Simpson et al., 2012). Particularly during periods of high variations, such as frontogenesis and frontolysis, higher resolution maps would be more suitable to study frontal variability.

There are still a few points that require further investigation, such as the best method to deal with the *Flcear* effect. In order to be able to compare the outcomes with previous research, it would be useful to test the approach used in this study a) in other locations and b) on frontal variability spatially averaged

over large areas. Furthermore, different statistics were investigated during data exploration, such as the median and maxima instead of using the mean, but the mean provided the most meaningful results. However, it would be useful to test the most suitable statistic for each metric and how it affects the analytical outcome.

This study provides some information on the differences and limitations of commonly used frontal metrics and gives advice for their use in statistical analyses. However, it appears essential to produce a full and coherent guide on frontal metrics and the basics of frontal map processing, particularly addressed to scientist not working in remote sensing. The guide should include a complete list of frontal metrics, their underlying algorithms, advantages, limitations and potentially their suitability for a particular type of analysis, e.g. spatial versus temporal. Furthermore, a guide could include advice on how to prepare the data before analysis and the most suitable statistic for each metric.

2.4.6 Conclusions

There were significant differences in the temporal variability of *Fprob* and *Fmean*, due to the distinctiveness of the underlying algorithms and meaning of each metric. *Fmean* describes frontal gradient strength and displayed a natural oscillation over time with periods of stronger (decrease between 1990 to 2000) and weaker fronts (increase since 2001). *Fprob* on the other hand, represents frontal persistence and did not change significantly from 1990 to 2010. In addition, there were high correlations between *Fprob*, *Fpers*, *Fcomp* as well as *Fmean* and *Fdens*. It is recommended to use *Fmean* to study temporal variability of frontal strength and *Fprob* for frontal persistence. The more complex metrics are not recommended for temporal analyse, because they do not add information that is not already provided by the simpler metrics *Fmean* and *Fprob*, but are a lot more difficult to interpret. It is important to note that the demonstrated difference between the frontal metrics only relate to their temporal variability. Spatially, the relationship between the metrics is different. Generally, the complex metrics (*Fcomp*, *Fdens*, *Fpers*) are highly correlated, whereas the simple metrics (*Fmean*, *Fprob*) do not have a strong similarity with other metrics. The complex metrics are more suitable for spatial analyses in

certain cases, because their maps highlight persistent features that are cleared off noise. Therefore, the choice of metric should be carefully based on the research questions and type of the study. *Fprob* and *Fmean* were strongly affected by *Fclear* and temporal analyses of frontal metrics should always account for the changes in available data. How to best account for *Fclear* still requires further research. Intraannual variability of both fronts described in this research is in agreement with findings of previous studies. This consistency provides confidence that frontal maps are suitable and useful tools to study temporal pattern of dynamic fronts. However, frontal maps were initially created for visualisation purposes and have therefore, some limitations when used in statistical analyses. A guide on frontal map processing, available metrics and advice on their use in quantitative analyses would be useful, particularly for scientists not working in remote sensing.

2.5 Supplementary material

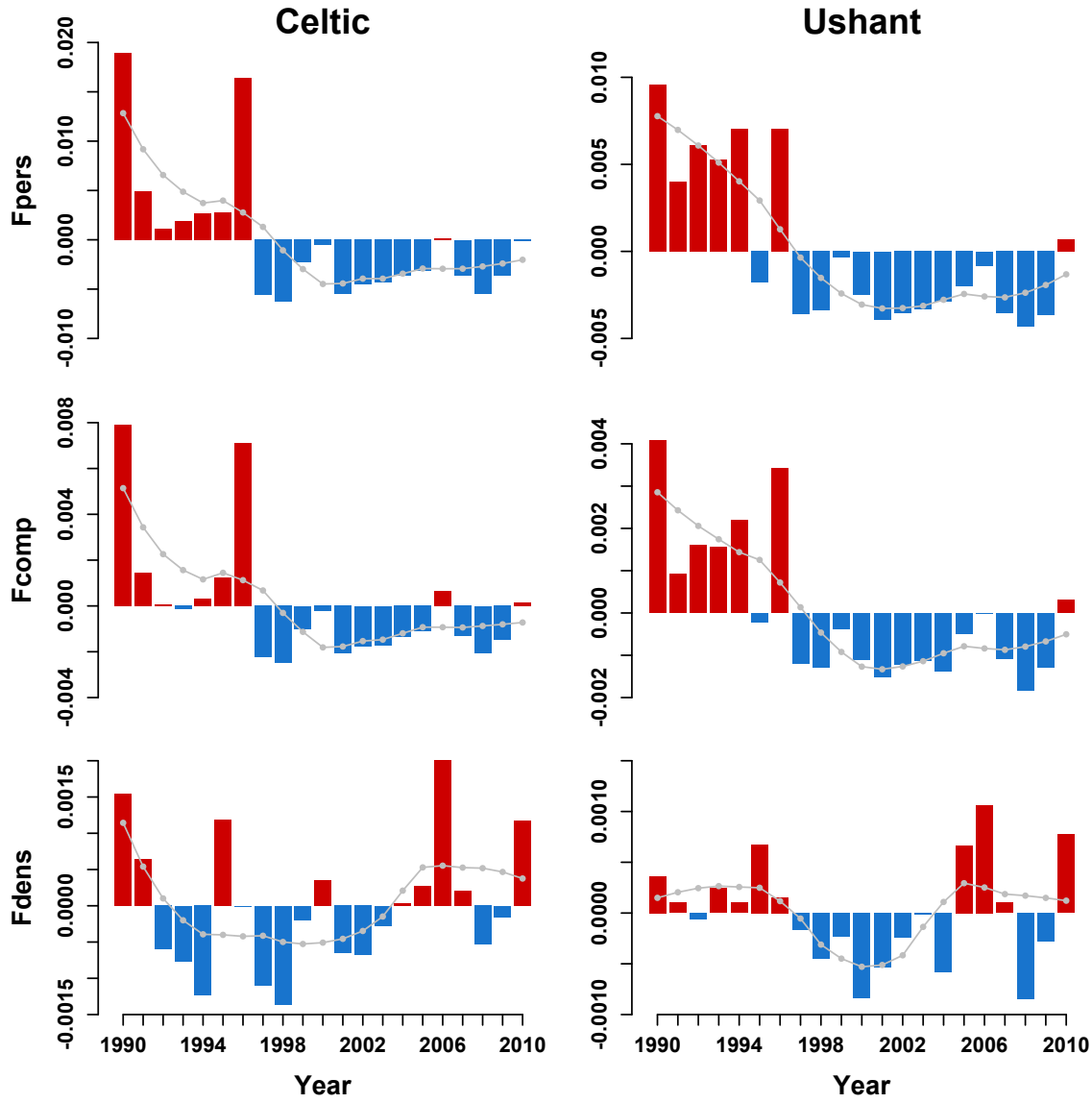

Sup.Figure 2.1: Yearly anomalies with loess smoother (α= 0.6, grey line) for metrics not included in the analysis: *Fpers*, *Fcomp* and *Fdens* at the Celtic Sea and Ushant Front from 1990 to 2010. Blue bars represent negative anomalies and red positive anomalies.

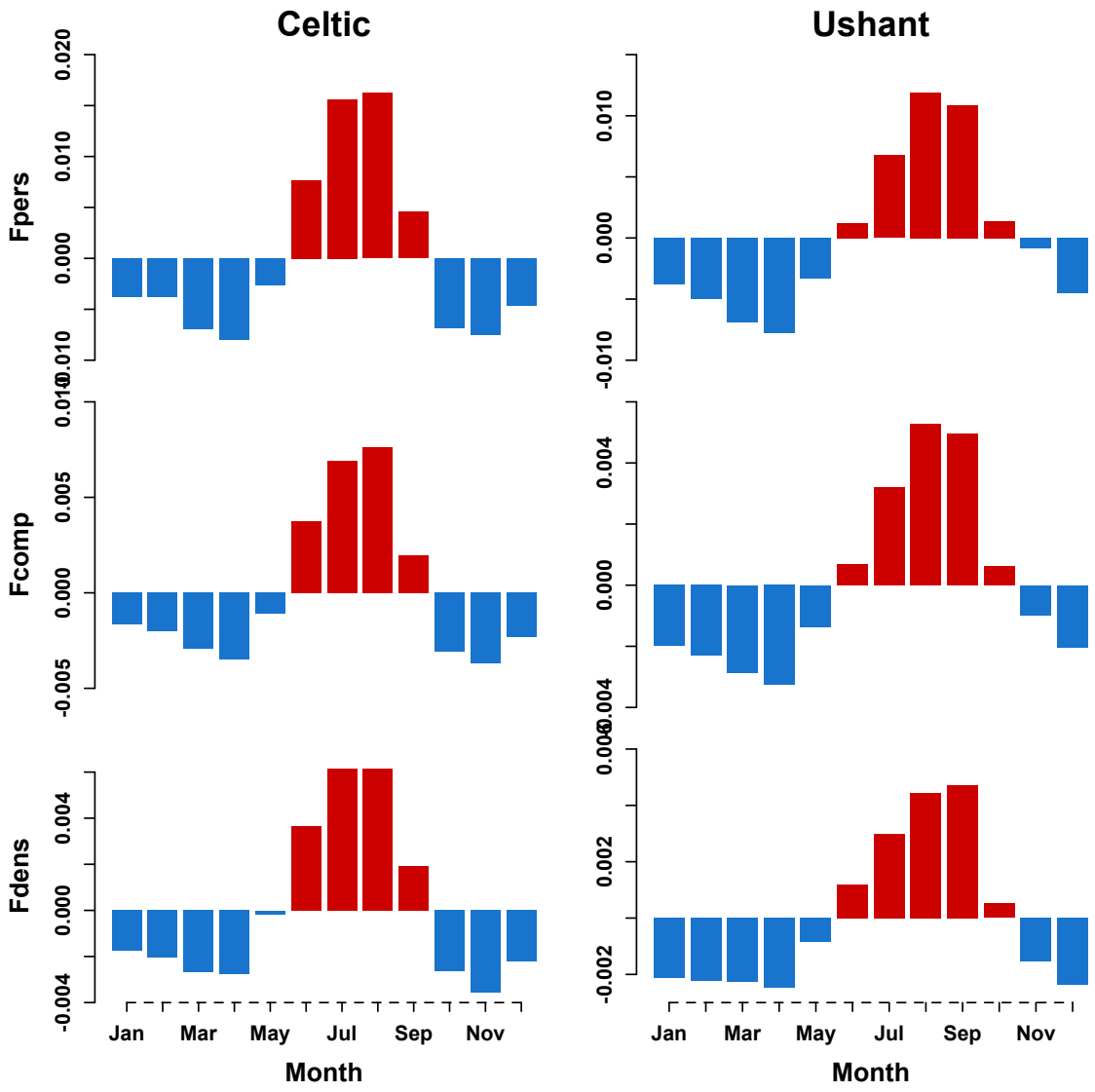

Sup.Figure 2.2: Seasonal anomalies for metrics not included in the analysis: *Fpers*, *Fcomp* and *Fdens* at the Celtic Sea and Ushant Front. Blue bars represent negative anomalies and red positive anomalies.

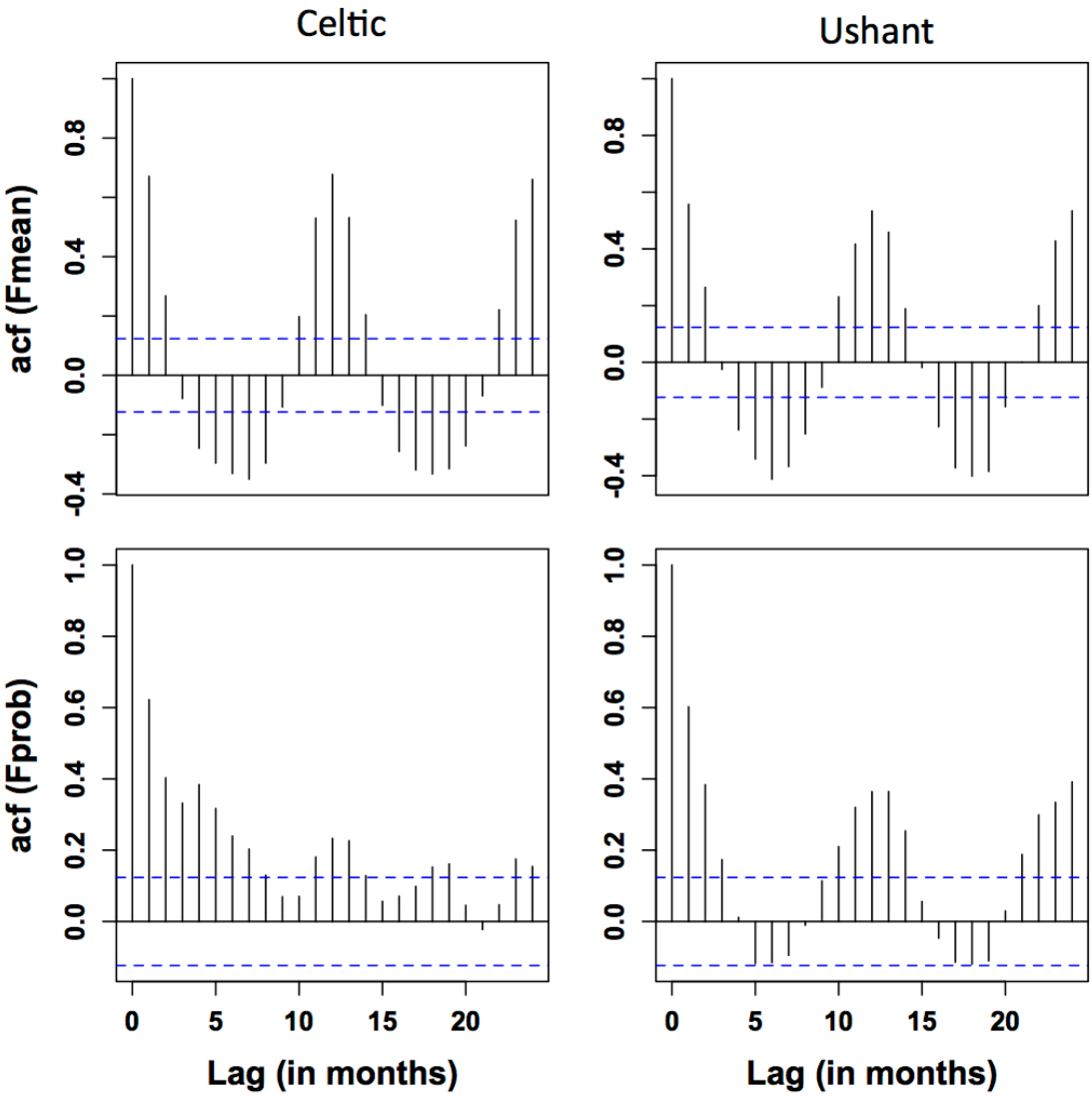

Sup.Figure 2.3: Autocorrelation functions (acf) for *Fmean* and *Fprob* at the Celtic Sea and Ushant Front.

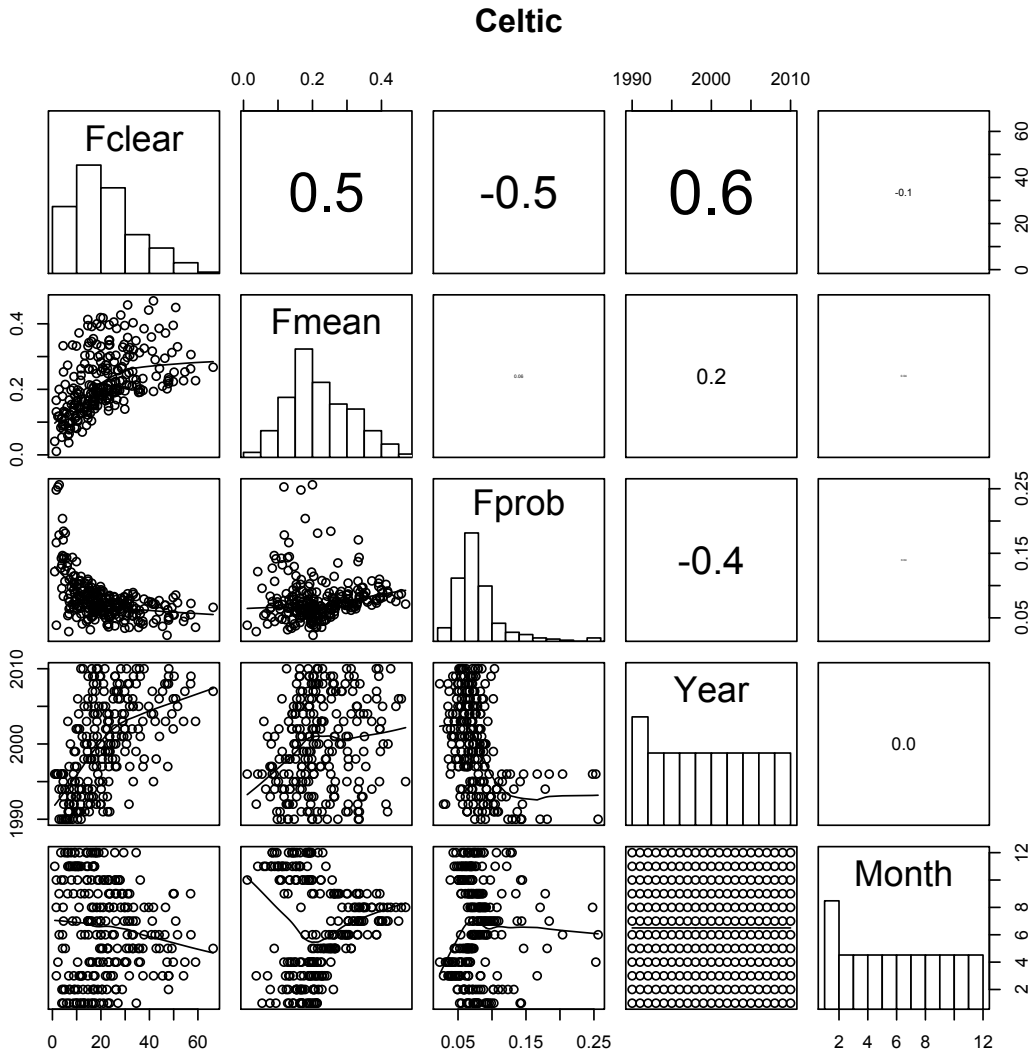

Sup.Figure 2.4: Histograms, Pearson correlation coefficients and scatter plots with loess smoother, showing the relationship between the frontal metrics *Fprob* and *Fmean* and explanatory variables *Fclear*, year and month at the Celtic Sea Front.

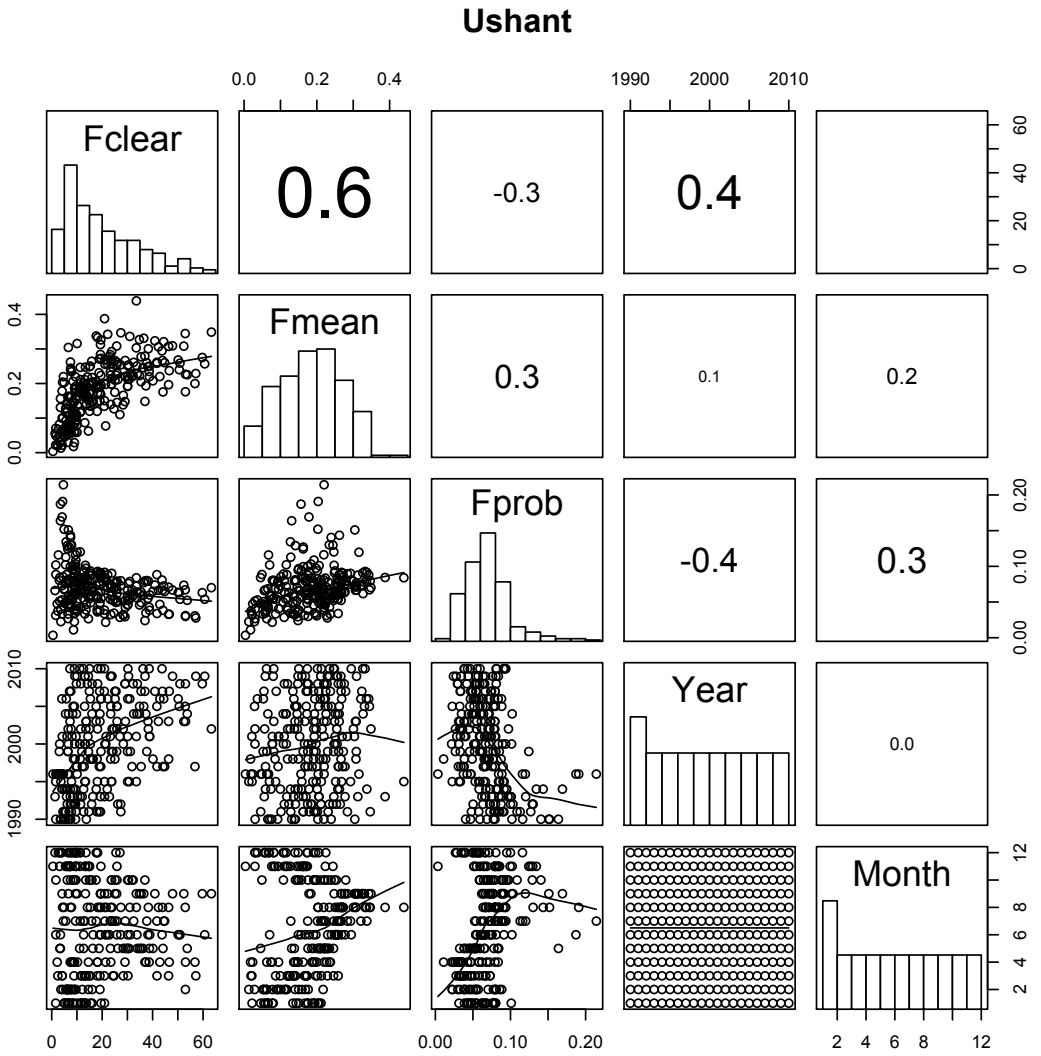

Sup.Figure 2.5: Histograms, Pearson correlation coefficients and scatter plots with loess smoother, showing the relationship between the frontal metrics *Fprob* and *Fmean* and explanatory variables *Fclear*, year and month at the Ushant Front.

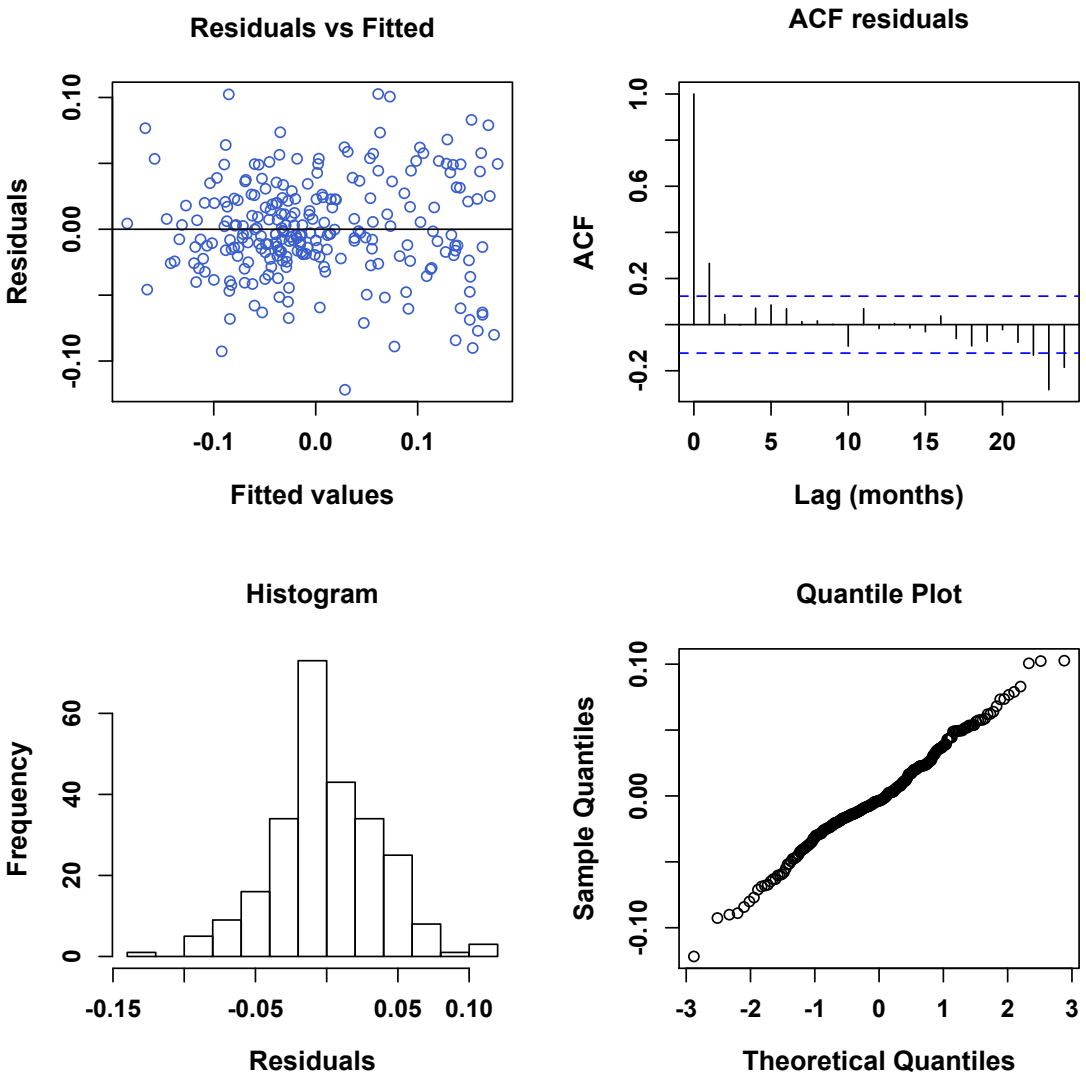

Sup.Figure 2.6: Model validation plots of residual analysis for *Fmean* at the Celtic Sea Front. Top left: fitted values against normalized residuals; top right: autocorrelation function of residuals with 95% confidence intervals as blue dashed line; bottom left: histogram of residuals and bottom right: Quantile plot.

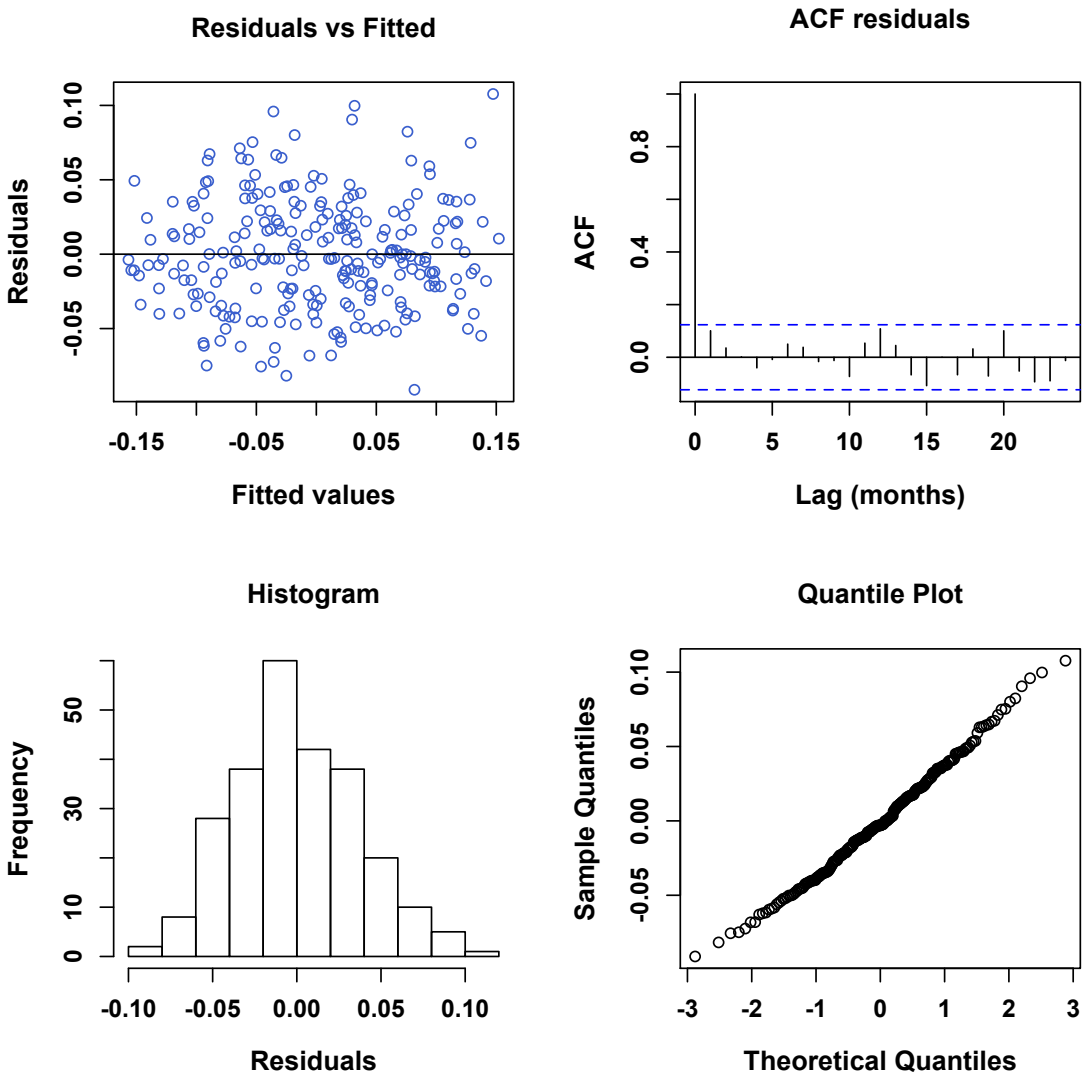

Sup.Figure 2.7: Model validation plots of residual analysis for *Fmean* at the Ushant Front. Top left: fitted values against normalized residuals; top right: autocorrelation function of residuals with 95% confidence intervals as blue dashed line; bottom left: histogram of residuals and bottom right: Quantile plot.

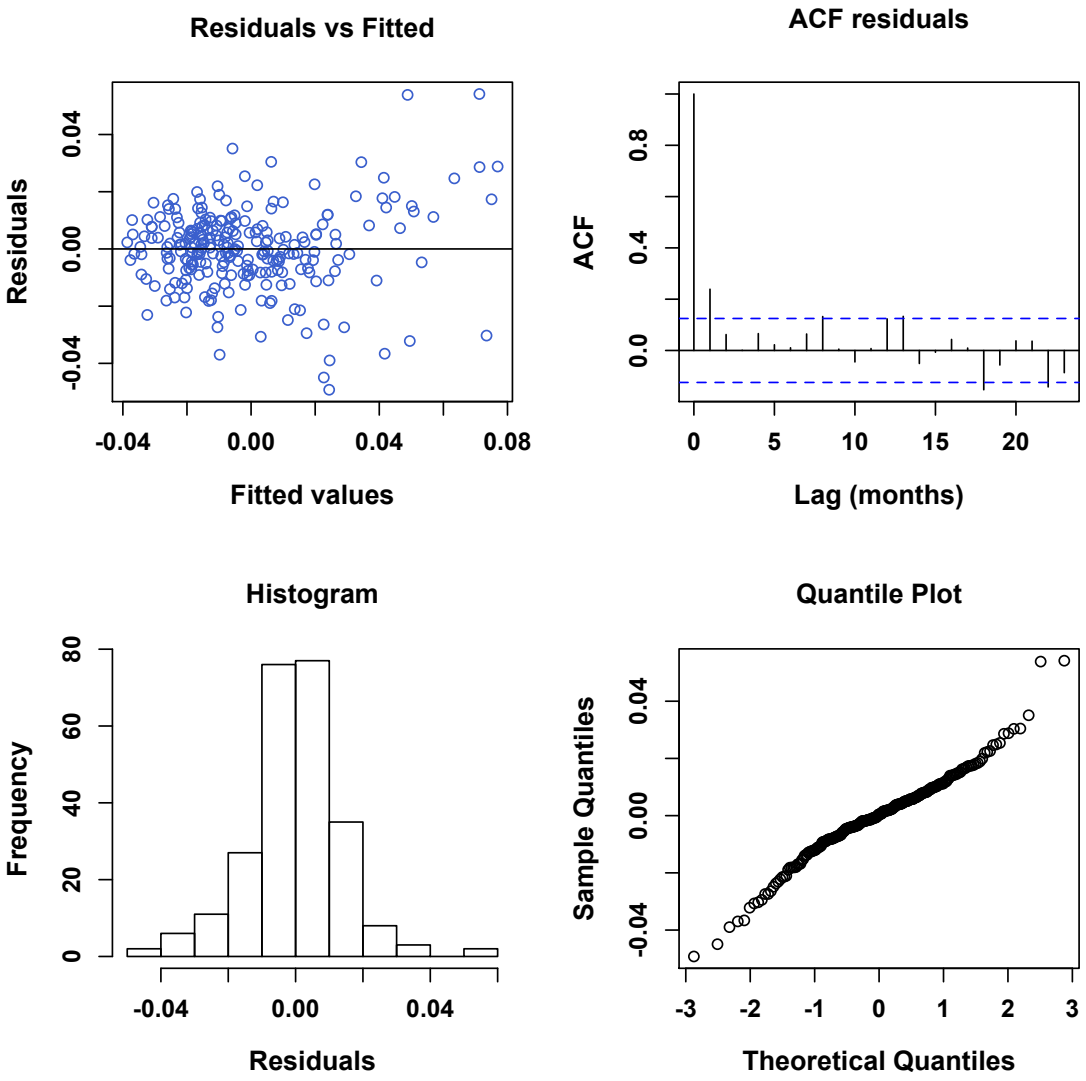

Sup.Figure 2.8: Model validation plots of residual analysis for *Fprob* at the Celtic Sea Front. Top left: fitted values against normalized residuals; top right: autocorrelation function of residuals with 95% confidence intervals as blue dashed line; bottom left: histogram of residuals and bottom right: Quantile plot.

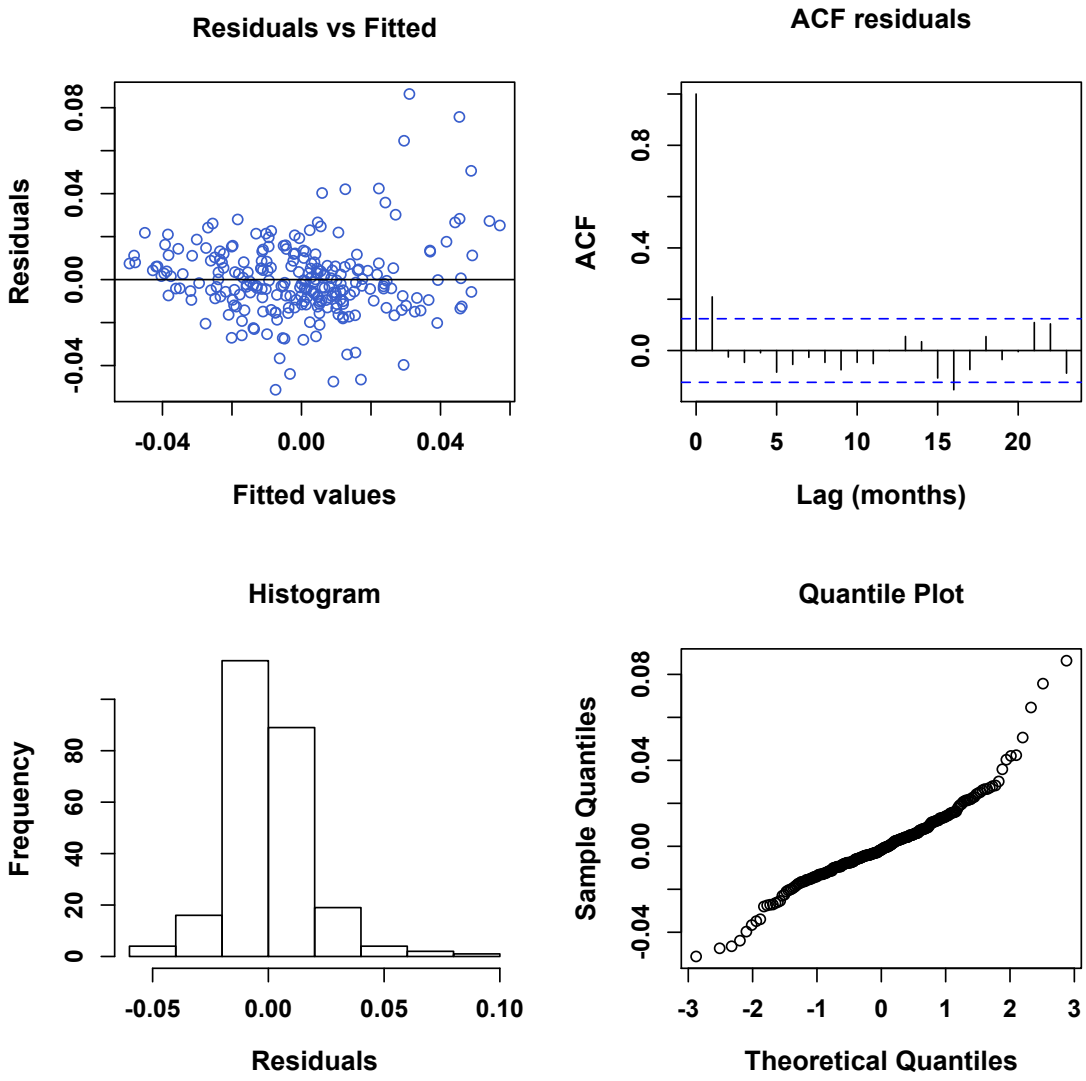

Sup.Figure 2.9: Model validation plots of residual analysis for *Fprob* at the Ushant Front. Top left: fitted values against normalized residuals; top right: autocorrelation function of residuals with 95% confidence intervals as blue dashed line; bottom left: histogram of residuals and bottom right: Quantile plot.

Sup.Table 2.1: Spatial similarities between all metrics based on all pixels within subset 1 for both fronts from March to November. Due to non-normality, Kendalls *tau* was computed. Green shading refers to Celtic Sea Front and blue shading to Ushant Front correlations. Coefficients ≥0.7 are highlighted in bold (all *p-values* were significant).

Metric/*r*	***Fprob***	***Fpers***	***Fcomp***	***Fmean***	***Fdens***
Fprob	1.0	**0.73**	**0.74**	0.36	0.57
Fpers	**0.7**	1.0	**0.93**	0.65	0.68
Fcomp	**0.72**	**0.92**	1.0	0.63	**0.75**
Fmean	0.32	0.64	0.62	1.0	0.54
Fdens	0.56	0.69	**0.76**	0.54	1.0

3 Physical drivers of inter-and intraannual variability of two tidal mixing fronts on the northwest European shelf

Tidal mixing fronts separate tidally-mixed from stratified shelf waters and play a vital role in oceanographic and biological shelf-sea processes during the summer. Despite the importance of tidal mixing fronts, not much is known about their long-term variability and the underlying environmental drivers. This information is needed to predict potential impacts of climate change on tidal mixing fronts and consequences for shelf-sea ecosystems in the future. This research uses meteorological time series from the NCEP/NCAR reanalysis and satellite-derived frontal maps from 1990 to 2010 at monthly resolution to investigate the key environmental drivers of interannual variability of two tidal mixing fronts (Celtic Sea and Ushant Front) in the Celtic Sea. Seasonal patterns of these fronts are well studied, but an analysis of drivers of intraanual variability is included for comparison purposes. Temporal variability of tidal mixing fronts was assessed using the frontal metrics *Fmean*, which represents the frontal gradient strength, and *Fprob*, which is a measure of frontal persistence. Generalized additive mixed models with temporal correlation structure AR1 revealed that net heat flux (at monthly lags of one or two, depending on front) to be the key driver of seasonal variability pattern for both metrics and fronts, which is in accordance with previous studies. Long-term variability on the other hand, was best explained by variations in sea surface temperature (SST), which indicates a potential sensitivity of tidal mixing fronts to climate change. The consequences of changing weather pattern on these fronts are not yet resolved, but could include an extension of the frontal season, strengthening of the frontal density gradient or spatial displacements of the fronts. Overall, the results were consistent between both metrics and both fronts. Only minor variations occurred, such as the importance of wind stress or precipitation, which can be attributed to location-specific differences at the two fronts (e.g. bathymetry and tidal regime).

3.1 INTRODUCTION

Tidal mixing fronts separate tidally-mixed, from seasonally stratified waters. They are a characteristic component of shelf-seas during the summer and play an important role in shaping oceanographic and biological processes (Holt et al., 2008b; Sharples et al., 2013). Density driven currents associated with these fronts make a significant contribution to the shelf-sea circulation, including the movement of large quantities of water over vast distances (several 100km) and with it the transport of organic and inorganic material, e.g. pollutants and plankton (Brown et al., 2003; Hill et al., 2008; Holt et al., 2008a). Tidal mixing fronts act as semi-permeable boundaries between different water masses and govern the exchange of nutrients from one side to the other (Holt et al., 2012). Front-specific hydrodynamics lead to elevated levels of primary productivity and passive and active accumulation of plankton, which is believed to have a cascading effect up the food chain (Bost et al., 2009; Weeks et al., 2015). Increasing research suggests that tidal mixing fronts are important foraging areas for organisms from a range of taxonomic groups, including various development stages of commercially important fish (Alemany et al., 2009; Munk et al., 2009), sharks (Miller et al., 2015; Priede et al., 2009; Queiroz et al., 2012), marine mammals (Goold, 1998) and seabirds (Begg et al., 1997; Durazo et al., 1998).

Despite the importance of tidal mixing fronts for shelf-sea biology and oceanography, comprehensive statistical analyses on their long-term variability and the influence of climate change on these fronts are limited. Understanding the predominant causes of interannual variability of tidal mixing fronts is important to predict potential impacts of changing weather patterns on these fronts and understand knock-on effects on marine organisms in the future.

Tidal mixing fronts have been intensively studied over the last five decades, particularly on the North Western European Shelf (e.g. Brown et al., 2003; Guillou et al., 2013; Holt et al., 2008b; Pingree et al., 1978; Simpson, 1977; 1981; Simpson et al., 1981; Young et al., 2004), Georges Bank (US East coast) (e.g. Drinkwater et al., 2001; Ji et al., 2008; Lough et al., 2001; Mavor et al., 2001; Ullman et al., 2003; Wishner et al., 2006) and Patagonian shelf

(Argentina) (e.g. Pisoni et al., 2015; Rivas et al., 2010). Tidal mixing fronts display a clear seasonal cycle, which is linked to the development of the shelf-sea stratification (Holt et al., 2008b; Pringree, 1980). During winter the shelf-seas are vertically homogenous due to the mixing effects of wind and tides. In early summer, the water column begins to stabilize, because of persistent solar heating and a reduction in wind forcing. The surface layer of the sea stores heat from solar radiation, whereas the bottom part remains cold and subject to mixing by tidal forcing. Between the warm top and cold bottom layers the summer thermocline develops. In shallower waters towards the coast, the heat from solar radiation is distributed throughout the entire water column by tidal mixing and the water body remains vertically homogenous.

During autumn, temperature and solar radiance decrease. Convection and turbulences caused by autumn storms cause a destabilization of the layering system of the shelf-seas (Horsburgh et al., 1998; Neil et al., 2012). Consequently, stratification and tidal mixing fronts retreat offshore and weaken until mixed scenarios are fully established in early winter (Hill et al., 2008; Schumacher et al., 1979). The exact timing of frontal breakup depends on meteorological, atmospheric and tidal forcing as well as location specific parameters, such as depth, riverine input and local hydrodynamics (Bowers et al., 1987; Dooley, 1981; Simpson et al., 2012).

In the Celtic Sea, which is the focus of this study, the two dominant tidal mixing fronts are the Celtic Sea and Ushant Front (Figure 1.1). In the Celtic Sea, the stratification season begins in early April south of Ireland, near the Celtic Sea Front and this front begins to establish (Elliott et al., 1991; Pingree et al., 1978). The thermocline advances over the shelf, but does not manifest around Western English Channel (location of the Ushant Front) until mid to late April due to stronger tidal currents in this area (Pringree, 1980). Celtic Sea and Ushant Front are well established by May and reach their peak around August. Frontolysis occurs in September, October and well-mixed conditions are fully restored by November, December at both frontal locations (Pringree, 1980; Pingree et al., 1976).

The establishment and breakup of tidal mixing fronts is large driven by meteorological and atmospheric factors. Hence, inter-annual variations in the onset and length of the frontal period have been observed in response to interannual variations in climatic forcing (Young et al., 2004). Consequently, long-term alterations in our climate are expected to affect frontal occurrence in the future, e.g. leading to an intensification of frontal gradients or an earlier frontal establishment (Holt et al., 2010). However, only limited research is available investigating long-term variability of thermal fronts and the underlying drivers. The lack of information is likely due to the difficulties of collecting data on fronts over long time scales and at adequate spatial extend. For example, tidal mixing fronts in the Celtic Sea are several hundred kilometres in length and spatially variable (Sharples, 2008; Sharples et al., 2006). Frontal characteristics (e.g. SST gradient) can be vary along a single front due to location specific factors, such as variations in local bathymetry or tidal forcing.

In order to account for the size and high spatio-temporal variability of certain types of fronts, studies investigating drivers of interannual frontal variability are generally based on model simulations or satellite-derived data (e.g. Kahru et al., 2012; Marsh et al., 2015; Tomita et al., 2010). For example, an increase in frontal frequency has been found in the California Current System based on satellite-derived frontal maps from 1997 to 2010 (Kahru et al., 2012). Interannual variations in frontal frequency were attributed to variability in large scale SST, upwelling favourable winds and the ENSO index. On the northwest European, Holt et al. (2010) predict in a model simulation that a) stratification will strengthen by up to 20% and b) and the stratification period will be extended by ten to 15 days by the end of the century compared to the recent past. Both phenomena are mainly attributed to an increase in water temperature. Due to the direct link between stratification and tidal mixing fronts, similar scenarios can be expected for the fronts, e.g. an extension of the frontal season. How these changes in frontal occurrence will impact upon density currents on the shelf, primary productivity and the food chain, still remains largely unknown.

This research uses satellite-derived frontal metrics from 1990 to 2010 (21 years) to identify the predominant physical drivers of inter-and intraanual

variability of two tidal mixing fronts (Celtic Sea and Ushant Front) on the northwest European shelf. Frontal metrics employed are *Fmean*, which provides information on the strength of the frontal gradient; and *Fprob*, which is a measure of frontal persistence (for details see section 2.2.2). Using two metrics allows a comparison between the impacts of meteorological forcing on different characteristics of tidal mixing fronts. The Celtic Sea and Ushant Front are about about 300km apart from one another. Comparison between the two fronts will demonstrate differences between individual fronts caused by location-specific interactions, such as riverine input or bathymetry. Intraanual variability and its underlying drivers of both fronts are already well established. This knowledge provides a good background to verify the results of the interannual analysis of meteorological forcing on temporal variability of *Fmean* and *Fprob*.

3.2 METHODS

The processing of frontal maps, calculation of the frontal metrics *Fmean* and *Fprob* and the calculation of monthly time series for each of the two metrics at the Celtic Sea and Ushant Front respectively is described in section 2.2.5. This section lists the environmental variables used in the analysis and describes their origin and processing. This is followed by a description of the statistical analysis to test for the main meteorological drivers that best explain the inter- and intraannual variation of *Fmean* and *Fprob*. All statistical analysis was performed in 'R' (R Core Team, 2013), figures and geographic maps were created in either 'R', Matlab or ArcMap10.1 (ArcMap, 2012).

3.2.1 Explanatory variables used in the analyses

This analysis investigates the main meteorological drivers that best explain inter-and intraannual variability of frontal strength (*Fmean*) and frontal persistence (*Fprob*). The variables and the reasoning for their inclusion in the analysis, e.g. their effect on tidal mixing fronts, are described below.

3.2.1.1 Meteorological variables

Meteorological variables were obtained from the NCEP/NCAR reanalysis model (National Centre for Environmental Predictions/ National Centre for Atmospheric

Research (Kalnay et al., 1996): http://www.iridl.ldeo.columbia.edu/SOURCES/.NOAA/.NCEP-NCAR/.CDAS-1/.MONTHLY/.Diagnostic. The NCEP/NCAR Reanalysis Project provides atmospheric data gridded at 2.5°x2.5° spatial resolution. The data is available at different temporal resolutions, from four times daily to monthly means. Because monthly frontal composites were used, the NCAR monthly means time series was downloaded. The monthly averages represent the arithmetic mean of all values available for a given month, usually four data points per day. Table 3.1 provides a summary of variables included in the analyses and information on their spatio-temporal resolution.

Net heat flux: The net heat flux is the amount of energy, which is absorbed or released by the oceans. During the summer months, the oceans take up heat and sea temperatures increase, while in the winter, heat is lost to the atmosphere and sea temperatures decrease. Negative net heat flux values imply ocean heat loss and positive values heat gain. When net heat flux values are positive, the sea is taking up heat, the surface layer is warming and the sea progressing towards stratification, which is directly linked to the establishment of tidal mixing fronts (Holt et al., 2010; Pingree et al., 1978). Mean monthly net heat flux is expressed in W/m² and was calculated by adding mean monthly downward solar flux, upward longwave radiation, sensible heat flux and latent heat flux.

Wind stress: Wind causes disturbance in the ocean-atmosphere boundary layer by creating waves, increasing stirring and mixing processes (Raitsos et al., 2006), which weakens stratification. Wind stress affects tidal mixing fronts in particular when they are weak during periods of frontolysis- and genesis (Pringree, 1980). A strong storm can cause the destabilisation of stratification during its establishment in spring as well as cause its break up in late autumn. Wind stress is expressed as Pascal (Pa) and was calculated by: wind stress= $\sqrt{v^2 + u^2}$; where $'v'$ represents the zonal momentum flux and $'u'$ the meridional component. The *v*- and *u*-components were downloaded as monthly means from the NCEP/NCAR Reanalysis Project and used to calculate the monthly wind stress mean.

Wind direction: Not just the wind speed, but also the wind direction can affect tidal mixing fronts. Wind directions that promote Ekman transport can result in denser mixed water being pushed over lighter stratified water and subsequently, lead to an offshore retreat of the front (Wang et al., 1990). Mean monthly wind direction was calculated form the monthly mean *v*- and *u*- components by first converting radians to degrees and then computing the arctangents from the two wind components:

Wind direction = $\frac{180}{\pi}\ x\ atan2\ (-u, -v)$. This is the direction the wind is blowing form. The wind direction was converted to **wind blowing to** by adding 180 degrees.

SST: Studies suggest that an increase in SST due to climate change could lead to an intensification of stratification and affect the strength of tidal mixing fronts (Holt et al., 2010). The monthly mean SST was included as a variable to examine if the increase in SST in the last decade has caused an increase in *Fmean* and *Fprob*.

Precipitation: Precipitation was included in the analysis as it might affect the surface signal of a front by causing disturbance at the water surface and influencing surface temperatures (short term) and by directly affecting the available satellite data due to correlation with cloud cover. Mean monthly precipitation data are presented in kg/m^2/day.

North Atlantic Oscillation (NAO): The NAO is a major teleconnection and influences weather patterns worldwide over large time scales (Hurrell, 1995). Negative NAO-years are associated with strong westerly winds, whereas positive NAO-anomalies are correlated with warmer temperatures, but more rainfall. Large teleconnections have been found to affect spatial and temporal variability of fronts in other regions of the world (Hopkins et al., 2010; Kahru et al., 2012; Tomita et al., 2010). Normalized monthly mean NAO-anomalies were data obtained from NCEP: http://www.cpc.ncep.noaa.gov/products/precip/CWlink/pna/nao.shtml. To test whether there is a response in frontal variability in accordance with the

variations in the NAO, the summertime NAO-trend (obtained by *loess* smoothing, window size= 6) was used for the analysis instead of the raw monthly anomalies (mean of all daily values available for a given month), because the NAO is not expected to affect weather instantly, but over monthly scales (Hurrell, 1995).

3.2.1.2 Other variables

Fclear was included as a covariate in the models, because an increase in satellites and subsequently, satellite passes, resulted in an increase of available data over time, which strongly affects temporal variability of *Fmean* and *Fprob* (for details see section 2.4.2). Hence, temporal variability is not only caused by environmental variables, but also by the changes in data availability over time, which needs to be accounted for.

Table 3.1: Summary of explanatory variables used in the analysis and their spatio-temporal resolution.

Variable	Spatial resolution	Temporal scales
Net heat flux (W/m²)	2.5°x2.5°	Monthly mean (1990-2010)
Precipitation (kg/m^2/day)	2.5°x2.5°	Monthly mean (1990-2010)
Wind stress (Pa)	2.5°x2.5°	Monthly mean (1990-2010)
Wind direction (blowing to)	2.5°x2.5°	Monthly mean (1990-2010)
SST (°C)	2.5°x2.5°	Monthly mean (1990-2010)
NAO	-	Monthly, weighted 6 months average (1990-2010),
Fclear	See subsets Figure 2.3	Total number per month (1990-2010)

3.2.2 Creation of time series of meteorological variables

The NCAR data set is based on 2.5°x2.5° grid cells. The NCAR grid cell with the centre coordinates 52.37N; 5.625W covered the spatial extend of the Celtic Sea Front subset 1 (see Figure 2.3). Therefore, only data of meteorological variables from this particular grid cell were used for the statistical analysis of drivers of temporal variability at the Celtic Sea Front. Because the NCAR data was already provided as monthly averages, each monthly data point of the

meteorological variables was assigned to the corresponding *Fmean* and *Fprob* time series points (for details of creation of time series of *Fmean* and *Fprob* see section 2.2.5). The Ushant Front is spatially more variable than the Celtic Sea Front and its sampling area much larger. Data from four different NCAR grid cells had to be averaged to cover the spatial extend of the sampling area of the Ushant Front and to create a monthly time series of meteorological variables. The Ushant Front was not present in equal parts in each of the four grid cell (centre coordinates: a) 48.57N, 5.625W, b) 48.57N, 3.75W, c) 50.475N, 5.625W and d) 50.475N, 3.75W). For example, the northern part of the Ushant Front is spatially more variable than the southern part and therefore, less frequently present in the northern grid cells than in the southern ones. In order to account for the different frequencies per grid cell, a weighted average was applied to create time series of the meteorological variables at the Ushant Front. The weights were based on the total number of frontal observations in each of the NCAR grid cells. Only data March to November (1990 – 2010) was considered, which covers the frontal season, in order to avoid noise from wintertime fronts. For example, only 3% of the total frontal observations were located in the upper left grid cell. Therefore, the contribution of meteorological data form this grid cell in the monthly averages was only 3%.

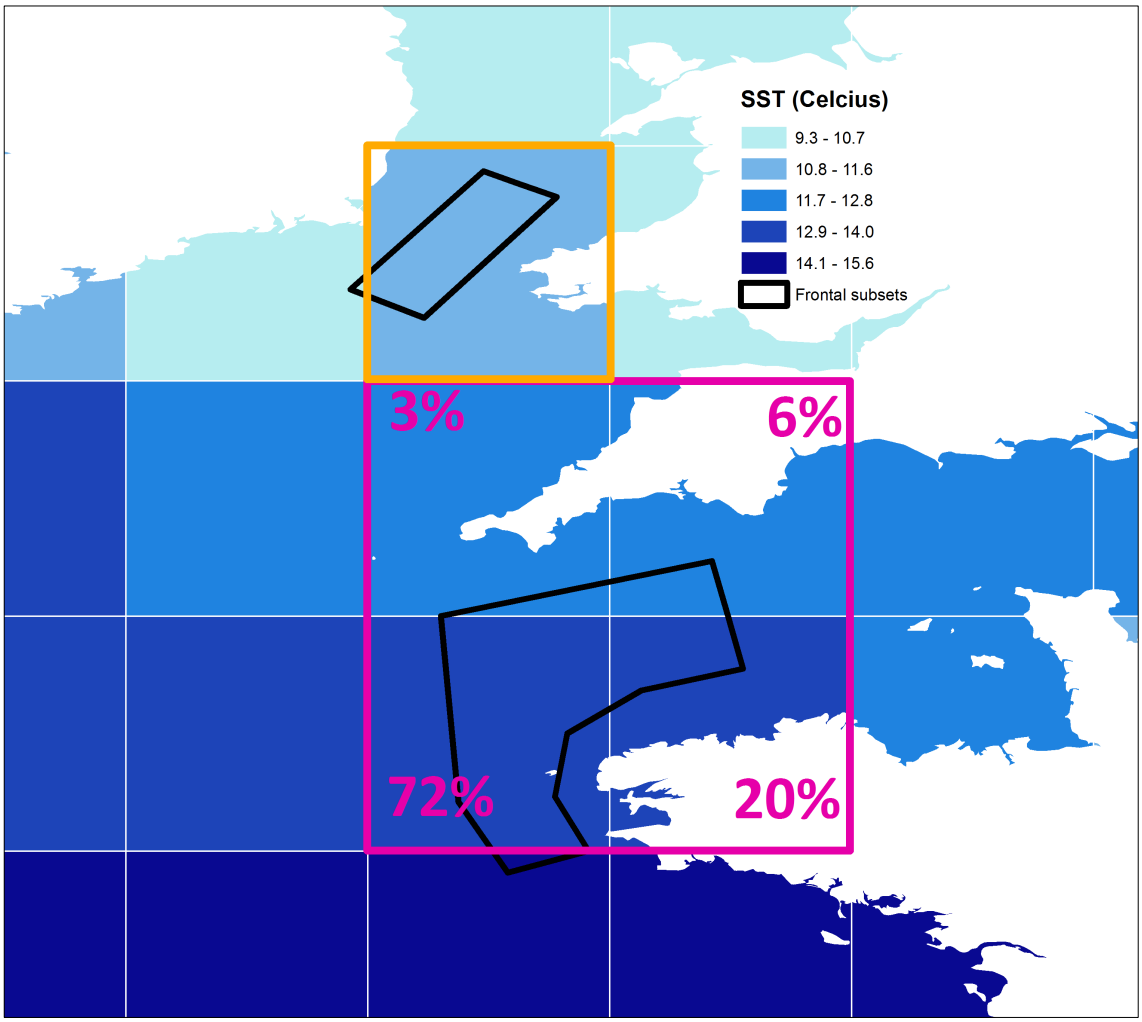

Figure 3.1: Map of NCAR grid cells showing SST (°C) for each grid averaged from March to November 1990 – 2010. NCAR grid cells used in the statistical analysis for the Celtic Sea Front are framed in orange and pink for the grid cells used for the Ushant Front. Meteorological data from only one grid cell was considered for the Celtic Sea Front meteorological time series (centre coordinate: 52.37N, 5.625W). Data points of the Ushant Front meteorological time series comprise of a weighted average of four NCAR grid cells. The weights are based on the total number of frontal observations (from March to November 1990 – 2010) in each of the NCAR grid cells. Influence of each grid cell in the average is given in percentage. Centre coordinates of the Ushant Front grid cells are: a) 48.57N, 5.625W, b) 48.57N, 3.75W, c) 50.475N, 5.625W and d) 50.475N, 3.75W.

3.2.3 Statistical modelling of meteorological drivers of frontal variability

Tidal mixing fronts only occur during the stratification period. The previous chapter revealed that the frontal season runs from March to October and April to November at the Ushant Front. In addition, *Fprob* showed some noise (increased *Fprob* values, although these should be near zero) during the winter months. Therefore, only data from March to November was considered for the analysis of both fronts and metrics. Anomalies were created for all response and explanatory variables, as described in section 2.2.6. Statistical analyses were based on anomalies of *Fmean* and *Fprob*, but the original values were used for the explanatory meteorological variables. However, some figures that show inter-and intrannual variability of meteorological variables were produced using yearly and monthly anomalies (Figure 3.2 and Figure 3.8). Figure captions state if anomalies or original values were used.

3.2.3.1 Analysis of meteorological drivers of intraannual variability of *Fmean* and *Fprob*

In climate related processes, explanatory variables often lead the response variable, e.g. it can take time until an effect of the explanatory variable is actually expressed by a change in the response variable. In order to test for leading variables and the need to include temporal lags, cross-correlograms of explanatory variables and *Fmean* and *Fprob* were consulted. In addition, scatter plots and Pearson correlation coefficients of *Fmean* and *Fprob* with the meteorological variables heat flux, precipitation, wind stress, SST and *Fclear* were created on the original data set (no lag) and at monthly lags of one, two and three to test for the need of including lags. The final dataset for the Celtic Sea Front included lags for *Fmean* and heat flux (one month) as well as *Fprob* and heat flux (two months), precipitation (two months) and wind stress (one month) (**Table 3.2**). Final datasets at the Ushant included lags for *Fmean* and heat flux (two months) as well as *Fprob* and heat flux (two months), precipitation (two months) and wind stress (two months).

Table 3.2: Summary of lagged dataset that were created for each metric and meteorological variable at the Celtic Sea and Ushant Front. Lags are in months and are highlighted in blue.

	Celtic Sea Front		Ushant Front	
Variable/Metric	***Fmean***	***Fprob***	***Fmean***	***Fprob***
Heat flux	Lag1	Lag 2	Lag 2	Lag 2
SST	No lag	No lag	No lag	No lag
Wind stress	No lag	Lag 1	No lag	Lag 2
Precipitation	No lag	Lag 2	No lag	Lag 2

Before the modelling process, all covariates were examined for collinearity using Pearson-correlation and Variance Inflation Factors (VIF) (*corvif* function in 'HighstadLibV4' by Zuur et al. ((2009)). A Pearson-correlation coefficient ≥0.7 and/or VIF-values ≥3.0 indicate collinearity (Zuur et al. 2009). Tests for collinearity were performed on the final datasets (e.g. lagged as summarized in **Table 3.2**).

Preliminary analysis indicated a non-linear relationship between the response and some of the explanatory variables as well as temporal autocorrelation. Therefore, Generalized Additive Mixed Models (GAMMs) with an AR(1) correlation structure were used to investigate which meteorological variables best explain the intra-annual variability of *Fmean* and *Fprob* at both fronts. GAMMS were fitted as described in section 2.2.6.2. In order to model the relationship between environmental variables and the seasonal variability of *Fmean* and *Fprob* only, the interannual component needed to be accounted for. Interannual variability was resolved by simply including the temporal variable 'year' in the model and checking for pattern in the relationship between the final model residuals and fitted values with the factor 'year'.

Model selection was conducted using manual stepwise-forward selection. In this approach, one starts with a series of models, each containing only one of the explanatory variables. The explanatory variable resulting in the lowest AIC is added to each of the remaining models. This procedure is repeated until no decrease in AIC of at least 2.0 per added term is achieved or the R^2 does not improve by at least 0.01 or an added covariate is not significant (*p-value* >

0.05). Preliminary analysis indicated collinearity between some explanatory variables. Therefore, only the variable resulting in the lower AIC during stepwise forward modelling, was retained and the collinear variable not further consider for analysis. Model fit was examined by means of residual analysis (Sup.Figure 3.1 to Sup.Figure 3.8). In the case of *Fprob* a couple of outliers were removed to improve model fit at both fronts.

3.2.3.2 Analysis of meteorological drivers of interannual variability of *Fmean* and *Fprob*

The analysis of the main meteorological drivers of interannual variability was conducted as described in section 3.2.3.1. However, no lagged datasets were considered. In order to account for the strong seasonal component of the dataset, the factor 'month' was included in the models and checking for pattern in the relationship between the final model residuals and fitted values with the factor 'month'.

3.3 RESULTS

3.3.1 Meteorological drivers of intraannual variability of *Fmean* and *Fprob*

3.3.1.1 Description of intraannual variability pattern of frontal metrics *Fmean, Fprob* and *Fclear* and the meteorological variables

A detailed description of intraannual variability of *Fmean* and *Fprob* can be found in the previous chapter (chapter 2) and therefore, the description of seasonal pattern of both metrics is reduced to the main points. In chapter 2, intraannual variability pattern of *Fmean* and *Fprob* were investigated under consideration of the effect of *Fclear.* Accounting for an *Fclear* effect, the seasonal cycle of *Fmean* and *Fprob* was predicted to run between April and October at the Celtic Sea Front and May to November at the Ushant Front (Figure 2.7 and Figure 2.8). Peaks in frontal strength occurred in July and August at the Celtic Sea Front and between August and September at the Ushant Front. A notable increase in *Fprob* already occurred in June and lasts until August (Celtic) or September (Ushant).

Based on monthly anomalies, intraannual variability of meteorological variables was almost identical at both fronts (Figure 3.2) and only small differences in minima and maxima for some variables were evident. Net heat flux displayed a defined seasonal cycle. The sea takes up heat from March to September, with peak values in May to July. In real values, the net heat gain and loss was greater at the Celtic Sea Front compared to the Ushant Front. The overall range between minimum and maximum net heat flux was 451.3 compared to 414.5 at the Ushant Front.

SST displayed almost identical seasonal pattern to heat flux, but lagged behind by about two months (Figure 3.2). SST anomalies were positive form June to November and reached maxima during August to September. SST at the Ushant Front was about two degrees higher (14.71 ± 2.4) than at the Celtic Sea Front (12.91 ± 2.69).

Wind stress at both fronts increased notably form October onwards, reaching its peak in January and decreasing thereafter (Figure 3.2). At the Ushant Front, wind stress anomalies were negative form March onwards and April at the Celtic Sea Front. Throughout the stratification period, wind stress did not show any major fluctuations. The predominant winds at the Celtic Sea Front were southwesterlies. In the Ushant Front region westerlies and southwesterlies dominated (Figure 3.3).

Precipitation displayed similar intraannual pattern to wind stress (Figure 3.2). Precipitation increased notably from October onwards and lowest rates occurred in May and June at both fronts. Precipitation was higher in the Celtic Sea Front region (1.8 ± 1.1) than at the Ushant Front (1.35 ± 1.12).

The seasonal cycle of *Flcear* is similar to net heat flux (Figure 3.2). Anomalies are positive between March and approximately October. However *Fclear* maxima occur in May and June at both fronts. In addition, the seasonal curve is not as clearly defined as in net heat flux and displays some up and downs over the summer months.

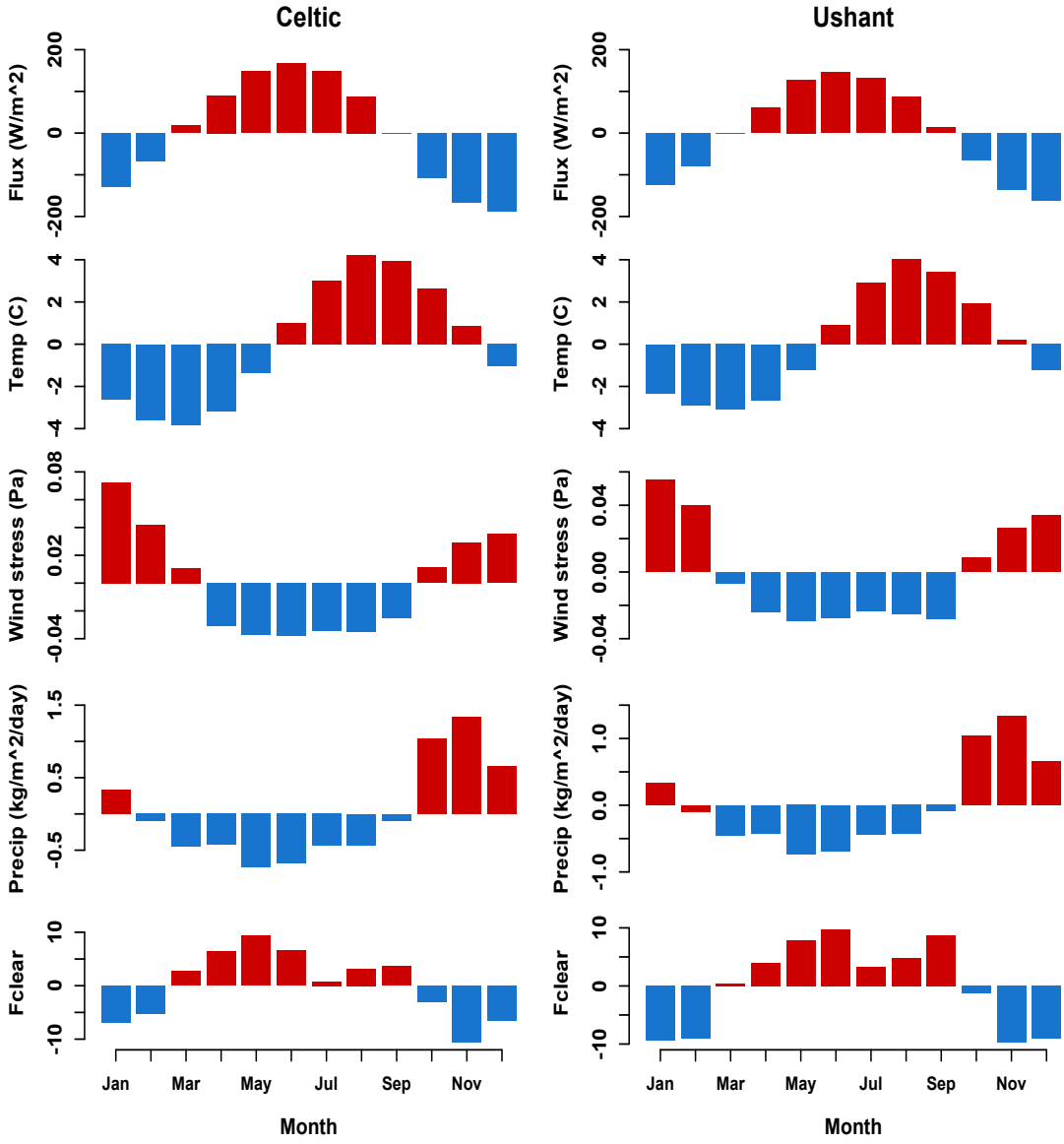

Figure 3.2: Monthly anomalies of net heat flux (Flux), SST (Temp), wind stress, precipitation (Precip) and *Fclear* at the Celtic Sea (left panel) and Ushant Front (right panel). Blue bars represent negative anomalies and red anomalies.

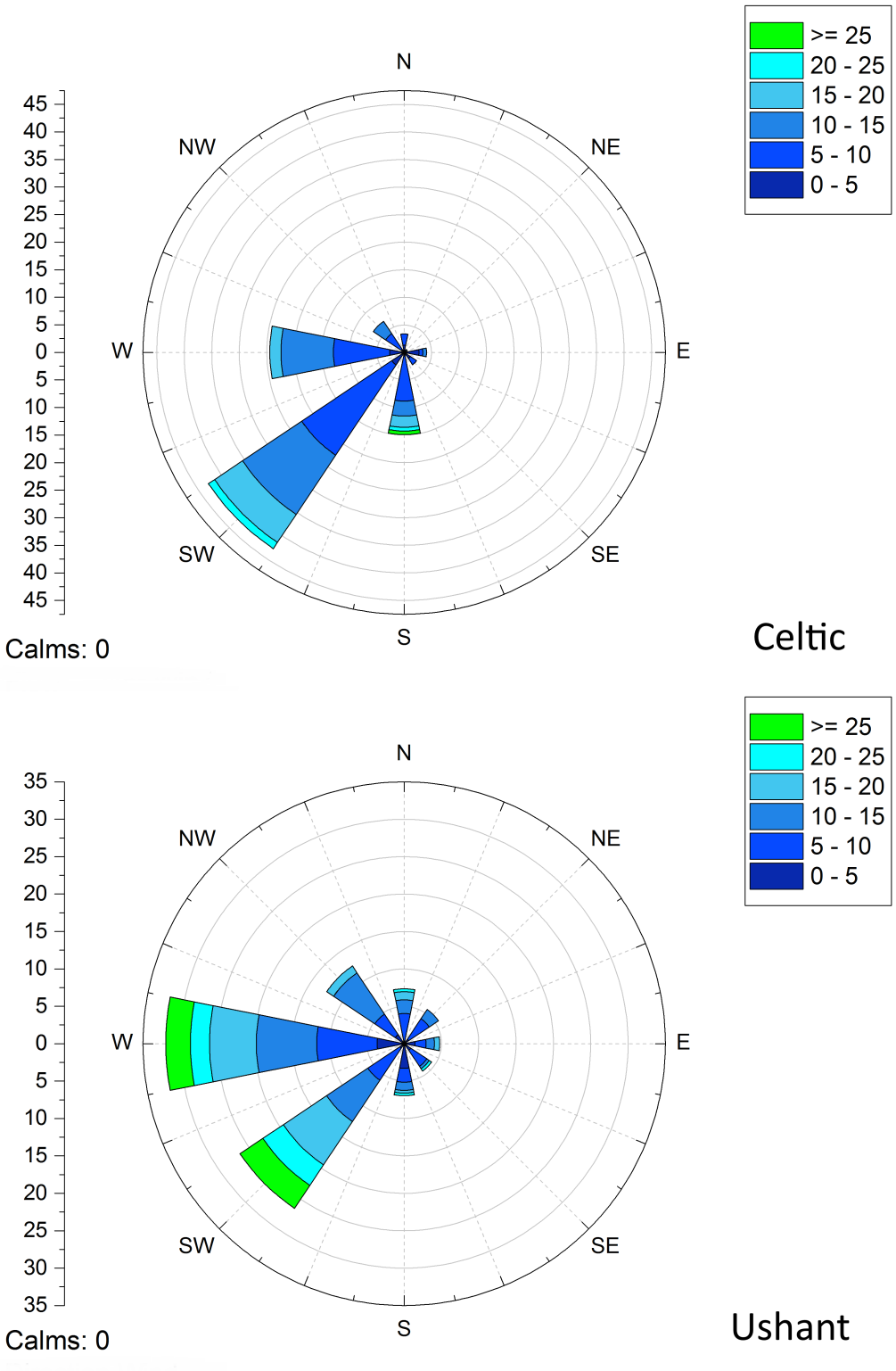

Figure 3.3: Wind roses for Celtic Sea Front (top panel) and Ushant Front (bottom panel), showing the wind speeds and direction the wind is blowing from for the months March-November over the entire time series (1990-2010). Scale bar on left shows percentage frequency.

3.3.1.2 Meteorological drivers of interannual variability of *Fmean* and *Fprob*

The majority of the seasonal variation of *Fmean* and *Fprob* at both fronts was explained by *Fclear* and meteorological variables related to the heating budged: heat flux and SST (**Table 3.3**). The effect of *Fclear* on *Fmean* and *Fprob* has been explained in detail in section 2.4.2 and will not be discussed here any further. Net heat flux (at lag 1 and 2 respectively) was the most important meteorological driver of seasonal variability of *Fmean* at the Celtic Sea and Ushant Front as well as of *Fprob* at the Celtic Sea Front (**Table 3.3**). The relationship was positive, but an increase in *Fmean* and *Fprob* was only observed once the net heat flux became positive (Figure 3.4 to Figure 3.6). The oceans begin to take up heat (positive net heat flux), but it takes about one to two months until the energy intake results in stratification of the water column. At the Ushant Front on the other hand, the meteorological variable explaining most of the seasonal variation of *Fprob* was SST (**Table 3.3**). The relationship was linear positive (Figure 3.7). In addition, the temporal variable 'year' explained some variation in seasonal variability of all metrics, apart form *Fprob* at the Celtic Sea Front (**Table 3.3**). The GAMMs predicted a strong decrease in *Fprob* and *Fmean* until 2000 and a gentle increase thereafter (Figure 3.4, Figure 3.6 and Figure 3.7). A detailed description of temporal variability of *Fmean* and *Fprob* at both fronts can be found in chapter 2. A small amount of the seasonal variability of *Fmean* at both fronts was also explained by precipitation (at lag 2) at both fronts (Figure 3.4 and Figure 3.6). Precipitation had a negative effect on *Fmean*. Wind stress caused some minor temporal variability in *Fprob* at the Celtic Sea Front (**Table 3.3**)

Table 3.3: Summary of GAMMs with AR1 structure for a seasonal subset of *Fmean* and *Fprob* (March to November) at the Celtic Sea and Ushant Front, testing for meteorological drivers of intraannual variability of *Fmean* and *Fprob*. Only significant covariates are listed, including their estimated degrees of freedom (edf), F-values, p-values, reduction in AIC and the increase in adjusted R^2 (Adj.R^2). The overall R^2 is given in bold. Flux= net heat flux, Precip= precipitation, Wind= wind stress.

Front	Metric	Variable (edf)	*F-value*	*p-value*	Δ-AIC	Adj. R^2
CELTIC SEA	***Fmean***	Flux at lag 1 (4.13)	63.51	<0.001	120.91	0.51
		Fclear (3.91)	15.66	<0.001	54.45	0.12
		Year (2.46)	4.52	<0.001	1.92	0.03
		Precip (1.0)	10.59	<0.001	6.21	0.01
						(**0.78**)
	Fprob	*Fclear* (4.73)	38.71	<0.001	97.92	0.5
		Flux at lag 2 (3.71)	17.62	<0.001	53.77	0.24
		Wind at lag 1 (1.81)	4.89	0.0115	0.92	0.02
						(**0.68**)
USHANT	***Fmean***	*Fclear* (4.45)	32.27	<0.001	113.11	0.3
		Flux (3.24) at lag 2	66.06	<0.001	81.44	0.34
		Precip (2.49) at lag 2	10.39	<0.001	22.87	0.05
			5.05	0.0022	4.2	0.02
		Year (3.0)				(**0.79**)
	Fprob	SST (1.84)	142.7	<0.001	93.17	0.39
		Fclear(3.74)	27.52	<0.001	73.45	0.36
		Year(3.28)	14.1	<0.001	24.36	0.08
						(**0.72**)

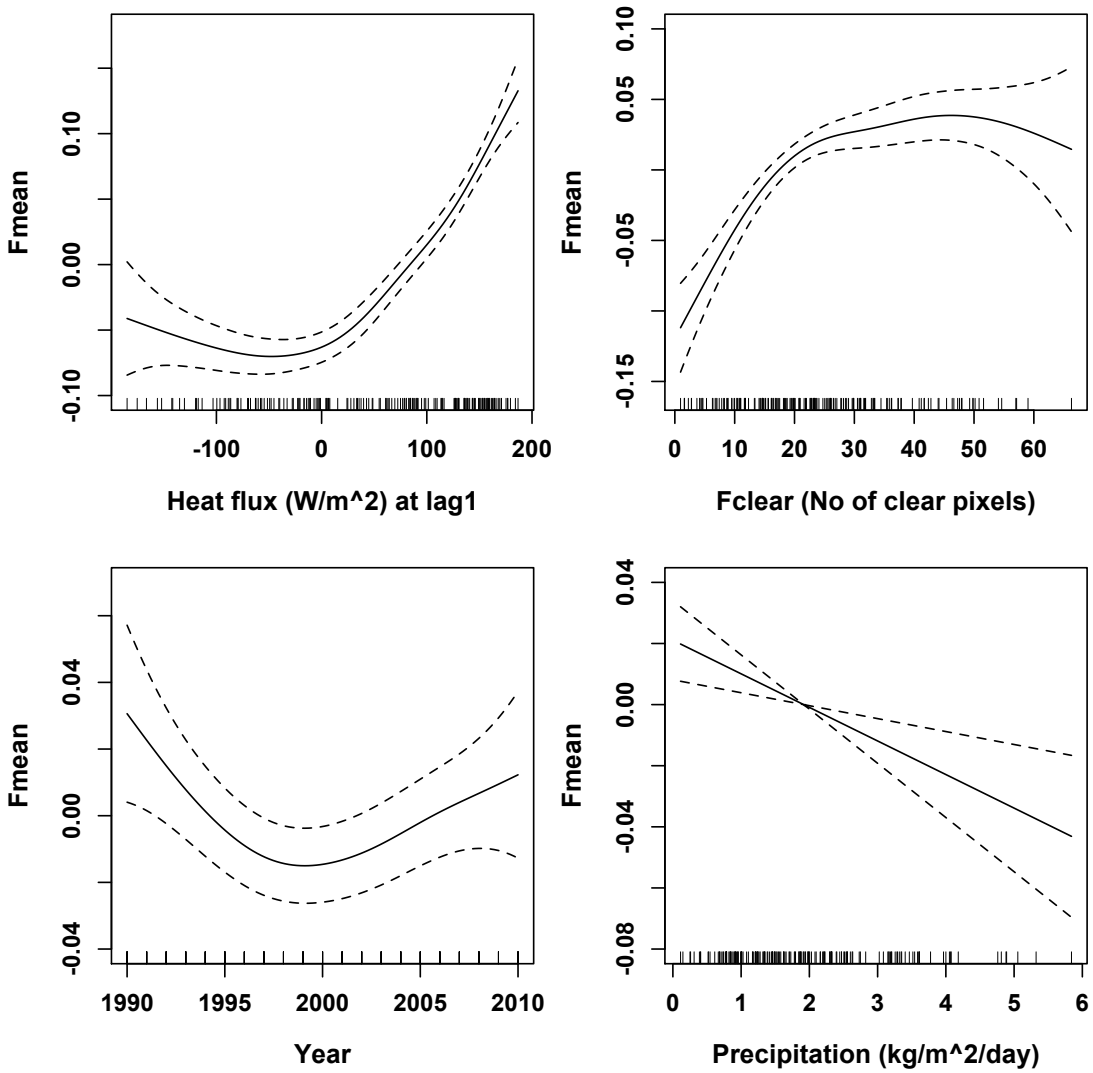

Figure 3.4: Results of GAMM with AR1 structure for a seasonal subset of *Fmean* (March to November, *N*=188) at the Celtic Sea Front as a function of heat flux (at lag1), *Fclear* and precipitation. Solid black line represents fitted values, dotted lines 95% confidence intervals.

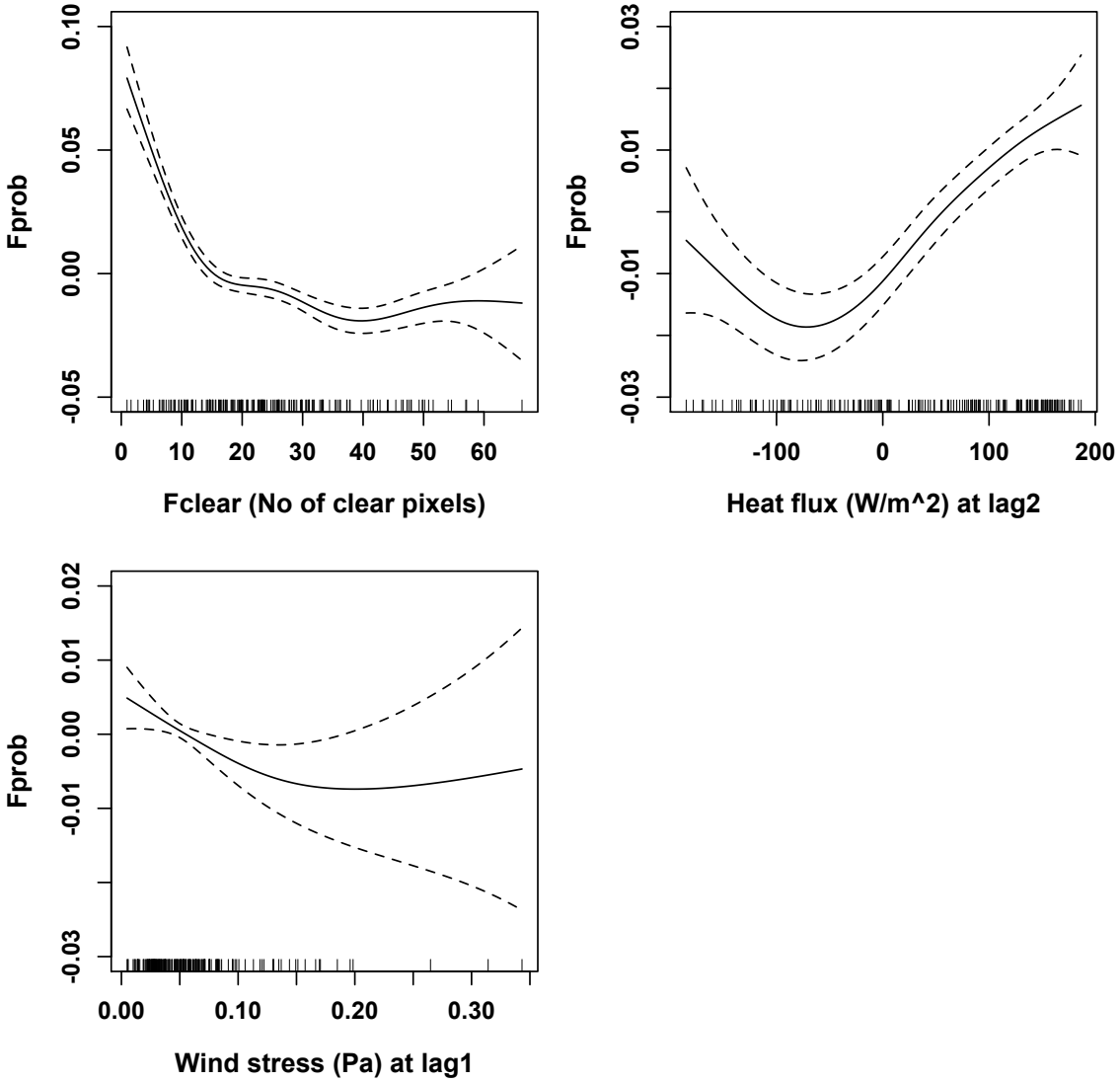

Figure 3.5: Results of GAMM with AR1 structure for a seasonal subset of *Fprob* (March to November, *N*=185) at the Celtic Sea Front as a function of *Fclear,* heat flux (at lag2) and wind stress (at lag1). Solid black line represents fitted values, dotted lines 95% confidence intervals.

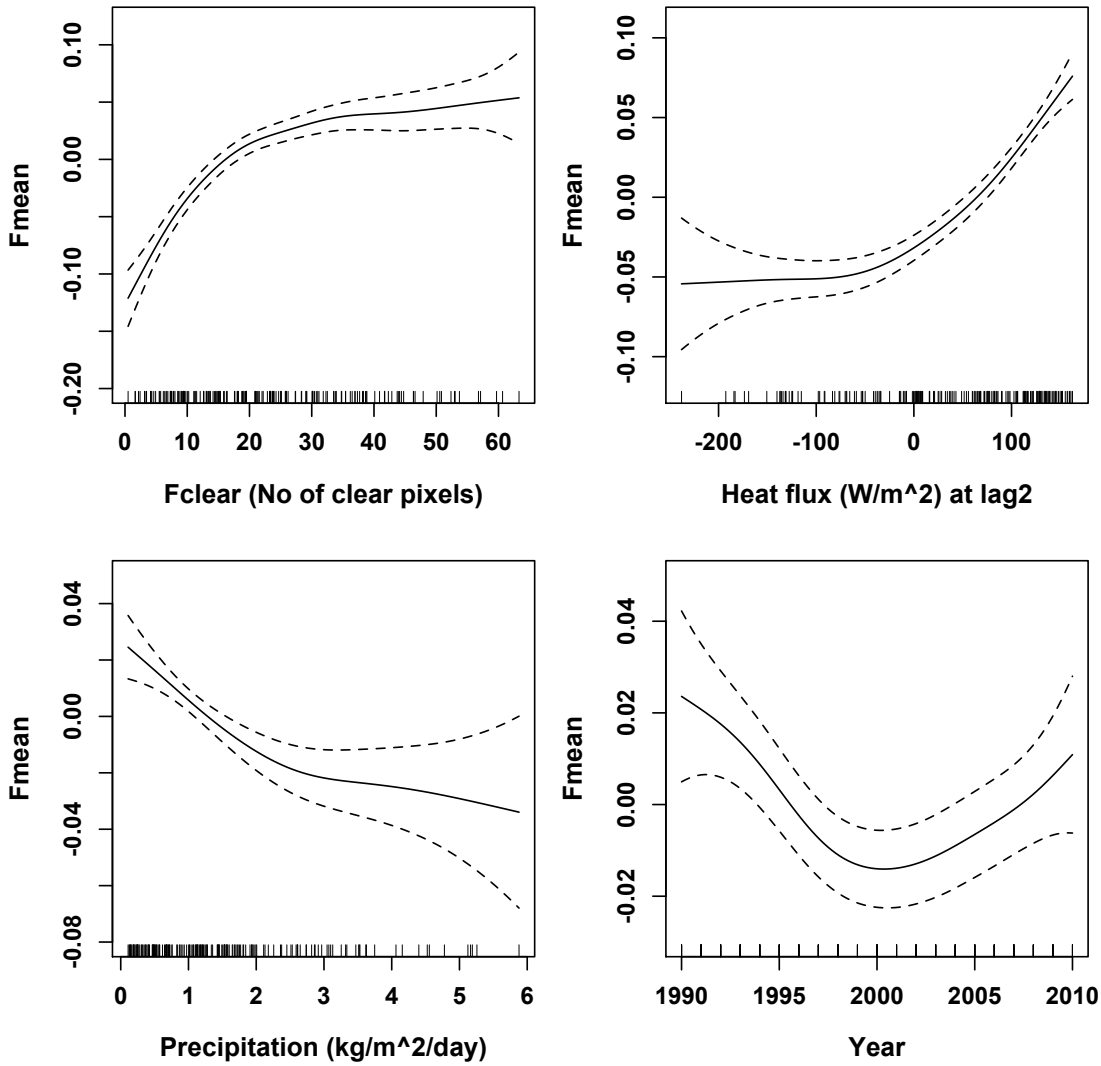

Figure 3.6: Results of GAMM with AR1 structure for a seasonal subset of *Fmean* (March to November, *N*=188) at the Ushant Front as a function of *Fclear,* heat flux (at lag2), precipitation and year. Solid black line represents fitted values, dotted lines 95% confidence intervals.

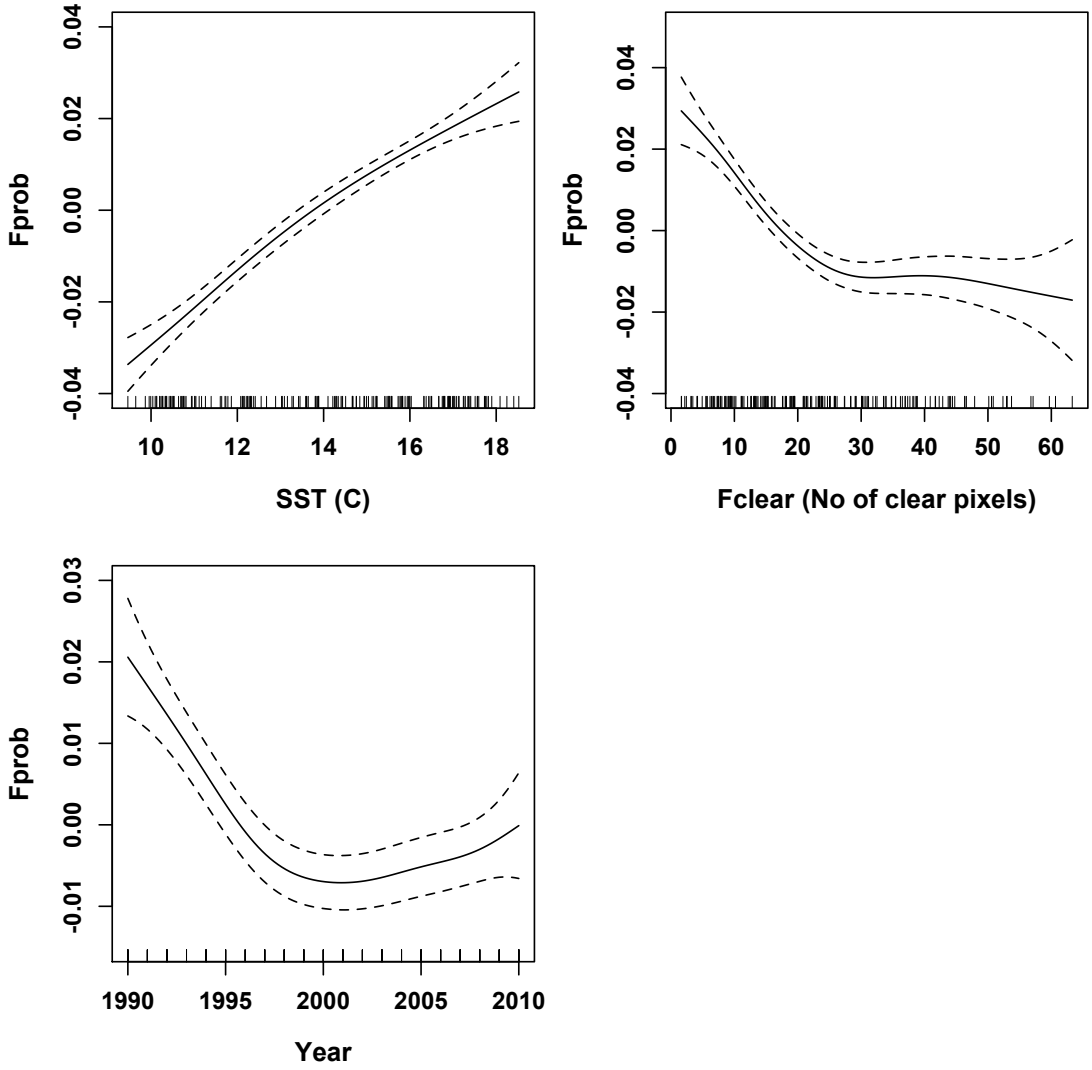

Figure 3.7: Results of GAMM with AR1 structure for a seasonal subset of *Fprob* (March to November, *N*=184) at the Ushant Front as a function of SST, *Fclear* and year. Solid black line represents fitted values, dotted lines 95% confidence intervals.

3.3.2 Meteorological drivers of interannual variability of *Fmean* and *Fprob*

3.3.2.1 Description of interannual variability pattern of frontal metrics *Fmean, Fprob* and *Fclear* and the meteorological variables

A detailed description of interannual pattern of *Fmean* and *Fprob* can be found in the section 2.3.1 and therefore, the description of long-term variability of both metrics is reduced to the main points. In chapter 2, interannual variability pattern of *Fmean* and *Fprob* were investigated under consideration of the effect of *Fclear.* Accounting for an *Fclear* effect, no significant interannual differences

in *Fprob* occurred at any of the two fronts (Figure 2.9 and Figure 2.10). However, a sinusoidal pattern was predicted for *Fmean*, with an initial decrease until around 2000, followed by an increase at both fronts (Figure 2.7 and Figure 2.8).

Similar to the pattern of *Fmean*, yearly net het flux anomalies at the Celtic Sea Front showed a decrease until the late 1990's and a gentle increase thereafter (Figure 3.8). Although years of positive and negative anomalies alternate throughout the time series, the magnitude of the positive anomalies decreased until the late 1990's, which caused an overall decrease in net heat flux in the first half of the time series. The increase thereafter is caused by a decrease in the magnitude of negative anomalies. At the Ushant Front on the other hand, the decrease in net heat flux was continuous from 1990 to 2010 (Figure 3.9). Interannual pattern of SST at both fronts were identical (Figure 3.8 and Figure 3.9). Despite some years of decreasing SST, there has been a strong overall increase of SST from 1990 to 2010. Precipitation and wind stress both displayed an oscillating pattern with alternating periods of higher and lower precipitation rates at both fronts (Figure 3.8 and Figure 3.9). The amplitude between high and low precipitation periods was higher at the Celtic Sea Front compared to the Ushant Front. As already discussed in chapter 2, *Fclear* has strongly and consistently increased from 1990 to 2010 at both fronts (Figure 3.8 and Figure 3.9). Apart from some minor deviations, the NAO displayed a generally decreasing trend at both fronts throughout the time series (Figure 3.8 and Figure 3.9).

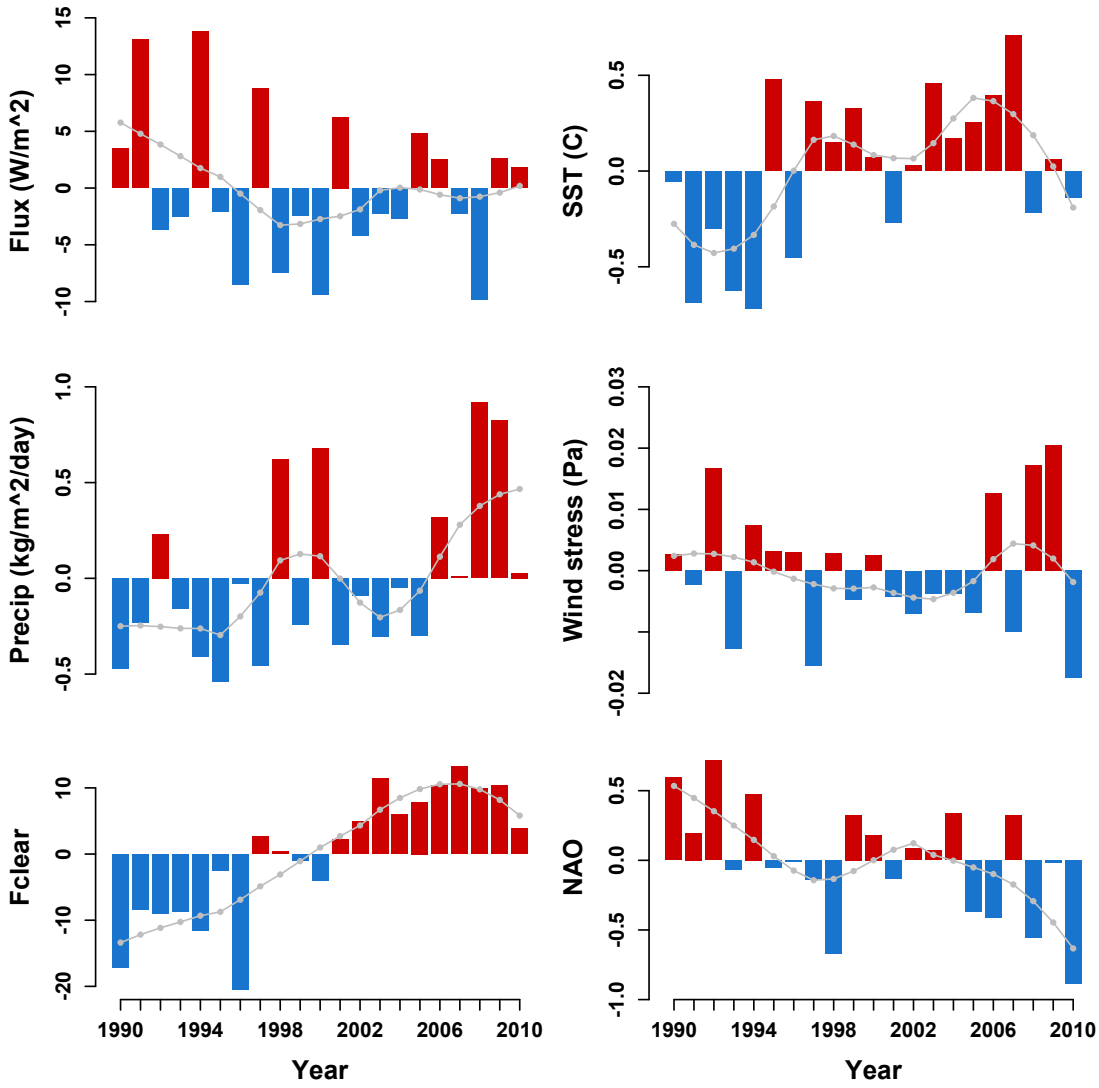

Figure 3.8: Time series of anomalies of net heat flux (Flux), SST (Temp), precipitation (Precip), wind stress, *Fclear* and the NAO at the Celtic Sea Front. Light grey line shows trend obtained by *loess* smoothing (span width= 0.6) Blue bars represent negative anomalies and red anomalies.

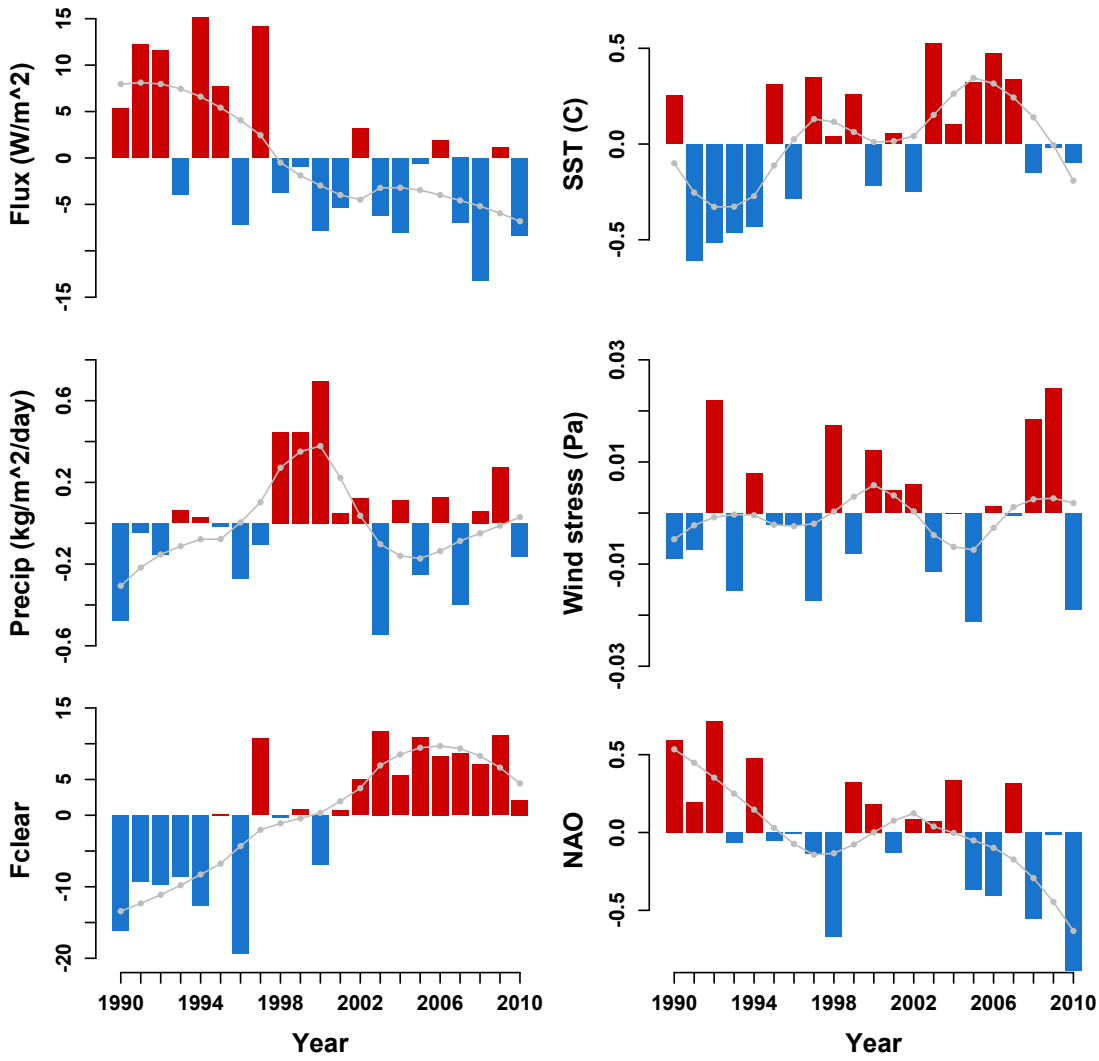

Figure 3.9: Time series of anomalies of net heat flux (Flux), SST (Temp), precipitation (Precip), wind stress, *Fclear* and the NAO at the Ushant Front. Light grey line shows trend obtained by *loess* smoothing (span width= 0.6) Blue bars represent negative anomalies and red anomalies.

3.3.2.2 Meteorological drivers of intraannual variability of *Fmean* and *Fprob*

As mentioned earlier, the largest variation in temporal pattern of *Fmean* and *Fprob* was contained in the seasonal component. Therefore, the factor 'months' explained, together with *Fclear*, most of the temporal variability of *Fmean* and *Fprob* at both fronts (**Table 3.4**). The relationship between factor month and the two frontal metrics was non-linear and expressed in a typical seasonal curve (Figure 3.10, Figure 3.11 and Figure 3.12). However, month was insignificant for *Fprob* at the Ushant Front (**Table 3.4**). The remaining temporal variability of

both metrics at both fronts was small and largely attributed to changes in SST and heat flux (**Table 3.4**). The relationship between both frontal metrics and SST and heat flux was almost linear positive (Figure 3.11, Figure 3.12 and Figure 3.13). Exception was the relationship between SST and *Fmean* at the Celtic Sea Front, which only became positive at about 13°C (Figure 3.10). In addition, precipitation and wind stress explained some of the variation of *Fmean* and *Fprob* at the Ushant Front only (**Table 3.4**). The relation between both metrics and precipitation and wind stress was negative (Figure 3.12 and Figure 3.13).

Table 3.4: Summary of GAMMs with AR1 structure for a seasonal subset of *Fmean* and *Fprob* (March to November) at the Celtic Sea and Ushant Front, testing for meteorological drivers of interannual variability of *Fmean* and *Fprob*. Only significant covariates are listed, including their estimated degrees of freedom (edf), F-values, p-values, reduction in AIC and the increase in adjusted R^2 (Adj.R^2). The overall R^2 is given in bold. Flux= net heat flux, Precip= precipitation, Wind= wind stress.

Front	Metric	Variable (edf)	*F-value*	*p-value*	∆-AIC	Adj. R^2
CELTIC SEA	***Fmean***	Month (5.47)	30.89	<0.001	160.79	0.56
		Fclear (4.47)	18.81	<0.001	69.78	0.14
		SST (4.97)	7.57	<0.001	18.85	0.04 (**0.83**)
	Fprob	*Fclear* (4.87)	103.77	<0.001	140.06	0.67
		Month (4.25)	13.14	<0.001	81.39	0.27
		Flux (1.0)	10.2	0.0017	5.71	0.01 (**0.8**)
USHANT	***Fmean***	*Fclear* (5.65)	27.06	<0.001	101.44	0.24
		Month (5.21)	5.8	<0.001	90.54	0.36
		Precip (2.61)	18.5	<0.001	29.19	0.06
		SST (1.0)	7.7	0.0061	3.11	0.001 (**0.8**)
	Fprob	SST (1.68)	86.2	<0.001	87.07	0.35
		Fclear (4.17)	47.8	<0.001	77.24	0.41
		Wind (1.0)	13.17	<0.001	7.5	0.04 (**0.66**)

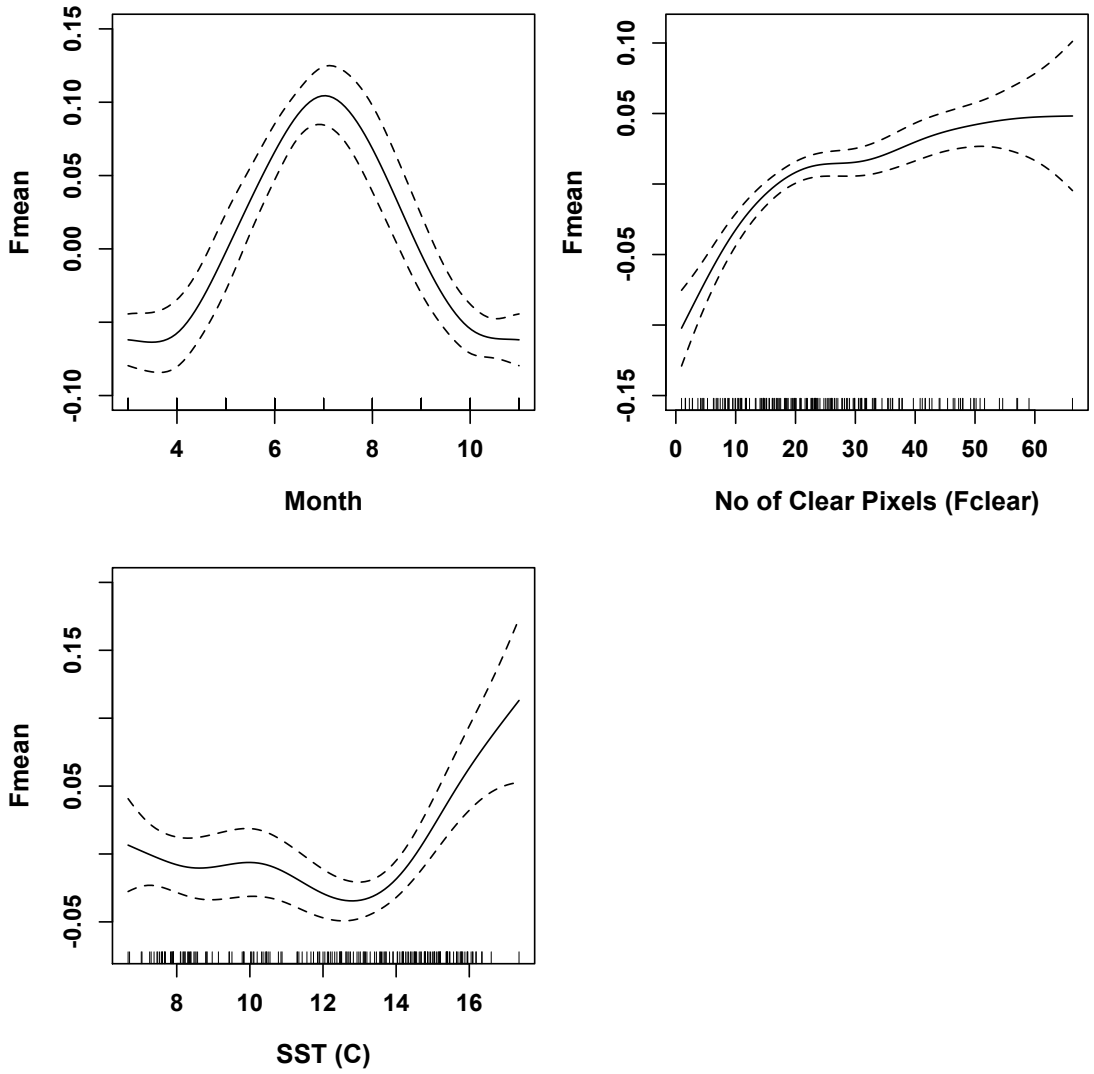

Figure 3.10: Results of GAMM with AR1 structure for a seasonal subset of *Fmean* (March to November, *N*=188) at the Celtic Sea Front as a function of month, *Fclear* and SST. Solid black line represents fitted values, dotted lines 95% confidence intervals.

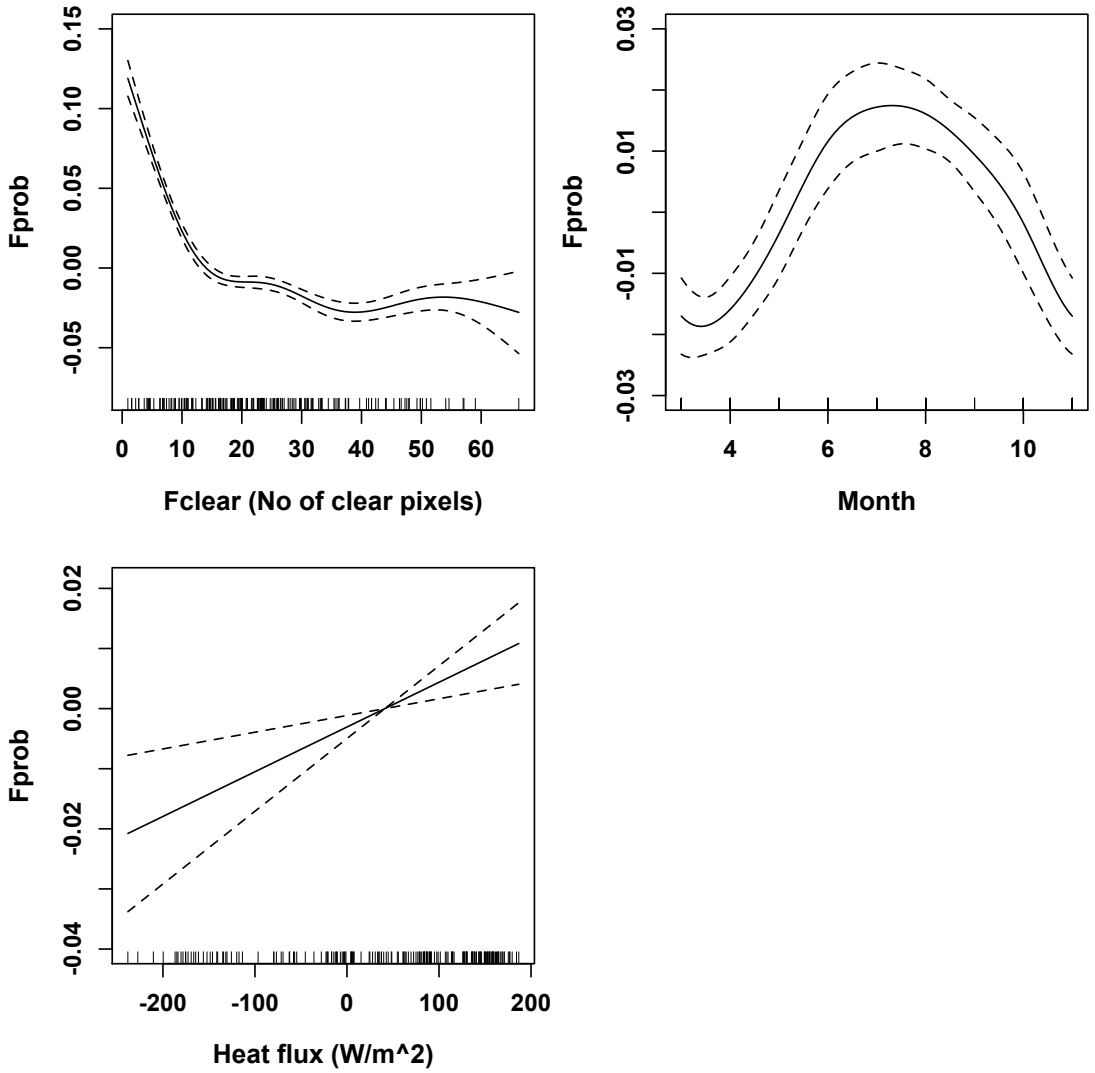

Figure 3.11: Results of GAMM with AR1 structure for a seasonal subset of *Fprob* (March to November, *N*=187) at the Celtic Sea Front as a function of *Fclear,* month and heat flux. Solid black line represents fitted values, dotted lines 95% confidence intervals.

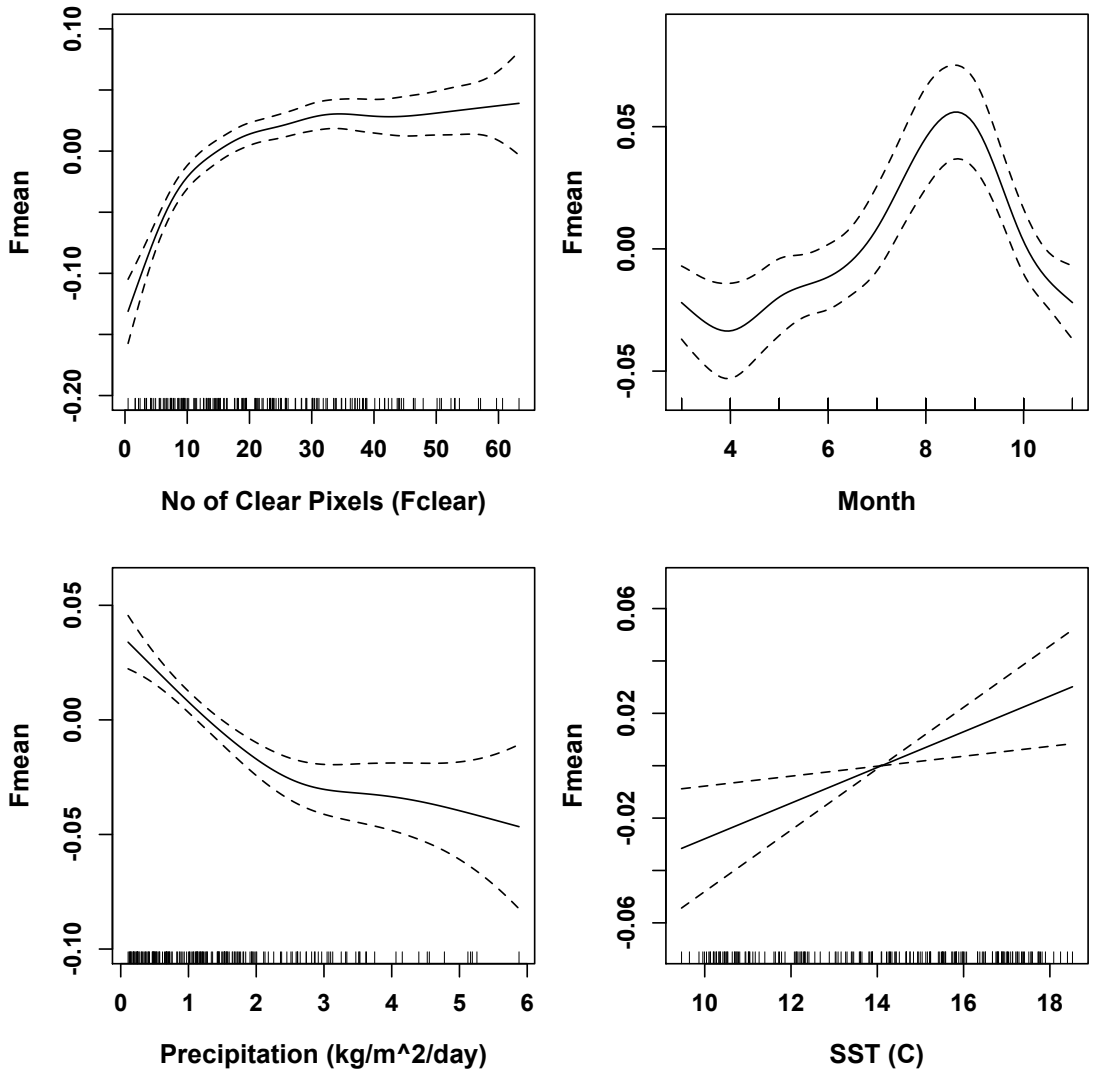

Figure 3.12: Results of GAMM with AR1 structure for a seasonal subset of *Fmean* (March to November, *N*=188) at the Ushant Front as a function of *Fclear,* month, precipitation and SST, precipitation and year. Solid black line represents fitted values, dotted lines 95% confidence intervals.

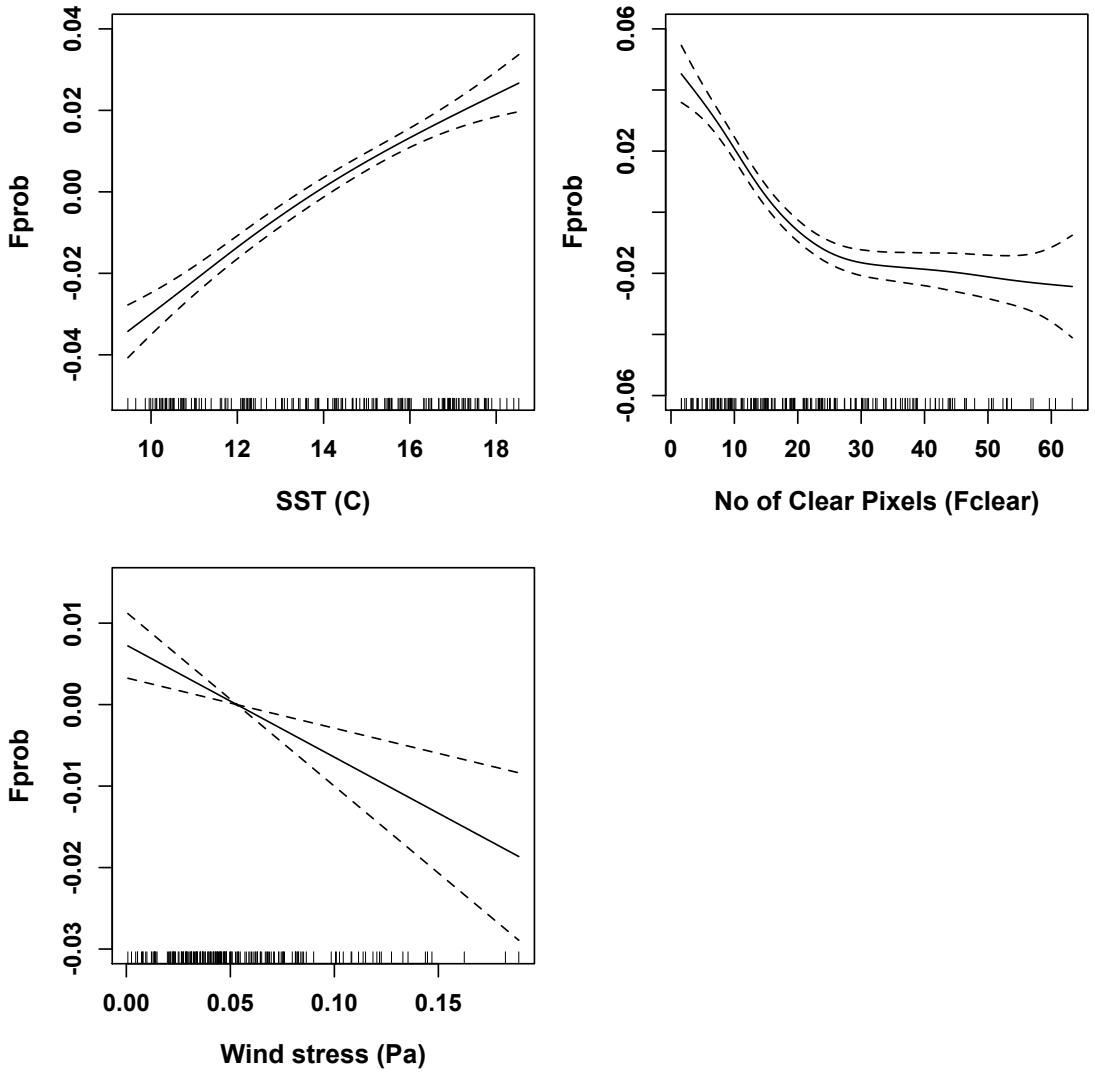

Figure 3.13: Results of GAMM with AR1 structure for a seasonal subset of *Fprob* (March to November, *N*=185) at the Ushant Front as a function of SST, *Fclear* and wind stress. Solid black line represents fitted values, dotted lines 95% confidence intervals.

3.4 DISCUSSION

3.4.1 Meteorological drivers of inter- and intraannual variability of *Fmean* and *Fprob*

3.4.1.1 Meteorological drivers of intraannual variability of *Fmean* and *Fprob*

Variables related to the heat budget of the shelf-seas, namely net heat flux and SST, were the most important contributors to seasonal variability of frontal gradient strength (*Fmean*) and frontal persistence (*Fprob*). Heat flux showed

best correlations with *Fmean* and *Fprob* at lags of 2 month. This is in agreement with previous studies and mechanisms of frontogenesis and frontolysis. It takes about two months after net heat flux has become positive (oceans contain energy instead of releasing it). At this point, surface waters retain enough heat for stratification to develop that is strong enough to counteract the mixing forces of tides and wind (Pringree, 1980). Stratification and tidal mixing fronts intensify with increasing SST (Holt et al., 2010), which explains the linear positive relationship between SST and *Fprob* at the Ushant Front.

Wind stress and precipitation were found to play only minor roles in the seasonal development of tidal mixing fronts. An intensification of wind stress negatively affects tidal mixing fronts, because it can weaken stratification due to its mixing effect. This happens predominantly during times of frontal establishment and break up (Marsh et al., 2015) and therefore, the contribution of wind stress was small compared to factors acting throughout the entire frontal season. Overland rainfall causes increased riverine input, which can lead to a temporal intensification of the density gradient at tidal mixing fronts (Holt et al., 2010). However, a precipitation effect is thought to be comparatively small and only evident in the Ushant Front region (Holt et al., 2010). The negative relationship between precipitation and *Fmean* at both fronts found in this research is likely to arise from confounding factors between increased precipitation and with bad weather periods. For example, precipitation is usually correlated with increased cloud cover and wind stress. Particularly frontogenesis and –lysis wind stress can weaken the frontal structure (Bowers et al., 1987). It is also possible that disturbances on the water surface caused by raindrops blur the surface signal of a front, which makes it harder to identify frontal temperature gradients on satellite imagery and in return, result in lower *Fprob* and *Fmean*.

In general, the results of the analysis of meteorological drivers of seasonal variations were consistent between both fronts and metrics. Interannual variability of *Fmean* and *Fprob* was strongly influenced by SST or heat flux. Minor differences between the Celtic Sea and Ushant Front were found in the importance of wind stress and precipitation. This is likely a reflection of the

local-specific differences at the two fronts, such as strength of tidal flows or bathymetry. Compared to the Celtic Sea Front, shallower depth and stronger tides in the Ushant region require extended periods of heating to counteract mixing forces and for stratification to develop and make the Ushant Front more sensitive to kinetic forcing during frontogenesis and –lysis.

Overall, the results of the analysis of meteorological drivers of seasonal variability of tidal mixing fronts are in agreement with previous studies. Tidal mixing fronts are temporally dynamic features, which are sensitive to parameters that change at temporal scales of a few days to weeks, such as the spring neap adjustment or a strong storm. Therefore, the monthly resolution used in this research is not sufficient to study environmental causes of smaller scale variations in frontal occurrence (e.g. days). For example, the importance of wind stress appears to have been underestimated in this analysis. However, the consistency between previous studies and this analysis provides confidence that frontal maps and meteorological model data used here are capable of identifying at least the main drivers of temporal variability pattern of frontal metrics.

3.4.1.2 Meteorological drivers of interannual variability of *Fmean* and *Fprob*

SST was the main driver of interannual variability of all metrics, but *Fprob* at the Celtic Sea Front, which was primarily governed by net heat flux. The strong correlation between seasonal variability and net heat flux was not replicated at interannual timescales. This shows that the effect of environmental drivers of frontal variability differ over different temporal scales. The positive relationship between frontal metrics and SST indicate a potential sensitivity of tidal mixing fronts to climate change. Modelling studies suggest an extension of the frontal period by ten to 15 days by the end of the century due to higher SST (Holt et al., 2010). However, an increase in frontal strength was not predicted. Interestingly, this study found significant interannual variations in *Fprob*, which were not found to be significant in the previous chapter (**Table 2.4**). In the chapter 2 *Fprob* was modelled as a function of temporal variables (year and month) and *Fclear* only. This provides some evidence that the statistical model in chapter 2 indeed overestimated an *Fclear* effect and more of the temporal variability in

Fprob (and likely in *Fmean* as well) was caused by genuine fluctuations of the front in response to environmental conditions.

As satellite data only concern the very surface signal of a front, it is not possible to discuss potential effects of warming temperatures on subsurface components of the front. However, Holt et al. (2012) suggested that most of the change on shelf-seas will occur in the surface layer, because the bottom layer is less sensitive towards warming SST. Similar, consequences of climate change on spatial variability of tidal mixing fronts in the Celtic Sea are unclear. Some models suggest an expansion of the stratification area (Holtet al., 2012), which could affect the location of tidal mixing fronts. Other research does not predict a significant change in frontal positions (Holt et al., 2010). Likewise, knock-on effects of future alterations in frontal location, intensity or period on biological and hydrodynamic processes of the Celtic Sea ecosystem remain largely unknown.

At the Ushant Front, wind stress and precipitation explained a small part of the interannual variability of *Fmean* and *Fprob*. As described above, precipitation is likely to be correlated to frontal variability due to confounding factors with bad weather phenomena and data availability (*Fclear*). Wind stress is expected to play a more significant role in seasonal variability of tidal mixing fronts rather than interannual variability. However, years of increased wind stress are to some degree accompanied with years of other weather variables that weaken fronts, such as more cloud cover and colder temperatures. The correlation between bad weather periods and data availability is one of the limitations of satellite-derived data sets, which will be discussed in section 3.4.2.

The findings of this research are in agreement with model predictions of long-term variability of shelf-sea stratification and impacts of rising SST on stratification in the Celtic Sea. Overall, the meteorological drivers of interannual variability are similar between *Fmean* and *Fprob* and between both fronts. Only small differences occurred, which can be attributed to differences in location-specific characteristics of both fronts. Therefore, individual fronts may respond differently to changing weather patterns in the future.

3.4.2 Limitations and recommendations

Some limitations of satellite-derived data have already been discussed in the previous chapter (section 2.4.5) and therefore, a couple of the following points are a repetition, but included for completeness. As mentioned above, satellite-derived data only considers the very surface signal of thermal fronts. In the case of a three-dimensional structure like a tidal mixing front, this means a large part of the feature is not accounted for. In addition, the bottom part of a tidal mixing front is less subject to atmospheric forcing and hence, much more stable in time and space. Because the bottom front is primarily driven by tides, bathymetry and the differences between winter and summer temperatures (e.g. the greater the differences the stronger the density gradient will be), its response to climate change could be very different to that of a surface front, but can not be studied using satellite-derived data (Brown et al., 2003; Le Boyer et al., 2009).

Satellite-derived datasets are limited in studying effects of meteorological variability on tidal mixing fronts because of confounding effects of the seasonal nature of these fronts and similar seasonal pattern in data availability and bad weather phenomena (e.g. cloud cover and wind stress). Overall, the findings of this research are in agreement with previous studies, which provides confidence in the results. However, the discussion of some findings remains speculative, such as a potential effect of climate change due to rising SST in the last decade.

In this analysis, spatial averages of monthly composites of *Fprob* and *Fmean* were used, because the mean summarizes and provides information on the entire front. However, it could be useful to expand the analysis of meteorological drivers of frontal variability using monthly maxima (e.g. extract the upper 5% from each sampling area). Analysis on the maxima would extract specific information the potential intensification of fronts over time and its meteorological causes.

The spatial resolution of the meteorological data set used in this research was about the same size as the spatial extent of the fronts. It would be useful to investigate how higher spatial resolution data of meteorological variables would

affect the outcomes of the analysis. The Celtic Sea Front is spatially fairly stable, but the northern part of the Ushant Front moves several 100km over the seasonal cycle and performs smaller spatial adjustments in response to wind or tidal forces. Investigating distinct sections of the Ushant Front separately might even show that the effect of atmospheric forcing on spatio-temporal variability differ along a single front. Furthermore, additional parameters such as evaporation rate, air temperature, and interactions between the investigated variables could increase explanatory power of the statistical models. It might also be worth to explore the effect of teleconnections other than the NAO on interannual frontal variability.

In this research, monthly composites of frontal metrics were used, because higher resolution maps were too affected by cloud cover, particularly during the first half of the time series (early 90's). However, the amount of available data has drastically increased over the last decade, because more satellites are in use. A reduced data set e.g. starting from 2000), would allow the use of higher resolution frontal maps (e.g. fortnightly composites). Higher temporal resolution can provide additional insights into temporal variability pattern of tidal mixing fronts and the underlying meteorological drivers. Particularly during periods of fontal establishment and breakup, changes in frontal activity occur quickly and frontal variability is high. This variability can be blurred when using monthly composites. In addition, higher resolution frontal maps would allow for a temporally refined investigation of a potential extension of the frontal season.

3.4.3 Conclusion

The key meteorological drivers of temporal variability of frontal gradient strength and persistence at both fronts were related to the heat budget of the water column. Overall, net heat flux explained most of the variations in intraannual pattern, whereas SST was the most important contributor to interannual variability of *Fmean* and *Fprob*. The positive correlation between long-term variability of both frontal metrics and SST indicate a potential sensitivity of tidal mixing fronts to climate change. The consequences are not yet fully resolved, but could include an extension of the frontal season, strengthening of the frontal density gradients or spatial displacements of tidal mixing fronts. Likewise,

knock-on effects of changes in frontal occurrence on oceanographic biological processes on the shelf remain unclear.

Generally, the key meteorological drivers of frontal variability were consistent between the Celtic Sea and Ushant Front as well as between the two metrics. Only minor differences in the significance of environmental causes of temporal variability were evident between the two fronts, which can be attributed to location-specific differences, such as bathymetry or the tidal regime. The results are in agreement with previous studies concerning intraannual variability of tidal mixing fronts in the Celtic Sea and provide confidence in the suitability of frontal maps for this kind of analysis. However, the use of frontal maps is limited by confounding factors between bad weather phenomena and data availability. Also, the low temporal resolution was likely to lead to an underestimation of some meteorological drivers of frontal variability, such as wind stress during periods of frontogenesis and -lysis.

3.5 Supplementary material

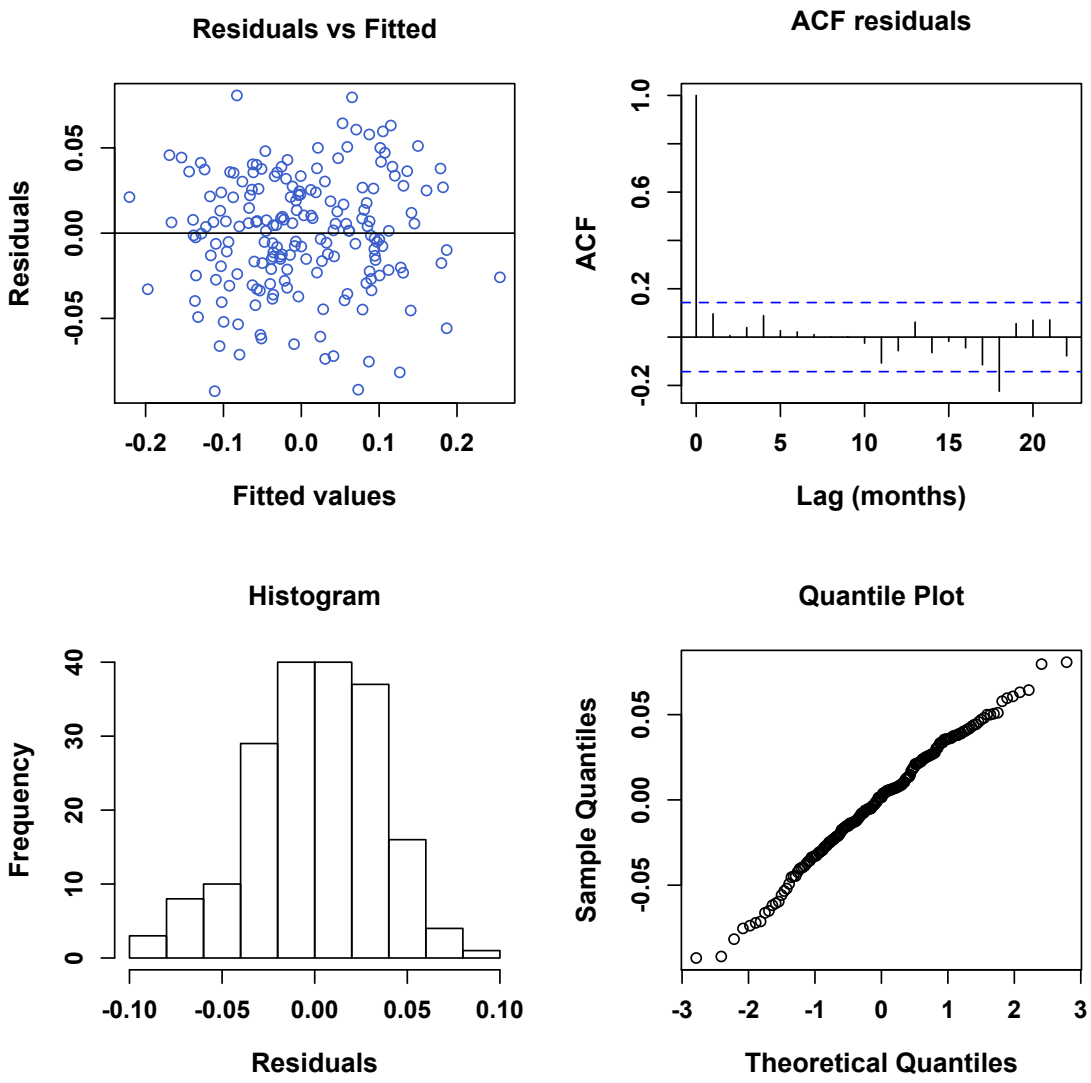

Sup.Figure 3.1: Model validation plots of residual analysis for meteorological drivers of intraannual variability of *Fmean* at the Celtic Sea Front. Top left: fitted values against normalized residuals; top right: autocorrelation function of residuals with 95% confidence intervals as blue dashed line; bottom left: histogram of residuals and bottom right: Quantile plot.

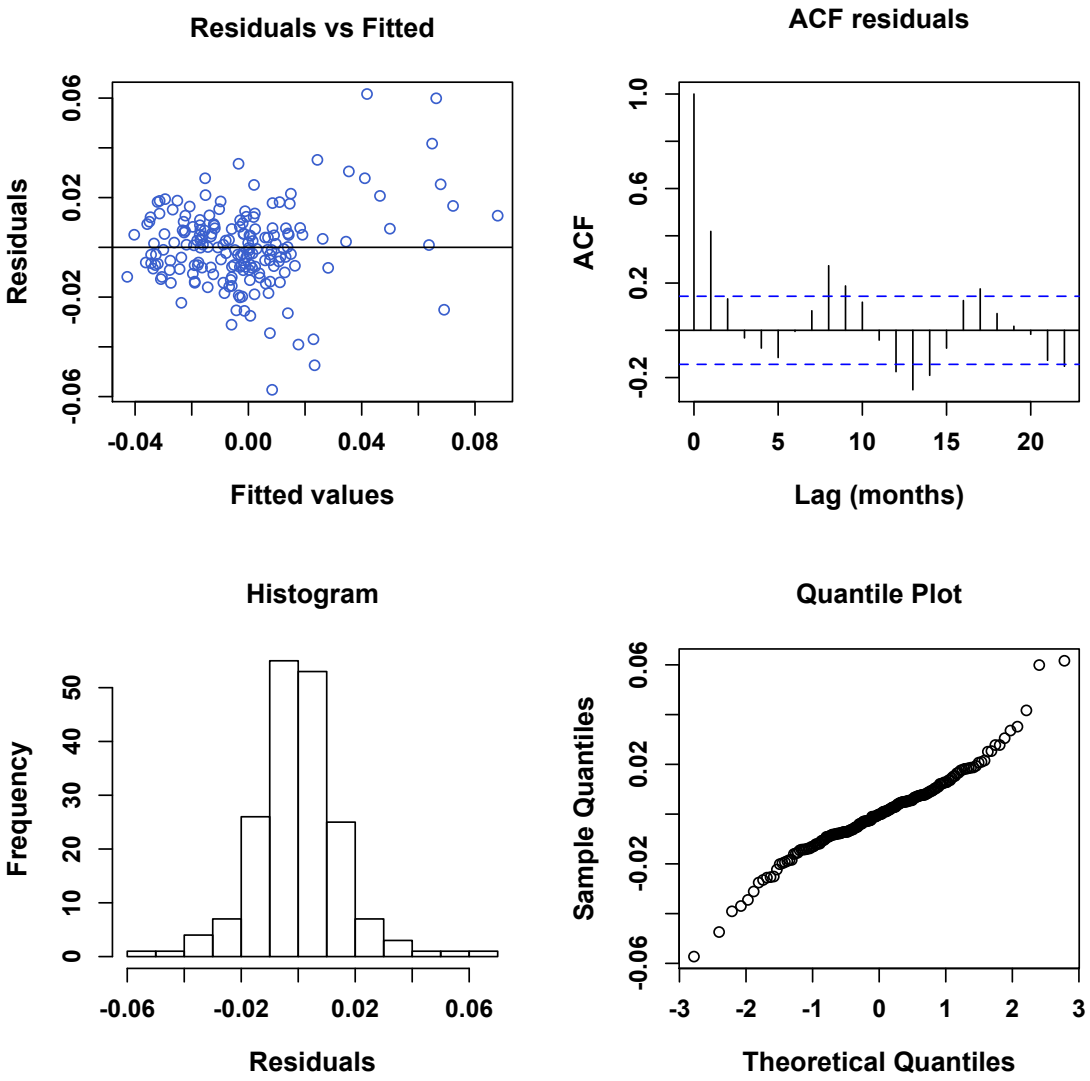

Sup.Figure 3.2: Model validation plots of residual analysis for meteorological drivers of intraannual variability of *Fprob* at the Celtic Sea Front. Top left: fitted values against normalized residuals; top right: autocorrelation function of residuals with 95% confidence intervals as blue dashed line; bottom left: histogram of residuals and bottom right: Quantile plot.

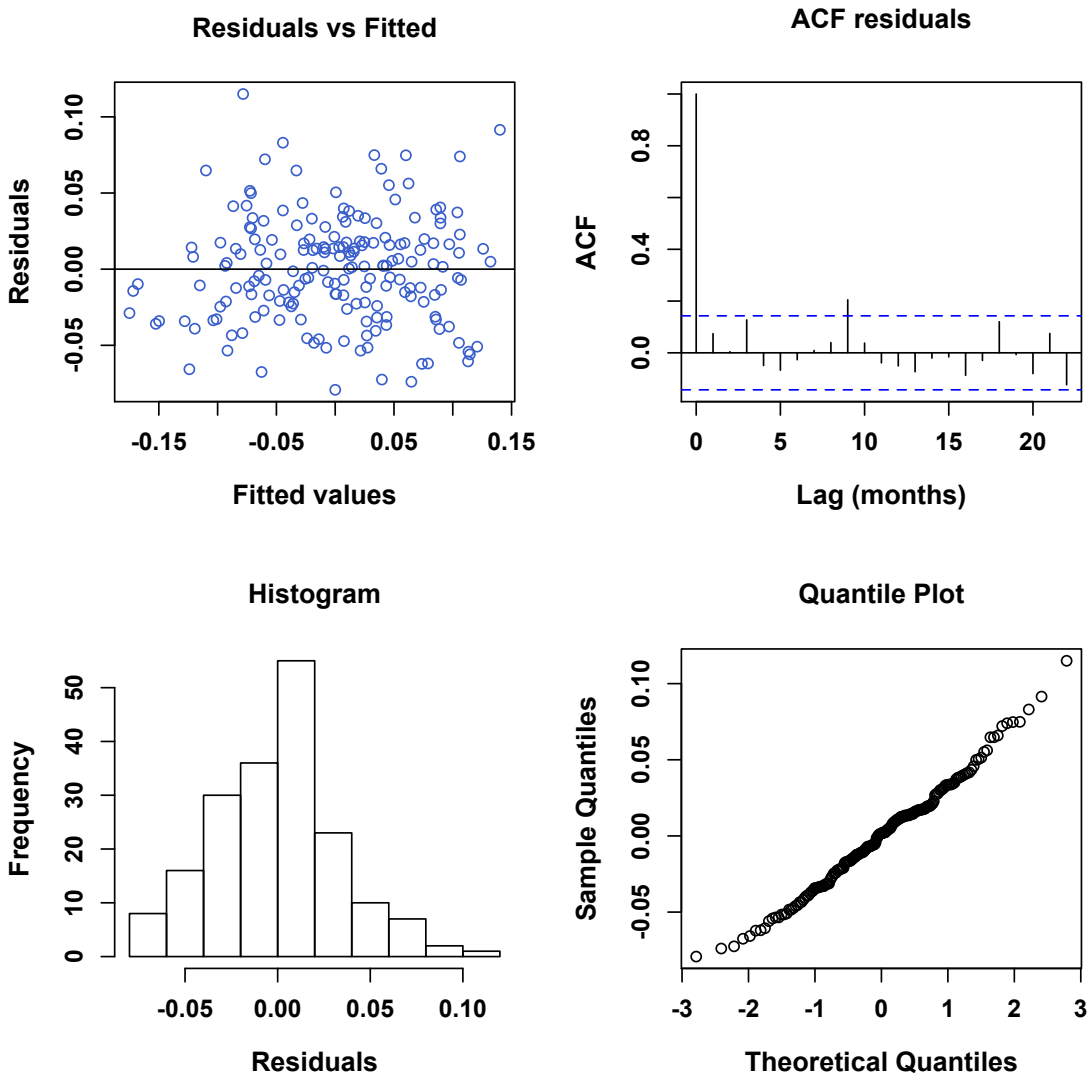

Sup.Figure 3.3: Model validation plots of residual analysis for meteorological drivers of intraannual variability of *Fmean* at the Ushant Front. Top left: fitted values against normalized residuals; top right: autocorrelation function of residuals with 95% confidence intervals as blue dashed line; bottom left: histogram of residuals and bottom right: Quantile plot.

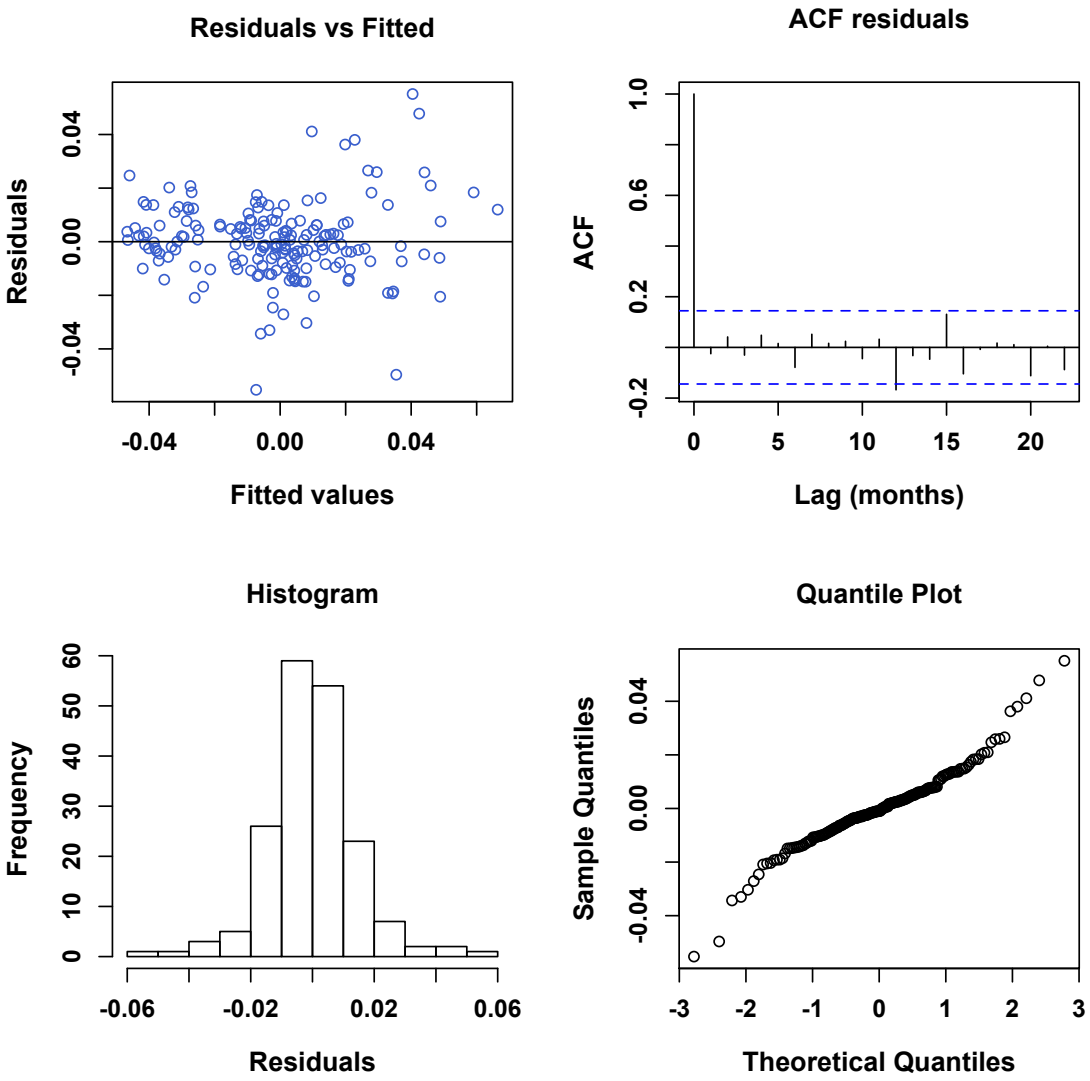

Sup.Figure 3.4: Model validation plots of residual analysis for meteorological drivers of intraannual variability of *Fprob* at the Ushant Front. Top left: fitted values against normalized residuals; top right: autocorrelation function of residuals with 95% confidence intervals as blue dashed line; bottom left: histogram of residuals and bottom right: Quantile plot.

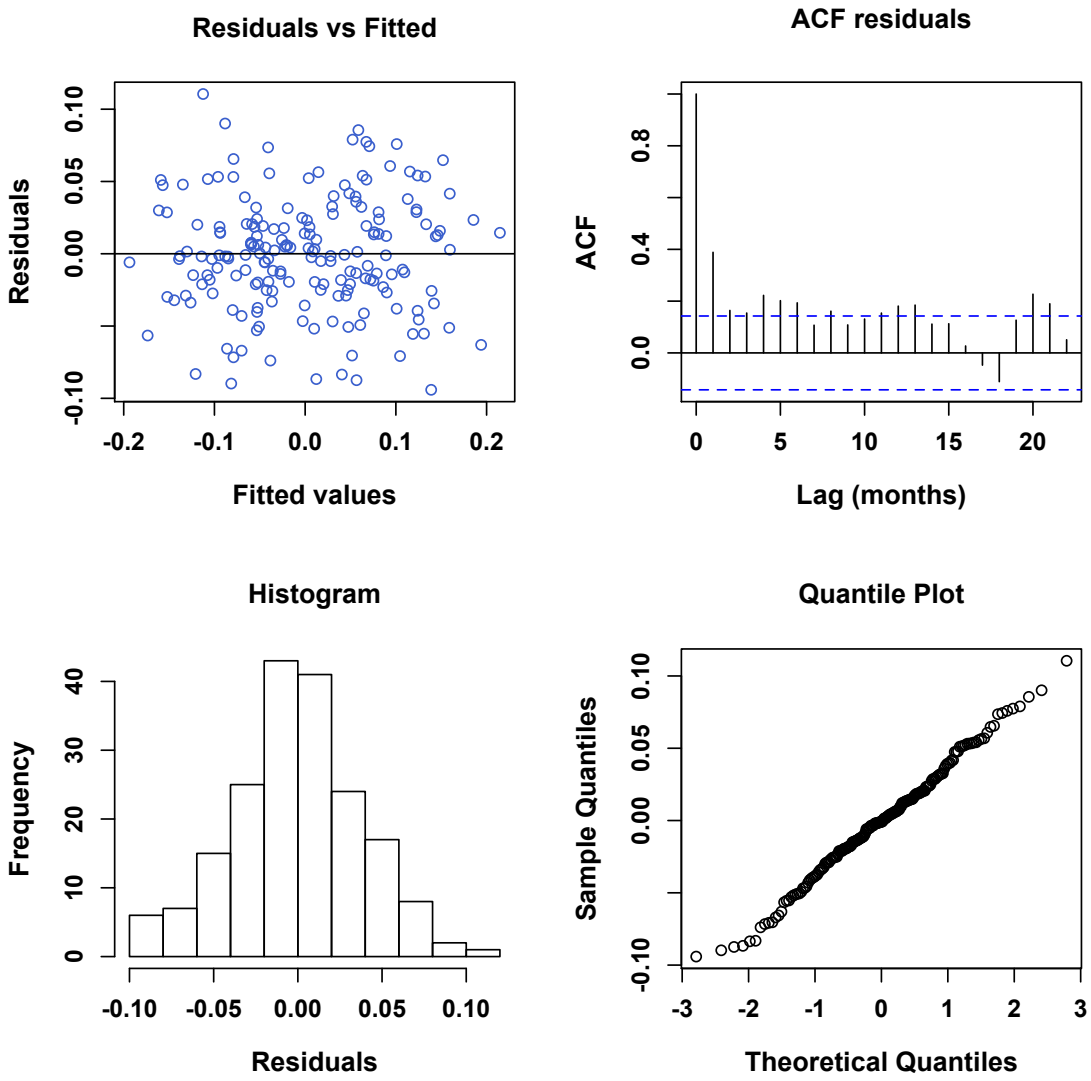

Sup.Figure 3.5: Model validation plots of residual analysis for meteorological drivers of interannual variability of *Fmean* at the Celtic Sea Front. Top left: fitted values against normalized residuals; top right: autocorrelation function of residuals with 95% confidence intervals as blue dashed line; bottom left: histogram of residuals and bottom right: Quantile plot.

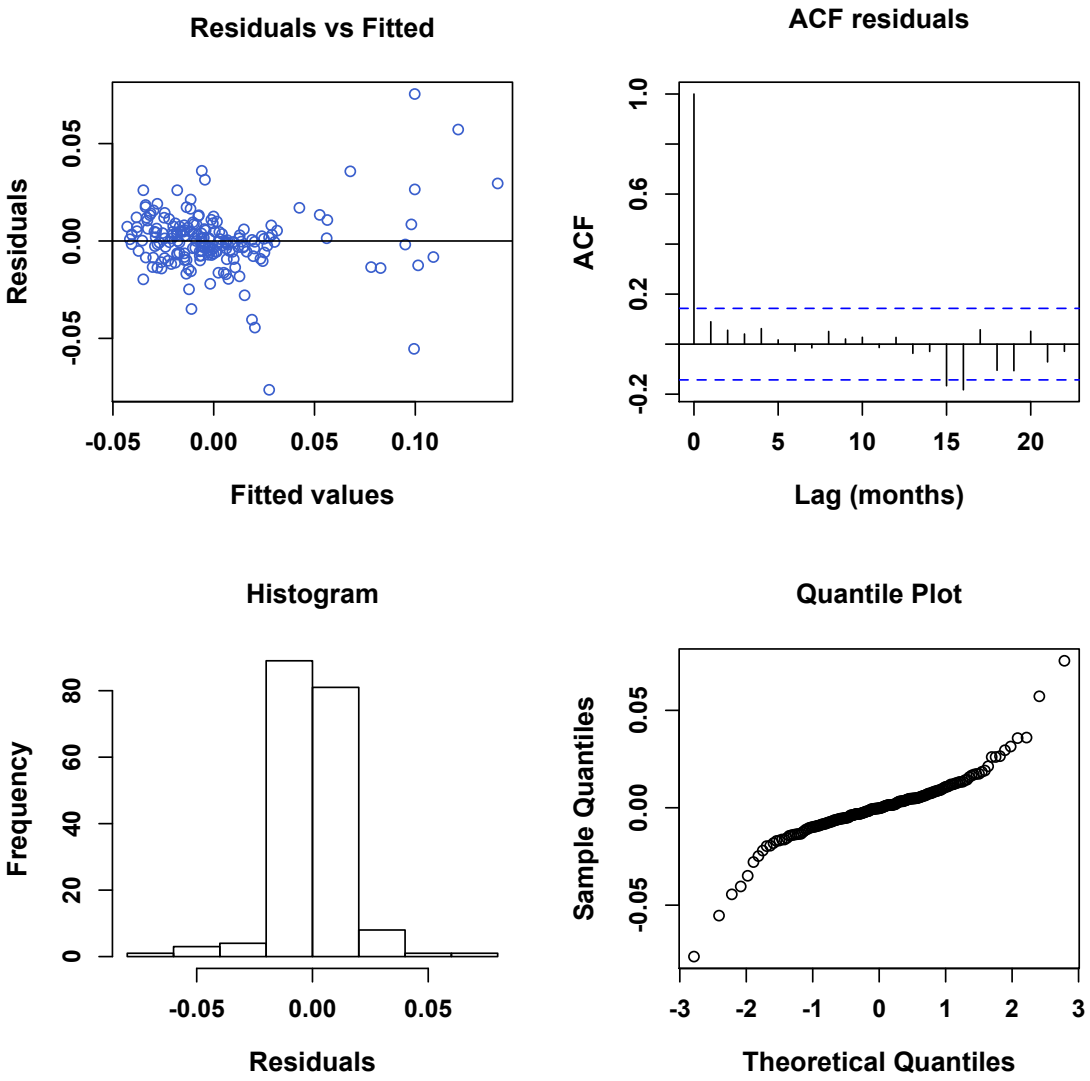

Sup.Figure 3.6: Model validation plots of residual analysis for meteorological drivers of interannual variability of *Fprob* at the Celtic Sea Front. Top left: fitted values against normalized residuals; top right: autocorrelation function of residuals with 95% confidence intervals as blue dashed line; bottom left: histogram of residuals and bottom right: Quantile plot.

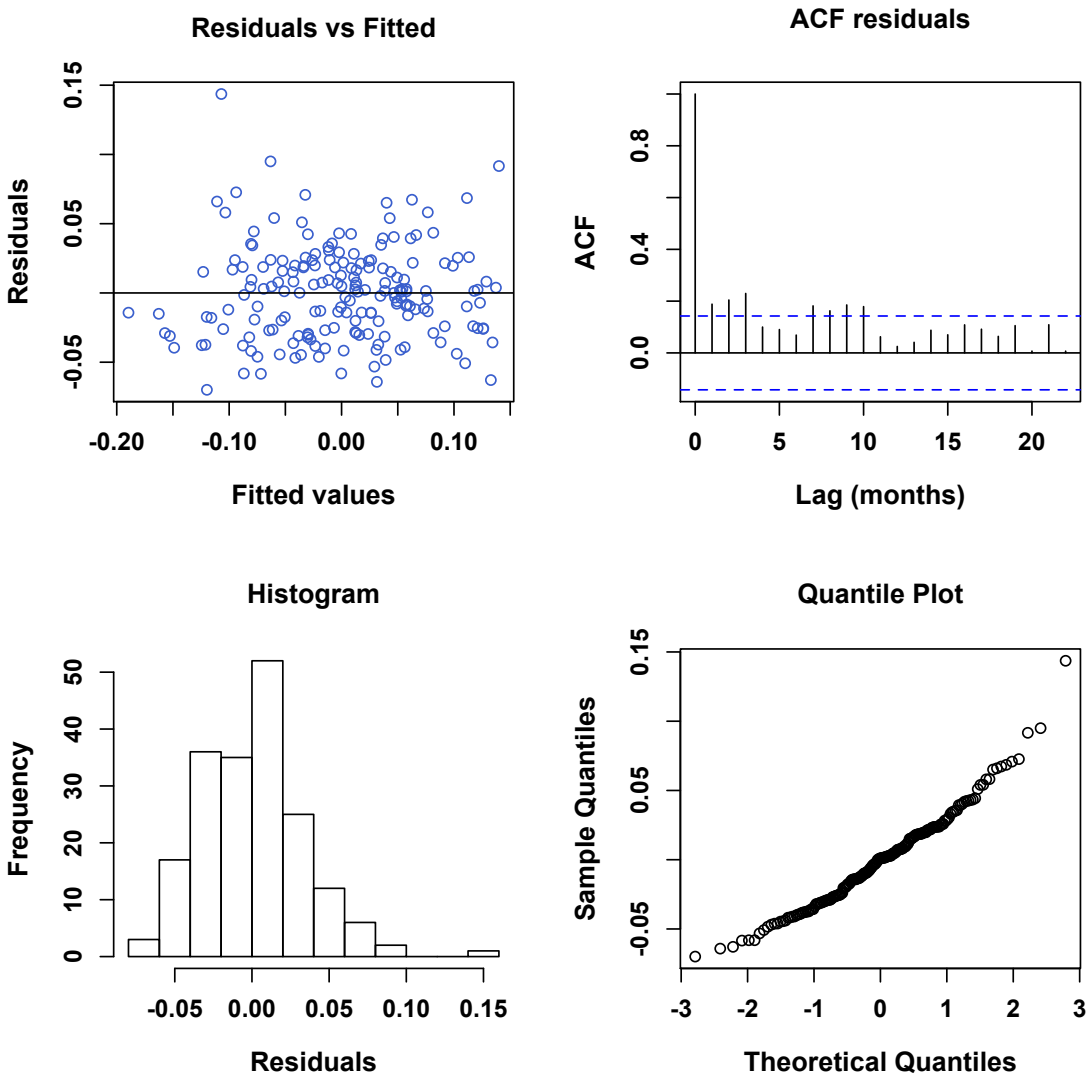

Sup.Figure 3.7: Model validation plots of residual analysis for meteorological drivers of interannual variability of *Fmean* at the Ushant Front. Top left: fitted values against normalized residuals; top right: autocorrelation function of residuals with 95% confidence intervals as blue dashed line; bottom left: histogram of residuals and bottom right: Quantile plot.

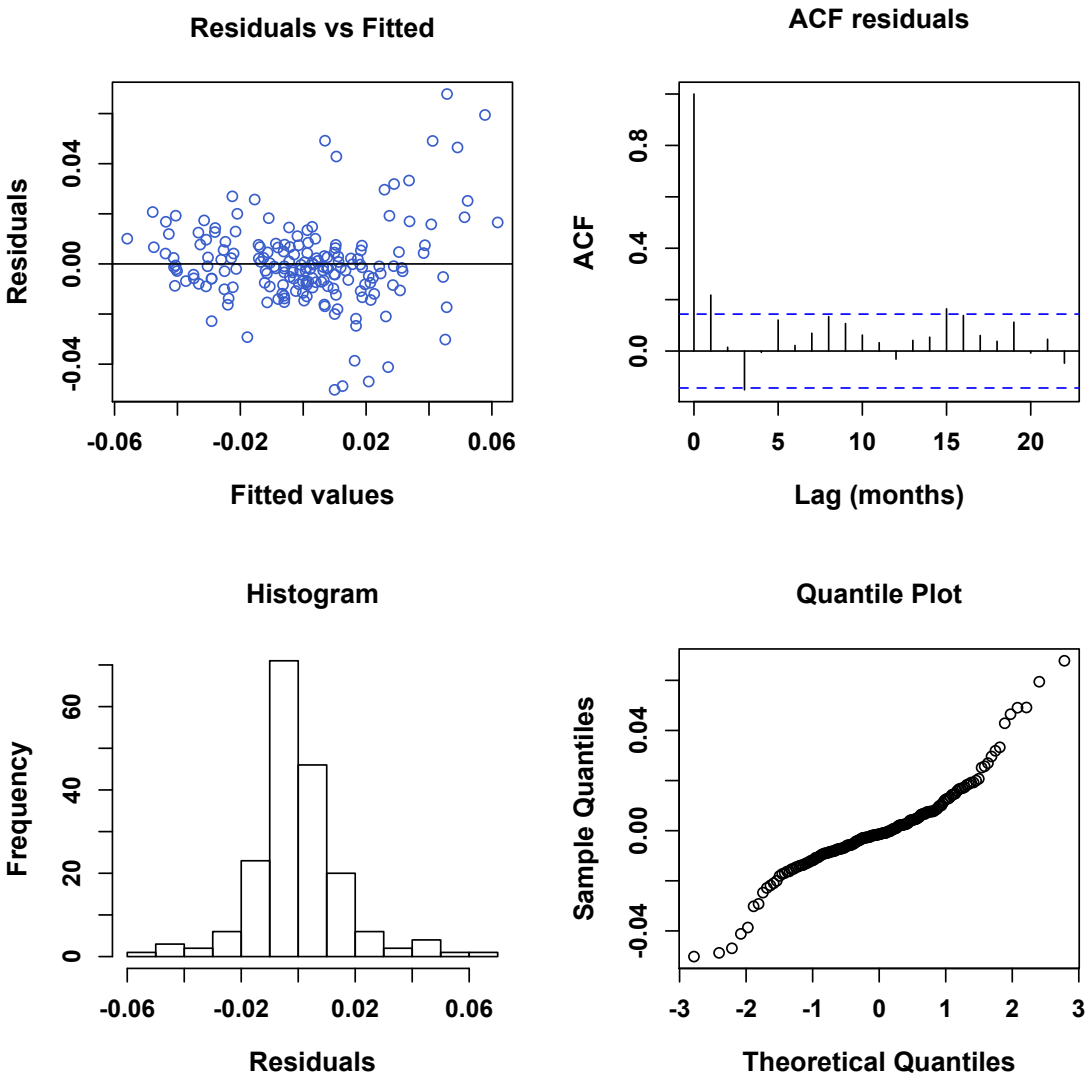

Sup.Figure 3.8: Model validation plots of residual analysis for meteorological drivers of interannual variability of *Fprob* at the Ushant Front. Top left: fitted values against normalized residuals; top right: autocorrelation function of residuals with 95% confidence intervals as blue dashed line; bottom left: histogram of residuals and bottom right: Quantile plot.

4 Fronts as boundaries: Frontal density gradients restrict dispersal of passive floating organisms on shelf-seas

Distribution and abundance of zooplankton directly affects dependent predator species (e.g. commercially important fish) and populations dynamics of organisms with planktonic life cycle (e.g. the benthos). Consequently, identifying distribution drivers and dispersal mechanisms of zooplankton is essential for our understanding of ecosystem functioning. This research investigates a boundary effect of tidal mixing fronts on zooplankton distribution in the English Channel. The influence of local movements of the Ushant Front on abundance of *Calanus helgolandicus* and echinoderm larvae was investigated using monthly satellite-derived frontal maps and Continuous Plankton Recorder (CPR) data from a fixed route between 1990 and 2009. The CPR-route crosses the English Channel from France to England and samples in mixed water conditions, when the front is located to the west of the route and in stratified water when the front is located to the east. The centre of distribution of *Calanus helgolandicus* and echinoderm larvae is in the Celtic Sea to the west of the route. A barrier effect of the Ushant Front was expected to be expressed in changes in plankton abundance in response to the movement of the front (different water mass scenarios). Other environmental drivers of zooplankton distribution were considered (including satellite-derived sea surface temperature and phytoplankton colour index). The movement of the front clearly affected *Calanus helgolandicus* and echinoderm larvae abundance. Abundances of both plankter were low in mixed water conditions and significantly increased when the fronts moved to the other side of the ferry route. A barrier effect of fronts can influence interannual variability in habitat connective, diversity and density of the benthos as well as of plankton-dependent predator species. Phenological shifts in the plankton, such as an earlier spawning of the benthos and larvae development before frontal establishment, could open pathways into other water masses for echinoderm larvae or extent their dispersal range in the future.

4.1 INTRODUCTION

Fronts are hydrodynamic features that separate water masses of different physical properties (e.g. temperature and salinity, see **Table 1.1**) (Belkin et al., 2009). A range of frontal types exist (e.g. estuarine fronts, shelf break fronts), which occur at various spatio-temporal scales (e.g. a few days to persistent features) and are maintained by distinct formation mechanisms (Owen, 1981). Still, common features of fronts are steep gradients in physical, chemical and/or biological properties and often strong current flows, divergences and convergences (Pedersen, 1994; Ryan et al., 2010; Simpson, 1981). Fronts have received considerable attention in recent years as biodiversity and productivity hotspots. Many are considered as sites of ecological significance as they can host elevated numbers of organisms across various trophic levels, have been shown to be associated with frequently re-occurring feeding events and high encounter probabilities of top-predators (Bost et al., 2009; Scales et al., 2014b; Weeks et al., 2015; Worm et al., 2005).

Less attention has been paid to ability of fronts to act as semi-permeable boundaries between differing water masses, affecting the exchange of nutrients and other particles from one side to the other and partitioning ecosystems into distinct habitats (Nihoul, 1981; Sournia, 1994). While a barrier function does not affect mobile species, such as cetaceans and fish as much, it can have impacts on the distribution of the zooplankton. Zooplankton are passive drifters, only capable of minor spatial adjustments and are therefore, subject to currents and other hydrodynamic forces (Sameoto et al., 2010). In addition, most species have a limited physiological capacity of adapting to changes in their physical environment (Fransz et al., 1991). Therefore, a frontal structure, which is accompanied by steep changes in physical characteristics of the water column, can limit the distribution range of zooplankton.

Changes in zooplankton assemblages over frontal gradients have been reported from a variety of fronts, including shelf break, tidal mixing and river plume fronts (Greer et al., 2015; Otero et al., 2009; Sabatini et al., 2002). The affect of fronts on zooplankton assemblages has been attributed to a combination of three main mechanisms: a) physiological inability of zooplankton

species to deal with the magnitude of environmental change or the switch in hydrodynamic regime (e.g. greater turbulence) occurring from one side to the other, b) higher abundance of the preferred food source on one side and c) inability to actively penetrate through the density barrier associated with a front (Franks et al., 1996; Wishner et al., 2006). Hence, the frontal density gradient can affect the dispersal capacities and distributional range of passive drifting organisms and partially control the connectivity between different habitats (Hill et al., 2008; Lee et al., 2005; Munk et al., 1999).

During the stratification season from approximately April to November, the Ushant tidal mixing front develops between the Celtic Sea and the English Channel (Pringree, 1980; Pingree et al., 1978). The front separates the tidally-mixed cooler waters of the English Channel from the seasonally stratified waters of the Celtic Sea. This front is spatially very mobile. Its position depends on the advance and retreat of the thermocline over the seasonal cycle. In addition, the front also performs smaller spatial movements in response to the spring neap adjustment or strong storm events (Sharples, 2008; Sharples et al., 2006). At the beginning and end of the stratification season the Ushant Front tends to run in almost a straight line between England and France at the very western mouth of the English Channel (LeFevre, 1986). During peak frontal season, the front predominantly runs east along the coast of Brittany and then winds north towards the English coast.

Relatively little is known about a potential barrier effect of the Ushant Front. Few existing research found a distinct composition of zooplankton on each side of the Ushant Front and in the actual transition zone (Beaugrand et al., 2000; Grall et al., 1980; Holligan, 1981; Robinson et al., 1986; Schultes et al., 2013). The distribution pattern and changes in species assemblages were attributed to the above-described mechanism, e.g. limited capacity of zooplankton species to deal with large changes in physical properties of different water masses. However, most of these studies focused on the influence of the Ushant Front on community structure, but did not consider an effect of the spatial variability of the front on zooplankton distribution. In addition, the majority of these studies were carried out more than three decades ago and lacked sufficient sample size

to investigate the distribution pattern statistically. Consequently, the majority of these studies are mainly descriptive.

The height of the Ushant Front season, July to September, coincides with the autumn abundance peak of the copepod *Calanus helgolandicus* (Bonnet et al., 2005). The Celtic Sea is the centre of distribution of this copepod that can make up 90% of the zooplankton biomass on the shelf during peak abundance (Bonnet et al., 2005). *Calanus helgolandicus* plays a vital part in transferring energy from the base of the food web to higher trophic levels (Bonnet et al., 2005). The copepod is an important food source for marine organisms from a range of taxonomic groups, such as different development stages of commercially important fish, such as cod, herring and mackerel. Another integral part of the Celtic Sea food web is echinoderm larvae, which are the larval stages of benthic organisms. During the summer months (peak abundance between May and August), echinoderm larvae can make up a large proportion of the zooplankton (Fransz et al., 1991). Although the Celtic Sea provides ideal physical environment for echinoderm larvae and *Calanus helgolandicus*, they are physiologically capable of coping with the ranges of environmental conditions found in the English Channel, including lower temperatures and salinity (Wilson et al., 2015). Still, they are almost absent from the English Channel.

The distribution of both plankter and the spatial variability of the Ushant Front provide a unique setting to study the effect of the front as a potential distribution barrier for zooplankton. If spatial advances of echinoderm larvae and *Calanus helgolandicus* into the eastern English Channel are associated with a spatial displacement of the Ushant Front in the same direction and under consideration of other bio-physical factors known to affect the distribution of the two plankter (e.g. temperature and phytoplankton availability), it is possible to separate a frontal barrier effect from one caused solely by changes in environmental conditions. A barrier effect of seasonally occurring shelf-sea fronts may have direct implications for predator species, larval dispersal and the respective adult population. In addition, knowledge of the causes of small-scale spatial variability

in zooplankton is important when choosing a sampling location for zooplankton studies.

Zooplankton has generally a patchy distribution pattern. In combination with high temporal variability in zooplankton abundance due to sensitivity to climatic forcing, a sufficient large data set is required to investigate zooplankton distribution quantitatively. Even more so at tidal mixing fronts, which can stretch over several 100km, and where differences in zooplankton composition can occur along a single front (Gomez-Gutierrez et al., 2007; Robinson et al., 1986). Only few available datasets have the spatio-temporal resolution to cover an entire frontal feature over sufficiently large enough time scales to capture an association between spatial variations in frontal location and zooplankton distribution.

This research uses satellite-derived frontal maps and Continuous Plankton Recorder (CPR) data from 1990-2009 to investigate the effect of spatial variability of the Ushant Front on small-scale distribution changes of *Calanus helgolandicus* and echinoderm larvae. A selected CPR- route, the Plymouth to Roscoff route (PR-route) runs in a straight line between Plymouth (UK) and Roscoff (France) (Figure 4.1). Due to the mobile nature of the Ushant Front, the PR-route runs either to the east or to the west side of the front. If the front is located to the east of the route, samples should be characterized by shelf water abundances of zooplankton. It is hypothesized that abundance decreases when the front is located to the west of the route, because a boundary effect would hinder specimen to disperse further into the English Channel. The large spatio-temporal extend of the frontal and CPR dataset provides enough data to quantitatively investigate the effect of the spatial displacement of the Ushant Front on *Calanus helgolandicus* and echinoderm larvae abundance under considerations of other known factors that influence zooplankton distribution, such as temperature and phytoplankton.

4.2 METHODS

4.2.1 Plankton collection

Plankton data were collected by the CPR from January 1990- December 2009 in the English Channel along the PR-Route (Figure 4.1) and were provided by Sir Hardy Alister Foundation for Ocean Science (SAHFOS). The CPR is an autonomous recorder, which is towed behind ships of opportunity at about 7-9m depth, at an average speed of ~20kmh (Richardson et al., 2006). Water enters the CPR through a square 1.61cm^2 aperture and is directed through a tunnel, which exits through the rear of the device. Samples are filtered onto a constantly moving band of silk of mesh size approx. 270µm, covered by another band of silk and captured between the two silk layers. On average 3m^3 of water are filtered in each 10nm (18km) transect. However, for time efficiency reasons only alternate samples are counted for most routes. A spatial error of 10-20nm (18- 37km) can be associated with the location of each CPR sample, because transect-midpoint positions are calculated based on navigational information logged by the towing ship whenever the ship changes direction not based short, regular time intervals, which would provide more accurate location data. However, the spatial error can be considered negligible here due to the shortness of the PR-route itself (appr. 145km) and the shortness of the transects (29.0km±0.5km). Therefore, it is assumed that the sampling positions were precise. For specimens smaller than 2mm (e.g. echinoderm larvae), only subsamples are analysed and counts are extrapolated based on a category system. For large zooplankton (>2mm), e.g. *Calanus helgolandicus*, the entire sample is considered. Detailed descriptions of the CPR device, the sampling methodology and analysis can be found elsewhere (e.g.Batten et al., 2003; Richardson et al., 2006; Warner et al., 1994).

4.2.2 Statistical analysis of the effect of spatial variations of the Ushant Front on abundance of *Calanus helgolandicus* and echinoderm larvae

In order to test whether spatial movements of the Ushant Front are associated with changes in the abundance of *Calanus helgolandicus* and echinoderm larvae, only samples from the Plymouth-Roscoff route (PR- route) were considered (Figure 4.1). The PR-route crosses the Western English Channel in

the Ushant Front region. Due to the mobile nature of the front, the PR-route can be located either to the right or to the left side of the front. Monthly maps of frontal density (*Fdens*) at 1km resolution (details in section 2.2.2) and synoptic maps (*Fsyn*) (details in section 2.4.4.1) were consulted for each transect and, depending on the location of the front, the CPR samples were categorized as either: a) '**S': Shelf** water= front is to the right of the route, b) **'C': Channel** water= front is to the left of the route and c) **'M': Mixed** = front is either in line with the route or no clear distinction could be made due to high spatial variability of the front during this month (Figure 4.1). *Fsyn* maps show persistent fronts as two-coloured lines, where each colour refers to either the cold (e.g. blue) or warm side (e.g. red) of a front (Miller, in preperation). This colour coding aids the differentiation between different types of fronts, e.g. tidal mixing fronts and estuarine fronts. Temporarily short-lived features are not included and only strong, persistent fronts are shown. *Fdens* maps combine the strength and persistence of a front (Scales et al., 2014a). In order to highlight areas of frequent frontal occurrence, a spatial filter is applied to smooth out ephemeral frontal segments.

Only samples from April to October were considered in the analysis of *Calanus helgolandicus;* and May to September in the analysis of echinoderm larvae. These months represent the seasonal peak abundance period of each plankter. In addition, months without frontal activity (e.g. due to unfavourable meteorological conditions or insufficient data) were excluded. CPR samples collected close to shore (>49.95°N and <48.9°N) were discarded, because they are likely to be a) influenced by coastal processes, which might have a stronger impact on zooplankton distribution than the Ushant Front and b) are outside of the frontal zone.

Calanus helgolandicus and echinoderm larvae counts were *log10+1* transformed, because initial models on the actual counts of both species were overdispersed. The transformed data were modelled in a Gaussian linear mixed effects model (LMM) with random effects for transect ID (*lmer* function, package 'lme4', R) (Bates et al., 2014; J. Fox, 2002). The **factor 'scenario'** with three levels (C= Channel water, M= Mixed conditions, S= Shelf water) was created to

test whether movements of the front result in changes in *Calanus helgolandicus* and echinoderm larvae numbers. Movements of the front across the PR-route are accompanied with changes in the water mass the CPR is sampling in. Channel water scenarios occur when the front is located to the west of the PR-route and zooplankton abundance is expected to be lower compared to when the front is located to the east of the route and the sample are dominated by shelf water. Mixed scenarios relate to mixed conditions, when no clear distinction between shelf and Channel water can be made. An interaction term between the factors 'scenario' and 'month' was considered to account for scenarios being more frequently encountered in specific months. For example, the Ushant Front moves with the advance of the stratification over the seasonal cycle. Therefore, channel water might dominate at the beginning and end of the season (e.g. May and October), but is less frequently encountered during the peak of the frontal season between July and September.

To distinguish a boundary effect of the Ushant Front from sole influences of environmental and biological parameters known to affect zooplankton distribution, the following variables were considered in the statistical analysis: **SST** was modelled as a continuous linear variable. Monthly gridded SST (°C) composites from 1990-2009, derived from NOAA's Advanced Very High-resolution Radiometry (AVHRR), were provided by PML at 1km^2 resolution. CPR samples from each transect were spatially matched to the SST raster data. CPR samples from the PR-route are based on segments of approximately 28km length. Therefore, each segment crossed multiple SST raster cells. The values of all SST raster cells that were crossed by a single sample segment were averaged and assigned to the corresponding CPR sample. The **Phytoplankton Colour Index (PCI),** added as a factor with four levels and represents a measure of chlorophyll. The PCI is collected by the CPR itself and is obtained by visually assigning a greenness factor to each sample. There are four levels of greenness, which represent the amount of chlorophyll pigments present in the silk, giving an estimate of phytoplankton biomass. The levels are assigned numerical values based on a ratio-scale, derived from acetone extracts using spectrophotometric methods (Richardson et al., 2006). In order to account for temporal autocorrelation caused by the seasonal variability in

zooplankton abundance and the seasonal variability in the location of the Ushant Front as well as interannual differences, the factors **'month'** and **'year'** were included in the model. Depth was not included as an explanatory variable, because the sampling stations along the route were quasi-fixed and no considerable changes in depth over the route occurred, apart from stations near the coast, but these were excluded for the reason described above. A summary of explanatory variables used in the analysis is given in **Table 4.1**.

Prior to the model selection process, collinearity between variables was assessed via Variance Inflation Factors (VIFs) and Pearson correlation. If VIFs were ≥3 or correlation coefficients >6, variables were thought to be collinear (Zuur et al., 2009). Where two covariates were co-linear, only the one producing a lower Akaike Information Criteria (AIC) was considered in the model selection process (Akaike, 1981). To account for autocorrelation caused by continuous line sampling, random effects for 'transect ID' were included in the model. Autocorrelation can result in violation of the independence assumption of linear regression models, which can lead to incorrect model conclusions due to falsely estimated uncertainties and significances (Panigada et al., 2008). The best combination of covariates was based on forward model selection. A series of models with just one covariate were run and the one resulting in the lowest AIC was retained to enter the next round of model selection. If the addition of a new covariate did not decrease the model AIC by >2.0 (for each additional term), the term was not included. Non-significant terms (*p-value* > 0.05) were excluded from the final model. All statistical analysis was performed in 'R' (R Core Team, 2013)and frontal maps were processed in Matlab *v2014b* (Matlab, 2009).

Table 4.1: Summary of explanatory variables used in the analysis

Variable	
Scenario	Factor with three levels (S= shelf water, M=mixed water, C=Channel water), referring to the different water masses
SST (°C)	Continuous, based on monthly SST composites at 1km^2 resolution
Phytoplankton Colour Index (PCI)	Factor with four levels: 1, 2, 3, 4. referring to the greenness of the sample. The higher the number, the greener and the higher the chlorophyll concentration
Month	Factor with 7 levels (April- October) for *Calanus helgolandicus* and 5 levels (May- September) for echinoderm larvae
Year	Factor with 20 levels (1990-2009)
Month*Scenario	Interaction term between 'month' and 'scenario' to account for certain month—scenario combinations occurring more frequently than others

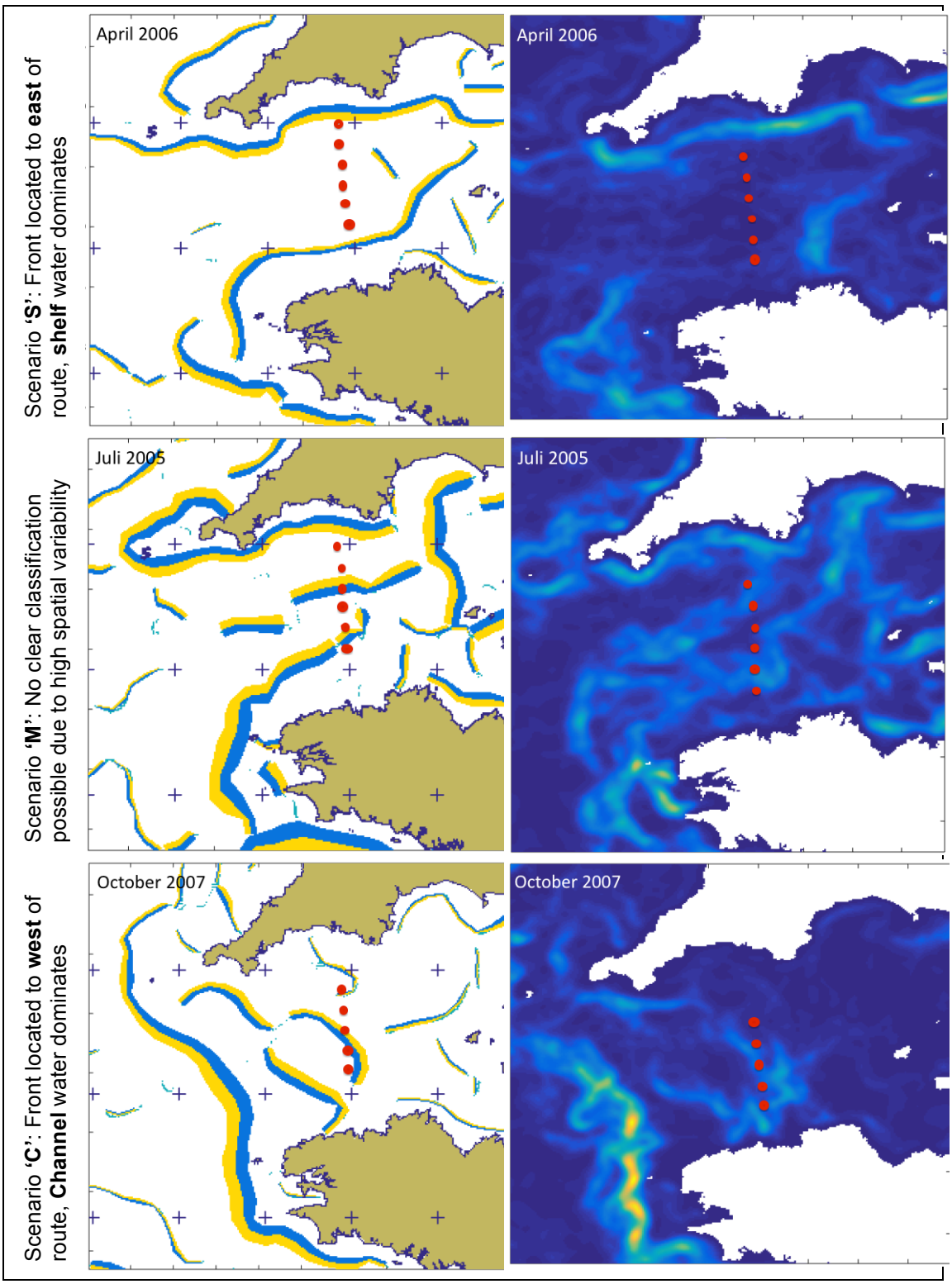

Figure 4.1: Selected Synoptic (left panel) and frontal density (right panel) maps to demonstrate the different classification scenarios: Upper panel: 'S'=Shelf water: the front is located to the east of the PR-route (red dots); 'C'=Channel water: the front is located to the west of the route and 'M'=mixed water: no clear distinction can be made due to a high degree of spatial variability in that month. Synoptic maps show fronts as two-coloured lines, where 'blue' indicates the cold-water side of a front and 'orange', the warm-water side. The thickness of the line represents the strength of the front. Frontal density maps show strong and persistent fronts in yellow and weak ones in blue. The date is shown in upper left corner. The red dots show locations of CPR samples for the corresponding month (PR-route only).

4.3 RESULTS

4.3.1.1 Effect of tidal mixing fronts on small-scale changes in *Calanus helgolandicus* and echinoderm larvae abundance

The analysis tested a boundary effect of the Ushant tidal mixing front by investigating variations in *Calanus helgolandicus* and echinoderm larvae abundance in relation to movements of the front. Although environmental and temporal variables (PCI, SST, month and year) were included in the analysis, they did not explain any variability in the log-transformed abundances of the two plankter, apart from one exception (Table 4.2). Month was significant in explaining some of the variation found in echinoderm larvae abundance. The LMM indicated clear differences in abundances of *Calanus helgolandicus* between the three different scenarios (Figure 4.2). When the Ushant Front was located to the west of the PR-route (Channel water scenario), *Calanus helgolandicus* abundance was significantly lower compared to months when the front was to the east (shelf water scenario) or during mixed conditions. When shelf water dominated (scenario S= front to the east of the route), *Calanus helgolandicus* abundance was highest. In contrast, no clear distinction between echinoderm larvae samples from the different scenarios could be made and only factor 'month' was significant (Table 4.2). Still, echinoderm larvae abundance was higher in mixed and shelf water scenarios than in Channel water (Figure 4.2).

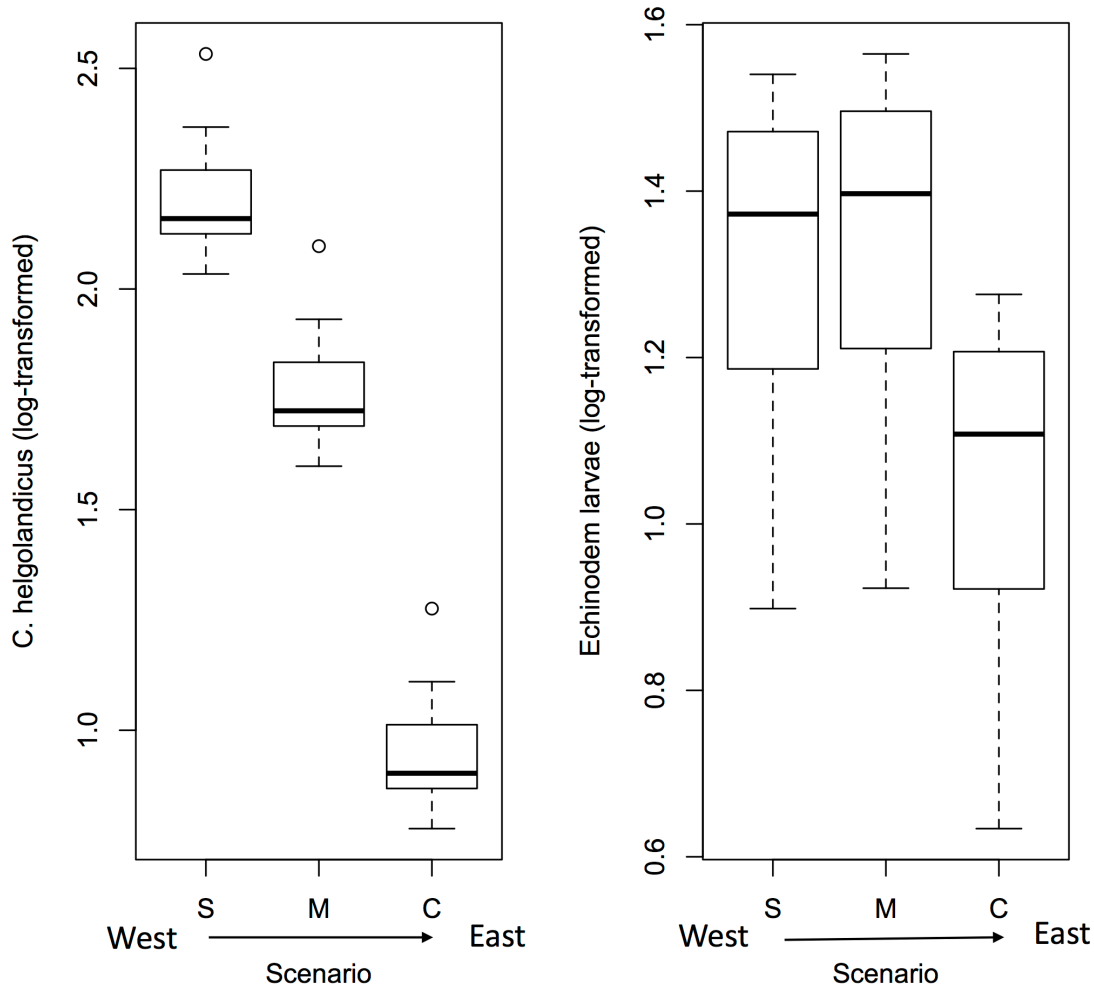

Figure 4.2: LMM (with random effects for transect ID) predictions of *Calanus helgolandicus* (left) and echinoderm larvae (right) abundances (log-transformed) for each scenario: C=Channel: front is located to the west of the PR-route; M=Mixed: no clear distinction is made due to high spatial variability of the front in a given month and S=Shelf: the front is located to the east of the route.

Table 4.2: Summary of LMM (with random effects for transect ID) of log-transformed abundances of *Calanus helgolandicus* (*N*=187) and echinoderm larvae (*N*=135). Significant *p-values* are in bold.

Species	***Calanus helgolandicus***			**Echinoderm larvae**		
Variable	**χ^2**	**df**	***p-value***	**χ^2**	**df**	***p-value***
Scenario	7.06	2	**0.029**	Not significant		
Month	Not significant			9.43	4	**0.051**

4.4 DISCUSSION

4.4.1 Influence of small-scale spatial variability of the Ushant Front on *Calanus helgolandicus and* echinoderm larvae abundance

Spatial variability of the Ushant Front significantly affected the distribution of *Calanus helgolandicus.* Abundance of the copepod was highest when shelf water scenarios were present and lowest when Channel water dominated. *Calanus helgolandicus* is generally associated with warm shelf-waters and the centre of its distribution is the Celtic Sea (Wilson et al., 2015). Dedicated zooplankton studies at the Ushant Front reported highest abundance of *Calanus helgolandicus* in the stratified region, slightly lower numbers within the frontal zone and a decline in numbers on the mixed side (Holligan, 1981; McGinty et al., 2011; Robinson et al., 1986; Schultes et al., 2013). These patterns have previously been attributed mainly to changes in the bio-physical environment, e.g. changes in temperaute, salinity or food availability, rather than a barrier effect caused by a frontal density gradient. Monthly SST values (from 1990 to 2009) corresponding to each CPR sample in this research ranged from 11.0°C to 17.5°C in Channel water conditions and from 9.0°C to 18.2°C in stratified water conditions. The overall SST minima and maxima between the two scenarios was relative small and the temperatures of both water masses are well within the temperature range of *Calanus helgolandicus* (Wilson et al., 2015). In addition, this research did not find a significant effect of SST or PCI on *Calanus helgolandicus* abundance. Therefore, environmental conditions might not be the sole reason for the lower copepod numbers found in Channel water samples. There are some environmental factors that this research did not accounted for, such as salinity, more precise measures food availability other than the PCI or the hydrodynamic regime (e.g. differences in turbulence). Nevertheless, this research suggests that the Ushant Front density gradient affects the distribution of *Calanus helgolandicus* by limiting its dispersal into adjacent water masses.

Although this research did not find significant differences in echinoderm larvae abundance between the three water masses, echinoderm numbers were considerably higher in mixed waters (3.9±3.0) compared to the Channel water (2.8±2.9). Patchy distribution and generally low abundance of echinoderm larvae in the CPR samples lead to large within group variability and is probably one of the reasons why the this study failed to find statistically significant differences in echinoderm abundance between the three scenarios.

Previous studies have reported changes in echinoderm larvae numbers across fronts and often found an increased abundance of larvae right in the frontal zone (Robinson et al., 1986; Weidberg et al., 2014), similar to the pattern seen in this research. Echinoderm larvae are very limited in adjusting their position in the water column and strongly subject to currents (Sameoto et al., 2010). Convergence processes near the front can lead to an entrapment of passive floating organisms and may explain higher echinoderm larvae numbers in mixed scenario conditions (Weidberg et al., 2014). In addition, primary productivity is often elevated near fronts, which would provide favourable foraging conditions for larvae. Furthermore, strong currents associated with tidal mixing fronts could serve echinoderm larvae as dispersal highways. However, it is questionable if echinoderm larvae actively approach fronts or if frontal zones are specifically frequented by the adult population during spawning.

The CPR does not record echinoderm larvae at species level. However, genetic studies conducted on CPR samples collected in the North Sea revealed that the predominant echinoderm larvae species was the sea urchin *Echinocardium cordatum* (Kirby et al., 2005). The development and abundance of this species is heavily dependent on temperature and phytoplankton availability (Kirby et al., 2007). Therefore, it is particularly difficult to attribute the abrupt change in echinoderm numbers in the Channel found in this study to a frontal boundary effect, because the dependency of the larvae to environmental factors is so strong. However, previous research has shown that spatial movements of mobile fronts in California can significantly affect benthic larvae dispersal, settlement rates and in

consequence, adult population diversity (Gosnell et al., 2014). For example, areas that are subject to frequent frontal movements have been found to have a higher benthic diversity than areas mostly dominated by a single water mass. A barrier effect of the Ushant Front on echinoderm larvae distribution could potentially affect benthic population dynamics and provide additional explanations for temporal variations in the benthic community.

4.4.2 Limitations and recommendations

CPR samples were collected over the course of just a few hours, but the different water mass scenarios were based on monthly frontal maps. Even if the predominant position of the Ushant Front in a given month was to the west of the PR-route, there could have been periods where it was located to the east, but that would have not been considered in the analysis. It is therefore possible that a CPR sample was assigned a wrong scenario, e.g. the scenario was shelf water because the predominant position of the front was to the east of the route during that month, but when the CPR transect was performed, the fronts was located to the west of the route.

The CPR samples the surface waters at about 7m depths. However, *Calanus helgolandics* performs vertical migrations at various stages of its life cycle, over the season and even daily at certain times of the year. Similarly, a front is a complex, three-dimensional structure expanding all the way to the sea floor and front-biota interactions cannot sufficiently be resolved by considering the surface layer only. For example, it is not possible to resolve how a frontal barrier function affects horizontal species distribution differently when the organisms are located at greater depth.

Ideally, zooplankton samples should be taken at different depth from a fixed station, which will be repeatedly crossed by the front. Differences between bottom and surface front at various states of the season and with simultaneous measurements of bio-physical variables would be needed to entangle the

confounding information incorporated within seasonal, environmental and biological factors and the actual density barrier.

4.4.3 Conclusion

This research revealed a boundary function of the Ushant tidal mixing front by investigating the effect of the spatial movements of the front on abundance of *Calanus helgolandicus* and echinoderm larvae. A boundary effect of tidal mixing fronts on plankton has direct implications for larvae dispersal, the respective adult population and indirectly affects the distribution of dependent predator species higher up the food chain. Tidal mixing fronts are seasonally occurring and strongly driven by climatic forces. There is some evidence that changing weather pattern can cause alterations in frontal properties in the future, such as an increase in gradient strength, shifts in the timing of the frontal season or expansion of the frontal season. All of these potential consequences of climate change can increase the fontal barrier function in the future. Vice versa, phenological shifts in the plankton, such as an earlier spawning of the benthos and larvae development before frontal establishment, could open pathways into other water masses for echinoderm larvae or extent their dispersal range. Subsequently, this will affect habitat connective and the diversity and density of benthic adult populations.

5 Shelf-sea fronts as conservation sites for marine megavertebrates with specialist foraging ecology

Spatial conservation measures for marine megavertebrates benefit from the identification of diversity hotspots, where multiple species occur in elevated numbers and can be protected within limited available space. While large frontal features have received considerable attention in this regard, tidal mixing fronts have been less well studied. These fronts establish during the summer on shelf-seas and could represent potential conservation sites for megavertebrates in seas heavily used by humans. This study investigates if the Ushant tidal mixing front effects sighting rates of megavetebrate species with different foraging ecologies: a) surface feeding kittiwakes and storm petrels, which benefit from food sources made available near the water surface, b) harbour porpoises, which need to feed frequently to refuel energy deposits and c) for comparison purposes a generalist feeder, the gannet. 16 years of Presence/Absence data (1996- 2010), a range of satellite-derived frontal metrics (strength, persistence, frequency and distance to nearest front) at monthly resolution and other habitat variables (depth, chlorophyll, SST), covering the English Channel and Celtic Sea were used to identify the key environmental drivers of spatial variability of the four study species. Generalized Additive Models (GAM), with Generalized Estimating Equations (GEE-GAM) to account for spatial autocorrelation, revealed a strong positive relationship between frontal strength and kittiwakes, storm petrels and harbour porpoises. In contrast, a significant relationship between any frontal metric and gannets was not found. In addition, frontal metrics relating to persistence of fronts (frontal frequency and frontal persistence) were consistently more significant in describing spatial variations in megavertebrate sightings with specialist feeding ecology than chlorophyll *a*. This research suggest that a) shelf-sea fronts represent predictable feeding locations for animals that rely on food sources in their vicinity and easy accessibility of prey near the surface and b) frontal metrics are more important descriptors of specialist species distribution than productivity Therefore, shelf-sea fronts could be significant conservation areas for vulnerable species.

5.1 INTRODUCTION

The manner in which marine megavertebrates use the seascape is complex and highly variable over differing spatio-temporal scales, habitats and depends on species-specific ecology (Block et al., 2011; Young et al., 2015). This makes conservation efforts more challenging as only limited space is available for the protection of species, which are often highly mobile (Game et al., 2009). Understanding ecosystem dynamics, bio-physical coupling and drivers of species distribution can significantly improve marine conservation planning (Hobday et al., 2014). Identifying biodiversity hotspots and the mechanisms leading to such have therefore, become a key topic in marine ecology. It has become evident that heterogeneous-hydrodynamic features, such as eddies (e.g. Jaquemet et al., 2014), upwelling events (e.g. Hazen et al., 2011) and frontal zones (e.g. Bailey et al., 2010), represent potential conservation areas (Hazen et al., 2013; Hyrenbach et al., 2006), because they support and promote food webs, resulting in bio-aggregations of different trophic levels and recurring feeding events within a small area (Bost et al., 2009; Weeks et al., 2015).

Frontal zones, which separate water masses of different physical properties, have been the subject of a considerable amount of research in this context. Fronts can develop from a variety of mechanisms and occur at a multitude of different spatio-temporal scales, such as the large Polar Current or small temporally variable tidal intrusion fronts (Table 1.1) (Owen, 1981). However, all are characterized by a set of physical processes that lead to a refuelling of nutrients and elevated productivity. Higher phytoplankton standing stocks as well as convergence and current flows along the front are believed to lead to passive and active accumulation of zooplankton, resulting in a cascading effect up the food chain. Aggregations of large pelagic fish as well as small bait fish and larvae have been reported from fronts (Chassot et al., 2011; Klemas, 2013; Woodson et al., 2015), resulting in recurring feeding events (Weeks et al., 2015). For marine megavertebrates, these fronts provide predictable foraging opportunities, higher biomass and easy accessibility of prey (Davoren, 2013).

Tidal mixing fronts, which separate mixed-coastal from stratified shelf waters, develop during the summer stratification on shelf-seas and coincide with the productive season here (Pingree et al., 1975; Simpson, 1981). Primary productivity is greatly enhanced at these features and active as well as passive accumulation of zooplankton promotes the development of biodiversity hotspots (Franks, 1992a; Franks et al., 1996; Gomez-Gutierrez et al., 2007; Pingree et al., 1975; Wishner et al., 2006). However, research on bio-physical coupling at tidal mixing fronts, particular in relation to top predators and mobile species, is extremely limited. This is rather surprising, given that these features are seasonally persistent, far ranging (up to >100km in length), and closer to shore than other known hotspots, for instance the shelf break. These characteristics could make them particularly attractive for breeding birds or smaller cetacean species that have higher energy constraints and rely on predictable and proximate food sources. Some evidence suggests that organisms over a range of taxonomic groups use tidal mixing fronts as foraging areas, such as ocean sun fish (*Mola mola*) (Sims et al., 2002), blue (*Prionace glauca*) and basking (*Cetorhinus maximus*) sharks (Miller et al., 2015; Priede et al., 2009; Queiroz et al., 2012; Sims et al., 1998) or common dolphins (*Delphinus delphis*) (Goold, 1998) and a variety of seabird species, despite having different feeding ecologies (Begg et al., 1997; Durazo et al., 1998). However, most of these studies are conducted at the small-scale, focusing on processes occurring at the fronts themselves rather than investigating a general larger-scale influence of fronts on species distribution. In addition, datasets are often limited as they are based on isolated tagging data or temporally restricted vessel surveys.

The seasonally stratified Celtic Sea and mixed waters of the Western English Channel are considered to be one of the most productive areas on the European Continental shelf and represent foraging ground for a variety of seabirds, cetaceans and other megafauna, some of which are considered vulnerable or endangered (Lauria et al., 2012; Rodriguez-Rodriguez et al., 2015). At the same time, the Celtic Sea and especially the English Channel are subject to anthropogenic pressures directly and indirectly due to heavy shipping traffic, commercial fisheries, recreational activities and high population densities along the

coast (Dauvin, 2012), requiring direct conservation management. Although a network of Marine Protected Areas (MPAs) of various categories have been established on both sides of the Channel (Rodriguez-Rodriguez et al., 2015), there is limited focus on the protection of pelagic biodiversity.

The Ushant tidal mixing front delineates the boundary between the seasonally stratified Celtic Sea and the mixed waters of the English Channel (Figure 5.1). A considerable amount of research has demonstrated enhancement of primary productivity and aggregation of zooplankton (e.g. Grall et al., 1980; Holligan, 1981; Le Boyer et al., 2009; Pingree et al., 1975; Schultes et al., 2013; Sharples, 2008), but no serious effort has been made to extend studies on bio-physical coupling at the Ushant Front to higher trophic levels and subsequently, evaluate its potential as a conservation site for pelagic species.

This study investigates the influence of the Ushant tidal mixing front on the large-scale distribution of multiple mobile marine species at different spatio-temporal scales by means of long-term opportunistic sightings data and a variety of newly available frontal metrics. The frontal metrics include a) the distance to the nearest persistent front (*Fdist*), b) 'Frontal frequency' (*Ffreq*), which is the highlight areas of frequently occurring frontal activity over multiple years and c) frontal probability (*Fprob*), which denotes how often a front was observed in a given time period. The sightings dataset covers a 16-year period (from 1997 to 2010), collected from opportunistic surveys repeatedly crossing distinct hydrodynamic and geographic features on the shelf, including the Ushant Front. It provides a unique opportunity to test whether encounter probabilities of mobile animals at tidal mixing fronts are enhanced and thus, their potential as conservation sites for mobile species.

Species considered in this research are harbour porpoise (*Phocoena phocoena*), kittiwake (*Rissa tridactyla)* and European storm petrel (*Hydrobates pelagicus*), because their foraging ecologies would suggest they use fronts as feeding areas. Kittiwakes and storm petrels are seabirds that pick for zoo- and ichthyo-plankton and, for kittiwakes, small fish near the water surface (D'Elbee et al., 1998; Lewis et

al., 2001) and therefore, benefit from physical processes that make food available near the surface (Embling et al., 2012). Increased feeding activity and abundance at mesoscale features, such as eddies and fronts, has been reported for both these species (Ainley et al., 2009; Begg et al., 1997). Harbour porpoises are small cetaceans that need to feed frequently, making them reliable on predictable prey sources (Brodie, 1995; Lockyer, 2007) and therefore, the physical processes causing such, for example fronts, eddies and tidal forcing (Jones et al., 2014; Mikkelsen et al., 2013; Scott et al., 2010). Northern Gannets (*Morus bassanus*), which are large-bodied generalist piscivors (Lewis et al., 2003), are included in the analysis for comparison purposes.

The combination of the newly available frontal metrics and extensive sightings data, covering multiple species allows for the first time a) to test whether the location and strength of the Ushant tidal mixing front affects the sightings probability of selected mobile marine species, including harbour porpoises, kittiwakes, storm petrels and gannets; b) to test if the association between the front and these animals differ in specialist (harbour porpoises, kittiwakes, storm petrels) and generalist feeders (gannets); c) to evaluate the importance of the Ushant Front in context with other known environmental drivers of species distribution; and d) to asses which frontal metrics best describe the front-biota association for each of the study species, e.g. does the spatial persistence of a front (e.g. a high frontal frequency) have the same effect on animal distribution than the contemporaneous occurrence of a front (e.g. frontal probability).

5.2 METHODS

5.2.1 Data collection

Cetacean and seabird sightings data were provided by MarineLife, an UK-based charity that regularly conducts megafauna surveys in the English Channel, Celtic Sea and Bay of Biscay (www.marine-life.org.uk). Data used in this research were collected between May and October from 1996 to 2010 onboard the following vessels:

2. 1996-2010: the P&O passenger ferry 'Pride of Bilbao', operating between Portsmouth, UK and Bilbao, Spain; and
3. 2008-2010: Brittany Freight Ferries, operating between Poole, UK and Santander, Spain (Figure 5.1).

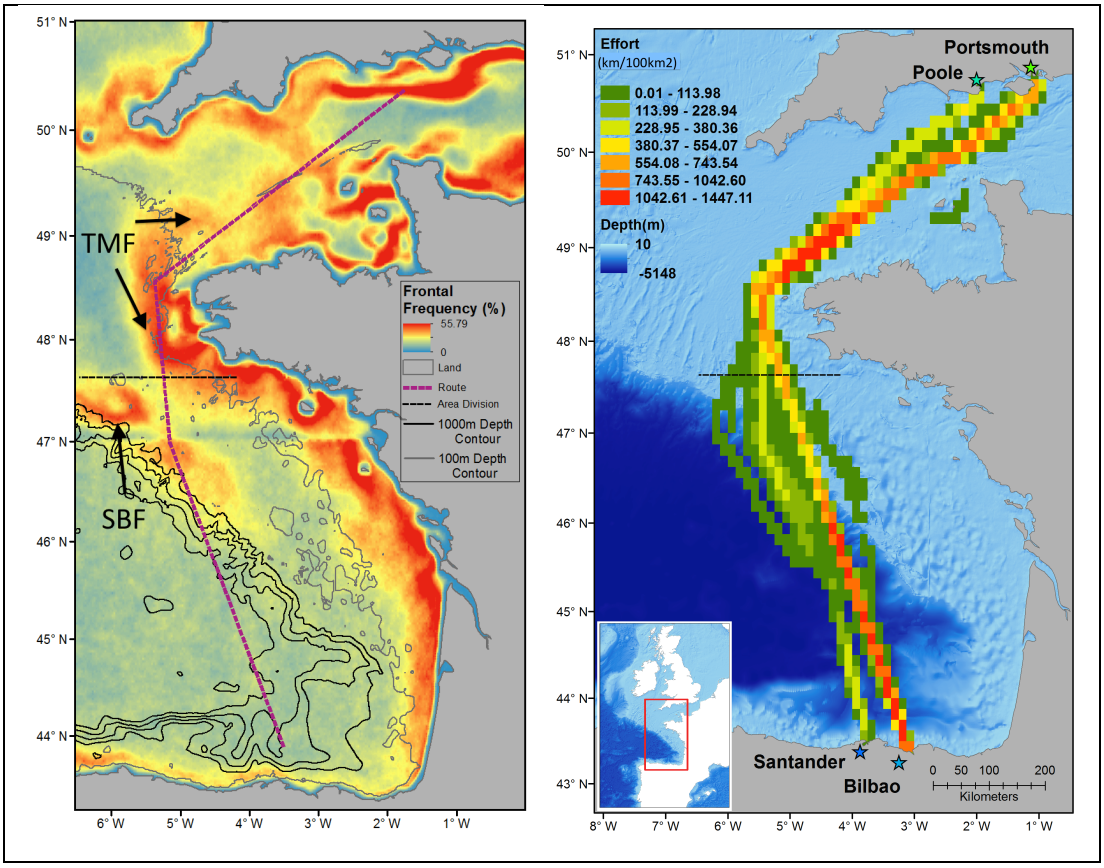

Figure 5.1: Frontal frequency (left) and effort (right) map of the survey area. Frontal frequency map displays areas of frontal frequency in percentage, where blue relates to low and red to frequent frontal areas. The purple dotted line (right map) shows the ferry route. Only data north of the black dotted line was considered for the analysis in this research. Light grey lines refer to 100m depth contours, black lines to 1000m depth contour. Arrows point to the shelf break and the Ushant tidal mixing front, where SBF= Shelf break front and TMF= Ushant tidal mixing front. Effort map shows total km travelled in each 10x10km grid cell during 'on effort' periods (for time scale of analysis only: May-October 1996-2010). Green indicates less, red highest effort areas. Stars refer to the home (UK: Poole and Portsmouth) and destination ports (Spain: Santander and Bilbao) of ferry trips. Underlying bathymetry layer represents depth in metres, where darker areas relate to deeper water. Inset shows sampling area in relation to the UK and Spain.

The ferries followed a dedicated route and hence, transects were not randomized, but repeatedly transited roughly the same routes and associated hydrodynamic features. For the purpose of this research only transects covering the shelf area were considered (shelf habitat), because the focus lies on the tidal mixing fronts (Figure 5.1: shows data collected over the entire ferry route, but only data north of the black line was used for the analysis). Frontal maps cannot distinguish between different types of thermal fronts, such as shelf break or river plume. In order to avoid signal from other frontal features, such as the shelf break, the data set was spatially limited to the south based on the extend of the Ushant Front. Surveys were conducted during daylight hours from the bridge (height: 24-32m) by at least two observers (max. 4) at a time, scanning the sea surface with the naked eye and binoculars. Effort and survey variables were recorded every 15-30min, whenever the vessel changed course or when a sighting was made.

Cetaceans were recorded by a dedicated cetacean observer within a 2000m-wide, 180° arc ahead of the vessel without any distance information until May 2001. Thereafter, distance sampling was employed (Buckland et al., 1992), but without a double-observer platform, which would be required for abundance estimates. Whenever an animal or group of animals was encountered, sightings information (position, number of animals, species, distance, certainty, behaviour, age group) and survey parameters (number of observers, sea state, visibility, cloud cover and swell) were recorded.

Seabirds were recorded by a dedicated seabird observer within. Each seabird observed ahead of the ship was counted once only, with sightings grouped into two minute-long periods and observations were made in two distance categories: within

1. a 300m square box on the starboard side of the ship and
2. a 1000m-wide 180° arc ahead of the vessel.

5.2.2 Data processing

Survey tracks were reconstructed from effort-waypoints and divided into 10km-segments, which were used as the sampling unit. This resolution was chosen in order to account for the spatial scale of the environmental variables and to reduce zero-inflation (e.g. smaller segment size would have resulted in 99% zeros for the most common cetacean species). Segments that were shorter than half a segment length (<5km) were discarded, which was predominantly the case at the end of each transect or shift.

All entries missing information essential for data analysis, such as sea state and visibility, were excluded. Cetacean sightings made at distances of >2000m were not considered, because species records prior to 2001 did not include sightings outside this distance range. Furthermore, effort and sightings made when visibility was <2000m and in sea states ≥4 were excluded.

5.2.3 Explanatory variables

5.2.3.1 Frontal metrics

A variety of frontal metrics were used to investigate the importance of fronts on marine top megavertebrate distribution at different temporal scales and time lags. A detailed methodology on frontal detection and processing of frontal maps employed in this research is given in Miller (2009), but here we focus only on information relevant to this particular analysis.

All frontal metrics described below are based on Advanced Very High-resolution Radiometer (AVHRR) data from National Oceanic and Atmospheric Administration (NOAA) satellites. Fronts are detected on each satellite image by application of the Single Image Edge Detection algorithm (SIED; Cayula and Cornillon (1992)), where the definition threshold of the cross-frontal temperature gradient is set to 0.4°C. Due to frequent cloud cover over the survey area, monthly composites (weekly ones would have been largely obscured by clouds) at 1.1km^2 resolution were used for all metrics, unless stated otherwise.

Firstly, maps of **frontal probability** (*Fprob*) were produced to investigate the influence of contemporaneous fronts on animal distributions. *Fprob* represents a proportion of how many times a front was observed in a given area and hence, indicates frontal occurrence at a given location. *Fprob* can range between 0 and 1 (Miller, 2009). In addition, *Fprob* lags of 1-3 months were included in the analysis to account for the time it may take a frontal effect to reach the upper trophic levels. Lags of more than 3 months were not considered, because data exploration suggested no relationships with response variables at higher lags. Please note that the term frontal probability is slightly misleading as *Fprob* is not a probability, but a proportion of the number of frontal occurrences in a given location over a given time period. However, the term frontal probability has been widely used for this particular metric in the literature and is therefore, used in this study as well.

The ratio between two consecutive monthly *Fprob* maps (***Fprob*_Ratio**= Map_t/Map_t-1) was used as a proxy for frontal establishment (frontogenesis) and break-up (frontolysis). The processes of frontogenesis and –lysis have been linked to steep increases in primary productivity and might therefore, be of particular importance to marine organisms. Each pixel on a *Fprob-Ratio* map represents the ratio between the *Fprob* value of this pixel of the current month and the previous months. High values indicate areas with either frontogenesis (values>1), or -lysis (values <1). Monthly lags for *Fprob_Ratio* were likewise included in the analysis.

Although animals may be encountered at higher numbers at the frontal zones, there might also be increased abundance in its vicinity, because of spill-over effects from productivity gradients associated with a feature or animal movements to/away from the front. Furthermore, the different spatio-temporal scales of the sightings and oceanographic datasets (sightings made at a given time versus temporal averaged oceanographic data) can result in an offset between sightings and frontal occurrence. Therefore, **distance to the nearest front** (*Fdist*) was included in the analysis, which presents the distance (as in number of pixels) from a given location to the nearest major front (obtained by smoothing each map with a Gaussian filter of five pixel width) (Scales et al., 2014a).

Frontal frequency maps (*Ffreq*) were employed to investigate the importance of frontal regions 'known' to marine megavertebrates. In contrast to *Fprob*, *Ffreq* maps show areas of persistent frontal occurrence over large time scales rather than contemporaneous fronts. Instead of reacting to immediate features only, mobile marine species may also frequent areas where they have experienced frontal processes and associated productivity in the past (Nabe-Nielsen et al., 2013). *Ffreq* is expressed as the percentage of time a strong front was observed in a given location, where 'strong' is defined by an arbitrary threshold value (*Fcomp* ≥0.015) (Miller et al., 2014). *Ffreq* maps are based on averaged *Fprob* data that has been collected over a given time frame. In this study, a single *Ffreq* map was created from data obtained between 1997-2010 during the months May to October.

5.2.3.2 Other environmental covariates

In order to assess the degree to which fronts affect species distribution in a realistic context, environmental variables, known to influence animal occurrence, were also considered: Satellite-derived **chlorophyll *a*** was used as a representative for primary productivity. Areas of enhanced primary productivity often lead to the establishment of food webs and a positive relationship has been well established for a large variety of marine megavertebrates, including the ones considered in this research (Tremblay et al., 2009). Due to the temporal extent of this analysis, products from MODIS-Aqua, SeaWiFS and MERIS were combined by the ESA Ocean Colour Climate Change Initiative (OC_CCI) to create a dataset consisting of monthly chlorophyll *a* composites at 4km^2 resolution from 1997-2010 (OC-CCI Product User Guide, www.esa-oceancolour-cci.org/index.php?q=webfm_send/318). As for the frontal metrics, lagged chlorophyll *a* of 1-3 months was assessed in order to allow the effect of primary productivity to work up the food chain to the top levels (Jaquet, 1996). Monthly **SST** (°C) composites from 1997-2010, derived from NOAA's Advanced Very High-resolution Radiometry (AVHRR) were provided by NEODAAS at 4.8 km^2 resolution. SST is a known driver of distribution of a range of marine species (Tremblay et al., 2009).

General Bathymetric Chart of the Oceans (GEBCO) 1-minute gridded **bathymetry** data was obtained from the British Oceanographic Data Centre (BODC) and displayed as negative values in meters (Hunter et al., 2003). **Percentage slope** (%) was based on the GEBCO bathymetry dataset and calculated using the '*Slope'* tool in ArcMap 10.1 (ArcMap, 2012). The Slope tool calculates the maximum rate of change between cell and its eight neighbouring cells. The maximum change in elevation over the distance between the cell and its eight neighbors is assigned to the centre cell. Bathymetric variables, such as depth and slope are particular important to cetaceans, but have also been shown to be linked to seabird distribution. For instance, harbour porpoises have a limited diving range (max 200m depth) and are therefore usually not found in deeper waters (Westgate et al., 1995). Locations of high slope are often associated with physical processes, such as upwelling events. These, in turn may lead to the establishment of feeding events as described in section and their importance for multiple taxonomic group is well documented (e.g. Correia et al., 2015; Gill et al., 2015; Tremblay et al., 2009). A summary of environmental, temporal and survey variables can be found in **Table 5.1**.

Assigning environmental covariates to the sightings data was done in Matlab 7.8 (Matlab, 2009). Environmental variables were provided in raster format. Each 10km-sightings segment crossed multiple raster cells. Instead of just averaging all values of raster cells that were crossed by a given 10km-segment to obtain a single value, the following approach was used: Each 10km-segment was first split into 1km long sub-segments. Explanatory covariate values were then interpolated to the midpoint of each 1km-segment via weighted linear interpolation using the closest four data points (*interp* function, Matlab 7.8). Subsequently, the mean of extracted values for each sub-segment was taken to obtain an overall value for a given 10km-segment. This approach provided a more precise value of the underlying environmental data. For instance, raster cells that were only covered by a small portion of a 10km-segment, are given less weight than a cell that is crossed entirely by a segment.

5.2.3.3 Additional variables

Survey conditions can significantly affect the detection probability of marine animals, particularly cetaceans during visual surveys. Therefore sea state, swell, cloud cover, visibility and number of observers were included in the analysis to parameterize bias introduced by varying survey conditions. Year was modelled as a continuous variable to assess changes over time.

Table 5.1: Information on spatial and temporal scale and numerical values of explanatory variables used in the analysis. Abbreviations are explained in the text. Chla: Chlorophyll *a*.

Variable	Unit	Spatial resolution	Temporal scales	Range
Fprob	Probability	1.1km^2	monthly+lags 1-3, 1996-2010	0- 1
Fprob_Ratio	Ratio	1.1km^2	monthly+lags 1-3, 1996-2010	0.1- 1.34
Fdist	No. of pixels	1.1km^2	monthly, 1996-2010	0- 112.68
Ffreq	%	1.1km^2	averaged 1996-2010	0- 100
Chla	mg/m^3	4.8km^2	monthly+lags 1-3, 1997-2010	0- 12.09
SST	°C	4.8km^2	monthly, 1996-2010	9.45- 24.6
Depth	m	2km^2	static	-4557- 1.0
Slope	%	2km^2	static	
Year			1996-2010	1996- 2010
Sea state	Beaufort	Recorded every 15-30min		0- 6
Swell	Douglas	Recorded every 15-30min		0- 3
Cloud-cover	Okta	Recorded every 15-30min		0- 8
Visibility		Recorded every 15-30min		0- 7
Observer No.	No of Obs.	Recorded every 15-30min		1- 4

5.2.4 Statistical analysis

Generalized Additive Models (GAMs), constructed within a Generalized Estimation Equations (GEEs) framework, were used to investigate environmental influences on species distribution (Hastie et al., 1987; Zeger et al., 1986). Presence/absence of each species 10km-segment was modelled using binomial GAM-GEEs (with logit link function). All statistical analyses were performed in R (R Core Team, 2013).

This dataset was collected on ships of opportunity and therefore, transects could not be randomized, but instead were repeatedly taken over the same vessel routes and often at the same times in the day due to the ferry timetables. Longitudinal data collected in this manner commonly displays spatial and temporal autocorrelation, resulting in violation of the independence assumption of linear regression models, including GAMs (Panigada et al., 2008). Ignoring autocorrelation can lead to incorrect model conclusions due to falsely estimated uncertainties and significances, suggesting insignificant covariates to be retained in the model (Panigada et al., 2008). To account for the dependence between consecutive segments, a correlation structure was added to the GAM using GEEs. GEEs are an extension of Generalized Linear Models (GLMs), allowing for errors to be correlated within pre-defined 'clusters', but independent between them (Zeger et al., 1986). Standard errors and parameter estimates are adjusted accordingly, avoiding false significances of model terms. Adequate choice of correlation structure and clusters are required, but GEEs have been shown to be generally robust to misspecifications of these parameters (Pan et al., 2002). The extent of the spatial and temporal autocorrelation in this dataset was examined during data exploration and clusters were specified as 'day within transect'. One transect describes a full return journey from England to Spain and back, which takes about 3 days including stop over. Competing correlation structures were tested using Quasi Likelihood under Independence Model Criterion (QIC) (Pan, 2001a; 2001b), as obtained by the *QIC* function in the R-package 'MESS' (Ekstrom, 2014). For all models the independence structure was chosen, because it resulted in the lowest *QIC*. In addition, Pan (2001b) advises to use the independence structure if the form or correlation between residuals is not entirely clear. Here, points within clusters are considered uncorrelated and model estimates remain unchanged, but standard errors are adjusted (Hardin et al., 2003).

Prior to the model selection process, collinearity between variables was assessed via Variance Inflation Factors (VIFs) and Pearson correlation. If VIFs were <3 and correlation coefficients >6, variables were thought to be collinear (Zuur et al., 2009).

The GAM-GEEs were built using the *geeglm* function in the R-packages 'geepack' (Halekoh et al., 2006), and 'splines' to extend the GLM to a GAM. The modelling approach used here is largely based on Pirotta *et al.* (2011). Survey variables were modelled as factor and all others as continuous. Initially, B-splines were fit for each of the continuous covariates with four degrees of freedom (df) and one internal knot at the mean of the value range. These were compared to the linear form of each variable and the one with lower QICu was retained for the model selection process. Similar, collinear variables were compared and only the one with the lowest QICu was kept during the model selection process. Forward selection was carried out by creating a series of models including one covariate only and an offset term to account for unequal segment length. The model with the lowest QICu was retained and extended by a set of new models, each containing one of the remaining covariates. This procedure was repeated until the addition of a new variable did not decrease the QICu by more than 2 for each parameter added. The significance of each covariate in the in final model was verified by running Wald's Test, obtained via the *anova* function in 'geepack'. Variables that were not significant were removed one by one and the model was re-run until only significant variables remained (p-value <0.05).

Model fit was assessed by constructing a receiver operating characteristic curve (ROC), where the area under the curve (AUC) indicates the goodness of fit (Boyce et al., 2002). Values below 0.7 are considered poor and 1.0 represents a perfect fit (Cumming, 2000).

5.3 RESULTS

5.3.1 Survey summary

During the study period from May to October 1995-2010, 99 transects were completed over 360 survey days, which corresponds to 85,289km of effort in total (entire dataset: 150,294km) (Table 5.2). A total of 9,001 of 10km-segments were used in the analysis with 81% of the data collected on the Portsmouth to Bilbao Route (PoB) from 1995- 2010 and 19% between Poole and Santander (PS) within

a three year (2008-2010). There was significant variability in survey effort between months (one-way ANOVA: $F_{5,86}$= 7.36; *p-value*: >0.001, Sup.Figure 5.1) and year (one-way ANOVA: $F_{14,86}$= 2.4; *p-value*: 0.024, Sup.Figure 5.1). Effort was highest in June/July and decreased August to October. In addition, a notable increase in the kilometres surveyed occurred in the last three years of the study period due to the addition of the PS-route.

Table 5.2: Summary effort and survey statistics. Numbers are based on data used in analysis only (May-October 1996-2010). One transect corresponds to a return journey from the UK to Spain and back.

Statistic	**Whole survey**	
Shelf only		
Total number of survey days	360	360
Total number of transects	100	99
Total effort (km)	150,294.4	85,289.46
Total number of 10km-segments	15,179	9001
Average segment length (km)	9.90	9.48
Range segment length (km)	5.0- 10.0	5.0- 10.0
Average ship speed (kmh)	34.7	35.2
Most frequently recorded visibility category	6	5
Most frequently recorded sea state (Beaufort)	3	3

Of the species considered in the analysis, gannets were by far the most commonly encountered and the most abundant species, followed by storm petrels, kittiwakes and harbour porpoises in that order (Table 5.3). Harbour porpoise and kittiwake distributions were restricted to the shelf, although occasional sightings were made beyond the shelf break (Figure 5.2). Harbour porpoises appeared to be clustered around the southern part of the Ushant Front. Storm petrels and gannets were found as far south as the Bay of Biscay, but in notably reduced numbers (Figure 5.2). No clear distribution patterns were identified for gannets. Within the study area, storm petrels were encountered most often around the southern Ushant Front and in the middle of the Channel.

Table 5.3: Summary statistics for cetacean and seabird species included in the analysis. Right columns: entire dataset (all months 1996-2010 and Sea states); left columns: time period considered in the analysis only (months May-October 1996-2010; Sea state ≤4).

	Data included in analysis		**Entire dataset**	
Species	**Total number**	**Total sightings**	**Total number**	**Total sightings**
Harbour Porpoises	977	375	1206	446
Kittiwakes	908	420	11857	3756
Storm Petrels	2228	647	2151	699
Gannets	48408	16949	75529	25432

5.3.2 Effect of the Ushant tidal mixing front on species distribution

A variety of frontal metrics was used in this study, with multiple temporal lags and ratios. However, the only metrics retained during model selection, displaying a significant relationship with species distribution were *Fprob* (concurrent and lagged versions) and *Ffreq* (Table 5.4).

Kittiwakes showed the strongest association with frontal features. *Fprob* with a three months lag was the most significant environmental variable to explain kittiwake occurrence in a strong, positive linear relationship (Figure 5.4, Sup.Figure 5.2 and Sup.Figure 5.3). Similarly, harbour porpoises displayed a significant positive association with *Fprob* (with no lag), but in contrast to kittiwakes it was not the most important covariate to describe their distribution (**Error! Reference source not found.**, Sup.Figure 5.2 and Sup.Figure 5.3). The relationship between storm petrels and *Ffreq* was non-linear and showed a strong increase at lower frontal values and then slowly levelled off. The distinct drop at high frontal frequencies may be due to low data coverage here (Figure 5.5, Sup.Figure 5.2 and Sup.Figure 5.3).. In contrast to the other study species, no significant relationship between gannets and any frontal metric was found (Figure 5.6, Sup.Figure 5.2 and Sup.Figure 5.3). Although *Fprob* entered the model selection process, post-hoc Wald's test found it to be insignificant and the covariate was excluded.

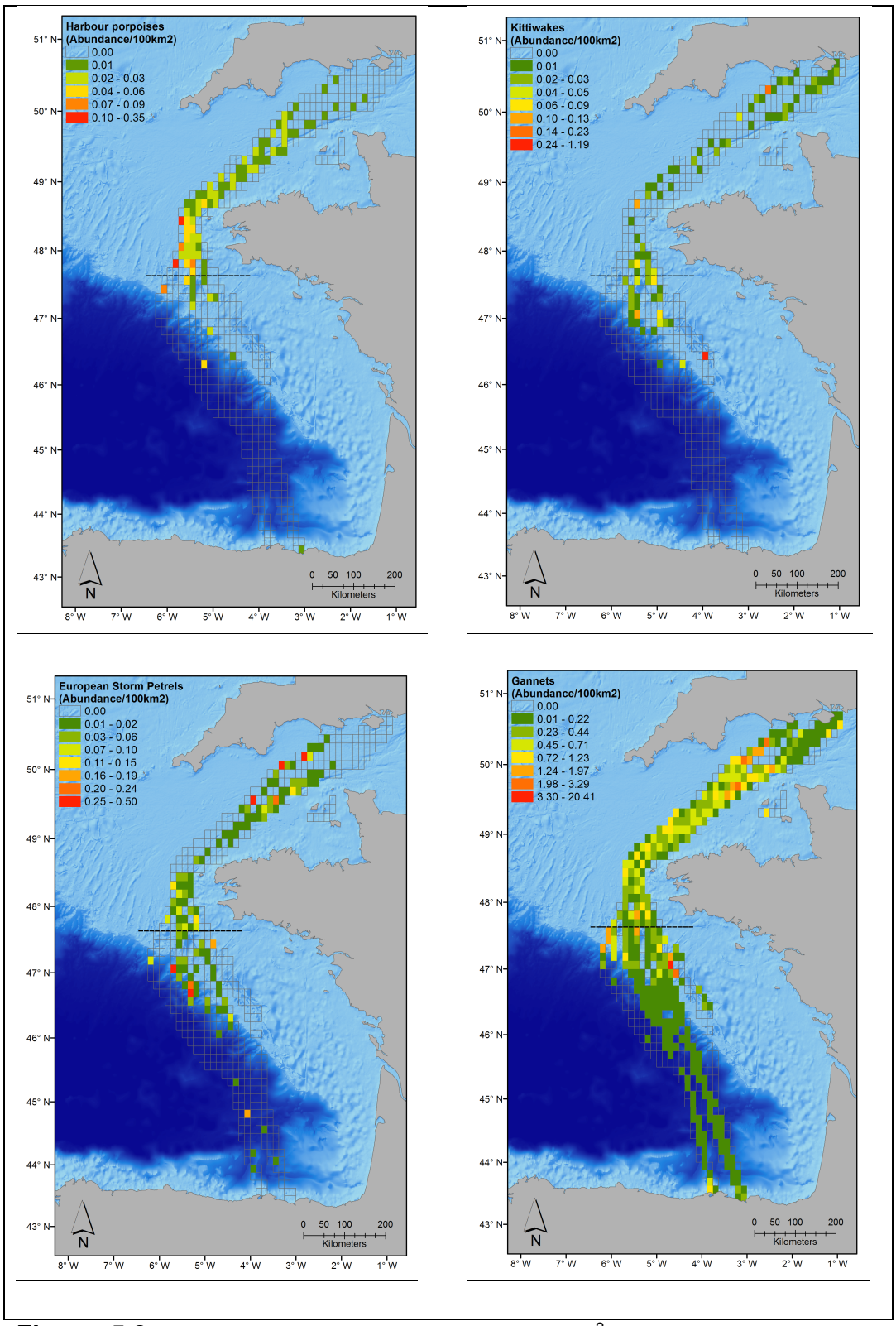

Figure 5.2: Effort corrected abundance per 100km^2 of study species, where green indicates low and red high abundance areas. Black dotted line represents habitat boundary between shelf and bay as used in the analysis.

5.3.3 Importance of frontal metrics in relation to other environmental variable

In comparison with other environmental variables, significant frontal metrics lie in the mid range in terms of their importance on species distribution. SST and, in particular, depth were the main drivers of distribution for most species, except kittiwakes (Table 5.4). Generally, the relationship between these variables and mobile marine species were non-linear, indicating particular depth and temperature preferences or seasonal patterns (Figure 5.3 to Figure 5.6, Sup.Figure 5.2 and Sup.Figure 5.3). Depth and SST are known descriptors of habitat preferences. Frontal metrics were the most significant variables to influence species distribution thereafter, displaying positive relationships with all species except gannets (**Table 5.4** and (Figure 5.3 to Figure 5.6, Sup.Figure 5.2 and Sup.Figure 5.3). It most cases fronts were more important than chlorophyll *a* (Table 5.4). The second most important covariate (after *Fprob* at lag3) to explain kittiwake occurrence was chlorophyll *a* with a lag of three months (Table 5.4). Chlorophyll *a* (lag 1 month) was also retained as a significant variable in the gannet models, but not for any other species (Table 5.4). A negative relationship between slope and harbour porpoises was found, which was positive for kittiwakes (**Table 5.4** and (Figure 5.3 and Figure 5.4, Sup.Figure 5.2 and Sup.Figure 5.3). Survey variables were highly significant factors in influencing animal detection, often more important than environmental variables (Table 5.4). The most important variables were sea state, which affected species occurrence negatively, and the numbers of observers, which increased species occurrence (**Table 5.4**, Sup.Figure 5.2 and Sup.Figure 5.3).

Table 5.4: Results of GAM-GEEs (Cluster: Day within transect; Correlation structure: Independence) of P/A of selected shelf species (*N*=9001), showing the degrees of freedom (df), Chi-squared values (χ^2), p-values and the decrease in QICu-score (QICu- difference) for a given covariate. Environmental variables are ordered by their relative importance based on the order they entered the model. Only significant environmental covariates are shown. AUC= 'Area under the curve' from the ROC-curve analysis serves as an indication of model fit; where 1 symbolises a perfect fit and values below 0.7 indicate poor fit.

HARBOUR PORPOISES (AUC= 0.83)				
Covariate	**df**	χ^2	***p-value***	**QICu-difference**
Sea state	4	66.7	<0.001	-183.57
Depth	4	16.45	<0.001	-86.67
Year	1	12.55	<0.001	-25.28
SST	4	19.75	<0.001	-31.08
No of observers	3	10.51	0.015	-20.02
Fprob	4	16.07	0.002	-17.08
Slope	4	11.71	0.014	-10.99
KITTIWAKES (AUC= 0.74)				
Fprob (Lag3)	1	57.72	<0.001	-48.77
Swell	3	39.2	<0.001	-28.11
Chlorophyll *a* (Lag3)	4	132.26	<0.001	-23.6
SST	4	10.42	0.034	-16.17
Depth	4	13.13	0.010	-15.24
Slope	1	10.21	0.001	-10.48
EUROPEAN STORM PETRELS (AUC= 0.79)				
SST	4	42.75	<0.001	-127.09
Depth	1	13.59	<0.001	-19.55
No of observers	3	22.85	<0.001	-57.02
Sea state	4	16.08	0.002	-29.85
Visibility	5	12.14	0.033	-22.35
Ffreq	4	12.91	0.012	-24.03
GANNETS (AUC= 0.71)				
No of observers	4	62.02	<0.001	-747.97
Depth	4	51.19	<0.001	-126.35
Visibility	5	35.6	<0.001	-104.33
Sea state	4	14.69	0.005	-45.87
Chlorophyll *a* (Lag1)	4	13.12	0.01	-26.07

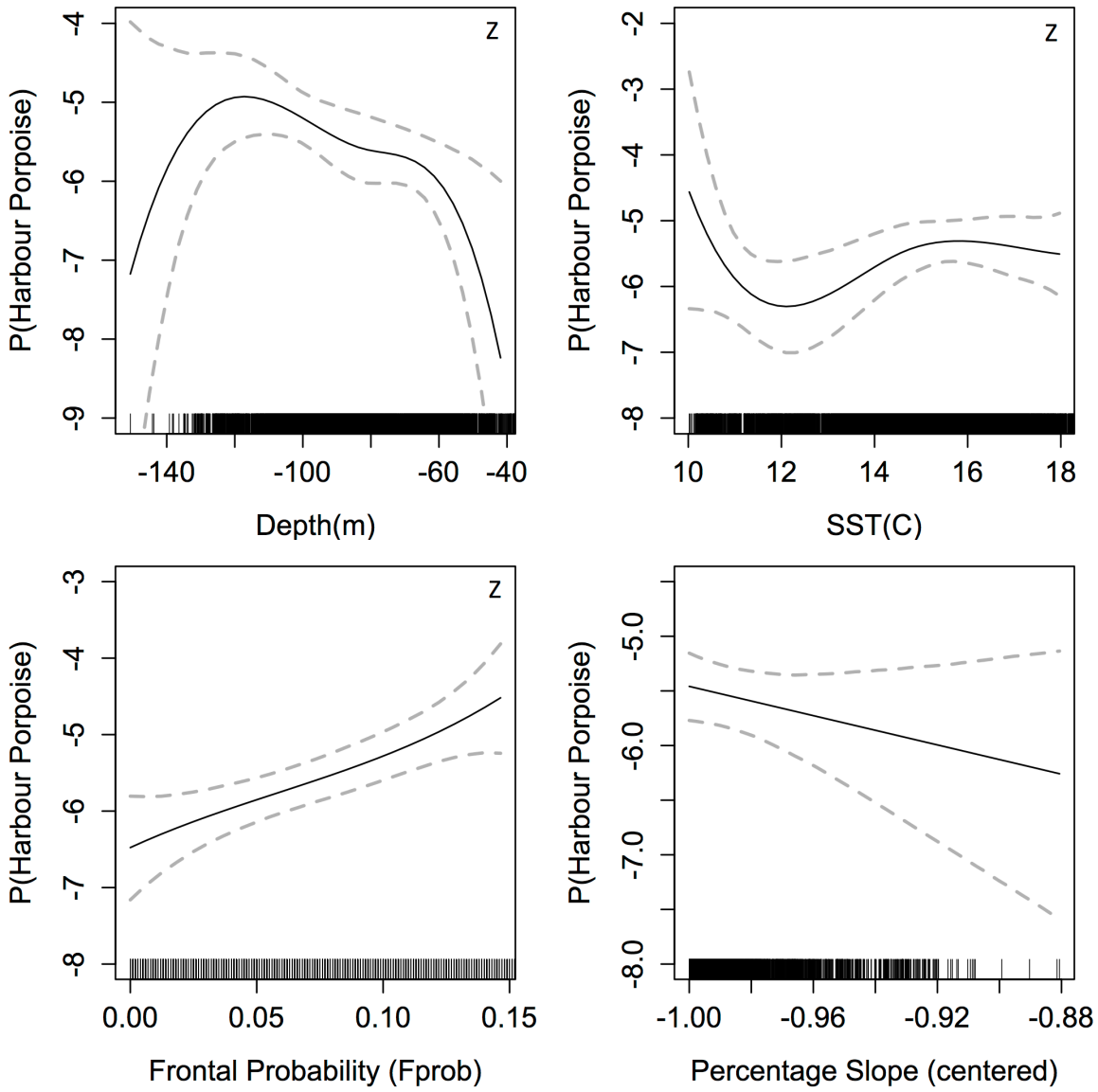

Figure 5.3: Partial fits of GAM-GEE results, showing the relationship between significant covariates and the probability of harbour porpoise sightings (partial residuals). Black lines show model fit and grey lines the GEE-based 95% confidence intervals. Black vertical lines on x-axis (rug-plot) represent real data values. In order to visualize the relationship between response and explanatory variables, some of the partial residual plots were zoomed into (marked with a 'Z'). Full fits and fits of survey variables can be found in the supplementary material (Sup.Figure 5.2 and Sup.Figure 5.3).

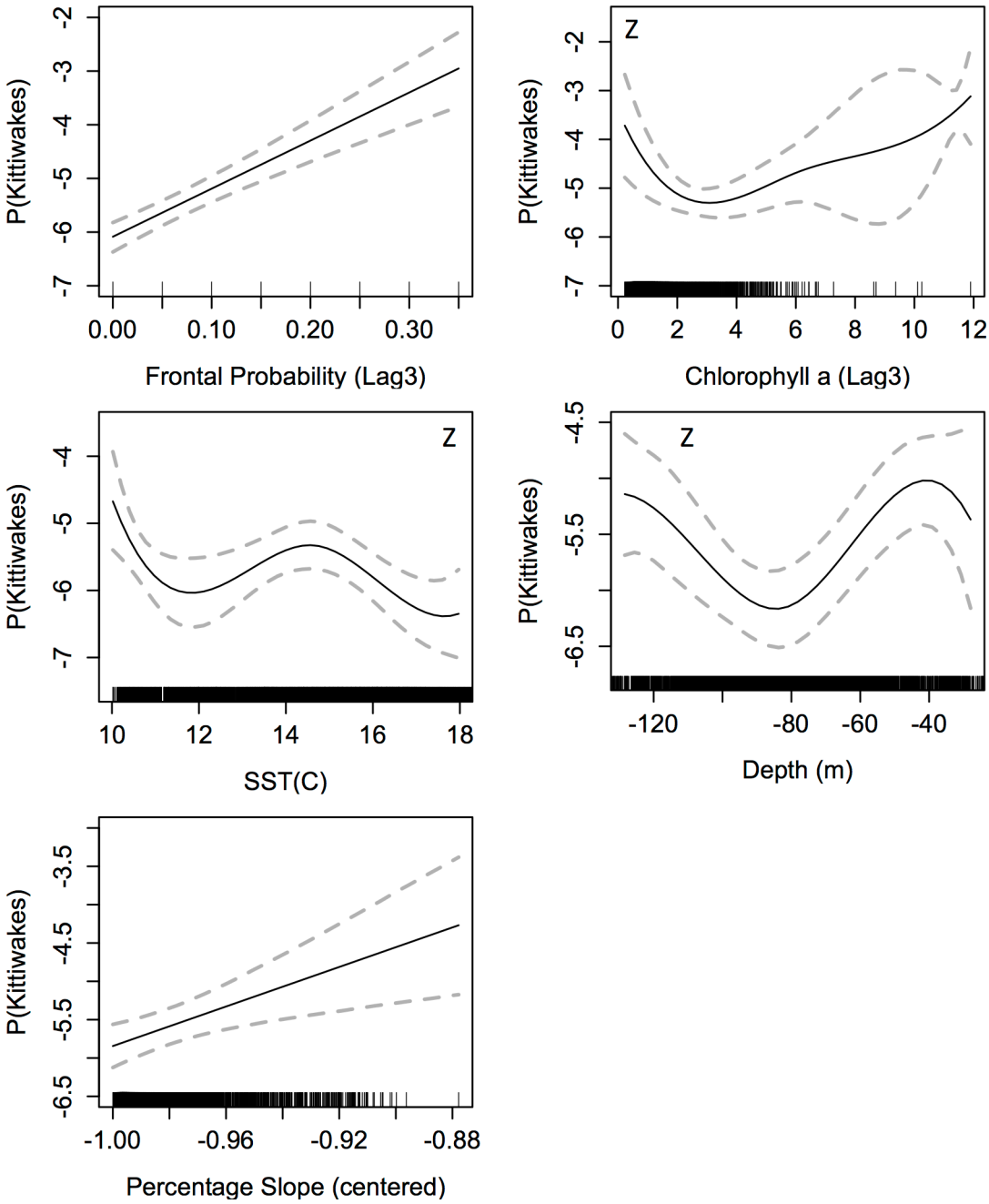

Figure 5.4: Partial fits of GAM-GEE results, showing the relationship between significant covariates and the probability of kittiwake sightings (partial residuals). Black lines show model fit and grey lines the GEE-based 95% confidence intervals. Black vertical lines on x-axis (rug-plot) represent real data values. In order to visualize the relationship between response and explanatory variables, some of the partial residual plots were zoomed into (marked with a 'Z'). Full fits and fits of survey variables can be found in the supplementary material (Sup.Figure 5.2 and Sup.Figure 5.3).

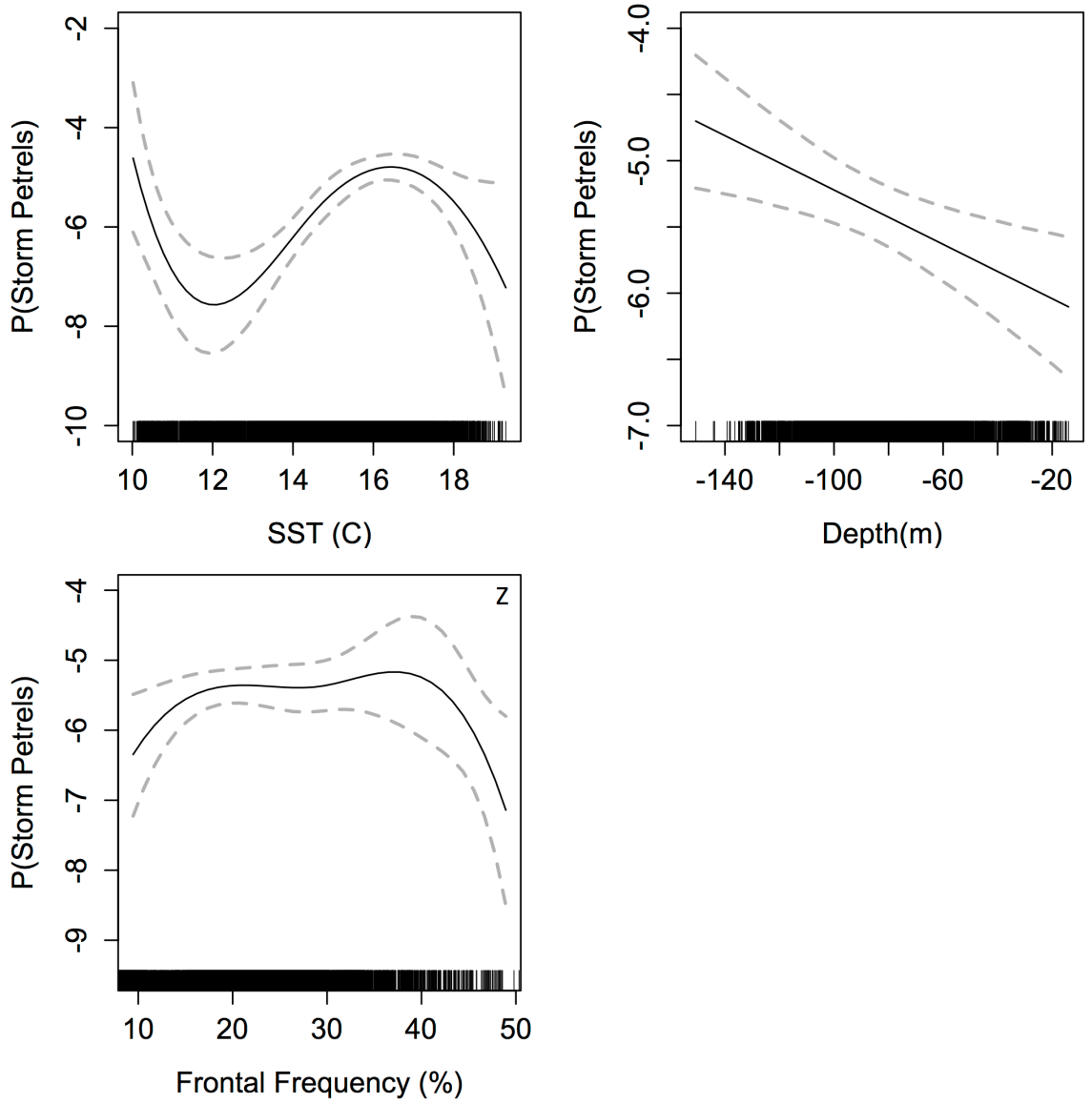

Figure 5.5: Partial fits of GAM-GEE results, showing the relationship between significant covariates and the probability of storm petrel sightings (partial residuals). Black lines show model fit and grey lines the GEE-based 95% confidence intervals. Black vertical lines on x-axis (rug-plot) represent real data values. In order to visualize the relationship between response and explanatory variables, some of the partial residual plots were zoomed into (marked with a 'Z'). Full fits and fits of survey variables can be found in the supplementary material (Sup.Figure 5.2 and Sup.Figure 5.3).

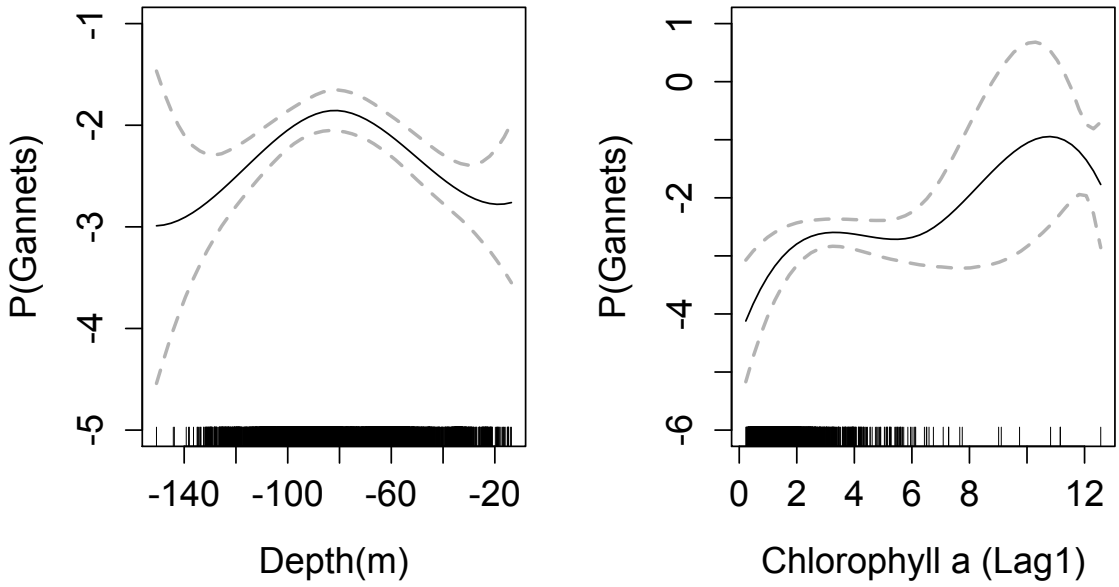

Figure 5.6: Partial fits of GAM-GEE results, showing the relationship between significant covariates and the probability of gannet sightings (partial residuals). Black lines show model fit and grey lines the GEE-based 95% confidence intervals. Black vertical lines on x-axis (rug-plot) represent real data values.

5.4 DISCUSSION

This study investigates the effect of tidal mixing fronts on broad scale distributions of different mobile megavertebrates. By combining long-term sightings data with newly developed frontal metrics, it was possible to analyse associations between species distributions and a selected frontal feature at multiple temporal lags, which has not been done before. All species with specialized feeding ecologies displayed a significant and positive correlation with the Ushant tidal mixing front. The relationship was particularly strong for kittiwakes and harbour porpoises. However, the strength and nature of the relationship differed between all species analysed, probably due to species-specific ecology and foraging strategies. Although different frontal metrics, ratios, and various lags, were considered in the analysis, only metrics that directly measure the magnitude of frontal persistence (*Fprob*) or frequency (*Freq*) were found to be significant variables.

5.4.1 Effect of the Ushant tidal mixing front on species distribution

Numbers of storm petrels and, in particular, kittiwakes were notably higher at the Ushant Front than in non-frontal areas and species distributions were significantly influenced by frontal metrics in the model. Other fine-scale studies have attributed associations between surface feeding seabirds, including storm petrels and kittiwakes, and hydrodynamic formations, such as fronts (e.g. Durazo et al., 1998), internal waves and other tidally driven processes directly to prey availability near the surface (Cox et al., 2013; Embling et al., 2012; Scott et al., 2013). For instance, kittiwakes have been found to take advantage of increased sandeel aggregations near the surface at a sandbank during high tide. Sandeel accumulations at the surface were thought to be due to stronger tidal velocities pushing zooplankton upwards during high tide (Embling et al., 2012). The At tidal mixing fronts zooplankton and other particles are retained within a convergence zone at the surface (Franks, 1992b), providing food for fish and to the seabirds themselves. Although information on the spatio-temporal distribution of prey fish around tidal mixing fronts is lacking, evidence suggests fish abundance is enhanced and more predictable at these fronts (Munk et al., 2009; Ocampo et al., 2013). For instance, the commercial hake fishery on the Patagonian shelf is concentrated over a tidal mixing front during the summer season (Ocampo et al., 2013) and areas of intensified spawning and elevated larval biomass (including cod, haddock and sandeel), spatially coincide with frontal systems in the North Sea (Munk, 2014; Munk et al., 2009), the eastern US shelf (Lough et al., 2001) and elsewhere (Woodson et al., 2015). However, vessel monitoring system (VMS) data from the Western Channel does not show increased levels of fishing activity around the Ushant Front (Campbell et al., 2014; Martinez et al., 2013), possibly due to elevated shipping traffic and controls, such as traffic separation schemes in this area.

Similar, recent studies have shown that harbour porpoises forage in locations of physical heterogeneity, often caused by a combination of bottom topography and tidal forcing (e.g. de Boer et al., 2014; Jones et al., 2014; Scott et al., 2010; Sveegaard et al., 2012). For instance, stronger tidal velocities during high tide over

irregular topography can cause entrapments for zooplankton and can provide enhanced feeding opportunities for harbour porpoises (de Boer et al., 2014). In the Western English Channel McClellan et al. (2014) showed that harbour porpoise distribution closely followed locations of tidal mixing fronts during the summer, but not in other seasons when the these features are absent. There was a strong association between harbour porpoises and frontal probability in this research and a in particular a clear clustering of animals around the southern part of the Ushant Front, which was not as prominent for the other study species. Due to their small body size, harbour porpoises need to refuel their energy reserves frequently and therefore more likely to rely on predictable food sources (Brody et al., 2013; Lockyer, 2007).

Seabirds in flight can scan large areas of the sea for prey, or indicators of prey, such as feeding events, other animals foraging or target hydrodynamic features directly by looking for e.g. frontal slicks that appear on the water surface. Cetacean on the other hand cannot rely on visual queues, but could resort to past experiences. The fact that clustering of harbour porpoises was observed at a particularly strong and stable domain of the Ushant Front, could indicate that cetaceans return to and relying on spatially stable and persistent features that have provided consistent foraging opportunities in the past.

The English Channel is one of the busiest shipping lanes in the world (Halpern et al., 2008), which greatly increases the probability of cetacean mortalities by ship strikes (Van Waerebeek et al., 2007) and causes disturbance by underwater noise (Dyndo et al., 2015; Hermannsen et al., 2014; Weilgart, 2007). Therefore, cetaceans are particularly vulnerable in this part of the European shelf and in need for targeted protection measures. An MPA was established in the vicinity of the Ushant Front in 2007, mainly because of the presence of rich kelp forests and high diversity across a range of taxonomic groups, including benthic and pelagic animals (Parc naturel marin d'Iroise) (www.parc-marin-iroise.fr). However, it also benefits from considerably less shipping traffic compared to the Channel and

provides recovery areas for cetacean, resulting in improved habitat conditions and potentially leading to higher harbour porpoise occurrence as seen in this research.

Although all harbour porpoises, kittiwakes and storm petrels displayed significant associations with fronts, there were clear differences between them in terms of strengths of the relationship, frontal metric and temporal scale. Frontal frequency, which represents locations of persistent frontal occurrence, affects the distribution of storm petrels, whereas kittiwakes (with a lag of 3 months) and harbour porpoises were most strongly linked to frontal probability, relating to concurrent frontal features. Temporal lags often relate to the time it takes biological processes to work up the food chain. For instance, the onset of summer phytoplankton growth can take several months to translate into elevated foraging opportunities for apex predators, such as increased biomass of krill or juvenile fish (Croll et al., 2005). The temporal lag seen in kittiwake occurrence however, is caused their seasonal distribution patterns. Abundance peaks occurred about three months after the main frontal season, which represent passaging birds leaving the colonies between August and October. Despite the frontal strength decreasing at the end of the season, the birds are still foraging in these areas, which suggests even weakening fronts are providing improved feeding conditions for kittiwakes. As discussed earlier, harbour porpoises are present during the frontal season and therefore, lags were not significant. It is difficult to draw any detailed conclusions here due to the restricted resolution of the datasets and lack of behavioural information relating to active foraging, but this most likely reflects species-specific foraging strategy and ecology.

As generalist feeders, it was not expected that gannets would show much of a relationship with fronts, and indeed this was the case. Other studies investigating front-gannet associations have shown weak relationships between this species movement patterns and fronts. Specifically, tagging studies found increased probability of gannets switching to area restricted search behaviour (ARS) around frequent frontal zones in the Celtic Sea (Scales et al., 2014a) and spatial correlations between gannet foraging trips and a tidal mixing front were found in

the North Sea (Skov et al., 2008). Using temperature-depth recorder (TDRs), Cox et al (unpublished data) recently discovered that gannets change their diving strategy from U-shaped to V-shaped at fronts, indicating the influence of oceanography on foraging. Nevertheless, this research suggests that tidal mixing fronts, in particular at the Ushant Front, are not of primary importance for generalist feeders, such as gannets, that have greater capability to adjust their foraging strategy. For instance, gannets are known to often forage around fishing vessels (Bodey et al., 2014; Votier et al., 2013). Specialist feeders and species with restricted physiological capacities however, may rely much heavier on natural predictable foraging areas, such as tidal mixing fronts.

5.4.2 Importance of frontal metrics in relation to other environmental variable

Depth and SST explained most of the spatial variability of the species studied here. Both variables are known habitat predictors for many marine organisms. They define broad scale species distribution, such as shelf versus deep-water habitats, are directly linked to species-specific ecologies, such as cold and warm water preferences and the seasonal distribution related to temperature, such as the breeding season for seabirds. After depth and SST, fronts were found to be the most important environmental factor influencing species distribution. In fact, it was more important than surface chlorophyll *a*, which is a known descriptor of variability of many marine organisms and used as a proxy for biodiversity (Tremblay et al., 2009). Although primary productivity is enhanced at frontal features, no perfect spatial overlap exists and high peaks are also found elsewhere in the Celtic Sea (Miller, 2009; Pingree et al., 1975). Therefore, frontal metrics could represent a better proxy for pelagic diversity of mobile species than surface chlorophyll *a*, because they are directly linked to hydrodynamic processes that can lead to aggregations of prey species, which may not be explained simply by primary productivity alone.

A variety of frontal metrics were used in this analysis, including their ratios and different temporal lags. However, only metrics that directly measure a magnitude in frontal persistence or strength were significant, namely frontal frequency and probability. Distance to front, frontal occurrence and ratios were not found to be important for explaining species distribution. This could imply that a) particularly strong and persistent features are preferentially targeted and b) species abundance abruptly changes near frontal zones. A gradient in animal numbers should have been reflected in *Fdist* being significant. Abrupt changes in abundance could provide some evidence for increased likelihood of feeding events, which tend to establish and disperse quickly. Ratios of *Fprob* were also not found to be significant, indicating established fronts are preferred over frontolysis- and genesis.

5.4.3 Limitations and recommendations

Although the dataset analysed here has proven very useful in revealing the effects of persistent frontal features on the distribution of multiple marine megavertebrate species, the spatio-temporal resolution of the data is not sufficient enough to examine the underlying physical mechanisms leading to the observed distribution patterns. To resolve in detail the aggregation processes, much higher sampling intervals and additional information on animal behaviour and particularly prey fish are required (e.g. Embling et al., 2013). Furthermore, a tidal mixing front is a complex 3-dimensional structure, which can be as small as 1km in width and is temporally variable over scales of just a few days. It is therefore, a simplification to describe a tidal mixing front by 4km monthly averaged satellite imagery that only considers the surface signal. Also, daily sightings data were matched to monthly frontal maps, which could result in a mismatch between the location of sightings and a front on the actual day of the sighting.

Nevertheless, using ships of opportunities provides a cost-effective alternative to dedicated vessel surveys and can deliver large-spatio temporal data sets for investigating relationships with fronts at the broad scale. This analysis has shown a broad scale effect of persistent frontal features on the distribution of multiple

megavertebrate species and provides useful information on the location of potential biodiversity hotspots. These areas can subsequently, be surveyed at high-resolution with a combination of vessel based sensors or underwater robotics and supplemented by tagging studies to tackle remaining questions about the mechanisms of bio-physical coupling and the importance of fronts. A lot of information is needed on the distribution, abundance and behaviour of prey fish at the time of feeding events as well as the establishment, temporal extent and frequency of feeding events themselves around fronts.

5.4.4 Conclusion

This research demonstrates that the occurrence of surface feeders and species with limited physiological capacities are greater at tidal mixing fronts, where they benefit from prey availability and accessibility. The findings suggest a key factor in shaping species distribution is the persistence of suitable oceanographic conditions. For instance, clustering of harbour porpoises was found in a particular strong and stable domain of the Ushant Front, indicating a constant and predictable foraging location. In addition, only frontal metrics directly measuring frequency and persistence were significant descriptors of species distribution. Frontal metrics were more important than most other environmental covariates, including surface chlorophyll *a*. Fronts might therefore, be a better proxy for pelagic diversity than satellite-derived primary productivity, because they are directly linked to hydrodynamic processes that lead to aggregations of prey species. This study provides strong evidence to consider shelf-sea fronts in marine management to safeguard mobile marine animals. They are easy to identify and conservation efforts can be focused on a fairly small area, where a front is particularly strong and spatially stable. Finally, this study shows how low resolution, but extensive datasets are extremely useful in identifying potential diversity hotspots, which can subsequently be surveyed at higher sampling intervals and with the collecting of additional covariates to tackle open question of bio-physical coupling at hydrodynamic features.

5.5 Supplementary material

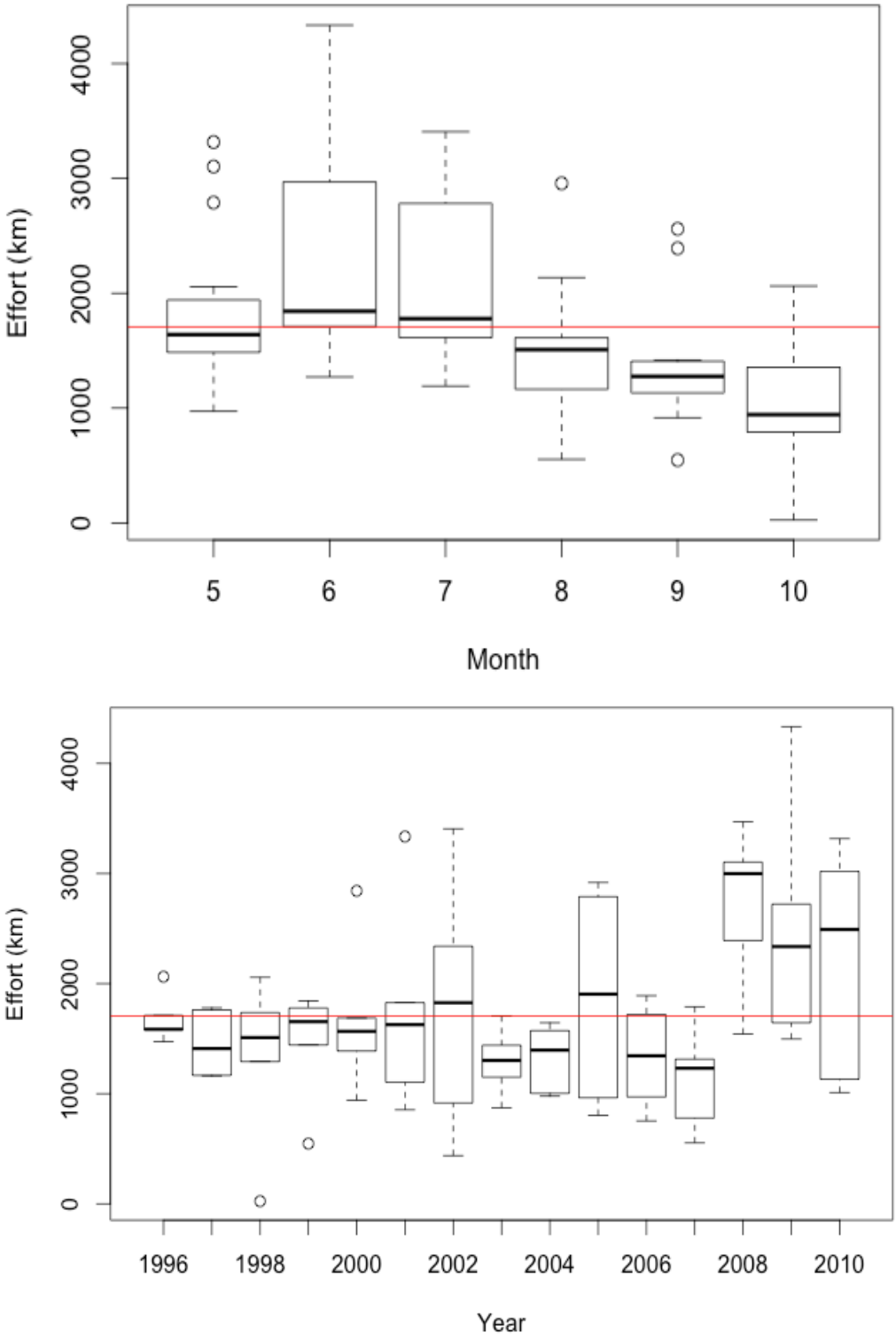

Sup.Figure 5.1: Boxplots showing effort in kilometres for month pooled over all years (top panel) and for year (bottom panel). Red line represents overall mean for month/year.

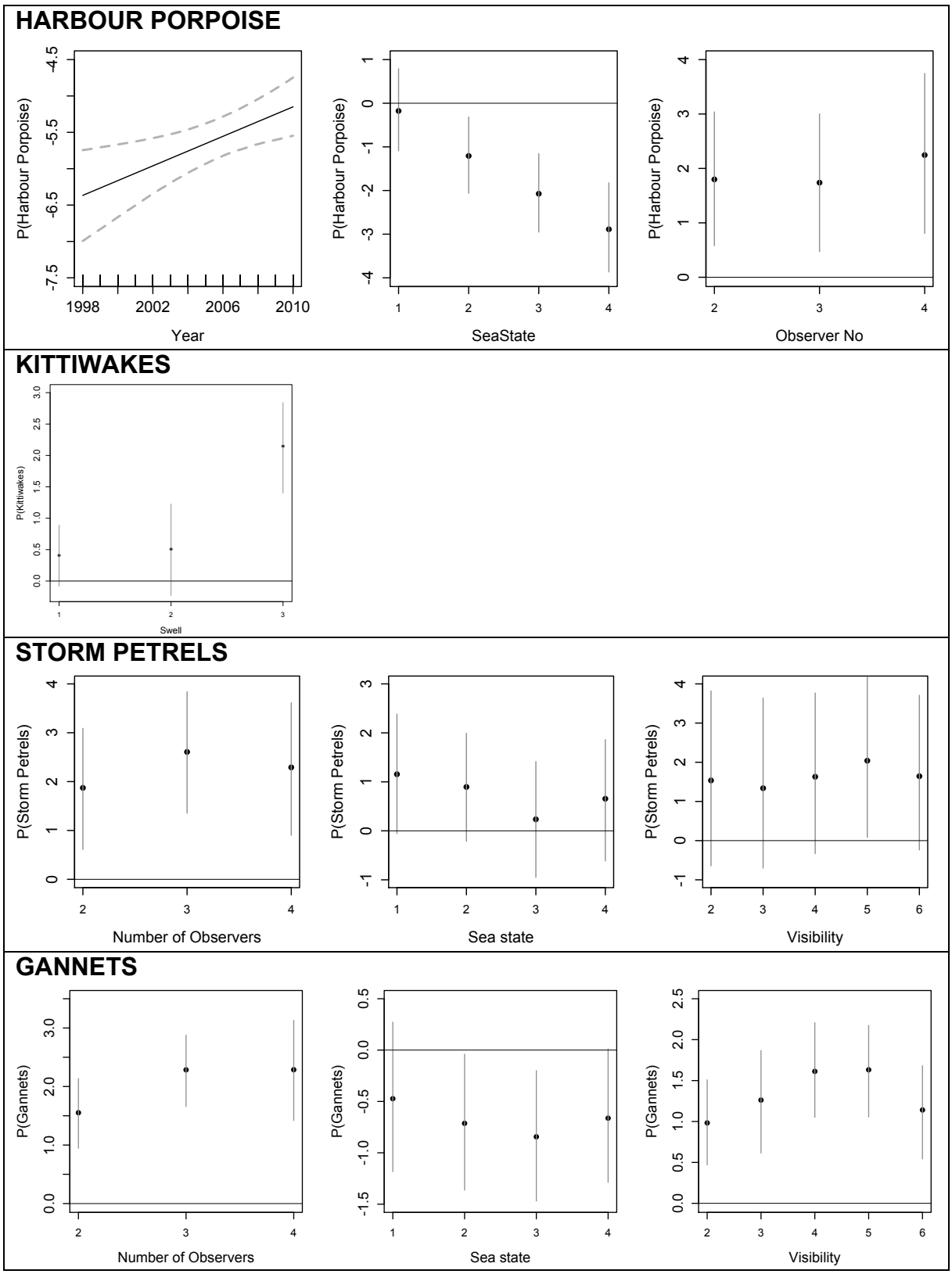

Sup.Figure 5.2: Partial fits of GAM-GEE results, showing the relationship between significant temporal/survey covariates and the P/A of a given species. Black lines/dots show model fit and grey lines the GEE-based 95% confidence intervals.

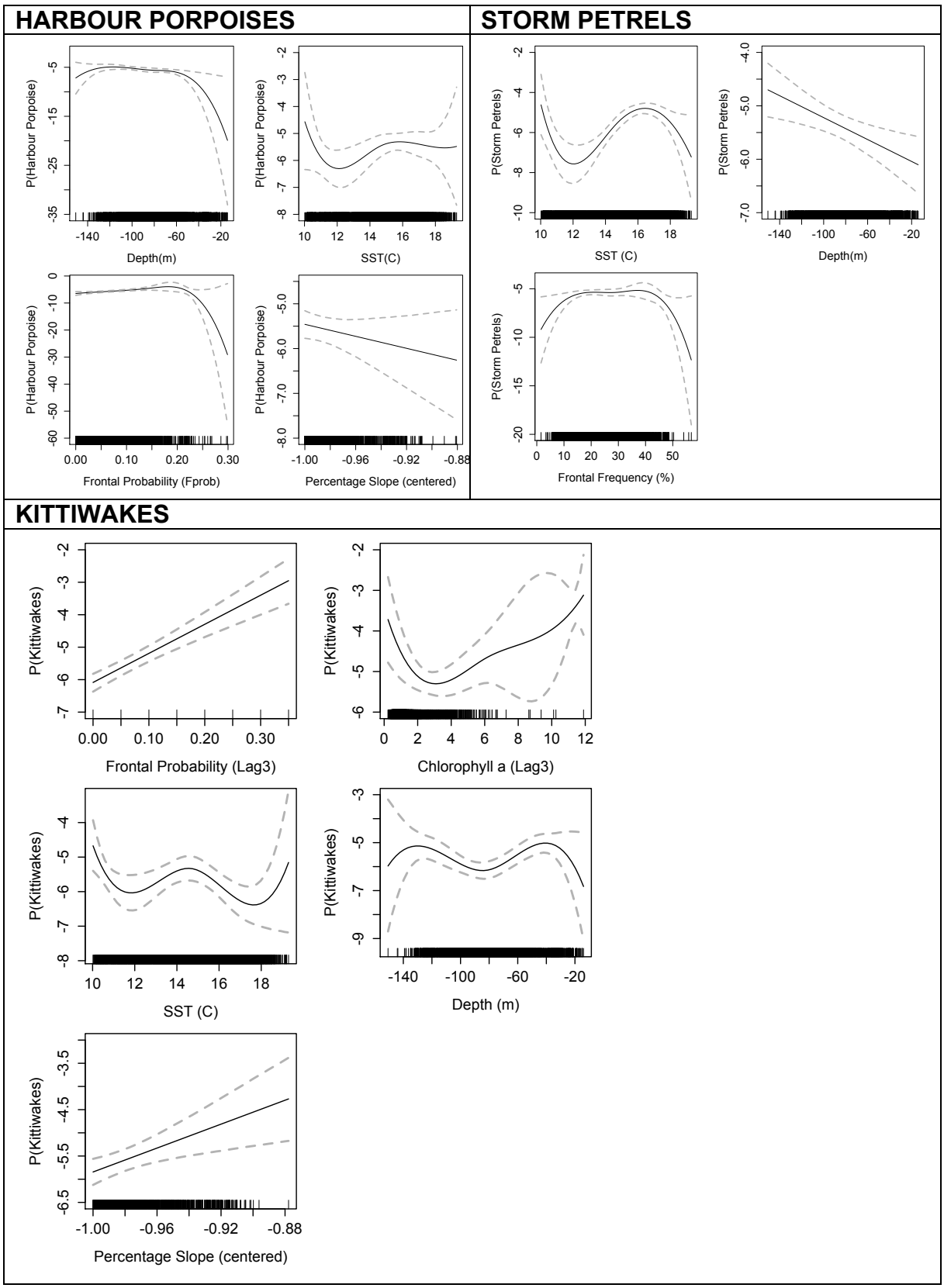

Sup.Figure 5.3: Full partial fits of GAM-GEE results, showing the relationship between significant covariates and the P/A of a given species.

6 Assessing the potential of autonomous submarine gliders for ecosystem monitoring across multiple trophic levels (plankton to cetaceans) and pollutants in shallow shelf-seas

A combination of scientific, economic, technological and policy drivers are behind a recent upsurge in the use of marine autonomous systems for environmental mapping and monitoring. Increased spatial-temporal resolution and coverage of data, at reduced cost, is particularly vital for effective spatial management of highly dynamic and heterogeneous shelf environments. This proof-of-concept study involves integration of a novel combination of sensors onto buoyancy-driven submarine gliders, in order to assess their suitability for ecosystem monitoring in shelf waters at a variety of trophic levels. Two shallow-water *Slocum* gliders were equipped with CTD and fluorometer to measure physical properties and chlorophyll, respectively. One glider was also equipped with a single-frequency echosounder to collect information on zooplankton and fish distribution. The other glider carried a Passive Acoustic Monitoring system to detect and record cetacean vocalisations, and a passive sampler to detect chemical contaminants in the water column. The two gliders were deployed together off southwest UK in autumn 2013, and targeted a known tidal-mixing front west of the Isles of Scilly. The gliders' mission took about 40 days, with each glider traveling distances of >1000km and undertaking >2500 dives to depths of up to 100m. Controlling glider flight and alignment of the two glider trajectories proved to be particularly challenging due to strong tidal flows. However, the gliders continued to collect data in poor weather when an accompanying research vessel was unable to operate. In addition, all glider sensors generated useful data, with particularly interesting initial results relating to subsurface chlorophyll maxima and numerous fish/cetacean detections within the water column. The broader implications of this study for marine ecosystem monitoring with submarine gliders are discussed.

6.1 INTRODUCTION

Shelf and adjacent coastal seas host highly productive ecosystems and are shared by an increasing variety of stakeholders utilizing limited space, e.g. shipping, fishing, aquaculture, recreation, hydrocarbon and aggregate extraction, and renewable energy (Collie et al., 2013; Sharples et al., 2013). These potentially conflicting demands require appropriate management, e.g. through Marine Spatial Planning, a complex task that is dependent upon high quality data and evidence (Douvere et al., 2011; Gilman, 2002).

In addition to the management of multiple stakeholders to ensure that ecosystem health and services are maintained, additional data from shelf-seas are required to meet international statutory obligations such as establishment of Marine Protected Areas (MPAs) and implementation of the EU Marine Strategy Framework Directive (MSFD) (Brennan et al., 2013; European Union, 2008). However, marine mapping and monitoring using dedicated research and survey vessels is expensive, and offshore operations can be hindered due to weather constraints (Schofield et al., 2013).In addition, the spatial and temporal resolution of vessel-based data are often insufficient to fully capture ecosystem dynamics, including the linkage of physical and biological processes, predator-prey interactions, community structure, and the spatio-temporal variability of different ecosystem components (Day, 2008). Satellite remote sensing of the oceans can provide useful supporting data at large spatial scales, but is restricted to sampling the uppermost layers of the sea surface (centimetre). Fixed moorings and profiling floats may provide long time series, but the former only collect data at a single point and the latter are difficult to spatially control (L'Heveder et al., 2013).

Submarine (buoyancy-driven) gliders are a type of Autonomous Underwater Vehicle (AUV) that oscillate through the water column and can remain unattended at sea for several weeks to months (Rudnick et al., 2012). Gliders carrying appropriate sensors can simultaneously monitor a range of physical and biological parameters, and regular surface communications with satellite allow their movement to be controlled and data to be uploaded in near real-time. However,

gliders are relatively slow moving (20-40cm/sec horizontally), making them prone to drift in areas of strong currents (Davis et al., 2009; Leonard et al., 2007). Their sensor load is limited and each mission necessitates a balance between battery life, mission duration, sampling frequency, and data quality (Willcox et al., 2001). Despite these limitations, the scientific research community is increasingly focusing on gliders as a tool for monitoring of features at the meso- and sub-mesoscale, including highly variable and dynamic phenomena such as oceanic fronts, eddies and upwelling regions (Davis et al., 2008).

Traditionally, gliders have been deployed with a basic set of sensors that enable measurement of physical oceanographic parameters such as temperature, salinity or currents (e.g. Bouffard et al., 2010; Merckelbach et al., 2010; M. J. Perry et al., 2008; Ruiz et al., 2009; Todd et al., 2013) and lower trophic levels of the ecosystem, such as phytoplankton and zooplankton (e.g. Baumgartner et al., 2008; R. D. Fox et al., 2009; Frajka-Williams et al., 2009; Guihen et al., 2014; Niewiadomska et al., 2008). More recently, new sensors have been integrated onto gliders that can measure abundance of higher trophic level organisms, e.g. fish and cetaceans (e.g. Baumgartner et al., 2008; Baumgartner et al., 2013; Ferguson et al., 2010; Klinck et al., 2012; Meyer-Gutbrod et al., 2012; Send et al., 2013). In addition, glider 'fleets' are increasingly used to establish ocean monitoring networks rather than single platform deployments (e.g. Alvarez et al., 2013; Alvarez et al., 2012; Bouffard et al., 2012; English et al., 2009). However, until now, there has been limited effort devoted to the simultaneous measurement of physical parameters and multiple biological components of the ecosystem using gliders.

This contribution describes a deployment of gliders carrying sensor loads capable of simultaneously monitoring multiple marine ecosystem components, from physical parameters and chlorophyll *a* fluorescence (CTD and fluorometer) to zooplankton and fish (echosounder), and cetaceans (hydrophone). This 'proof-of-concept' study involved the deployment of two shallow-water gliders off southwest UK in autumn 2013, targeting a known tidal-mixing front in a productive inner-shelf

environment. By targeting a frontal area, the gliders were expected to encounter steep vertical and horizontal gradients in physical parameters and potentially elevated levels of biomass. In addition, fronts in UK shelf waters are considered as potential targets for spatial protection measures (e.g. MPAs; (Miller et al., 2014)) and are therefore a particular target for multi-trophic-level monitoring.

The aims of the paper are therefore to: 1) describe the various sensors that were deployed on the gliders, 2) provide an overview of glider and sensor operations during the autumn 2013 deployment, 3) present some initial scientific results and examples of collected data, and 4) discuss some of the benefits and issues that arose from the glider missions. The intention is that this study will aid future assessment of submarine gliders as a suitable platform for cost-effective, long-term monitoring of shelf-sea ecosystems.

6.1.1 Survey area

The survey was conducted west of the Isles of Scilly, off southwest UK, where shelf waters are <100m deep (Figure 6.1). Here, tidal flows to the northeast and southwest peak at ~75cm/sec during spring tides, and are weakest towards the northwest and southeast. Residual currents flow northwest and northwards with speeds of up to 5cm/sec (Pingree et al., 1989). Shelf waters to the west of the Isles of Scilly are seasonally stratified (typically from late spring to late autumn), whereas inshore waters around the islands themselves remain mixed as a result of tidal-topographic interactions; a series of seasonal bottom and surface tidal-mixing fronts occur at the boundary between these stratified and mixed water masses (Simpson, 1981). Frontal dynamics lead to cooler, nutrient-rich waters being transferred into the photic zone and thus enhancing primary production (Pingree et al., 1976; Simpson et al., 1982), which can in turn lead to fronts (including the Isles of Scilly fronts) becoming hotspots for higher trophic levels such as marine mammals (Beaumont et al., 2007; Leeney et al., 2012). The recognition of a wide variety of important marine habitats around the Isles of Scilly has led to the designation of the Isles of Scilly Marine Conservation Zone (MCZ) in 2013 (Defra, 2013). In addition, the waters around the Isles of Scilly are valuable for marine

recreation and tourism (Beaumont et al., 2007). There is also significant commercial fishing activity in the area, including a nearshore industry for shellfish and crustaceans (Beaumont et al., 2007). There are three traffic separation zones (TSZ) surrounding the islands due to high levels of shipping traffic (Figure 6.1).

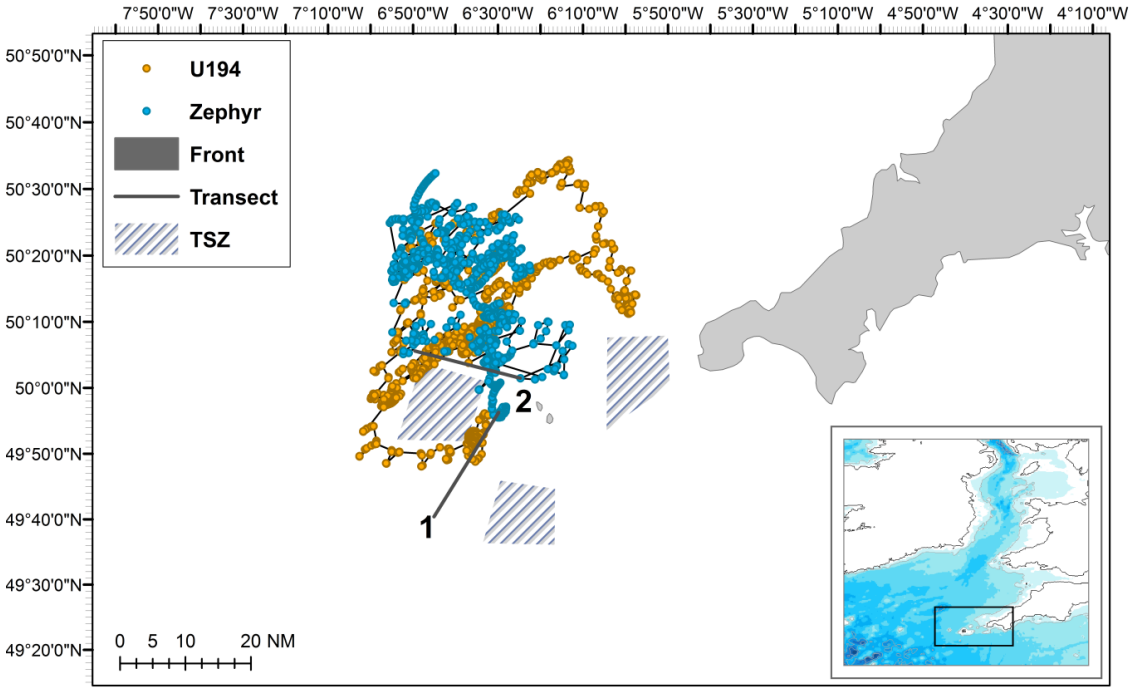

Figure 6.1: Map of survey area and glider positions. Inset shows geographic overview of the survey area and depth contours (dark blue = deeper water; white = land). Enlarged map shows land in grey (Isles of Scilly and west Cornwall). Dots represent glider GPS positions (blue: *Zephyr*; orange: *U194*); thin black lines indicate glider tracks between positions, based on linear interpolation. Large grey arrows indicate the approximate location of the Isles of Scilly tidal mixing front determined by remote sensing (Sup.Figure 6.1). Numbered dark grey lines indicate initial (1) and revised (2) transects. Shaded areas represent traffic separation zones (TSZ). Note that *U194* locations are only based upon GPS fixes received following re-deployment on 04 October 2013 (*cf*. Table 6.1 and Figure 6.3).

6.2 METHODS

6.2.1 Gliders

We used two shallow-water *Slocum* gliders, *Zephyr* and *U194* (Figure 6.2), developed by Teledyne Webb Research Corporation, which are specifically designed for shallow-water operations (<200m). A detailed description of the glider can be found in Webb et al. (2001), but here we focus on aspects relevant to this paper. *Slocums* move through the water column in a saw-tooth motion induced by changes in their buoyancy. A pump transfers seawater in and out of a holding chamber, which results in a change to the vehicle's density; this leads to a sequence of sinking and rising, which is translated into a forward motion by the attached wings. The average horizontal speed is 20-40cm/sec and vertical motion is 10-20cm/sec. Dive depth can be regulated by either a pressure sensor or an altimeter. Due to the shallow depth and varying bathymetry, we used the altimeter with an inflexion height of 10m above bottom to maximise dive depth. Forward and backward shifting of the battery packs controls dive angle; a rudder in the tail fin controls the yaw. When at the surface for communication, an air bladder at the tail is filled for additional buoyancy. Two-way communication is via Iridium satellite connection, allowing for near real-time transfer of subsets of data and manipulation of mission settings. Navigation is by Global Positioning System (GPS) when the vehicle is at the surface, and via dead reckoning during dives.

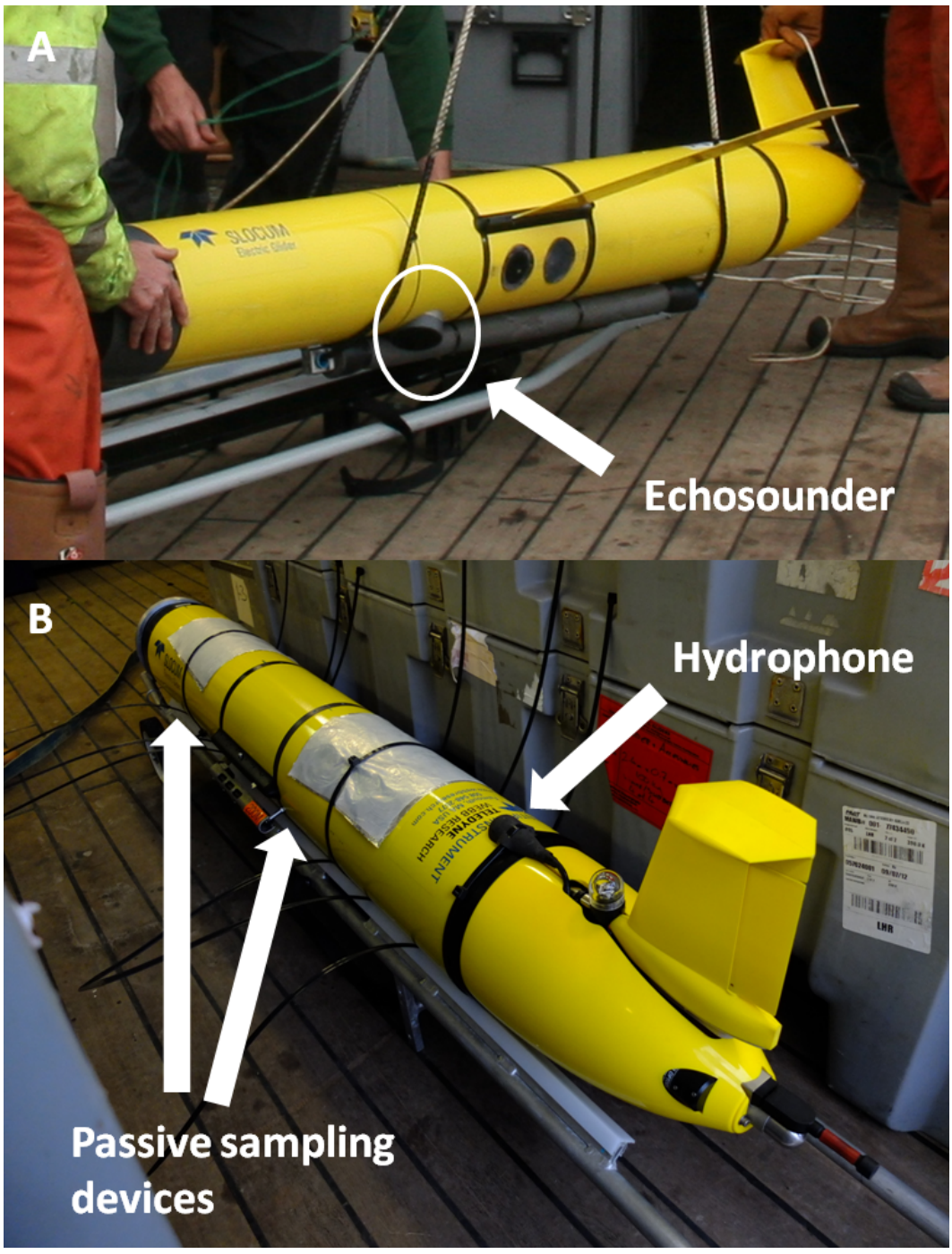

Figure 6.2: A) Picture of *U194* showing ES853 echosounder on the underside of the glider and B) picture of *Zephyr* (wings not yet attached), showing the d-tag hydrophone and silicone rubber passive sampling sheets attached to the glider body.

6.2.2 Glider sensors

6.2.2.1 Oceanographic sensors

Both gliders were equipped with the standard *Slocum* science package, which includes a non-pumped, low-drag, continuous profile Sea-bird SBE-41 CTD (temperature, conductivity and pressure) and WET Labs ECO pucks (BB2FLS, *Zephyr*; FlbbCD-SLK, *U194*), providing combined measurements of chlorophyll *a* fluorescence, coloured dissolved organic matter (CDOM), and backscatter. The excitation wavelengths were 470nm, 370nm and 700nm, the emission wavelengths 695nm, 460nm. The ECO pucks were mounted in the science bay, facing downwards. Also included are an Aanderaa Oxygen Optode 4835 and an altimeter. CDOM and backscatter provide information on organic and inorganic material in the water-column, which would be useful for an in-depth examination on ecosystem dynamics along a tidal mixing front. However, in this study, only temperature and chlorophyll *a* fluorescence measurements are considered for demonstration purposes, which were obtained on a 1Hz sampling frequency. All acquired data were stored internally and a subset transmitted via Iridium each time the glider surfaced.

Ensuring data quality from autonomous vehicles is an important, but potentially difficult task. The issues can be reduced by using stable instruments, such as ship-borne CTD rosettes, and taking calibration cats pre- and post- deployment. Therefore, we used two ship-based CTD casts, one taken directly after *Zephyr* retrieval (21st October 2013) and one taken at day 38 (19th October 2013) of the *U194* mission to correct the glider data (temperature and chlorophyll a) where necessary. Due to the problems of 'in-mission' calibration (e.g. aligning the ship and glider position), we were unable to take CTD casts at the same time and location as *U194*. Therefore, we present the ship-based profile with the nearest spatio-temporal *U194* match (Δ time: 27min; distance: 7.65km). Additional water samples at surface and bottom were taken for chlorophyll *a* measurement verification. A subset of oceanographic data was stored on the National Oceanography Centre (NOC) sftp server and made available to the Met Office via

the British Oceanographic Data Centre (BODC), for inclusion in their Forecasting Ocean Assimilation Models (FOAM).

6.2.2.2 Echosounder

In addition to the standard science payload, glider *U194* was equipped with an Imagenex ES853: a self-contained, single-beam 120kHz echosounder (**Figure 6.2**A). The ES853 was mounted in a science bay, aligned centrally along the short axis of the glider and at an angle of 64° from the long axis (towards the nose). This ensured that when the glider was in a downward glide (typical dive angle of -26°), the transducer pointed directly downwards, analogous with the downward-looking orientation of a ship's echosounder. The echosounder operates with a pulse length of 100μs, beam angle of 10°, range of 100m, configurable gain of either 20 or 40 dB, and measures mean volume backscattering (S_v, dB re $1m^{-1}$) per range bin interval of 0.5m. It requires power of 0.25W, drawn from a 24V DC supply, and can output values to a PC or record data to internal storage. The ES853 has a dynamic range of 120dB and records signals as integer values, thus the resolution in signal strength is reduced compared with typical floating-point recording of larger, ship-based echosounders. The glider-integrated ES853 was controlled via serial port and polled at a frequency of 0.25Hz, with data stored on the glider's internal memory. Upon retrieval of the glider the data were downloaded and processed following Guihen et al. (2014), where raw echo-intensity data were converted to mean volume backscattering strength (S_v), using the active version of the SONAR equation (Urick, 1983) and calibration and manufacturers' constants for echosounder receiving response and source level. Glider position data are used to locate individual pings in time, depth and aspect. These data were then processed using Myriax Echoview software (version 4.80), including subtraction of time-varied gain amplified background noise (after Watkins et al., 1996), and accounting for variability in aspect of the transducer (after Dunford, 2005) and depth of the echosounder. Due to operational difficulties, the ES853 was not calibrated using standard sphere methods (Foote et al., 1987), so data shown here are relative. However, Guihen et al. (2014) showed that a calibrated ES853, mounted on a glider, provided quantitative estimates of zooplankton distribution comparable to a

ship-borne echosounder, providing a suitable sampling strategy is employed. As a result we are confident that the ES853 data provide a relative index of zooplankton distribution.

6.2.2.3 Passive acoustic monitoring

Glider *Zephyr* was equipped with a Passive Acoustic Monitoring (PAM) system based on a modified d-tag sensor (Johnson et al., 2003). The d-tag was mounted in the glider's aft wet space close to the buoyancy bladder, with the hydrophone on top of the glider just forward of the rudder (Figure 6.2B). Power was taken from the glider's main batteries. The sensor was configured to sample at 480kHz, and an automatic detector was implemented to detect the narrow-band high-frequency clicks of harbour porpoise *Phocoena phocoena* (Villadsgaard et al., 2007). A 2ms waveform clip of detected clicks was stored to flash memory. Recordings were also made of acoustic data decimated to a sample rate of 96kHz for offline detection of other cetacean species and the measurement of noise. Although recordings were made using a lossless compression format, which typically gives a compression ratio of 4:1 (Johnson et al., 2013), continuous recording would have filled available storage in approximately two weeks. The recorder was therefore programmed to operate for 10 out of every 40 seconds and only at water depths >40m.

Recovered data were processed offline with PAMGuard software (Douglas Gillespie et al., 2008) to detect cetacean clicks and whistles and to measure noise in third octave bands between 22Hz and 45kHz. An operator (KG) viewed all detections manually, viewing click waveforms and whistle time frequency contours, and listening to sections of data to confirm detections and classify groups of transient sounds as either 'cetacean clicks' or as 'pump noise'.

6.2.2.4 Passive sampling devices for trace organic contaminant monitoring

Passive sampling devices made of a thin layer of polymer were deployed on *Zephyr* (Figure 6.2B). These polymer sheets are made of AlteSil® silicone rubber (24cm x 28cm x 0.5mm thick), and were Soxhlet extracted with ethyl acetate

before further soaking in methanol. Performance reference compounds (PRC; perdeuterated polycyclic aromatic hydrocarbons and fluorinated polychlorinated biphenyls) were then uniformly spiked into the batch of samplers according to a method similar to that described by (Booij et al., 2002). Samplers were kept in closed containers at -20°C until deployment. Control samplers were used to assess possible contamination during transport, deployment and retrieval operations, and to measure initial PRC concentrations. Two sampling sheets were placed on top of the glider and fastened using cable ties (Figure 6.2B). A thin sheet of aluminium foil (muffle furnaced prior to exposure) was placed between the samplers and the glider body to minimize possible contamination of the samplers by direct diffusion from the glider hull itself.

After retrieval, the surface of the samplers was thoroughly cleaned in the laboratory to remove any bio-fouling before static batch extraction with pentane (three times 300mL over 72 hours). Extracts were combined and reduced in volume. The solvent was changed to dichloromethane before clean-up by gel permeation chromatography. The extracts were then reduced in volume and analysed by gas chromatography-mass spectrometry for polycyclic aromatic hydrocarbons (PAHs), polychlorinated biphenyls (PCBs) and other chlorinated organic compounds. Field and laboratory procedures have been described elsewhere in more detail (e.g. Allan et al., 2010; Allan et al., 2013).

6.2.3 Glider mission

Both gliders were deployed southwest of the Isles of Scilly from the RV *CEFAS Endeavour* on 12 September 2013, in order to conduct repeated transects over the targeted tidal-mixing front (Figure 6.1, ‘transect 1’). The approximate location of the front was monitored prior to the survey via satellite-derived front maps (Miller, 2009). A ship-based pre-deployment transect was performed in order to ensure the area was free of static fishing gear (which is common in this area and represents a potential hazard to any glider) and to take repeated CTD and water samples to affirm the transect was located over the target front. A ship-based transect was

performed on 21 October 2013 along the glider survey line (Figure 6.1, 'transect2'), in order to 1) compare the ES853 echosounder data with those collected using the calibrated multi-frequency (38, 120 and 200kHz) split-beam Simrad EK60 on the RV *CEFAS Endeavour*, and 2) to collect CTD and water samples for *U194* calibration purposes. Due to glider control problems encountered during the mission, the initial glider transect (Figure 6.1, 'transect 1') was shifted to the north of the Isles of Scilly on 24 September 2013 (Figure 6.1, 'transect2'). *Zephyr* was recovered from the RV *CEFAS Endeavour* on 21 October 2013 and on this occasion, a CTD cast was conducted for glider-sensor calibration. Due to quickly deteriorating weather, retrieval of *U194* had to be abandoned and the glider was picked up via rib-boat three weeks later on 13 November 2013.

6.3 RESULTS

6.3.1 Mission summary

Strong tidal flows and northwards density currents deflected both gliders to the northwest of the Isles of Scilly soon after deployment on 12 September 2013 (Hill et al., 2008). Unable to counteract these currents, *U194* was pushed into very shallow water West of the islands on 17 September 2013, where manoeuvring was impossible and the glider needed to be recovered. Emergency recovery and subsequent repairs were carried out between 20 September and 04 October 2013 (Table 6.1).

U194 was redeployed on 4 October 2013 via fast-boat northwest of the Isles of Scilly. This also provided an opportunity to update faulty software on the *Zephyr* d-tag; both gliders then resumed their mission. The planned glider transect was repositioned to the north of the western TSZ (Figure 6.1), where tidal flows and currents were weaker and where *Zephyr* had been located for most of the previous three weeks. Using a more dynamic piloting approach (e.g. regularly adjusting waypoints according to tidal flows, changing current correction setting), control of the flight path of *U194* was much improved. In contrast, piloting of *Zephyr* became increasingly challenging following redeployment, possibly due to the hydrocarbon

sensor sheets loosening and adding extra drag to the vehicle (making it more susceptible to current drift). Nevertheless, both gliders executed the mission without any further problems until retrieval. A summary of key events and a timeline of sensor activity are given in Table 6.1 and Figure 6.3, respectively.

Table 6.1: Key events in chronological order

Date	Event
12/09/2013	Deployment
14/09/2013	*Zephyr* d-tag memory card full (no data stored hereafter) until re-deployment
17/09/2013	*U194* 'beached'
21/09-03/10/2013	Recovery and repairs *U194*
04/10/2013	Re-deployment *U194*; exchange *Zephyr* d-tag
10/10/2013	*Zephyr* d-tag stops recording: no power supply due to damaged cable
21/10/2013	Retrieval *Zephyr*
13/11/2013	Retrieval *U194*

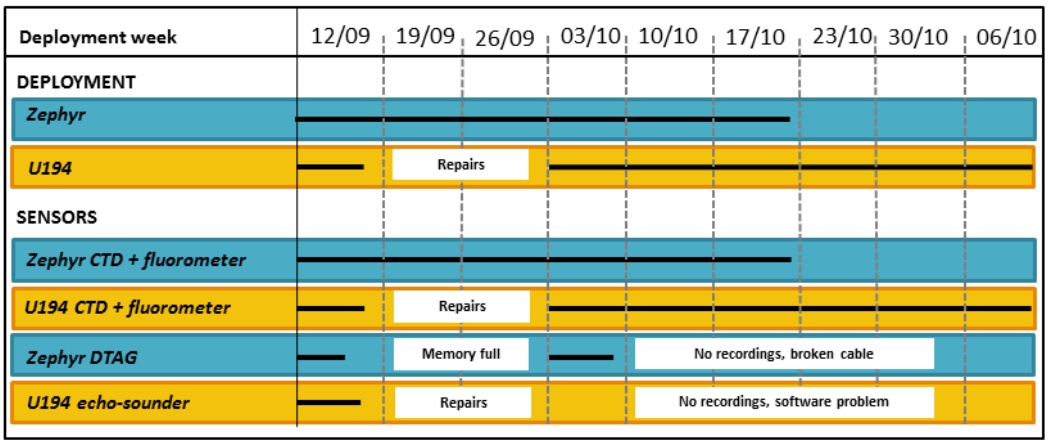

Figure 6.3: Timeline glider deployments (blue shading: *Zephyr*; yellow: *U194*) and sensor activity, represented by black lines. Dates indicate beginning of each week of the deployment, white boxes provide information on sensor malfunctions.

Table 6.2: Mission statistics. Statistics only consider dives of ≥10m (to exclude non-mission dives) and GPS fixes of ≥100m apart. *U194* statistics based on post-redeployment dives only.

Statistic	*Zephyr*	*U194*
Total deployment days	38	39
Total number of dives	2654	2821
Total horizontal distance (km)	1080	1309
Mean horizontal distance b/w GPS fixes (km)	0.9	0.85
Max distance b/w GPS fixes (km)	13.7	10.3
Mean dive depth (m)	44.55	40
Max dive depth (m)	101.49	103.89

Over the six-week deployment, the two gliders performed a total of 5474 dives (each dive comprising one up- and downcast, based on dives of ≥10m) to a maximum depth of 101m (*Zephyr*) and 104m (*U194*) (Table 6.2). The total horizontal distance covered was 2389km, with an average distance of ~0.9km between GPS fixes.

6.3.2 Physical environment

Figure 6.4 shows the glider data is in good agreement with measurements obtained from ship-based CTD-casts. However, *U194* chlorophyll *a* displayed a significant offset (Sup.Figure 6.2) and data shown here are corrected based on the vessel-profile by applying an ordinary linear model and adjusting the *U194* chlorophyll *a* data by the slope and offset ($U194_{corrected} = U194_{raw} \times 1.33 + 0.084$). Although there is a slight offset between Zephyr and ship chlorophyll *a*, no correction was applied, because the water samples suggest the glider fluorometer is giving a better reflection of the true chlorophyll than the vessel data. No correction of temperature measurements was necessary.

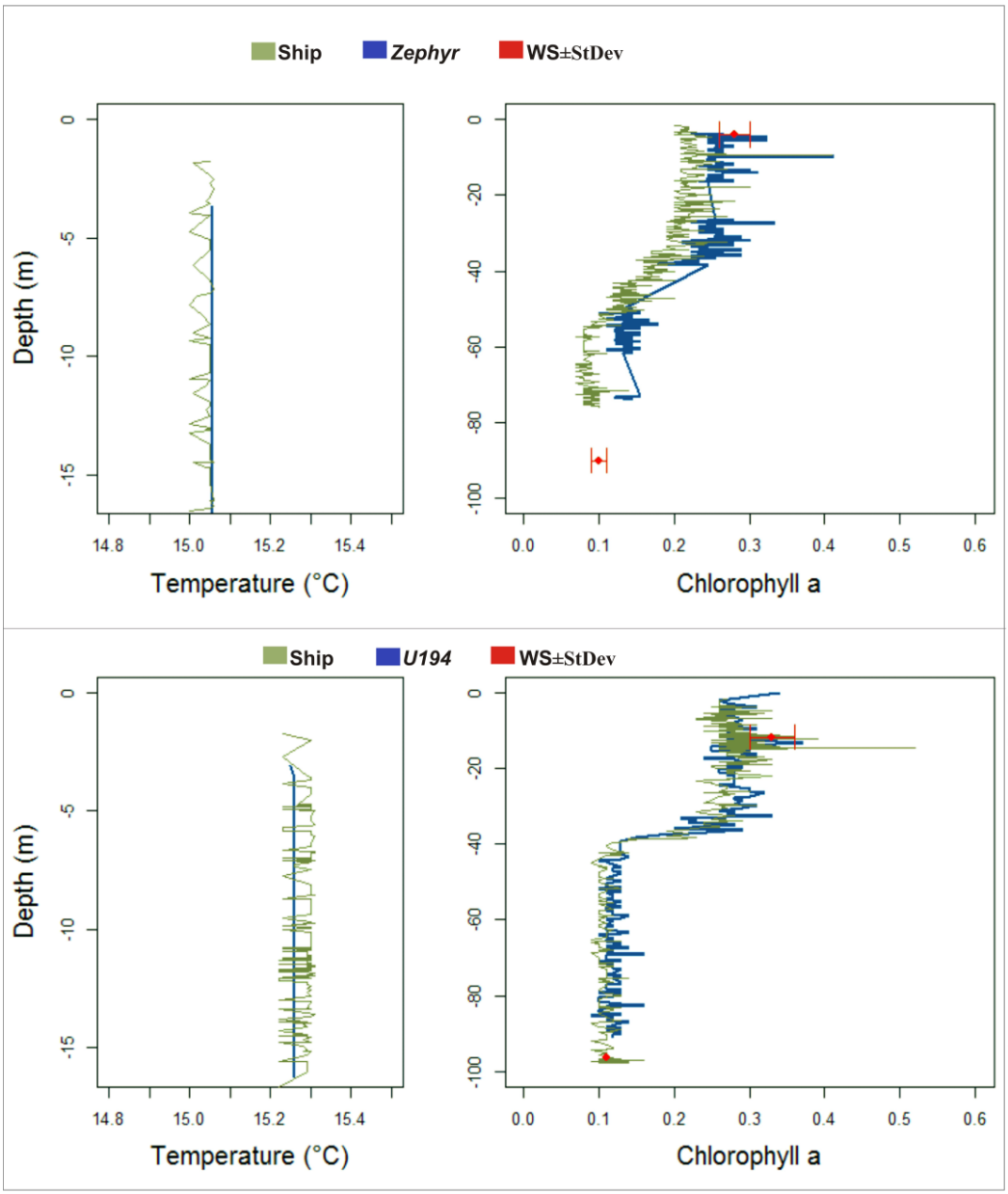

Figure 6.4: Comparison between ship and glider derived temperature and chlorophyll for *Zephyr* (upper panel) and *U194* (lower panel). Green: Ship; blue: glider; red points show chlorophyll *a* from water samples ± standard deviation (*N*=3).

Glider *Zephyr* predominantly sampled thermally stratified waters during its mission, although it crossed the targeted tidal-mixing front several times in the first 500 hours (Figures 6.5A, SupFigure 6.3). A strong thermocline at 20-40m depth is particularly evident after ~500 hours (Figure 6.5A). Elevated levels of chlorophyll *a* fluorescence are visible in the water column towards the base of the thermocline,

particularly around 300 hours (Figure 6.5B). Fluorescence increases notably where the thermocline crops towards the surface in the frontal region, e.g. during a frontal crossing at ~200 hours (Figure 6.5B). High levels of chlorophyll *a* fluorescence remain visible even after the equinox (21 September 2013; ~200hours), which is usually taken as the end of the primary production period elsewhere on the UK shelf (Weston et al., 2005).

Glider *U194* also predominantly sampled thermally stratified waters throughout its mission, but spent less time in frontal regions (Figure 6.1 and 6.5C). Subsurface chlorophyll maxima at ~30m depth, associated with the thermocline, are clearly visible in *U194* profiles until ~800 hours into the mission (Figure 6.5D). The deployment of *U194* was substantially longer than that of *Zephyr* (Figure 6.3), and included a major storm event on 27 October 2013 (1080 hours into the mission, Figure 6.5C). Interestingly, the water mass remained stratified (although much weaker) after this storm event, although surface waters had cooled significantly and the thermocline depth increased to ~50m (Figure 6.5C).

An interesting feature visible on the *Zephyr* temperature profile is the lack of an obvious relationship between bottom temperature gradients and surface gradients, particularly around 400-600 hours (Figure 6.5A). Consistently high surface temperatures were experienced throughout this period (>15°C), whereas the bottom temperature alternated between ~11-13°C. In general, the transition zone along the bottom appears wider than at the surface (Figure 6.5A, Sup.Figure 6.3). In addition, clear bottom front crossings occurred on nine occasions, whereas the surface front was intersected six times only (Figure 6.5A, Sup.Figure 6.3).

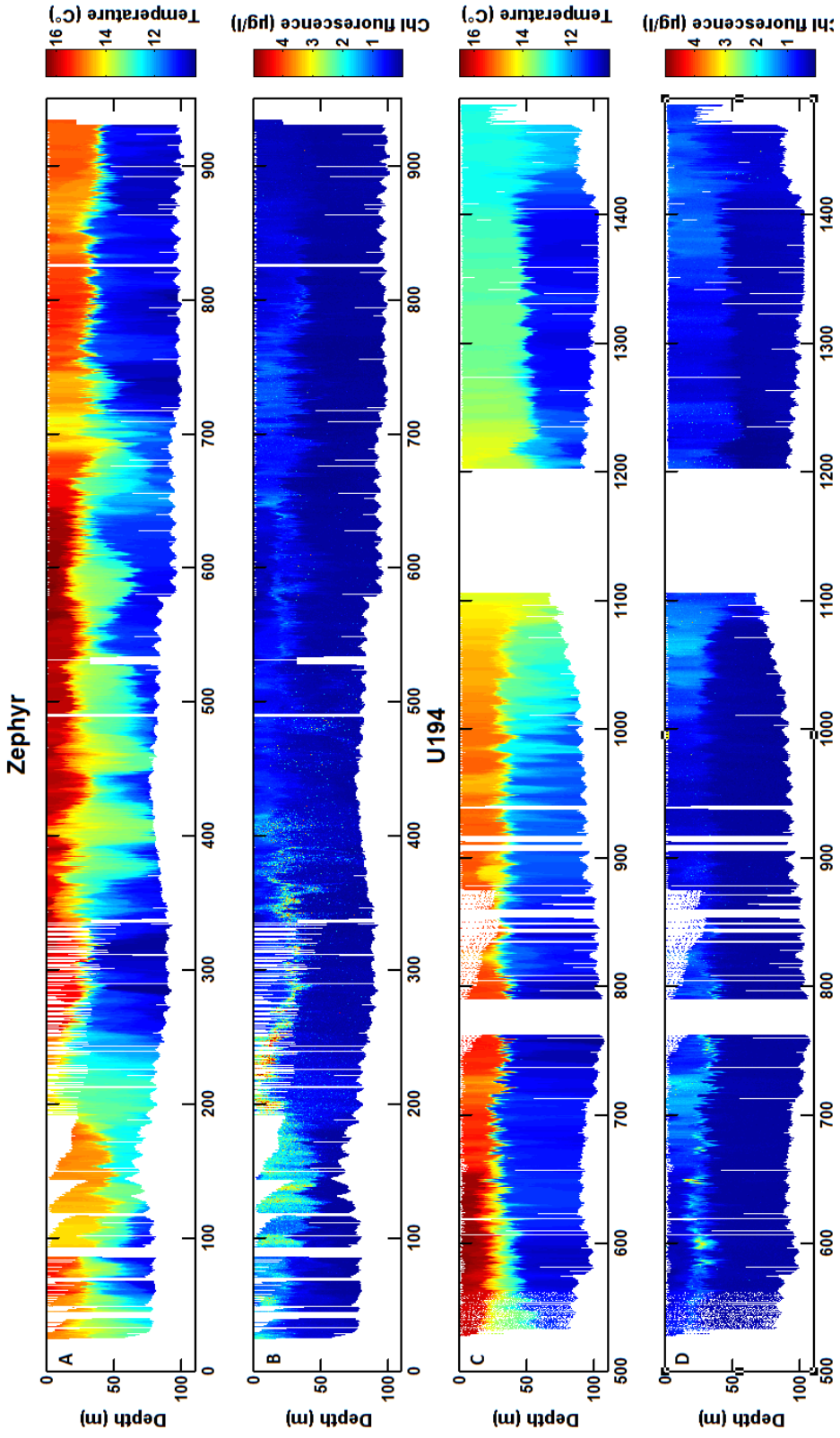

Figure 6.5: Time series plots of temperature and chlorophyll concentration of both gliders against depth (panels A-B, *Zephyr*; panels C-D, *U194*). Time refers to hours since mission start on 12 September 2013 at 1200 hrs. Note shifted time axis for *U194*, which only considers data since re-deployment from 04 October

6.3.3 Echosounder

The ES853 120kHz echosounder, integrated onto *U194* (Figure 6.2A), successfully recorded acoustic data from the water column during the first five-day deployment (Figures 6.3 and 6.6). Unfortunately, after redeployment a technical error prevented communication between the echosounder and the glider and, as a consequence, acoustic data for the rest of the mission were not stored on the internal memory of glider and echosounder. Focussing on the downcast, when the echosounder is vertically orientated and most comparable to a ship-based echosounder, typical features observed in echograms include the seabed and fish shoals (Figure 6.6A). Similar acoustic features were observed in an echogram derived from the ship-based echosounder in the same area at the same time of year (Figure 6.6B).

A band of scattered targets, consistently present within 20-25m of the glider echosounder during both down-and up-casts (Figure 6.6A), was interpreted to represent small organisms such as zooplankton. The vessel-based echogram at 120kHz revealed similar scattered targets throughout the water column, with some evidence for elevated concentrations at ~30-40m depth associated with the thermocline (Figure 6.6B). Due to the reduced signal-to-noise ratio of the glider echosounder, these small targets were only observed within a limited range of the transducer. In contrast, the stronger water column targets related to fish shoals that were recorded throughout the water column on glider data (Figure 6A). These targets appeared similar to those recorded from RV *CEFAS Endeavour* during its annual pelagic fish survey in the area (Figure 6B), and were thought to consist of boarfish (*Capros aper*). Due to differing ping rates (4 vs 0.25 s^{-1}) and vehicle speeds (5 ms^{-1} vs 0.3 ms^{-1}), the horizontal resolution of acoustic data obtained from the glider was nearly twice as high compared to the vessel (1.2m vs 2.5m per ping), which suggests that the fish shoals imaged on the glider echogram are possibly small examples of these boarfish shoals.

A noticeable feature on glider acoustic profiles is the presence of high backscatter patches in the uppermost water column, observed down to ~20m water depth

during upcasts (Figure 6.6A). Adverse weather conditions, with large waves or swell, are known to introduce bubbles into surface waters; however, weather conditions were favourable during the period that these features were observed so this cause is doubtful. Technical issues, such as side-lobe detection of the sea surface, are also thought to be unlikely as these patches were not always present, absent during previous trial deployments, and no changes had been applied to the echosounder settings. Vessel-derived echograms did not show the same features, although the transducer depth of the vessel-based echosounders was 8.2m below the surface and so did not cover the surface layer. It is therefore possible that these high backscatter patches have a biological origin, representing organisms restricted to surface layers. However, their unusually high backscatter, widespread occurrence, and consistent appearance throughout the deployment, also make this an unlikely source. Therefore, further investigation is required to determine the true origin.

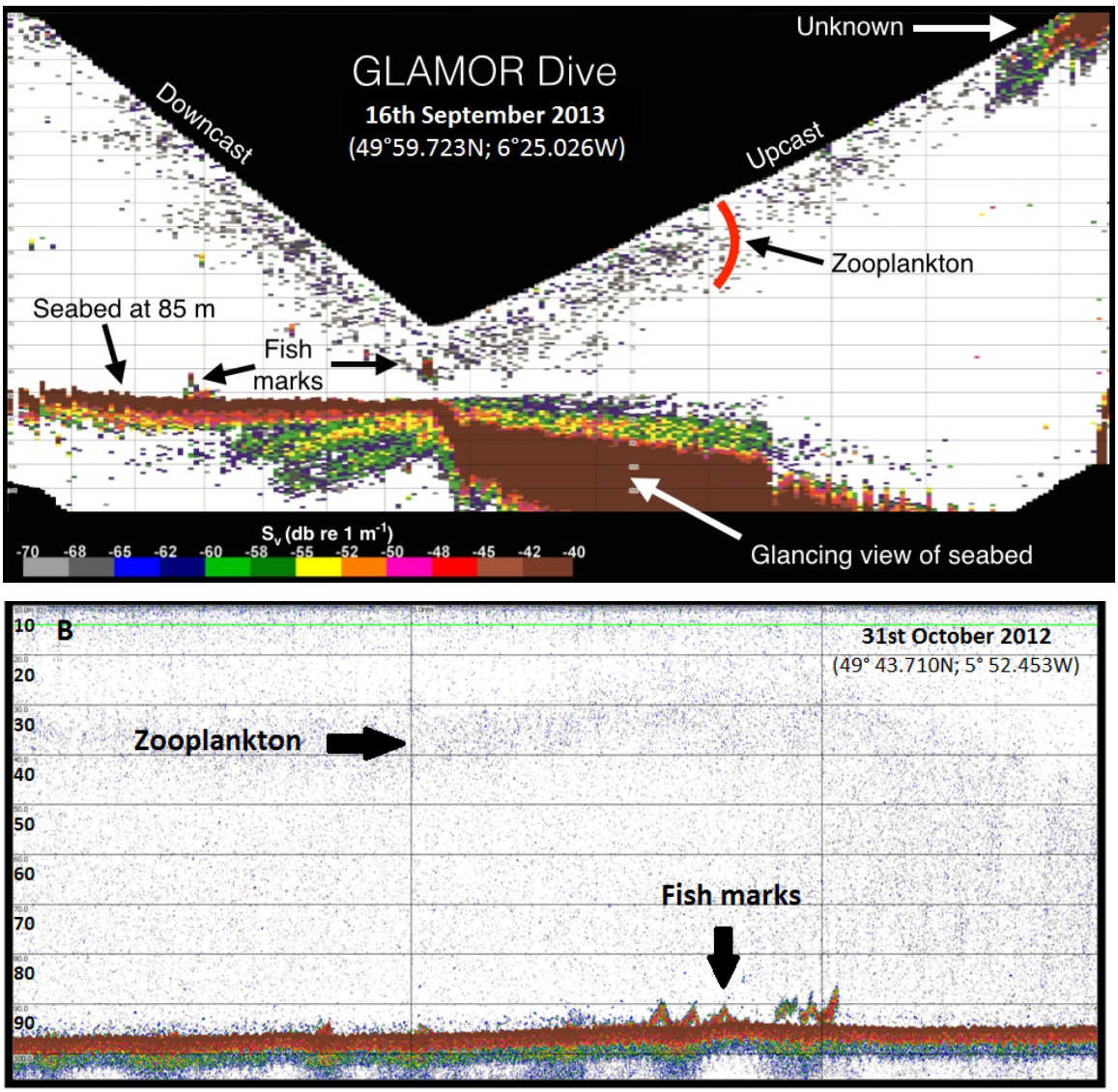

Figure 6.6: Echograms of glider-integrated ES853 at 120 kHz (A) and equivalent vessel based EK60 120 kHz (B). Distance between the two sites 43.3km. Features such as the seabed, fish shoals and zooplankton scattering have been indicated. Gain thresholds for both echograms were set to -70dB.

6.3.4 Passive acoustic monitoring

The power cable to the d-tag acoustic sensor was damaged during or soon after installation, so PAM data were only collected between 4 and 10 October (Figure 6.3). These data included 2413 10s recordings over 291 separate dive cycles, with an average of eight recordings per dive. Harbour porpoise clicks were detected during two separate dives, although one of these consisted of only a single click.

Dolphin clicks and whistles were detected during 194 dives: 145 of these were clicks only, 49 whistles only, and 42 both (for map of locations of recordings see Sup.Figure 6.4). Figure 6.7 shows the waveforms and power spectra of a typical dolphin and porpoise click. No other obvious noise sources, such as the pitch battery motor were apparent in the data.

Noise attributable to the glider pump was recorded on 169 occasions. The times of these noises corresponded to the times when the pump was 'on' in the glider log files, typically occurring for only a few seconds at the bottom of each dive. Figure 6.8 shows the distribution of noise in third octave bands with the pump on and the pump off. Median noise levels with the pump off are generally low indicating that the system can be used to make accurate measurements of ambient noise. Noise levels at all frequencies are considerably higher when the pump is in operation. However since the duration of these noisy periods is relatively short, it will have little effect on overall survey effort.

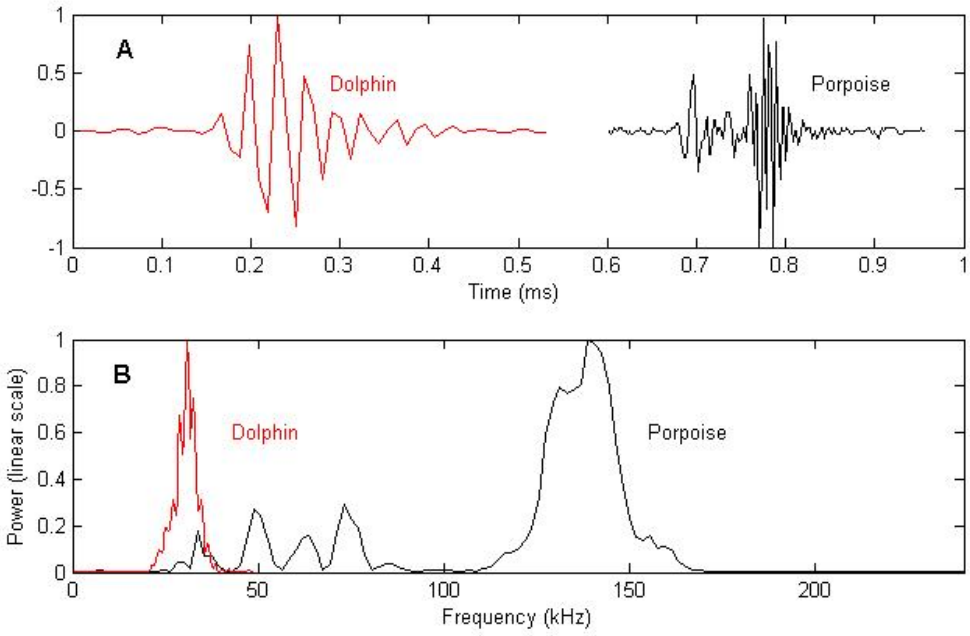

Figure 6.7: A) waveforms and B) power spectra of detected dolphin and porpoise clicks using the d-tag hydrophone on *Zephyr*.

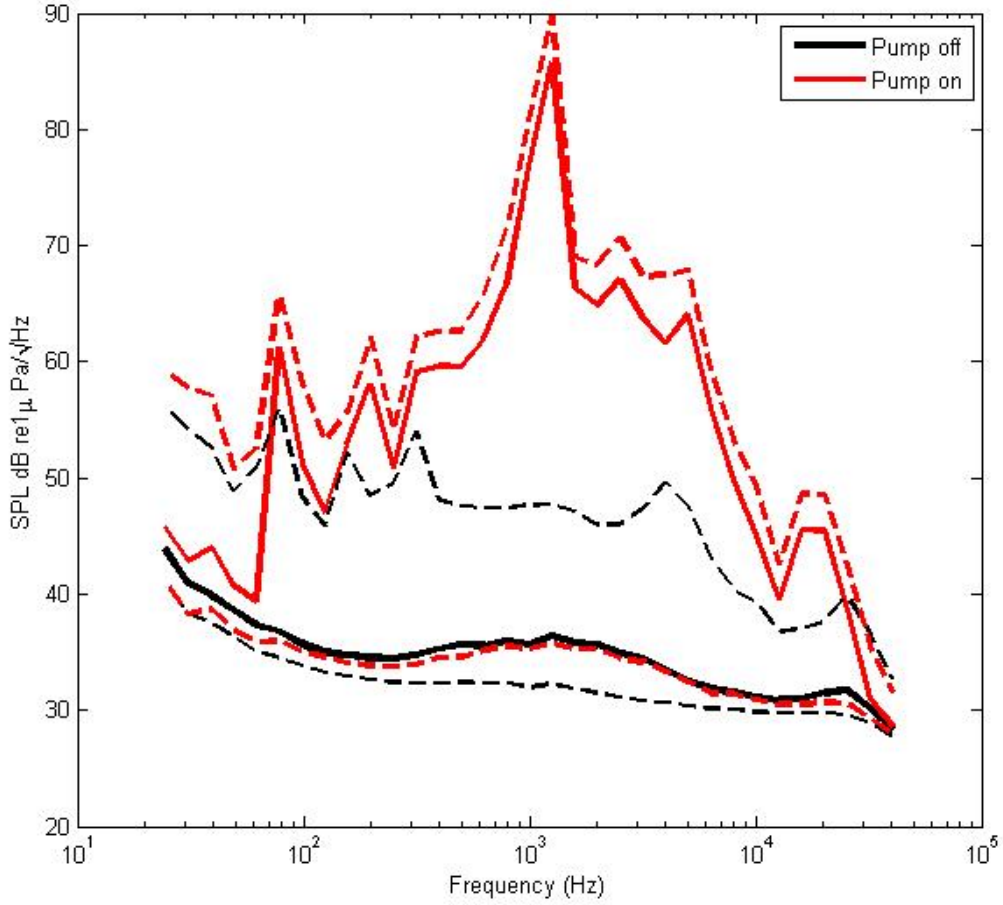

Figure 6.8: Spectrum-level noise measurements at third octave intervals for times when the Zephyr pump was on and when the pump was off. The three lines for each situation represent the median values and the lower and upper 90% intervals.

6.3.5 Passive sampling devices

Recovered silicone rubber sample sheets were visually inspected for bio-fouling before analysis (as this can affect the uptake of contaminants into passive samplers); bio-fouling levels were found to be very low compared to static exposures. Significant dissipation of performance reference compounds (PRC) was observed from sample sheets. PRC dissipation was used to estimate sampling rates using a published (Booij et al., 2011). These rates were in the range of 3 to 7 L d^{-1} depending on the chemical. Sampling rates were normalised to a standard surface area (Huckins et al., 1993) and compared with those observed during static

or other mobile deployments of passive samplers (e.g. Allan et al. (2011); Allan et al. (2011); Lohmann et al. (2012)) (Table 6.3). Sampling rates for the glider-mounted passive samplers used here are in a similar range to those commonly observed for static deployments, whereas mobile exposures with high velocities tend to achieve high sampling rates (Table 6.3). The PRC data from this passive sampler exposure (i.e. 50% dissipation for d_{10}-phenanthrene) indicate that sampling was time-integrative for substances with octanol-water partition coefficient (log K_{ow}) above 4.5. Since gliders are launched for periods of weeks to months, these exposures can still detect polycyclic aromatic hydrocarbons (PAH) and polychlorinated biphenyls (PCB) in the low pg L^{-1} range, i.e. levels at which these compounds typically occur in oceanic waters.

Freely dissolved concentrations of PAHs ranged from just over 1 ng L^{-1} for phenanthrene down to below 10 pg L^{-1} for higher molecular weight PAHs. Polychlorinated biphenyls (PCBs) were found at levels below 10 pg L^{-1} (except for PCB congener 28 with a concentration of 32 pg L^{-1}). The freely dissolved concentration of hexachlorobenzene was 45 pg L^{-1}. These concentrations were not corrected for temperature or salinity, but are generally in the range of those measured in open waters of the North Atlantic.

Table 6.3: Passive sampling rates, typical exposure times, and limits of detection for various passive sampler deployment modes.

Deployment mode	Sampling R_s ($L\ d^{-1}$)[a]	Exposure time	Limits of detection ($pg\ L^{-1}$)[b]	Reference
Static	1-20	0.5-3 months	0.3-30	(Allan et al., 2010; Allan et al., 2013; Prokes et al., 2012; Vrana et al., 2002)
Mobile[c]	18-27	4-6 days	3.0-7.0	(Booij et al., 2007)
Mobile[d]	70-200	5 and 48 hours	1.0-30	(Allan et al., 2011; Allan et al., 2011; Lohmann et al., 2012)
Calibration[e]	60-200	15 days	0.2-0.6	(Booij et al., 2003)
Glider[f]	3-7[g]	39 days	2.0-4.0	Present study

[a]for a standard semipermeable membrane device sampling surface area of 460 cm^2

[b]Limits of detection in water for PAHs/PCBs in the linear phase of uptake ($C_{w,lim} = m_{lim}/[R_s\ t]$) with a arbitrarily set m_{lim} of 0.5 ng per sample

[c]Ship-based measurement using the ship's continuous water supply (water velocity in the pipe of 15 cm s^{-1})

[d]samplers towed behind a benthic trawl net (1.2-1.4 knot); towed behind a research vessel

[e]During sampler calibration with water velocity of 90 cm s^{-1} and water temperature of 30 °C

[f]Average glider velocity through water of 20-40 cm s^{-1} (horizontal velocity)

[g]Sampling rates corrected to a surface area of 460 cm^2

6.4 DISCUSSION

In this 'proof-of-concept' study, two submarine gliders were equipped with sensors capable of simultaneously measuring physical properties of the water column and multiple trophic levels, in order to test their potential for ecosystem monitoring. The results highlight the advantages and current limitations of utilizing gliders as autonomous platforms for the outlined purpose. The key outcomes relate to operational aspects, current sensor technology, instrument calibration and data validation.

6.4.1 Glider operations

The two gliders successfully completed their missions, which lasted for just under 40 days and which each comprised >2500 dives to depths of up to 100m over total

horizontal travel distances of 1000-1300 km. The gliders continued to collect data in weather conditions that stopped research vessel activity in the region, including a particularly severe storm on 27 October 2013 (Figure 6.5C).

The two major operational challenges were flight control and alignment of the two glider trajectories in space and time. Although previous deployments have demonstrated that gliders are capable of following a proposed transect in areas of strong tidal flow (e.g. Leonard et al., 2007), this proved extremely challenging in the present study (Figure 6.1). This is likely due to the combination of strong tidal and non-tidal residuals acting on the vehicles together. In order to fully understand the effect of hydrodynamics on our gliders, a detailed analysis is required including currents, tides and meteorological forcing in relation to the glider tracks and flight settings, which is beyond the scope of this paper.

The flight of *U194* was significantly improved by applying a more dynamic piloting approach, including e.g. increased monitoring, modifying dive angle and current correction settings, and adjusting waypoints depending on currents and tidal state. Hybrid *Slocums* equipped with a thruster are also now commercially available (Jones, 2012), which should further aid future deployments in tidally dominated environments. Furthermore, ongoing modelling and simulation research, dealing with optimal path planning and influences on glider trajectories, can be used to aid survey design (e.g. Fernandez-Perdomo et al., 2011; Ting et al., 2012).

Aligning the flight of multiple gliders is a key requirement in whole-ecosystem monitoring, as the sensors required to simultaneously measure multiple ecosystem components cannot currently be integrated onto a single vehicle due to limited payload capacity and energy constraints. In addition, certain instruments need to go onto different platforms due to acoustic interference problems (e.g. active echosounder and passive hydrophone). In order to obtain meaningful data on multiple parameters simultaneously, the vehicles should be aligned in time and space; ideally the maximum distance between the vehicles should not exceed the scale on which the variables change. This is a challenging task, because gliders

equipped with different sensors will display specific flight behaviours, e.g. due to different ballasting and external sensor configurations. For example, the hydrocarbon sheets used on *Zephyr* in this study are likely to have added extra drag to the vehicle resulting in different flight behaviour compared to *U194* (*cf*. Figure 6.1). If time and budget allows, extended trials focusing on simultaneous flight prior to a mission could improve piloting for individual gliders and, therefore, trajectory alignment.

6.4.2 Sensors

Throughout the mission, CTD and fluorometer sensors on both gliders provided water-column data at a spatio-temporal resolution and frequency not attainable through ship-based surveys or satellite imagery. For example, *Zephyr* crossed the Isles of Scilly tidal-mixing front several times (Figure 6.5A), with collected data highlighting the spatial offset of the surface and bottom fronts (Figure 6.5) as well as chlorophyll maxima associated with the thermocline (Figure 6.5B); these features would not be detected using remote sensing data. Glider *U194* dominantly sampled stratified waters, and monitored change in the water column from seasonally stratified to mixed over a period of six weeks (Figure 6.5C); within this period the glider continued collecting data during the severe storm event on 27 October 2013. Despite the high-resolution and amount of information collected, file sizes were small enough for a subset of data to be transmitted via Iridium during the mission.

The newly integrated ES853 echosounder and d-tag passive acoustic monitoring system provided promising data on the spatial distribution of higher trophic-level organisms. The hydrophone recorded numerous cetacean clicks and whistles from different species during the six days of operation (Figure 6.7 and Sup.Figure 6.4). The echosounder was capable of detecting targets, including fish and zooplankton, similar to targets detected by vessel-based data echosounders (Figure 6.6).

The novel hydrocarbon sheets trialed here can easily be attached to gliders and AUVs, and collect supplementary information on water quality. This has particular

application for regulatory monitoring, e.g. in response to European legislation such as the Water Framework Directive and the Marine Strategy Framework Directive. The sampling scheme can be extended from hydrophobic compounds (as used in this study) to samplers specifically designed to sample hydrophilic substances and metals.

Limitations of glider-integrated instrumentation include the need for data calibration and validation, particularly over long-term surveys. CTD and fluorometer calibration procedures are generally undertaken during glider deployment and retrieval using calibrated ship-based CTDs and by taking water samples. However, depending on survey area and season, a considerable amount of bio-fouling can affect the glider-integrated instruments; this causes sensor drift in a non-linear fashion, which is difficult to account for with calibration procedures at the beginning and end of a mission. In addition, collection of water samples remains essential for phytoplankton biomass estimations or species identification.

Although the echosounder and PAM system are capable of collecting data on the distribution of higher trophic level organisms over large spatio-temporal scales, they are significantly harder to calibrate compared with the physical sensors. Single-beam single-frequency echosounders provide a limited capability for target identification, which are normally undertaken using multi-frequency discrimination methods (Korneliussen et al., 2003). However, these instruments are currently too large and powerful to be integrated into underwater gliders. To establish fish species with absolute certainty, verification via net sampling also remains essential. Size-length relationships needed for target strength, model parameterization for conversion to biomass and information on age-class distribution are additional parameters that can only be acquired with dedicated net sampling from vessel-based surveys. There has been some success at classifying cetacean whistles collected by PAM systems to species level (Gillespie et al., 2013), although considerable problems remain in estimating absolute animal abundance from glider-based data. Critical data for the estimation of abundance are the range at which animals are detected and either the rate of vocalization or

the ability to isolate and count individuals (Marques et al., 2013). Gliders are too slow moving to use target motion analysis to localize animals in the water columns, as is commonly done for sperm whales (e.g. Lewis et al., 2007) and vocalisation rate is poorly known for most species. Finally, echosounder and PAM system development should focus on methods for summarizing the complex data to enable transmission of a subset of collected data, rather than after retrieval. This would enable the glider to target, on the fly, hotspots of animals.

6.4.3 Conclusions and recommendations

This proof-of-concept study has highlighted some of the advantages and current limitations of utilizing submarine gliders for the purpose of ecosystem monitoring. Advantages include cost efficiency, capability of working in adverse weather, and collection of 3D water-column data at high spatio-temporal resolution over periods of weeks to months. This is not achievable with other single platforms, but is essential in order to detect change and its effect on an ecosystem, e.g. breakdown of seasonal stratification, impact of short-duration storm events. All of the novel glider-integrated sensors used in this study delivered usable data, although they could only provide information on distribution of biological indicators rather than accurate estimates of abundance or biomass. More broadly, glider sensor calibration and data validation remains challenging and dependent upon supporting infrastructure (ships, moorings), so acquired data are often only suitable for qualitative analysis. In addition, for the purpose of multi- vehicle surveys, aligning glider trajectories and flight control are significant issues that require further improvement (especially in dynamic tidally-dominated environments). Nevertheless, the promising results achieved in this study have led to a further deployment targeting oceanic fronts off southwest UK (planned for autumn 2014) using unmanned surface vehicles (USVs) as an in addition to submarine gliders.

For effective whole-ecosystem monitoring in the future, a range of autonomous platforms will need to be deployed within a marine monitoring network, including USVs, AUVs and gliders. Successful implementation of an autonomous monitoring network has already been demonstrated in the California Current Ecosystem,

where satellite imagery, vessel surveys, gliders, floats and moorings are used in combination to provide compatible data on ecosystem dynamics at various spatio-temporal scales (Ohman et al., 2013). Satellite remote sensing provides information on large-scale surface processes, which is supplemented by submarine gliders measuring water column properties. Moorings and targeted vessel surveys utilize more powerful sensors working at high frequency, and are used to calibrate satellite and glider data; vessels are also used to run structured experimental surveys, which require ship-based equipment. Together, the sampling network efficiently provides a synoptic view of an ecosystem at multiple scales, which can significantly advance our understanding of marine ecosystem functioning and drivers of change.

6.5 Supplementary Material

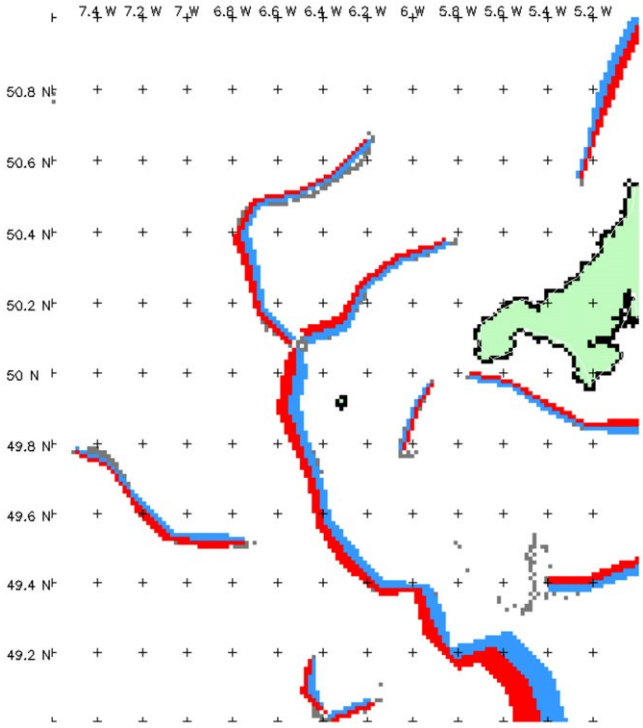

Sup.Figure 6.1: Composite satellite-derived front map of the survey area off southwest UK, based on data from 12 September- 17 October 2013. Red indicates warm-water (stratified) side of tidal mixing front, blue the cold-water (mixed) side. Line thickness equates to the strength of the front (the thicker the line, the stronger the front). Note the stratified waters to the west from tidally-mixed waters to the east (cf. Figure 6.1). (For interpretation of the references to colour in this figure legend, the reader is referred to the web version of this article).

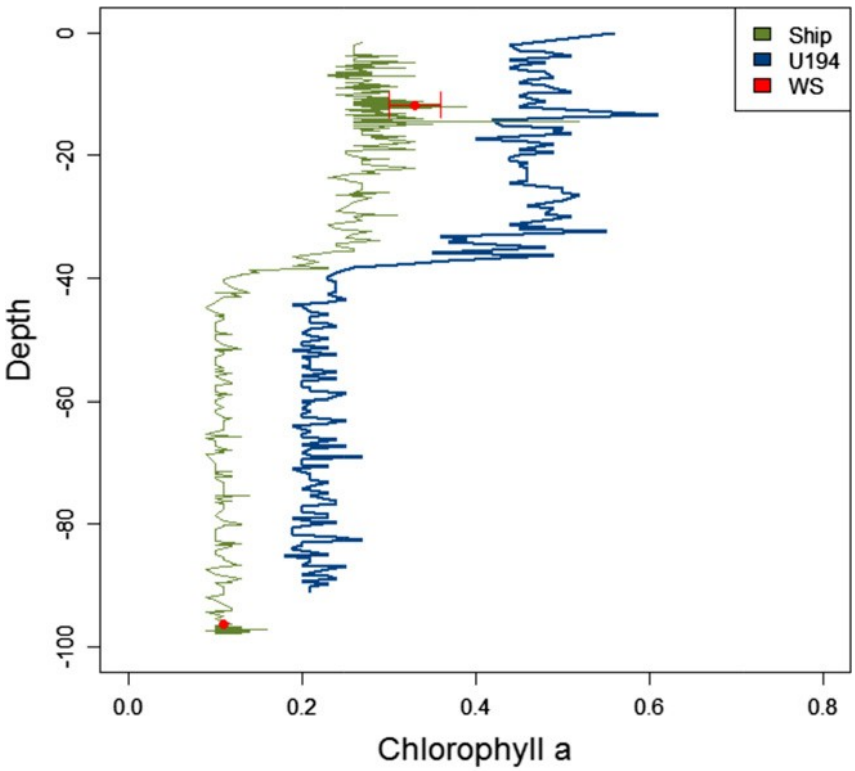

Sup.Figure 6.2 Calibration profiles between ship (green) and U194 (blue) showing uncorrected chlorophyll *a* data, Red points show values from water samples ± standard deviation (*N*= 3). (For interpretation of the references to colour in this figure legend, the reader is referred to the web version of this article).

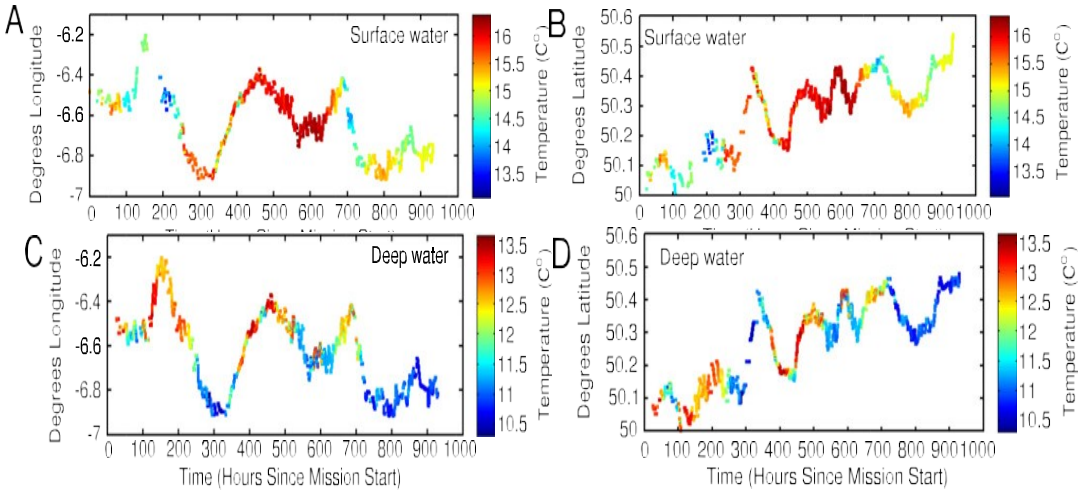

Sup.Figure 6.3: Temperature of surface waters (A and B, between 5-10m depth) and deeper waters (C and D, between 60-70m depth) as a function of time and longitude (A and C) and latitude (B and D).

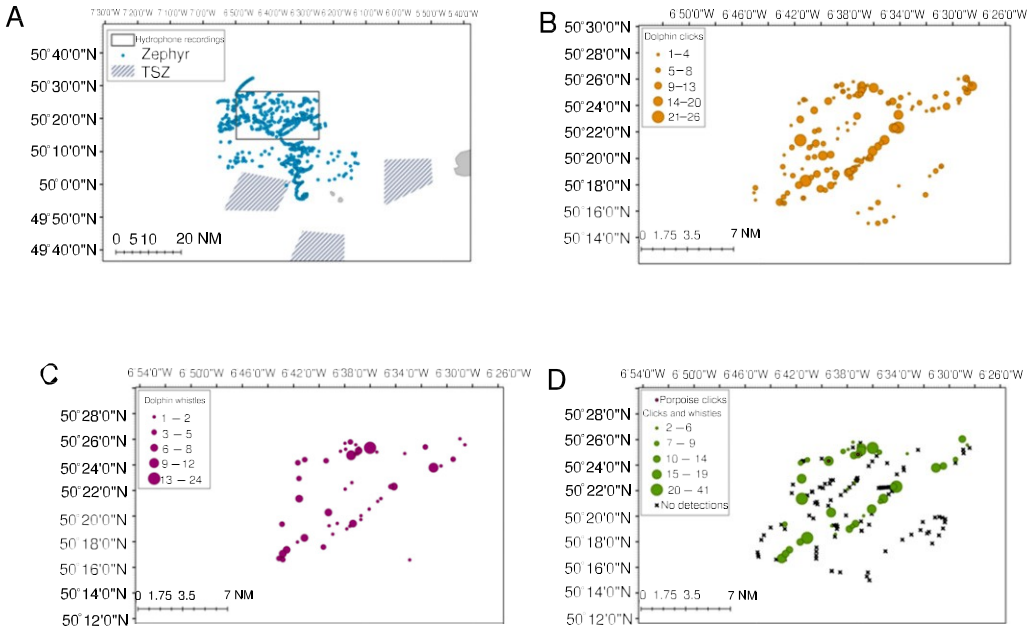

Sup.Figure 6.4: Map showing the area where the d-tag hydrophone on Zephyr was active (A) and recorded dolphin clicks (B), whistles (C) and dives with both and porpoises clicks (D). Black crosses refer to locations of dives without recordings.

7 GENERAL DISCUSSION

6.1 Summary

The primary objective of this thesis was to gain a better understanding of the ecological significance of tidal mixing fronts in shelf-sea ecosystems. The majority of studies concerning front-biota interactions are based on high-resolution, but small-scale surveys to entangle the underlying mechanisms of bio-physical coupling. In contrast, this research employed large spatio-temporal datasets (up to 21 years and covering the entire Celtic Sea) to investigate the influence of tidal mixing fronts at regional scale. The breadth of the data allowed for the first time an analytical assessment of long-term variability of tidal mixing fronts, its effect on distribution of marine organisms from different trophic levels and across multiple species. The spatial scale made it possible to compare between more than one frontal feature and the length of the time series enabled accounting for seasonal and inter-annual variability occurring in natural systems.

This thesis also takes a critical look at the shortcomings and advantages of currently available datasets and provides alternative sampling solutions to improve data collection in bio-physical coupling research. For example, this research highlights a range of issues with satellite-derived frontal metrics, which seriously can affect the outcomes of quantitative analyses. Yet, hardly any comprehensive information is available for scientists intending to use frontal maps in their research. In addition, satellite-derived datasets are useful to study large scale processes, but lack the resolution and multidimensionality (e.g. subsurface data) necessary to investigate mechanisms leading to front-biota interactions. At the same time, high-resolution surveys also have shortcoming, because they are usually undertaken over short periods of time (days to few weeks) and provide just a snapshot in time and space, often do not account for multiple trophic levels at once and are partially restricted to the surface (e.g. sightings or tracking data of megavetebrates). To resolve this problem, a proof of concept study was undertaken, using underwater gliders for synoptic data collection of physical parameters and across multiple trophic levels at high-

resolution and throughout the entire water column, which provided some promising results.

7.1 A guide to frontal metrics

Chapter two highlighted complex issues with the use of satellite-derived frontal metrics in quantitative analyse, which have not been described in detail before and are largely unknown to many researchers using frontal metrics. The complexity of the frontal metrics themselves and the number of factors to consider when analysing them, call for the production of a comprehensive guide to the correct application of frontal metrics. This guide should be aimed at researchers not working in remote sensing directly and who are likely not aware of some of the here highlighted issues with satellite data.

It is likely that even simple things, such as the choice of an appropriate metric for a given study or research question is made incorrectly, simply because the definitions of the various metrics are not always clear to everyone. Frontal metrics are based on sometimes complex algorithms, which can make it difficult to understand what information each metric provides. Some researchers might not be aware of the different meanings of the various metrics and assume they all represent information on frontal strength. While certain metrics are indeed similar, chapter two also illustrated profound differences in temporal variability between distinct metrics. Consequently, just the choice of a metric can significantly influences the outcomes of an analysis.

A guide to frontal metrics should provide a list of currently available metrics, a simple description of their meaning and the information they entail. The guide could make some suggestions what type of analyses a metric might be useful for or not. For example, *Fcomp* could be useful for investigations of the influence of persistent, strong fronts on animal distribution. However it would not be recommended for temporal analyses because of its complexity. *Fprob* provides almost identical information, but is much simpler and variability in *Fprob* can be directly attributed to the ratio of valid to clear pixels. The description of each metric needs to include a comprehensive explanation of

their mathematical derivation. It could be useful to explain underlying frontal detecting algorithms with illustrative examples as well.

Further sections of a guide to frontal metrics need to include discussions about factors to consider when processing and analysing frontal metrics. Scientists should be advised to think about e.g. how to define the sampling area or how to reduce noise from unwanted frontal segments that do not belong to the front of interest. Further discussion should concern the choice of statistic to describe the front when spatially averaging frontal metrics over the sampling area for time series analysis. For example, the spatial mean, median, maximum or variance will each provide distinct information on the spatial character of the front. Chapter two also revealed the need to account for *Fclear* in quantitative analyses in order to avoid wrong estimates of the temporal variability of frontal metrics. Ideally these issues are discussed with a remote sensing scientist before producing of the frontal maps for analysis.

While chapter two aimed to illustrate some of the differences between commonly used metrics and provided advice on their processing and analysis, it only represents a snap-shot of what a detailed guide to fontal metrics could look like. Chapter two only considered temporal analyses of frontal metrics, but especially marine ecologists use them for spatial analyses. Although it appears that there are fewer issues to consider when using frontal metrics for spatial analyses, it might proof useful to explore the differences and potential caveats of frontal metrics in spatial analyses in more detail as well.

7.2 Meteorological drivers of inter-and intraannual variability of frontal strength and persistence: potential implication of the effect of climate change on tidal mixing fronts and associated ecosystems

This study provides first long-term statistical analysis of inter-and intrannual variability of frontal persistence and gradient strength in the Celtic Sea and identifies their key meteorological drivers. Frontal gradient strength (*Fmean*) displayed a natural oscillation from 1990 to 2010, with periods of stronger and

weaker fronts. Frontal persistence (*Fprob*) on the other hand, did not change significantly from 1990 to 2010 when accounting for *Fclear* and including temporal variables (factor 'month' and 'year') only. However, *Fprob* did show similar oscillating pattern as *Fmean* at the Ushant Front, when meteorological variables were included in the statistical analyses. It is possible that the statistical models overestimates an *Fclear* effect and the temporal variability in *Fprob* (and likely in *Fmean* as well) was caused by genuine fluctuations of the front in response to changing environmental conditions.

The key meteorological drivers of temporal variability of frontal gradient strength and persistence at both fronts were related to the heat budget of the water column. Overall, net heat flux explained most of the variations in intraannual pattern, whereas SST was the most important contributor to interannual variability of *Fmean* and *Fprob*. The positive correlation between long-term variability of both frontal metrics and SST indicate a potential sensitivity of tidal mixing fronts to climate change. The long-term temporal variability of both metrics was small and the time series was not long enough to draw sound conclusions about a potential effect of climate change on tidal mixing fronts in the future. However, consequences could include an extension of the frontal season, strengthening of the frontal density gradients or spatial displacements of tidal mixing fronts. Some potential know-on effects on ecosystems were discussed in chapter four. For example, elongated frontal season could affect dispersal of benthic larvae and other passive floating organisms and consequently, affect density and diversity of adult populations.

Climate change is already impacting the ocean in several ways, for example through phonological shifts and trophic mismatch, leading to declines of sensitive species and the expansion of others, and resulting in competition with and displacement of local biota (Doney et al., 2012). Considering the diverse role that fronts play in the global oceans, climate-driven alterations in frontal occurrence could affect associated ecosystems. For instance, spatial displacement of fronts due to temperature changes or increased wind forcing can directly effect zooplankton distribution or the accessibility of foraging habitat for top predators (Constable et al., 2014).

On the other hand, fronts may be able to counteract the above scenarios by representing a location on the shelf where the exchange between nutrient-depleted and nutrient-rich domains still functions. Beaugrand *et al.* (Beaugrand et al., 2000) found that inter-annual variability in zooplankton abundance in the Ushant Front region is much lower than elsewhere in the Channel, the Celtic Sea or Bay of Biscay. They related that a 'buffering' effect of the Ushant Front, where the relationship between biota and climate is reduced. Frontal regions could provide a physically more stable environment where primary productivity is enhanced even during less favourable climatic conditions, and act as a save haven from climate change for marine biota.

7.3 Tidal mixing acting as boundaries for zooplankton distribution and dispersal

Research on front-biota associations has largely focused on fronts as high abundance and biodiversity sites. Generally, there is an appreciation of fronts acting as barriers between distinct bioregions, but this particular role of fronts has received considerably less attention. Differences in abundance, diversity and composition of marina biota across fronts have largely been attributed to the often abrupt changes in the environmental setting. Taking a different approach, this research showed that the density gradient associated with tidal mixing fronts contributes to the observed changes in community structure of marine biota from one side of the front to the other. The results suggest that the Ushant Front partially restricts distribution and dispersal of the two study organisms, *Calanus helgolandicus* and echinoderm larvae. The fronts could therefore play an important role in influencing habitat connectivity of benthic adult populations. Climate change induced phenological shifts, such as spawning of the adult benthos population before frontal establishment could result in wider echinoderm larvae dispersal in the future. Furthermore, increasing SST may lead to an extension of the frontal season, stronger density gradients in the future and increase a barrier effect. Taking into account effects of climate variations on the barrier effect of tidal mixing fronts could help explain interannual variations in the benthic adult populations.

7.4 Tidal mixing fronts as important foraging sites for species with specialist foraging ecology

Chapter five illustrates the role of tidal mixing fronts as foraging site for megavertebrates with specialist feeding ecology. The relationship between sightings probability of megavertebrates with specialist feeding ecology and frontal metrics, which represent frontal persistence or frequency was particularly strong. Specialist animals tend to be more vulnerable to alterations in their habitat or to variability in their food sources, because they do not have the means to react to changes as easily and just switch to other food sources (Peter E Robins et al., 2013). While a strong association between persistent fronts and these animals might be useful in identifying areas of conservation potential for vulnerable species, it might also have negative implications. Fronts are often places of elevated fishing activity (Ocampo et al., 2013) and consequently, there is an increased risk of fisheries interactions, e.g. food competition, risk of bycatch or physical trauma caused by ships or fishing gear, increased pollution, etc.

On shelf-seas the overlap between human activity and marine biota is particularly high. It is therefore necessary to identify and protect regions on the shelf that are critical for vulnerable species, such as socialising or resting sites for cetaceans, nursing grounds for fish or important foraging areas for megavertebrates. Knowing that temporally and spatially persistent parts of a front are frequent feeding places for a range of marine species, could aid refining diversity zones for conservation goals.

7.5 Assessing new technologies to improve data sampling of frontal characteristics and associated biota

The use of frontal maps is currently extremely popular in various scientific disciplines to study spatio-temporal variability of fronts or their associations with marine biota. Frontal maps have the advantage of providing information of different frontal characteristics (e.g. strength, persistence) over large spatio-temporal scales (30 years, global) for little money. However, this research illustrated a range of shortcomings of satellite-derived frontal metrics. There

always seems to be a trade-off between data resolution and quality versus temporal and spatial extent. The datasets used in this research are useful for identify broad scale patterns, but lack the resolution to understand the underlying mechanisms. Without information on bio-physical processes occurring at the subsurface and animal behaviour, a synoptic view on species-environment interactions at frontal systems is impossible to achieve. One solution is the combination of different methodologies that cover multiple resolutions and scales, such as satellite imagery to manage large spatio-temporal extents, biologging and vessel-based surveys for high-resolution 3D and behavioural information. However, linking different datasets incorporates some difficulties, because they are often sampled at different resolutions and often at different dates.

Chapter six showed that new ocean technologies like submarine gliders can sample the oceans autonomously, be deployed over extensive time scales and potentially cover large areas. Moreover, they have the capacity to collect information on a range of biological and physical variables simultaneously. These technologies are still in the early stages of development and have some limitations. However, they have the potential to account for many of the shortcomings of current available methodologies combined. In addition, they can be used in combination with satellite-derived oceanographic an biological data. The satellite data can be used to refine and improve glider surveys. Find high frequency areas in the first place via satellite information and then send out gliders to selected locations. Likewise, identify core frontal season using long-term satellite datasets and focus a glider survey on peak frontal periods.

Future scenarios of effective ocean monitoring and dynamic marine management could encompass the deployment of fleets of autonomous vehicles, including surface and underwater platforms carrying multiple sensors. In combination with satellite imagery, three dimensional, high-resolution data of multiple parameters and locations can be obtained simultaneously. If a feature or event of particular interest is discovered, such as bio-aggregations at a front, coverage can be increased or directed vessel-based surveys be undertaken. This will provide a) much more useful data for the understanding of ecosystem

functioning than is currently achieved by isolated surveys, and b) the possibility to undertake dynamic ocean management, where conservation measures are adjusted in direct response to near real-time events. Furthermore, autonomous vehicles could be used to patrol sensitive or remote areas of the oceans and finally provide the coverage necessary to reinforce current management regulations.

8 REFERENCES

Acha, E. M., Piola, A., Iribarne, O., & Mianzan, H. (2015). *Ecological Processes at Marine Fronts: Oases in the Ocean*: Springer.

Ainley, D. G., Dugger, K. D., Ford, R. G., Pierce, S. D., Reese, D. C., Brodeur, R. D., Tynan, C. T., & Barth, J. A. (2009). Association of predators and prey at frontal features in the California Current: competition, facilitation, and co-occurrence. *Marine Ecology Progress Series, 389*, 271-294. doi: 10.3354/meps08153

Akaike, H. (1981). Likelihood of a model and information criteria. *Journal of econometrics, 16*(1), 3-14.

Alemany, D., Acha, E. M., & Iribarne, O. (2009). The relationship between marine fronts and fish diversity in the Patagonian Shelf Large Marine Ecosystem. *Journal of Biogeography, 36*(11), 2111-2124. doi: 10.1111/j.1365-2699.2009.02148.x

Allan, I. J., & Harman, C. (2011). Global Aquatic Passive Sampling: Maximizing Available Resources Using a Novel Exposure Procedure. *Environmental Science & Technology, 45*(15), 6233-6234. doi: 10.1021/es2021022

Allan, I. J., Harman, C., Kringstad, A., & Bratsberg, E. (2010). Effect of sampler material on the uptake of PAHs into passive sampling devices. *Chemosphere, 79*(4), 470-475. doi: 10.1016/j.chemosphere.2010.01.021

Allan, I. J., Harman, C., Ranneklev, S. B., Thomas, K. V., & Grung, M. (2013). Passive sampling for target and nontarget analyses of moderately polar and nonpolar substances in water. *Environmental Toxicology and Chemistry, 32*(8), 1718-1726. doi: 10.1002/etc.2260

Allan, I. J., Nilsson, H. C., Tjensvoll, I., Bradshaw, C., & Naes, K. (2011). Mobile passive samplers: Concept for a novel mode of exposure. *Environmental Pollution, 159*(10), 2393-2397. doi: 10.1016/j.envpol.2011.06.039

Alvarez, A., Chiggiato, J., & Schroeder, K. (2013). Mapping sub-surface geostrophic currents from altimetry and a fleet of gliders. *Deep-Sea Research Part I-Oceanographic Research Papers, 74*, 115-129. doi: 10.1016/j.dsr.2012.10.014

Alvarez, A., & Mourre, B. (2012). Oceanographic Field Estimates from Remote Sensing and Glider Fleets. *Journal of Atmospheric and Oceanic Technology, 29*(11), 1657-1662. doi: 10.1175/jtech-d-12-00015.1

ArcMap. (2012). ArcMap10.1. Redlands, California: ESRI.

Armstrong, E. M., Wagner, G., Vazquez-Cuervo, J., & Chin, T. M. (2012). Comparisons of regional satellite sea surface temperature gradients derived from MODIS and AVHRR sensors. *International Journal of Remote Sensing, 33*(21), 6639-6651. doi: 10.1080/01431161.2012.692832

Azzellino, A., Gaspari, S., Airoldi, S., & Nani, B. (2008). Habitat use and preferences of cetaceans along the continental slope and the adjacent pelagic waters in the western Ligurian Sea. *Deep Sea Research Part I: Oceanographic Research Papers, 55*(3), 296-323.

Badin, G., Williams, R. G., Holt, J. T., & Fernand, L. J. (2009). Are mesoscale eddies in shelf-seas formed by baroclinic instability of tidal fronts? *Journal of Geophysical Research-Oceans, 114*. doi: C1002110.1029/2009jc005340

Bailey, H., & Thompson, P. (2010). Effect of oceanographic features on fine-scale foraging movements of bottlenose dolphins. *Marine Ecology-Progress Series, 418*, 223-233. doi: 10.3354/meps08789

Bakun, A. (2006). Fronts and eddies as key structures in the habitat of marine fish larvae: opportunity, adaptive response and competitive advantage. *Scientia Marina, 70*, 105-122.

Ballance, L. T., Pitman, R. L., & Fiedler, P. C. (2006). Oceanographic influences on seabirds and cetaceans of the eastern tropical Pacific: A review. *Progress in Oceanography, 69*(2-4), 360-390. doi: 10.1016/j.pocean.2006.03.013

Bargeron, C. P., Hydes, D. J., Woolf, D. K., Kelly-Gerreyn, B. A., & Qurban, M. A. (2006). A regional analysis of new production on the northwest European shelf using oxygen fluxes and a ship-of-opportunity. *Estuarine Coastal and Shelf Science, 69*(3-4), 478-490. doi: 10.1016/j.ecss.2006.05.015

Bates, D., Maechler, M., Bolker, B., Walker, S., Christensen, R. H. B., Singmann, H., Dai, B., Eigen, C., & Rcpp, L. (2014). Package 'lme4'. *R Foundation for Statistical Computing, Vienna*.

Batten, S. D., Clark, R., Flinkman, J., Hays, G. C., John, E., John, A. W. G., Jonas, T., Lindley, J. A., Stevens, D. P., & Walne, A. (2003). CPR sampling: the technical background, materials and methods, consistency and comparability. *Progress in Oceanography, 58*(2-4), 193-215. doi: 10.1016/j.poccan.2003.08.004

Baumgartner, M. F., & Fratantoni, D. M. (2008). Diel periodicity in both sei whale vocalization rates and the vertical migration of their copepod prey observed from ocean gliders. *Limnology and Oceanography, 53*(5), 2197-2209. doi: 10.4319/lo.2008.53.5_part_2.2197

Baumgartner, M. F., Fratantoni, D. M., Hurst, T. P., Brown, M. W., Cole, T. V. N., Van Parijs, S. M., & Johnson, M. (2013). Real-time reporting of baleen whale passive acoustic detections from ocean gliders. *The Journal of the Acoustical Society of America, 134*(3), 1814-1823. doi: 10.1121/1.4816406

Beaugrand, G., Ibanez, F., & Reid, P. C. (2000). Spatial, seasonal and long-term fluctuations of plankton in relation to hydroclimatic features in the English Channel, Celtic Sea and Bay of Biscay. *Marine Ecology-Progress Series, 200*, 93-102.

Beaumont, N. J., Austen, M. C., Atkins, J. P., Burdon, D., Degraer, S., Dentinho, T. P., Derous, S., Holm, P., Horton, T., van Ierland, E., Marboe, A. H., Starkey, D. J., Townsend, M., & Zarzycki, T. (2007). Identification, definition and quantification of goods and services provided by marine biodiversity: Implications for the ecosystem approach. *Marine Pollution Bulletin, 54*(3), 253-265. doi: http://dx.doi.org/10.1016/j.marpolbul.2006.12.003

Begg, G. S., & Reid, J. B. (1997). Spatial variation in seabird density at a shallow sea tidal mixing front in the Irish Sea. *Ices Journal of Marine Science, 54*(4), 552-565. doi: 10.1006/jmsc.1997.0259

Belkin, I. M., & Cornillon, P. C. (2005). Bering Sea thermal front from Pathfinder data: Seasonal and interannual variability. *Pacific Oceanography, 2*(3-4), 6-20.

Belkin, I. M., Cornillon, P. C., & Sherman, K. (2009). Fronts in Large Marine Ecosystems. *Progress in Oceanography, 81*(1-4), 223-236. doi: 10.1016/j.pocean.2009.04.015

Bertrand, A., Gerlotto, F., Bertrand, S., Gutierrez, M., Alza, L., Chipollini, A., Diaz, E., Espinoza, P., Ledesma, J., Quesquen, R., Peraltilla, S., & Chavez, F. (2008). Schooling behaviour and environmental forcing in relation to anchoveta distribution: An analysis across multiple spatial scales. *Progress in Oceanography, 79*(2-4), 264-277. doi: 10.1016/j.pocean.2008.10.018

Bisagni, J. J., Kim, H. S., & Drinkwater, K. F. (2006). Observations and modeling of shelf-slope front seasonal variability between 75 degrees and 50 degrees W. *Deep-Sea Research Part Ii-Topical Studies in Oceanography, 53*(23-24), 2477-2500. doi: 10.1016/j.dsr2.2006.08.005

Bisagni, J. J., Seemann, K. W., & Mavor, T. P. (2001). High-resolution satellite-derived sea-surface temperature variability over the Gulf of Maine and Georges Bank region, 1993-1996. *Deep-Sea Research Part Ii-Topical Studies in Oceanography, 48*(1-3), 71-94. doi: 10.1016/s0967-0645(00)00115-6

Block, B. A., Jonsen, I. D., Jorgensen, S. J., Winship, A. J., Shaffer, S. A., Bograd, S. J., Hazen, E. L., Foley, D. G., Breed, G. A., Harrison, A. L., Ganong, J. E., Swithenbank, A., Castleton, M., Dewar, H., Mate, B. R., Shillinger, G. L., Schaefer, K. M., Benson, S. R., Weise, M. J., Henry, R. W., & Costa, D. P. (2011). Tracking apex marine predator movements in a dynamic ocean. *Nature, 475*(7354), 86-90. doi: 10.1038/nature10082

Bodey, T. W., Jessopp, M. J., Votier, S. C., Gerritsen, H. D., Cleasby, I. R., Hamer, K. C., Patrick, S. C., Wakefield, E. D., & Bearhop, S. (2014). Seabird movement reveals the ecological footprint of fishing vessels. *Current Biology, 24*(11), R514-R515. doi: 10.1016/j.cub.2014.04.041

Bonnet, D., Richardson, A., Harris, R., Hirst, A., Beaugrand, G., Edwards, M., Ceballos, S., Diekman, R., Lopez-Urrutia, A., Valdes, L., Carlotti, F., Molinero, J. C., Weikert, H., Greve, W., Lucic, D., Albaina, A., Yahia, N. D., Umani, S. F., Miranda, A., dos Santos, A., Cook, K., Robinson, S., & de Puelles, M. L. F. (2005). An overview of Calanus helgolandicus ecology in European waters. *Progress in Oceanography, 65*(1), 1-53. doi: 10.1016/j.pocean.2005.02.002

Booij, K., Hofmans, H. E., Fischer, C. V., & Van Weerlee, E. M. (2003). Temperature-dependent uptake rates of nonpolar organic compounds by semipermeable membrane devices and low-density polyethylene membranes. *Environmental Science & Technology, 37*(2), 361-366. doi: 10.1021/es025739i

Booij, K., & Smedes, F. (2011). An Improved Method for Estimating in Situ Sampling Rates of Nonpolar Passive Samplers (vol 44, pg 6789, 2010). *Environmental Science & Technology, 45*(23), 10288-10288. doi: 10.1021/es203621m

Booij, K., Smedes, F., & van Weerlee, E. M. (2002). Spiking of performance reference compounds in low density polyethylene and silicone passive water samplers. *Chemosphere, 46*(8), 1157-1161. doi: 10.1016/s0045-6535(01)00200-4

Booij, K., van Bommel, R., Jones, K. C., & Barber, J. L. (2007). Air-water distribution of hexachlorobenzene and 4,4'-DDE along a North-South Atlantic transect. *Marine Pollution Bulletin, 54*(6), 814-819. doi: 10.1016/j.marpolbul.2006.12.012

Bost, C. A., Cotte, C., Bailleul, F., Cherel, Y., Charrassin, J. B., Guinet, C., Ainley, D. G., & Weimerskirch, H. (2009). The importance of oceanographic fronts to marine birds and mammals of the southern oceans. *Journal of Marine Systems, 78*(3), 363-376. doi: 10.1016/j.jmarsys.2008.11.022

Bouffard, J., Pascual, A., Ruiz, S., Faugere, Y., & Tintore, J. (2010). Coastal and mesoscale dynamics characterization using altimetry and gliders: A case study in the Balearic Sea. *Journal of Geophysical Research-Oceans, 115*. doi: C1002910.1029/2009jc006087

Bouffard, J., Renault, L., Ruiz, S., Pascual, A., Dufau, C., & Tintore, J. (2012). Sub-surface small-scale eddy dynamics from multi-sensor observations and modeling. *Progress in Oceanography, 106*, 62-79. doi: 10.1016/j.pocean.2012.06.007

Bowers, D. G., & Simpson, J. H. (1987). Mean position of tidal fronts in European shelf-seas. *Continental Shelf Research, 7*(1), 35-44.

Boyce, M. S., Vernier, P. R., Nielsen, S. E., & Schmiegelow, F. K. A. (2002). Evaluating resource selection functions. *Ecological Modelling, 157*(2-3), 281-300. doi: 10.1016/s0304-3800(02)00200-4

Brennan, J., Fitzsimmons, C., Gray, T., & Raggatt, L. (2013). EU marine strategy framework directive (MSFD) and marine spatial planning (MSP): Which is the more dominant and practicable contributor to maritime policy in the UK? *Marine Policy, 43*, 359-366. doi: 10.1016/j.marpol.2013.07.011

Brodie, P. F. (1995). The Bay of Fundy/Gulf of maine harbour porpoise (Phocoena phocoena): Some considerations regarding species interactions, energetics, density dependence and bycatch. In A. Bjorge & G. P. Donovan (Eds.), *Report of the International Whaling Commission Special Issue; Biology of the phocoenids: A collection of papers* (Vol. 16, pp. 181-187).

Brody, S. R., Lozier, M. S., & Dunne, J. P. (2013). A comparison of methods to determine phytoplankton bloom initiation. *Journal of Geophysical Research-Oceans, 118*(5), 2345-2357. doi: 10.1002/jgrc.20167

Brown, J., Carrillo, L., Fernand, L., Horsburgh, K. J., Hill, A. E., Young, E. F., & Medler, K. J. (2003). Observations of the physical structure and seasonal jet-like circulation of the Celtic Sea and St. George's Channel of the Irish Sea. *Continental Shelf Research, 23*(6), 533-561. doi: 10.1016/s0278-4343(03)00008-6

Buckland, S. T., & Turnock, B. J. (1992). A robust line transect method. *Biometrics, 48*(3), 901-909. doi: 10.2307/2532356

Campbell, M. S., Stehfest, K. M., Votier, S. C., & Hall-Spencer, J. M. (2014). Mapping fisheries for marine spatial planning: Gear-specific vessel monitoring system (VMS), marine conservation and offshore renewable energy. *Marine Policy, 45*, 293-300. doi: 10.1016/j.marpol.2013.09.015

Castelao, R. M., & Wang, Y. T. (2014). Wind-driven variability in sea surface temperature front distribution in the California Current System. *Journal of Geophysical Research-Oceans, 119*(3), 1861-1875.

Cayula, J. F., & Cornillon, P. (1992). Edge-detection algorithm for SST images. *Journal of Atmospheric and Oceanic Technology, 9*(1), 67-80. doi: 10.1175/1520-0426(1992)009<0067:edafsi>2.0.co;2

Chassot, E., Bonhommeau, S., Reygondeau, G., Nieto, K., Polovina, J. J., Huret, M., Dulvy, N. K., & Demarcq, H. (2011). Satellite remote sensing for an ecosystem approach to fisheries management. *Ices Journal of Marine Science, 68*(4), 651-666. doi: 10.1093/icesjms/fsq195

Collie, J. S., Adamowicz, W. L., Beck, M. W., Craig, B., Essington, T. E., Fluharty, D., Rice, J., & Sanchirico, J. N. (2013). Marine spatial planning in practice. *Estuarine Coastal and Shelf Science, 117*, 1-11. doi: 10.1016/j.ecss.2012.11.010

Constable, A. J., Melbourne-Thomas, J., Corney, S. P., Arrigo, K. R., Barbraud, C., Barnes, D. K. A., Bindoff, N. L., Boyd, P. W., Brandt, A., Costa, D. P., Davidson, A. T., Ducklow, H. W., Emmerson, L., Fukuchi, M., Gutt, J., Hindell, M. A., Hofmann, E. E., Hosie, G. W., Iida, T., Jacob, S., Johnston, N. M., Kawaguchi, S., Kokubun, N., Koubbi, P., Lea, M. A., Makhado, A., Massom, R. A., Meiners, K., Meredith, M. P., Murphy, E. J., Nicol, S., Reid, K., Richerson, K., Riddle, M. J., Rintoul, S. R., Smith, W. O., Southwell, C., Stark, J. S., Sumner, M., Swadling, K. M., Takahashi, K. T., Trathan, P. N., Welsford, D. C., Weimerskirch, H., Westwood, K. J., Wienecke, B. C., Wolf-Gladrow, D., Wright, S. W., Xavier, J. C., & Ziegler, P. (2014). Climate change and Southern Ocean ecosystems I: how changes in physical habitats directly affect marine biota. *Global Change Biology, 20*(10), 3004-3025. doi: 10.1111/gcb.12623

Correia, A. M., Tepsich, P., Rosso, M., Caldeira, R., & Sousa-Pinto, I. (2015). Cetacean occurrence and spatial distribution: Habitat modelling for offshore waters in the Portuguese EEZ (NE Atlantic). *Journal of Marine Systems, 143*, 73-85. doi: 10.1016/j.jmarsys.2014.10.016

Cotte, C., d'Ovidio, F., Dragon, A. C., Guinet, C., & Levy, M. (2015). Flexible preference of southern elephant seals for distinct mesoscale features within the Antarctic Circumpolar Current. *Progress in Oceanography, 131*, 46-58. doi: 10.1016/j.pocean.2014.11.011

Cox, S. L., Ingram, S. N., Embling, C., Votier, S. C., & Hosegood, P. unpublished data.

Cox, S. L., Scott, B. E., & Camphuysen, C. J. (2013). Combined spatial and tidal processes identify links between pelagic prey species and seabirds. *Marine Ecology Progress Series, 479*, 203-+. doi: 10.3354/meps10176

Croll, D. A., Marinovic, B., Benson, S., Chavez, F. P., Black, N., Ternullo, R., & Tershy, B. R. (2005). From wind to whales: trophic links in a coastal upwelling system. *Marine Ecology Progress Series, 289*, 117-130. doi: 10.3354/meps289117

Cumming, G. S. (2000). Using between-model comparisons to fine-tune linear models of species ranges. *Journal of Biogeography, 27*(2), 441-455.

Cyr, F., & Larouche, P. (2015). Thermal Fronts Atlas of Canadian Coastal Waters. *Atmosphere-Ocean, 53*(2), 212-236. doi: 10.1080/07055900.2014.986710

D'Elbee, J., & Hemery, G. (1998). Diet and foraging behaviour of the British Storm Petrel Hydrobates pelagicus in the Bay of Biscay during summer. *Ardea, 86*(1), 1-10.

Dauvin, J.-C. (2012). Are the eastern and western basins of the English Channel two separate ecosystems? *Marine Pollution Bulletin, 64*(3), 463-471.

Davis, R. E., Leonard, N. E., & Fratantoni, D. M. (2009). Routing strategies for underwater gliders. *Deep-Sea Research Part Ii-Topical Studies in Oceanography, 56*(3-5), 173-187. doi: 10.1016/j.dsr2.2008.08.005

Davis, R. E., Ohman, M. D., Rudnick, D. L., Sherman, J. T., & Hodges, B. (2008). Glider surveillance of physics and biology in the southern California Current System. *Limnology and Oceanography, 53*(5), 2151-2168. doi: 10.4319/lo.2008.53.5_part_2.2151

Davoren, G. (2013). Distribution of marine predator hotspots explained by persistent areas of prey. *Marine Biology, 160*(12), 3043-3058. doi: 10.1007/s00227-013-2294-5

Day, J. (2008). The need and practice of monitoring, evaluating and adapting marine planning and management - lessons from the Great Barrier Reef. *Marine Policy, 32*(5), 823-831. doi: 10.1016/j.marpol.2008.03.023

de Boer, M. N., Simmonds, M. P., Reijnders, P. J. H., & Aarts, G. (2014). The Influence of Topographic and Dynamic Cyclic Variables on the Distribution of Small Cetaceans in a Shallow Coastal System. *Plos One, 9*(1). doi: e8633110.1371/journal.pone.0086331

Defra. (2009). Guidance note on 'Selection and designation of Marine Conservation Zones' (Note 1). *Published by the Department for Environment, Food and Rural Affairs*.

Defra. (2012). 'Marine Strategy Framework Directive Consultation: UK initial assessment and proposals for Good Environmental Status': London: Department for Environment, Food and Rural Affairs.

Defra. (2013). 'The Isles of Scilly Marine Conservation Zones Designation Order 2013'. Ministerial Order. No 10: London: Department of Environment, Food and Rural Affairs.

Derisio, C., Alemany, D., Acha, E. M., & Mianzan, H. (2014). Influence of a tidal front on zooplankton abundance, assemblages and life histories in Peninsula Valdes, Argentina. *Journal of Marine Systems, 139*, 475-482. doi: 10.1016/j.jmarsys.2014.08.019

Diakhate, M., de Coetlogon, G., Lazar, A., Wade, M., & Gaye, A. T. (2016). Intraseasonal variability of tropical Atlantic sea-surface temperature: air-sea interaction over upwelling fronts. *Quarterly Journal of the Royal Meteorological Society, 142*(694), 372-386.

Doney, S. C., Ruckelshaus, M., Duffy, J. E., Barry, J. P., Chan, F., English, C. A., Galindo, H. M., Grebmeier, J. M., Hollowed, A. B., Knowlton, N., Polovina, J., Rabalais, N. N., Sydeman, W. J., & Talley, L. D. (2012). Climate Change Impacts on Marine Ecosystems. *Annual Review of Marine Science, Vol 4, 4*, 11-37. doi: 10.1146/annurev-marine-041911-111611

Dong, S. F., Sprintall, J., & Gille, S. T. (2006). Location of the antarctic polar front from AMSR-E satellite sea surface temperature measurements. *Journal of Physical Oceanography, 36*(11), 2075-2089.

Doniol-Valcroze, T., Berteaux, D., Larouche, P., & Sears, R. (2007). Influence of thermal fronts on habitat selection by four rorqual whale species in the Gulf of St. Lawrence. *Marine Ecology-Progress Series, 335*, 207-216.

Dooley, H. D. (1981). The role of axially varying vertical mixing along the path of a current generating phytoplankton production. *Philosophical Transactions of the Royal Society of London Series a-Mathematical Physical and Engineering Sciences, 302*(1472), 649-660.

Douvere, F., & Ehler, C. N. (2011). The importance of monitoring and evaluation in adaptive maritime spatial planning. *Journal of Coastal Conservation, 15*(2), 305-311. doi: 10.1007/s11852-010-0100-9

Drinkwater, K. F., & Loder, J. W. (2001). Near-surface horizontal convergence and dispersion near the tidal-mixing front on Northeastern Georges Bank. *Deep-Sea Research Part Ii-Topical Studies in Oceanography, 48*(1-3), 311-339. doi: 10.1016/s0967-0645(00)00084-9

Dunford, A. J. (2005). Correcting echo-integration data for transducer motion (L). *Journal of the Acoustical Society of America, 118*(4), 2121-2123. doi: 10.1121/1.2005927

Durazo, R., Harrison, N. M., & Hill, A. E. (1998). Seabird observations at a tidal mixing front in the Irish Sea. *Estuarine Coastal and Shelf Science, 47*(2), 153-164. doi: 10.1006/ecss.1998.0339

Dyndo, M., Wisniewska, D. M., Rojano-Donate, L., & Madsen, P. T. (2015). Harbour porpoises react to low levels of high frequency vessel noise. *Scientific Reports, 5*. doi: 10.1038/srep11083

Edwards, E. W. J., Quinn, L. R., Wakefield, E. D., Miller, P. I., & Thompson, P. M. (2013). Tracking a northern fulmar from a Scottish nesting site to the Charlie-Gibbs Fracture Zone: Evidence of linkage between coastal breeding seabirds and Mid-Atlantic Ridge feeding sites. *Deep-Sea Research Part Ii-Topical Studies in Oceanography, 98*, 438-444. doi: 10.1016/j.dsr2.2013.04.011

Ekstrom, C. (2014). MESS: Miscellaneous Esoteric Statistical Scripts. *R package version 0.3-2.* http://CRAN.R-project.org/package=MESS.

Elliott, A. J., & Clarke, T. (1991). Seasonal stratification in the Northwest European shelf-seas. *Continental Shelf Research, 11*(5), 467-492. doi: 10.1016/0278-4343(91)90054-a

Embling, C., Sharples, J., Armstrong, E., Palmer, M., & Scott, B. (2013). Fish behaviour in response to tidal variability and internal waves over a shelf-sea bank. *Progress in Oceanography, 117*, 106-117.

Embling, C. B., Illian, J., Armstrong, E., van der Kooij, J., Sharples, J., Camphuysen, K. C. J., & Scott, B. E. (2012). Investigating fine-scale spatio-temporal predator-prey patterns in dynamic marine ecosystems: a functional data analysis approach. *Journal of Applied Ecology, 49*(2), 481-492. doi: 10.1111/j.1365-2664.2012.02114.x

English, D., Chuanmin, H., Lembke, C., Weisberg, R., Edwards, D., Lorenzoni, L., Gonzalez, G., & Muller-Karger, F. (2009). Observing the 3-dimensional distribution of bio-optical properties of West Florida Shelf waters using gliders and autonomous platforms. *Oceans 2009*, 7 pp.-7 pp.

European Union. (2008). Directive 2008/56/EC of the European Parliament and the Council of 17 June 2008. Establishing a framework for community action in the field of marine environmental policy (Marine Strategy Framework Directive). . *Official Journal of the European Union, L164*, 19-40.

Evans, P. G., Pierce, G. J., & Panigada, S. (2010). Climate change and marine mammals. *Journal of the Marine Biological Association of the United Kingdom, 90*(08), 1483-1487.

Ferguson, B. G., Lo, K. W., & Rodgers, J. D. (2010, 24-27 May 2010). *Sensing the underwater acoustic environment with a single hydrophone onboard an undersea glider.* Paper presented at the OCEANS 2010 IEEE - Sydney.

Fernandez-Perdomo, E., Hernandez-Sosa, D., Isern-Gonzalez, J., Cabrera-Gamez, J., Dominguez-Brito, A. C., Prieto-Maranon, V., & Ieee. (2011). Single and Multiple Glider Path Planning using an Optimization-based Approach. *2011 Ieee - Oceans Spain*.

Flament, P., & Armi, L. (2000). The shear, convergence, and thermohaline structure of a front. *Journal of Physical Oceanography, 30*(1), 51-66.

Foote, K., Knudsen H., Vestnes G., Maclennan D.N., & Simmonds E.J. (1987). Calibration of acoustic instruments for fish density estimation: A practical guide. . *ICES Cooperative Research Report, 144*, 69.

Force, M. P., Santora, J. A., Reiss, C. S., & Loeb, V. J. (2015). Seabird species assemblages reflect hydrographic and biogeographic zones within Drake Passage. *Polar Biology, 38*(3), 381-392. doi: 10.1007/s00300-014-1594-7

Fox, J. (2002). Linear mixed models. *Appendix to An R and S-PLUS Companion to Applied Regression, URL* http://cran*. r-project. org/doc/contrib/Fox-Companion/appendix-mixed-models. pdf*.

Fox, R. D., Gower, J. F. R., & Curran, T. A. (2009). Slocum glider observations during the spring bloom in the Strait of Georgia. *Oceans 2009*, 9 pp.-9 pp.

Frajka-Williams, E., Rhines, P. B., & Eriksen, C. C. (2009). Physical controls and mesoscale variability in the Labrador Sea spring phytoplankton bloom observed by Seaglider. *Deep-Sea Research Part I-Oceanographic Research Papers, 56*(12), 2144-2161. doi: 10.1016/j.dsr.2009.07.008

Franks, P. J. S. (1992a). Phytoplankton blooms at fronts- Patterns, scales, and physical forcing mechanisms. *Reviews in Aquatic Sciences, 6*(2), 121-137.

Franks, P. J. S. (1992b). Sink or swim- Accumulation of biomass at fronts *Marine Ecology-Progress Series, 82*(1), 1-12.

Franks, P. J. S., & Chen, C. S. (1996). Plankton production in tidal fronts: A model of Georges Bank in summer. *Journal of Marine Research, 54*(4), 631-651. doi: 10.1357/0022240963213718

Fransz, H. G., Colebrook, J. M., Gamble, J. C., & Krause, M. (1991). The zooplankton of the North Sea. *Netherlands Journal of Sea Research, 28*(1-2), 1-52. doi: 10.1016/0077-7579(91)90003-j

Game, E. T., Grantham, H. S., Hobday, A. J., Pressey, R. L., Lombard, A. T., Beckley, L. E., Gjerde, K., Bustamante, R., Possingham, H. P., & Richardson, A. J. (2009). Pelagic protected areas: the missing dimension in ocean conservation. *Trends in Ecology & Evolution, 24*(7), 360-369. doi: 10.1016/j.tree.2009.01.011

Garrett, C. J. R., & Loder, J. W. (1981). Dynamical aspects of shallow sea fronts. *Philosophical Transactions of the Royal Society of London Series a-Mathematical Physical and Engineering Sciences, 302*(1472), 563-581.

Gill, P. C., Pirzl, R., Morrice, M. G., & Lawton, K. (2015). Cetacean Diversity of the Continental Shelf and Slope off Southern Australia. *Journal of Wildlife Management, 79*(4), 672-681. doi: 10.1002/jwmg.867

Gillespie, D., Caillat, M., Gordon, J., & White, P. (2013). Automatic detection and classification of odontocete whistles. *Journal of the Acoustical Society of America, 134*(3), 2427-2437. doi: 10.1121/1.4816555

Gillespie, D., Mellinger, D., Gordon, J., Mclaren, D., Redmond, P., McHugh, R., Trinder, P., Deng, X., & Thode, A. (2008). PAMGUARD: Semiautomated, open source software for real-time acoustic detection and localisation of cetaceans. *Journal of the Acoustical Society of America, 30*(5), 54-62.

Gilman, E. (2002). Guidelines for coastal and marine site-planning and examples of planning and management intervention tools. *Ocean & Coastal Management, 45*(6-7), 377-404. doi: 10.1016/s0964-5691(02)00076-5

Gomez-Gutierrez, J., Martinez-Gomez, S., & Robinson, C. J. (2007). Influence of thermo-haline fronts forced by tides on near-surface zooplankton aggregation and community structure in Bahia Magdalena, Mexico. *Marine Ecology-Progress Series, 346*, 109-125. doi: 10.3354/meps07019

Goold, J. C. (1998). Acoustic assessment of populations of common dolphin off the west Wales coast, with perspectives from satellite infrared imagery. *Journal of the Marine Biological Association of the United Kingdom, 78*(4), 1353-1368.

Gosnell, J. S., Macfarlan, R. J. A., Shears, N. T., & Caselle, J. E. (2014). A dynamic oceanographic front drives biogeographical structure in invertebrate settlement along Santa Cruz Island, California USA. *Marine Ecology Progress Series, 507*, 181-196. doi: 10.3354/meps10802

Grall, J. R., Le Corre, P., Le Fevre, J., Marty, Y., & Fournier, B. (1980). Caracteristiques estivales de la couche d'eau superficielle dans la zone de fronts thermiques Quest-Bretagne. *Oceanis, 6*, 235-249.

Greer, A. T., Cowen, R. K., Guigand, C. M., & Hare, J. A. (2015). Fine-scale planktonic habitat partitioning at a shelf-slope front revealed by a high-resolution imaging system. *Journal of Marine Systems, 142*, 111-125. doi: 10.1016/j.jmarsys.2014.10.008

Guihen, D., Fielding, S., Murphy, E. J., Heywood, K. J., & Griffiths, G. (2014). An assessment of the use of ocean gliders to undertake acoustic measurements of zooplankton: the distribution and density of Antarctic krill (*Euphausia superba*) in the Weddell Sea. *Limnology and Oceanography-Methods, 12*.

Guillou, N., Chapalain, G., & Duvieilbourg, E. (2013). Sea surface temperature modelling in the Sea of Iroise: assessment of boundary conditions. *Ocean Dynamics, 63*(7), 849-863. doi: 10.1007/s10236-013-0627-z

Halekoh, U., Hojsgaard, S., & Yan, J. (2006). The R Package geepack for Generalized Estimating Equations. *Journal of Statistical Software, 15*(2), 1-11.

Halpern, B. S., Walbridge, S., Selkoe, K. A., Kappel, C. V., Micheli, F., D'Agrosa, C., Bruno, J. F., Casey, K. S., Ebert, C., Fox, H. E., Fujita, R., Heinemann, D., Lenihan, H. S., Madin, E. M. P., Perry, M. T., Selig, E. R., Spalding, M., Steneck, R., & Watson, R. (2008). A global map of human impact on marine ecosystems. *Science, 319*(5865), 948-952. doi: 10.1126/science.1149345

Haney, J. C., & McGillivary, P. A. (1985). Midshelf fronts in the South Atlantic Bight and their influence on seabird distribution and seasonal abundance. *Biological Oceanography, 3*(4), 401-430.

Hardin, J. W., & Hilbe, J. M. (2003). *Generalized Estimating Equations* (2nd ed.). London: Chapman & Hall/CRC Press.

Hastie, T., & Tibshirani, R. (1987). Generalized additive models- Some applications. *Journal of the American Statistical Association, 82*(398), 371-386. doi: 10.2307/2289439

Hazen, E. L., Nowacek, D. P., Laurent, L. S., Halpin, P. N., & Moretti, D. J. (2011). The Relationship among Oceanography, Prey Fields, and Beaked Whale Foraging Habitat in the Tongue of the Ocean. *Plos One, 6*(4). doi: e1926910.1371/journal.pone.0019269

Hazen, E. L., Suryan, R. M., Santora, J. A., Bograd, S. J., Watanuki, Y., & Wilson, R. P. (2013). Scales and mechanisms of marine hotspot formation INTRODUCTION. *Marine Ecology Progress Series, 487*, 177-183. doi: Doi 10.3354/Meps10477

Hermannsen, L., Beedholm, K., Tougaard, J., & Madsen, P. T. (2014). High frequency components of ship noise in shallow water with a discussion of implications for harbor porpoises (Phocoena phocoena). *Journal of the Acoustical Society of America, 136*(4), 1640-1653. doi: 10.1121/1.4893908

Hickox, R., Belkin, I., Cornillon, P., & Shan, Z. (2000). Climatology and seasonal variability of ocean fronts in the east China, Yellow and Bohai Seas from satellite SST data. *Geophysical Research Letters, 27*(18), 2945-2948. doi: 10.1029/1999gl011223

Hidalgo, M., Reglero, P., Alvarez-Berastegui, D., Torres, A. P., Alvarez, I., Rodriguez, J. M., Carbonell, A., Zaragoza, N., Tor, A., Goni, R., Mallol, S., Balbin, R., & Alemany, F. (2014). Hydrographic and biological components of the seascape structure the meroplankton community in a frontal system. *Marine Ecology Progress Series, 505*, 65-80. doi: 10.3354/meps10763

Hill, A. E., Brown, J., Fernand, L., Holt, J., Horsburgh, K. J., Proctor, R., Raine, R., & Turrell, W. R. (2008). Thermohaline circulation of shallow tidal seas. *Geophysical Research Letters, 35*(11). doi: L1160510.1029/2008gl033459

Hobday, A. J., & Hartog, J. R. (2014). Derived Ocean Features for Dynamic Ocean Management. *Oceanography, 27*(4), 134-145. doi: 10.5670/oceanog.2014.92

Holligan, P. M. (1981). Biological implications of fronts on the Northwest European continental shelf. *Philosophical Transactions of the Royal Society of London Series a-Mathematical Physical and Engineering Sciences, 302*(1472), 547-&.

Holligan, P. M., Williams, P. J. L., Purdie, D., & Harris, R. P. (1984). Phytosynthesis, respiration and nitrogen supply of plankton populations in stratified, frontal and tidally-mixed shelf waters. *Marine Ecology-Progress Series, 17*(2), 201-213.

Holt, J., Butenschon, M., Wakelin, S. L., Artioli, Y., & Allen, J. I. (2012). Oceanic controls on the primary production of the northwest European continental shelf: model experiments under recent past conditions and a potential future scenario. *Biogeosciences, 9*(1), 97-117. doi: 10.5194/bg-9-97-2012

Holt, J., Hughes, S., Hopkins, J., Wakelin, S. L., Penny Holliday, N., Dye, S., González-Pola, C., Hjøllo, S. S., Mork, K. A., & Nolan, G. (2012). Multi-decadal variability and trends in the temperature of the northwest European continental shelf: A model-data synthesis. *Progress in Oceanography, 106*, 96-117.

Holt, J., & Proctor, R. (2008a). The seasonal circulation and volume transport on the northwest European continental shelf: A fine-resolution model study. *Journal of Geophysical Research-Oceans, 113*(C6). doi: C0602110.1029/2006jc004034

Holt, J., & Umlauf, L. (2008b). Modelling the tidal mixing fronts and seasonal stratification of the Northwest European Continental shelf. *Continental Shelf Research, 28*(7), 887-903. doi: 10.1016/j.csr.2008.01.012

Holt, J., Wakelin, S., Lowe, J., & Tinker, J. (2010). The potential impacts of climate change on the hydrography of the northwest European continental shelf. *Progress in Oceanography, 86*(3-4), 361-379. doi: 10.1016/j.pocean.2010.05.003

Hopkins, J., Shaw, A. G. P., & Challenor, P. (2010). The Southland Front, New Zealand: Variability and ENSO correlations. *Continental Shelf Research, 30*(14), 1535-1548. doi: 10.1016/j.csr.2010.05.016

Horsburgh, K. J., Hill, A. E., & Brown, J. (1998). A summer jet in the St George's Channel of the Irish Sea. *Estuarine Coastal and Shelf Science, 47*(3), 285-294. doi: 10.1006/ecss.1998.0354

Huckins, J. N., Manuweera, G. K., Petty, J. D., Mackay, D., & Lebo, J. A. (1993). Lipid-containing semipermeable membrane devices for monitoring organic contaminants in water. *Environmental Science & Technology, 27*(12), 2489-2496. doi: 10.1021/es00048a028

Hunter, P., & Macnab, R. (2003). The GEBCO Digital Atlas published by the British Oceanographic Data Centre on behalf of IOC and IHO. *North Atlantic region*.

Hurrell, J. W. (1995). Decadal trend in the North-Atlantic Oscilliation- Regional temperatures and precipitation. *Science, 269*(5224), 676-679. doi: 10.1126/science.269.5224.676

Hyrenbach, K. D., Forney, K. A., & Dayton, P. K. (2000). Marine protected areas and ocean basin management. *Aquatic conservation: marine and freshwater ecosystems, 10*(6), 437-458.

Hyrenbach, K. D., Veit, R. R., Weimerskirch, H., & Hunt, G. L., Jr. (2006). Seabird associations with mesoscale eddies: the subtropical Indian Ocean. *Marine Ecology-Progress Series, 324*, 271-279. doi: 10.3354/meps324271

Jameson, S. C., Tupper, M. H., & Ridley, J. M. (2002). The three screen doors: can marine 'protected' areas be effective? *Marine Pollution Bulletin, 44*(11), 1177-1183. doi: 10.1016/s0025-326x(02)00258-8

Jaquemet, S., Ternon, J. F., Kaehler, S., Thiebot, J. B., Dyer, B., Bemanaja, E., Marteau, C., & Le Corre, M. (2014). Contrasted structuring effects of mesoscale features on the seabird community in the Mozambique Channel. *Deep-Sea Research Part Ii-Topical Studies in Oceanography, 100*, 200-211. doi: 10.1016/j.dsr2.2013.10.027

Jaquet, N. (1996). How spatial and temporal scales influence understanding of Sperm Whale distribution: A review. *Mammal Review, 26*(1), 51-65. doi: 10.1111/j.1365-2907.1996.tb00146.x

Ji, R. B., Davis, C., Chen, C. S., & Beardsley, R. (2008). Influence of local and external processes on the annual nitrogen cycle and primary productivity on Georges Bank: A 3-D biological-physical modeling study. *Journal of Marine Systems, 73*(1-2), 31-47. doi: 10.1016/j.jmarsys.2007.08.002

Johnson, M., Partan, J., & Hurst, T. (2013). Low complexity lossless compression of underwater sound recordings. *Journal of the Acoustical Society of America, 133*(3), 1387-1398. doi: 10.1121/1.4776206

Johnson, M. P., & Tyack, P. L. (2003). A digital acoustic recording tag for measuring the response of wild marine mammals to sound. *Ieee Journal of Oceanic Engineering, 28*(1), 3-12. doi: 10.1109/joe.2002.808212

Joiris, C. R. (2011). A major feeding ground for cetaceans and seabirds in the south-western Greenland Sea. *Polar Biology, 34*(10), 1597-1607. doi: 10.1007/s00300-011-1022-1

Jones, A. R., Hosegood, P., Wynn, R. B., De Boer, M. N., Butler-Cowdry, S., & Embling, C. B. (2014). Fine-scale hydrodynamics influence the spatio-temporal distribution of harbour porpoises at a coastal hotspot. *Progress in Oceanography, 128*, 30-48. doi: 10.1016/j.pocean.2014.08.002

Jones, C. P. (2012). Slocum glider: persistent oceanography. *2012 IEEE/OES Autonomous Underwater Vehicles (AUV 2012)*, 6 pp.-6 pp. doi: 10.1109/auv.2012.6380738

Kahru, M., Di Lorenzo, E., Manzano-Sarabia, M., & Mitchell, B. G. (2012). Spatial and temporal statistics of sea surface temperature and chlorophyll fronts in the California Current. *Journal of Plankton Research, 34*(9), 749-760. doi: 10.1093/plankt/fbs010

Kai, E. T., Rossi, V., Sudre, J., Weimerskirch, H., Lopez, C., Hernandez-Garcia, E., Marsac, F., & Garcon, V. (2009). Top marine predators track Lagrangian coherent structures. *Proceedings of the National Academy of Sciences of the United States of America, 106*(20), 8245-8250. doi: 10.1073/pnas.0811034106

Kalnay, E., Kanamitsu, M., Kistler, R., Collins, W., Deaven, D., Gandin, L., Iredell, M., Saha, S., White, G., Woollen, J., Zhu, Y., Chelliah, M., Ebisuzaki, W., Higgins, W., Janowiak, J., Mo, K. C., Ropelewski, C., Wang, J., Leetmaa, A., Reynolds, R., Jenne, R., & Joseph, D. (1996). The NCEP/NCAR 40-year reanalysis project. *Bulletin of the American Meteorological Society, 77*(3), 437-471. doi: 10.1175/1520-0477(1996)077<0437:tnyrp>2.0.co;2

Kiorboe, T. (1993). Turbulence, phytoplankton cell-size and the structure of pelagic food webs. *Advances in Marine Biology, Vol 29, 29*, 1-72. doi: 10.1016/s0065-2881(08)60129-7

Kirby, R. R., Beaugrand, G., Lindley, J. A., Richardson, A. J., Edwards, M., & Reid, P. C. (2007). Climate effects and benthic-pelagic coupling in the North Sea. *Marine Ecology Progress Series, 330*, 31-38.

Kirby, R. R., & Lindley, J. A. (2005). Molecular analysis of Continuous Plankton Recorder samples, an examination of echinoderm larvae in the North Sea. *Journal of the Marine Biological Association of the United Kingdom, 85*(03), 451-459.

Kiszka, J., Macleod, K., Van Canneyt, O., Walker, D., & Ridoux, V. (2007). Distribution, encounter rates, and habitat characteristics of toothed cetaceans in the Bay of Biscay and adjacent waters from platform-of-opportunity data. *Ices Journal of Marine Science, 64*(5), 1033-1043. doi: 10.1093/icesjms/fsm067

Klemas, V. (2013). Fisheries applications of remote sensing: An overview. *Fisheries Research, 148*, 124-136. doi: 10.1016/j.fishres.2012.02.027

Klinck, H., Mellinger, D. K., Klinck, K., Bogue, N. M., Luby, J. C., Jump, W. A., Shilling, G. B., Litchendorf, T., Wood, A. S., Schorr, G. S., & Baird, R. W. (2012). Near-Real-Time Acoustic Monitoring of Beaked Whales and Other Cetaceans Using a Seaglider (TM). *Plos One, 7*(5). doi: e3612810.1371/journal.pone.0036128

Korneliussen, R. J., & Ona, E. (2003). Synthetic echograms generated from the relative frequency response. *ICES Journal of Marine Science: Journal du Conseil, 60*(3), 636-640.

L'Heveder, B., Mortier, L., Testor, P., & Lekien, F. (2013). A Glider Network Design Study for a Synoptic View of the Oceanic Mesoscale Variability. *Journal of Atmospheric and Oceanic Technology, 30*(7), 1472-1493. doi: 10.1175/jtech-d-12-00053.1

Lauria, V., Attrill, M. J., Pinnegar, J. K., Brown, A., Edwards, M., & Votier, S. C. (2012). Influence of Climate Change and Trophic Coupling across Four Trophic Levels in the Celtic Sea. *Plos One, 7*(10). doi: e4740810.1371/journal.pone.0047408

Le Boyer, A., Cambon, G., Daniault, N., Herbette, S., Le Cann, B., Marie, L., & Morin, P. (2009). Observations of the Ushant tidal front in September 2007. *Continental Shelf Research, 29*(8), 1026-1037. doi: 10.1016/j.csr.2008.12.020

Lee, M. A., Chang, Y., & Shimada, T. (2015). Seasonal evolution of fine-scale sea surface temperature fronts in the East China Sea. *Deep-Sea Research Part Ii-Topical Studies in Oceanography, 119*, 20-29. doi: 10.1016/j.dsr2.2014.03.021

Lee, O., Nash, R. D. M., & Danilowicz, B. S. (2005). Small-scale spatio-temporal variability in ichthyoplankton and zooplankton distribution in relation to a tidal-mixing front in the. *Ices Journal of Marine Science, 62*(6), 1021-1036. doi: 10.1016/j.icesjms.2005.04.016

Leeney, R. H., Witt, M. J., Broderick, A. C., Buchanan, J., Jarvis, D. S., Richardson, P. B., & Godley, B. J. (2012). Marine megavertebrates of Cornwall and the Isles of Scilly: relative abundance and distribution. *Journal of the Marine Biological Association of the United Kingdom, 92*(08), 1823-1833.

LeFevre, J. (1986). Aspects of the biology of frontal systems. *Advances in Marine Biology, 23*, 163-299.

Leonard, N. E., Paley, D. A., Lekien, F., Sepulchre, R., Fratantoni, D. M., & Davis, R. E. (2007). Collective motion, sensor networks, and ocean sampling. *Proceedings of the IEEE, 95*(1), 48-74.

Lewis, S., Sherratt, T. N., Hamer, K. C., Harris, M. P., & Wanless, S. (2003). Contrasting diet quality of northern gannets Morus bassanus at two colonies. *Ardea, 91*(2), 167-176.

Lewis, S., Wanless, S., Wright, P. J., Harris, M. P., Bull, J., & Elston, D. A. (2001). Diet and breeding performance of black-legged kittiwakes Rissa tridactyla at a North Sea colony. *Marine Ecology Progress Series, 221*, 277-284. doi: 10.3354/meps221277

Lewis, T., Gillespie, D., Matthews, L. J., Danbolt, M., Leaper, R., McLanaghan, R., & Moscrop, A. (2007). Sperm whale abundance estimates from acoustic surveys of the Ionian Sea and Straits of Sicily in 2003. *Journal of the Marine Biological Association of the United Kingdom, 87*(1), 353-357. doi: 10.1017/s0025315407054896

Lockyer, C. (2007). All creatures great and smaller: a study in cetacean life history energetics. *Journal of the Marine Biological Association of the United Kingdom, 87*(4), 1035-1045. doi: 10.1017/s0025315407054720

Loder, J. W., & Platt, T. (1985). *Physical controls on phytoplankton production at tidal fronts*.

Lohmann, R., Klanova, J., Kukucka, P., Yonis, S., & Bollinger, K. (2012). PCBs and OCPs on a East-to-West Transect: The Importance of Major Currents and Net Volatilization for PCBs in the Atlantic Ocean. *Environmental Science & Technology, 46*(19), 10471-10479. doi: 10.1021/es203459e

Lough, R. G., & Manning, J. P. (2001). Tidal-front entrainment and retention of fish larvae on the southern flank of Georges Bank. *Deep-Sea Research Part Ii-Topical Studies in Oceanography, 48*(1-3), 631-644.

Luyten, P. J., Jones, J. E., & Proctor, R. (2003). A numerical study of the long- and short-term temperature variability and thermal circulation in the North Sea. *Journal of Physical Oceanography, 33*(1), 37-56.

Macleod, C. D., Brereton, T., & Martin, C. (2009). Changes in the occurrence of common dolphins, striped dolphins and harbour porpoises in the English Channel and Bay of Biscay. *Journal of the Marine Biological Association of the United Kingdom, 89*(5), 1059-1065. doi: 10.1017/s0025315408002828

Mann, K. H., & Lazier, J. R. N. (2005). *DYNAMICS OF MARINE ECOSYSTEMS BIOLOGICAL-PHYSICAL INTERACTIONS IN THE OCEANS* (3rd ed.).

Marques, T. A., Thomas, L., Martin, S. W., Mellinger, D. K., Ward, J. A., Moretti, D. J., Harris, D., & Tyack, P. L. (2013). Estimating animal population density using passive acoustics. *Biological Reviews, 88*(2), 287-309. doi: 10.1111/brv.12001

Marsh, R., Hickman, A. E., & Sharples, J. (2015). S2P3-R (v1.0): a framework for efficient regional modelling of physical and biological structures and processes in shelf-seas. *Geoscientific Model Development, 8*(10), 3163-3178. doi: 10.5194/gmd-8-3163-2015

Martinez, I., Ellis, J., Scott, B., & Tidd, A. (2013). The fish and fisheries of Jones Bank and the wider Celtic Sea. *Progress in Oceanography*.

Matlab. (2009). Matlab 7.8 Natick, MA., United States

Mavor, T. P., & Bisagni, J. J. (2001). Seasonal variability of sea-surface temperature fronts on Georges Bank. *Deep-Sea Research Part Ii-Topical Studies in Oceanography, 48*(1-3), 215-243. doi: 10.1016/s0967-0645(00)00120-x

Maxwell, S. M., Hazen, E. L., Lewison, R. L., Dunn, D. C., Bailey, H., Bograd, S. J., Briscoe, D. K., Fossette, S., Hobday, A. J., Bennett, M., Benson, S., Caldwell, M. R., Costa, D. P., Dewar, H., Eguchi, T., Hazen, L., Kohin, S., Sippel, T., & Crowder, L. B. (2015). Dynamic ocean management: Defining and conceptualizing real-time management of the ocean. *Marine Policy, 58*, 42-50. doi: 10.1016/j.marpol.2015.03.014

McClellan, C. M., Brereton, T., Dell'Amico, F., Johns, D. G., Cucknell, A.-C., Patrick, S. C., Penrose, R., Ridoux, V., Solandt, J.-L., & Stephan, E. (2014). Understanding the Distribution of Marine Megafauna in the English Channel Region: Identifying Key Habitats for Conservation within the Busiest Seaway on Earth. *Plos One, 9*(2), e89720.

McGinty, N., Johnson, M. P., & Power, A. M. (2014). Spatial mismatch between phytoplankton and zooplankton biomass at the Celtic Boundary Front. *Journal of Plankton Research, 36*(6), 1446-1460. doi: 10.1093/plankt/fbu058

McGinty, N., Power, A. M., & Johnson, M. P. (2011). Variation among northeast Atlantic regions in the responses of zooplankton to climate change: Not all areas follow the same path. *Journal of Experimental Marine Biology and Ecology, 400*(1-2), 120-131. doi: 10.1016/j.jembe.2011.02.013

Merckelbach, L., Smeed, D., & Griffiths, G. (2010). Vertical water velocities from underwater gliders. *Journal of Atmospheric and Oceanic Technology, 27*(3), 547-563.

Meyer-Gutbrod, E., Greene, C., Packer, A., Dorn, H., & Griffith, J. (2012). *Long term autonomous fisheries survey utilizing active acoustics.* Paper presented at the Oceans, 2012.

Mikkelsen, L., Mouritsen, K. N., Dahl, K., Teilmann, J., & Tougaard, J. (2013). Re-established stony reef attracts harbour porpoises Phocoena phocoena. *Marine Ecology Progress Series, 481*, 239-248. doi: 10.3354/meps10260

Miller, P. (2004). Multi-spectral front maps for automatic detection of ocean colour features from SeaWiFS. *International Journal of Remote Sensing, 25*(7-8), 1437-1442. doi: Doi 10.1080/01431160310001592409

Miller, P. (2009). Composite front maps for improved visibility of dynamic sea-surface features on cloudy SeaWiFS and AVHRR data. *Journal of Marine Systems, 78*(3), 327-336. doi: 10.1016/j.jmarsys.2008.11.019

Miller, P. I. (in preperation). A line clustering algorithm with application to simplifying ocean front maps derived from satellite data. *Remote Sensing of Environment*.

Miller, P. I., & Christodoulou, S. (2014). Frequent locations of ocean fronts as an indicator of pelagic diversity: application to marine protected areas and renewables. *Marine Policy, 45*, 318–329.

Miller, P. I., Scales, K. L., Ingram, S. N., Southall, E. J., & Sims, D. W. (2015). Data from: Basking sharks and oceanographic fronts: quantifying associations in the north-east Atlantic. *Dryad*. doi: http://dx.doi.org/10.5061/dryad.d0h7s

Munk, P. (2007). Cross-frontal variation in growth rate and prey availability of larval North Sea cod Gadus morhua. *Marine Ecology-Progress Series, 334*, 225-235. doi: 10.3354/meps334225

Munk, P. (2014). Fish larvae at fronts: Horizontal and vertical distributions of gadoid fish larvae across a frontal zone at the Norwegian Trench. *Deep-Sea Research Part Ii-Topical Studies in Oceanography, 107*, 3-14. doi: 10.1016/j.dsr2.2014.01.016

Munk, P., Fox, C. J., Bolle, L. J., van Damme, C. J. G., Fossum, P., & Kraus, G. (2009). Spawning of North Sea fishes linked to hydrographic features. *Fisheries Oceanography, 18*(6), 458-469. doi: 10.1111/j.1365-2419.2009.00525.x

Munk, P., Larsson, P. O., Danielssen, D. S., & Moksness, E. (1999). Variability in frontal zone formation and distribution of gadoid fish larvae at the shelf break in the northeastern North Sea. *Marine Ecology-Progress Series, 177*, 221-233. doi: 10.3354/meps177221

Nabe-Nielsen, J., Tougaard, J., Teilmann, J., Lucke, K., & Forchhammer, M. C. (2013). How a simple adaptive foraging strategy can lead to emergent home ranges and increased food intake. *Oikos, 122*(9), 1307-1316. doi: 10.1111/j.1600-0706.2013.00069.x

Nakamura, H., Isobe, A., Minobe, S., Mitsudera, H., Nonaka, M., & Suga, T. (2015). 'Hot Spots' in the climate system-new developments in the extratropical ocean-atmosphere interaction research: a short review and an introduction. *Journal of Oceanography, 71*(5), 463-467. doi: 10.1007/s10872-015-0321-5

Neil, C., Cunningham, A., McKee, D., & Polton, J. A. (2012). Remote sensing of seasonal stratification dynamics in the southern Irish Sea. *Remote Sensing of Environment, 127*, 288-297. doi: 10.1016/j.rse.2012.09.010

Niewiadomska, K., Claustre, H., Prieur, L., & d'Ortenzio, F. (2008). Submesoscale physical-biogeochemical coupling across the Ligurian Current (northwestern Mediterranean) using a bio-optical glider. *Limnology and Oceanography, 53*(5), 2210-2225. doi: 10.4319/lo.2008.53.5_part_2.2210

Nihoul, J. C. J. (1981). Marine hydrodynamics at ecological scales. *Ecohydrodynamics: Proceedings of the 12th International Liège Colloquium on Ocean Hydrodynamics. Elsevier Oceanography Series, 32*, 1-12.

Nur, N., Jahncke, J., Herzog, M. P., Howar, J., Hyrenbach, K. D., Zamon, J. E., Ainley, D. G., Wiens, J. A., Morgan, K., Ballance, L. T., & Stralberg, D. (2011). Where the wild things are: predicting hotspots of seabird aggregations in the California Current System. *Ecological Applications, 21*(6), 2241-2257.

Obenour, K. M. (2013). *Temporal trends in global sea surface temperature fronts* (Master's Theses.). Retrieved from http://digitalcommons.uri.edu/theses/136 (Paper 136).

Ocampo Reinaldo, M., González, R., Williams, G., Storero, L. P., Romero, M. A., Narvarte, M., & Gagliardini, D. A. (2013). Spatial patterns of the Argentine hake Merluccius hubbsi and oceanographic processes in a semi-enclosed Patagonian ecosystem. *Marine Biology Research, 9*(4), 394-406.

Ohman, M. D., Rudnick, D. L., Chekalyuk, A., Davis, R. E., Feely, R. A., Kahru, M., Kim, H. J., Landry, M. R., Martz, T. R., Sabine, C. L., & Send, U. (2013). Autonomous ocean measurements in the California Current Ecosystem. *Oceanography, 26*(3), 18-25.

Oppel, S., Meirinho, A., Ramirez, I., Gardner, B., O'Connell, A. F., Miller, P. I., & Louzao, M. (2012). Comparison of five modelling techniques to predict the spatial distribution and abundance of seabirds. *Biological Conservation, 156*, 94-104. doi: 10.1016/j.biocon.2011.11.013

Otero, P., Ruiz-Villarreal, M., & Peliz, A. (2009). River plume fronts off NW Iberia from satellite observations and model data. *Ices Journal of Marine Science, 66*(9), 1853-1864. doi: 10.1093/icesjms/fsp156

Owen, R. (Ed.). (1981). *Fronts and Eddies in the Sea: mechanisms, interactions and biological effects*. New York: Academic Press.

Palacios, D. M., Bograd, S. J., Foley, D. G., & Schwing, F. B. (2006). Oceanographic characteristics of biological hot spots in the North Pacific: A remote sensing perspective. *Deep-Sea Research Part Ii-Topical Studies in Oceanography, 53*(3-4), 250-269. doi: 10.1016/j.dsr2.2006.03.004

Pan, W. (2001a). Akaike's information criterion in generalized estimating equations. *Biometrics, 57*(1), 120-125. doi: 10.1111/j.0006-341X.2001.00120.x

Pan, W. (2001b). Model selection in estimating equations. *Biometrics, 57*(2), 529-534. doi: 10.1111/j.0006-341X.2001.00529.x

Pan, W., & Connett, J. E. (2002). Selecting the working correlation structure in generalized estimating equations with application to the lung health study. *Statistica Sinica, 12*(2), 475-490.

Panigada, S., Zanardelli, M., MacKenzie, M., Donovan, C., Melin, F., & Hammond, P. S. (2008). Modelling habitat preferences for fin whales and striped dolphins in the Pelagos Sanctuary (Western Mediterranean Sea) with physiographic and remote sensing variables. *Remote Sensing of Environment, 112*(8), 3400-3412. doi: 10.1016/j.rse.2007.11.017

Parc naturel marin d'Iroise. (2007). Management Plan 2010-2025 (Vol. December 2007): Agence des aires marines protégées.

Pedersen, F. (1994). The oceanographic and biological tidal cycle succession in shallow sea fronts in the North Sea and teh English Channel. *Estuarine Coastal and Shelf Science, 38*(3), 249-269.

Pemberton, K., Rees, A. P., Miller, P. I., Raine, R., & Joint, I. (2004). The influence of water body characteristics on phytoplankton diversity and production in the Celtic Sea. *Continental Shelf Research, 24*(17), 2011-2028. doi: 10.1016/j.csr.2004.07.003

Peng, R. D. (2008). R package 'simpleboot': Simple Bootstrap Routines (version 1.1-3).

Perry, M. J., Sackmann, B. S., Eriksen, C. C., & Lee, C. M. (2008). Seaglider observations of blooms and subsurface chlorophyll maxima off the Washington coast. *Limnology and Oceanography, 53*(5), 2169-2179. doi: 10.4319/lo.2008.53.5_part_2.2169

Perry, R. I., Harding, G. C., Loder, J. W., Tremblay, M. J., Sinclair, M. M., & Drinkwater, K. F. (1993). Zooplankton distributions at the Geroges Bank frontal system- Retention or dispersion. *Continental Shelf Research, 13*(4), 357-383. doi: 10.1016/0278-4343(93)90056-4

Pikesley, S. K., Maxwell, S. M., Pendoley, K., Costa, D. P., Coyne, M. S., Formia, A., Godley, B. J., Klein, W., Makanga-Bahouna, J., Maruca, S., Ngouessono, S., Parnell, R. J., Pemo-Makaya, E., & Witt, M. J. (2013). On the front line: integrated habitat mapping for olive ridley sea turtles in the southeast Atlantic. *Diversity and Distributions, 19*(12), 1518-1530. doi: 10.1111/ddi.12118

Pingree, R. (1980). Physical oceanography of the Celtic Sea and English Channel. *The North–West European Shelf-seas: The Sea Bed and the Sea in Motion. II. Physical and Chemical Oceanography and Physical Resources*, 415-465.

Pingree, R. D. (1975). Advance and retreat of the thermocline on the continental shelf. *Journal of the Marine Biological Association of the United Kingdom, 55*(4), 965-974.

Pingree, R. D., & Griffiths, D. K. (1978). Tidal fronts on shelf-seas around British Isles. *Journal of Geophysical Research-Oceans and Atmospheres, 83*(NC9), 4615-4622.

Pingree, R. D., Holligan, P. M., & Head, R. N. (1977). Survival of dinoflagellate blooms in the Western English Channel. *Nature, 265*(5591), 266-269.

Pingree, R. D., Holligan, P. M., & Mardell, G. T. (1979). Phytoplankton growth and cyclonic eddies. *Nature, 278*(5701), 245-247. doi: 10.1038/278245a0

Pingree, R. D., Holligan, P. M., Mardell, G. T., & Head, R. N. (1976). Influence of physical stability on spring, summer and autumn phytoplankton blooms in the Celtic Sea. *Journal of the Marine Biological Association of the United Kingdom, 56*(4), 845-873.

Pingree, R. D., & Lecann, B. (1989). Celtic and Armorican slope and shelf residual currents. *Progress in Oceanography, 23*(4), 303-338. doi: 10.1016/0079-6611(89)90003-7

Pingree, R. D., Pugh, P. R., Holligan, P. M., & Forster, G. R. (1975). Summer phytoplankton blooms and red tides along tidal fronts in approaches to the English Channel. *Nature, 258*(5537), 672-677. doi: 10.1038/258672a0

Pirotta, E., Matthiopoulos, J., MacKenzie, M., Scott-Hayward, L., & Rendell, L. (2011). Modelling sperm whale habitat preference: a novel approach combining transect and follow data. *Marine Ecology Progress Series, 436*, 257-272. doi: 10.3354/meps09236

Pirotta, E., Thompson, P. M., Miller, P. I., Brookes, K. L., Cheney, B., Barton, T. R., Graham, I. M., & Lusseau, D. (2014). Scale-dependent foraging ecology of a marine top predator modelled using passive acoustic data. *Functional Ecology, 28*(1), 206-217. doi: 10.1111/1365-2435.12146

Pisoni, J. P., Rivas, A. L., & Piola, A. R. (2015). On the variability of tidal fronts on a macrotidal continental shelf, Northern Patagonia, Argentina. *Deep-Sea Research Part Ii-Topical Studies in Oceanography, 119*, 61-68. doi: 10.1016/j.dsr2.2014.01.019

Podesta, G. P., Browder, J. A., & Hoey, J. J. (1993). Exploring the association between swordfish catch rates and thermal fronts on United States longline grounds in the Western North Atlantic. *Continental Shelf Research, 13*(2-3), 253-&.

Priede, I. G., & Miller, P. I. (2009). A basking shark (Cetorhinus maximus) tracked by satellite together with simultaneous remote sensing II: New analysis reveals orientation to a thermal front. *Fisheries Research (Amsterdam), 95*(2-3), 370-372. doi: :10.1016/j.fishres.2008.09.038

Prokes, R., Vrana, B., & Klanova, J. (2012). Levels and distribution of dissolved hydrophobic organic contaminants in the Morava river in Zlin district, Czech Republic as derived from their accumulation in silicone rubber passive samplers. *Environmental Pollution, 166*, 157-166. doi: 10.1016/j.envpol.2012.02.022

Queiroz, N., Humphries, N. E., Noble, L. R., Santos, A. M., & Sims, D. W. (2012). Spatial Dynamics and Expanded Vertical Niche of Blue Sharks in Oceanographic Fronts Reveal Habitat Targets for Conservation. *Plos One, 7*(2). doi: e3237410.1371/journal.pone.0032374

R Core Team. (2013). R: A language and environment for statistical computing. *R Foundation for Statistical Computing, Vienna, Austria.*

Raitsos, D. E., Lavender, S. J., Pradhan, Y., Tyrrell, T., Reid, P. C., & Edwards, M. (2006). Coccolithophore bloom size variation in response to the regional environment of the subarctic North Atlantic. *Limnology and Oceanography, 51*(5), 2122-2130.

Reese, D. C., O'Malley, R. T., Brodeur, R. D., & Churnside, J. H. (2011). Epipelagic fish distributions in relation to thermal fronts in a coastal upwelling system using high-resolution remote-sensing techniques. *Ices Journal of Marine Science, 68*(9), 1865-1874. doi: 10.1093/icesjms/fsr107

Reid, J. B., Evans, P. G., & Northridge, S. P. (2003). *Atlas of cetacean distribution in north-west European waters*: Joint Nature Conservation Committee.

Ribic, C. A., Ainley, D. G., Ford, R. G., Fraser, W. R., Tynan, C. T., & Woehler, E. J. (2011). Water masses, ocean fronts, and the structure of Antarctic seabird communities: Putting the eastern Bellingshausen Sea in perspective. *Deep-Sea Research Part Ii-Topical Studies in Oceanography, 58*(13-16), 1695-1709. doi: 10.1016/j.dsr2.2009.09.017

Richardson, A. J., Walne, A. W., John, A. W. G., Jonas, T. D., Lindley, J. A., Sims, D. W., Stevens, D., & Witt, M. (2006). Using continuous plankton recorder data. *Progress in Oceanography, 68*(1), 27-74. doi: 10.1016/j.pocean.2005.09.011

Rivas, A. L., & Pisoni, J. P. (2010). Identification, characteristics and seasonal evolution of surface thermal fronts in the Argentinean Continental Shelf. *Journal of Marine Systems, 79*(1-2), 134-143. doi: 10.1016/j.jmarsys.2009.07.008

Robins, P. E., Neill, S. P., Gimenez, L., Jenkins, S. R., & Malham, S. K. (2013). Physical and biological controls on larval dispersal and connectivity in a highly energetic shelf-sea. *Limnology and Oceanography, 58*(2), 505-524. doi: 10.4319/lo.2013.58.2.0505

Robins, P. E., Neill, S. P., Giménez, L., Jenkins, S. R., & Malham, S. K. (2013). Physical and biological controls on larval dispersal and connectivity in a highly energetic shelf-sea. *Limnology and Oceanography, 58*(2), 505-524.

Robinson, G. A., Aiken, J., & Hunt, H. G. (1986). Synoptic surveys of the Western English Channel- Relationships between plankton and hydrography. *Journal of the Marine Biological Association of the United Kingdom, 66*(1), 201-218.

Rodriguez-Rodriguez, D., Rees, S., Mannaerts, G., Sciberras, M., Pirie, C., Black, G., Aulert, C., Sheehan, E. V., Carrier, S., & Attrill, M. J. (2015). Status of the marine protected area network across the English channel (La Manche): Cross-country similarities and differences in MPA designation, management and monitoring. *Marine Policy, 51*, 536-546. doi: 10.1016/j.marpol.2014.09.021

Rudnick, D. L., Crowley, M., Schofield, O., Baltes, R., Lee, C. M., Lembke, C., & Ieee. (2012). *A National Glider Network for Sustained Observation of the Coastal Ocean*. New York: Ieee.

Ruiz, S., Pascual, A., Garau, B., Faugere, Y., Alvarez, A., & Tintore, J. (2009). Mesoscale dynamics of the Balearic Front, integrating glider, ship and satellite data. *Journal of Marine Systems, 78*, S3-S16. doi: 10.1016/j.jmarsys.2009.01.007

Ryan, J. P., Fischer, A. M., Kudela, R. M., McManus, M. A., Myers, J. S., Paduan, J. D., Ruhsam, C. M., Woodson, C. B., & Zhang, Y. (2010). Recurrent frontal slicks of a coastal ocean upwelling shadow. *Journal of Geophysical Research-Oceans, 115*. doi: C1207010.1029/2010jc006398

Ryan, J. P., Harvey, J. B. J., Zhang, Y., & Woodson, C. B. (2014). Distributions of invertebrate larvae and phytoplankton in a coastal upwelling system retention zone and peripheral front. *Journal of Experimental Marine Biology and Ecology, 459*, 51-60. doi: 10.1016/j.jembe.2014.05.017

Sabarros, P. S., Gremillet, D., Demarcq, H., Moseley, C., Pichegru, L., Mullers, R. H. E., Stenseth, N. C., & Machu, E. (2014). Fine-scale recognition and use of mesoscale fronts by foraging Cape gannets in the Benguela upwelling region. *Deep-Sea Research Part Ii-Topical Studies in Oceanography, 107*, 77-84. doi: 10.1016/j.dsr2.2013.06.023

Sabatini, M., & Martos, P. (2002). Mesozooplankton features in a frontal area off northern Patagonia (Argentina) during spring 1995 and 1998. *Scientia Marina, 66*(3), 215-232.

Sabatini, M. E., Akselman, R., Reta, R., Negri, R. M., Lutz, V. A., Silva, R. I., Segura, V., Gil, M. N., Santinelli, N. H., Sastre, A. V., Daponte, M. C., & Antacli, J. (2012). Spring plankton communities in the southern Patagonian shelf: Hydrography, mesozooplankton patterns and trophic relationships. *Journal of Marine Systems, 94*, 33-51. doi: 10.1016/j.jmarsys.2011.10.007

Sameoto, J. A., Ross, T., & Metaxas, A. (2010). The effect of flow on larval vertical distribution of the sea urchin, Strongylocentrotus droebachiensis. *Journal of Experimental Marine Biology and Ecology, 383*(2), 156-163. doi: 10.1016/j.jembe.2009.11.014

Savidge, G. (1976). Preliminary study of distribution of chlorophyll a in vicinity of fronts in the Celtic and Western Irish Seas. *Estuarine and Coastal Marine Science, 4*(6), 617-625. doi: 10.1016/0302-3524(76)90070-0

Savidge, G., & Foster, P. (1978). Phytoplankton biology of a theral front in the Celtic Sea. *Nature, 271*(5641), 155-157. doi: 10.1038/271155a0

Scales, K. L., Miller, P. I., Embling, C. B., Ingram, S. N., Pirotta, E., & Votier, S. C. (2014a). Mesoscale fronts as foraging habitats: composite front mapping reveals oceanographic drivers of habitat use for a pelagic seabird. *Journal of the Royal Society Interface, 11*(100). doi: 10.1098/rsif.2014.0679

Scales, K. L., Miller, P. I., Hawkes, L. A., Ingram, S. N., Sims, D. W., & Votier, S. C. (2014b). On the Front Line: frontal zones as priority at-sea conservation areas for mobile marine vertebrates. *Journal of Applied Ecology, 51*(6), 1575-1583. doi: 10.1111/1365-2664.12330

Scales, K. L., Miller, P. I., Varo-Cruz, N., Hodgson, D. J., Hawkes, L. A., & Godley, B. J. (2015). Oceanic loggerhead turtles Caretta caretta associate with thermal fronts: evidence from the Canary Current Large Marine Ecosystem. *Marine Ecology Progress Series, 519*, 195-207. doi: 10.3354/meps11075

Schabetsberger, R., Okland, F., Aarestrup, K., Kalfatak, D., Sichrowsky, U., Tambets, M., Dall'Olmo, G., Kaiser, R., & Miller, P. I. (2013). Oceanic migration behaviour of tropical Pacific eels from Vanuatu. *Marine Ecology Progress Series, 475*, 177-190. doi: 10.3354/meps10254

Schofield, O., Glenn, S., & Moline, M. (2013). The Robot Ocean Network. *American Scientist, 101*(6), 434-441.

Schultes, S., Sourisseau, M., Le Masson, E., Lunven, M., & Marie, L. (2013). Influence of physical forcing on mesozooplankton communities at the Ushant tidal front. *Journal of Marine Systems, 109*, S191-S202. doi: 10.1016/j.jmarsys.2011.11.025

Schumacher, J. D., Kinder, T. H., Pashinski, D. J., & Charnell, R. L. (1979). Structural front over the continental shelf of the Eastern Bering Sea. *Journal of Physical Oceanography, 9*(1), 79-87.

Scott, B. E., Sharples, J., Ross, O. N., Wang, J., Pierce, G. J., & Camphuysen, C. J. (2010). Sub-surface hotspots in shallow seas: fine-scale limited locations of top predator foraging habitat indicated by tidal mixing and sub-surface chlorophyll. *Marine Ecology-Progress Series, 408*, 207-226. doi: 10.3354/meps08552

Scott, B. E., Webb, A., Palmer, M. R., Embling, C. B., & Sharples, J. (2013). Fine scale bio-physical oceanographic characteristics predict the foraging occurrence of contrasting seabird species; Gannet (Morus bassanus) and storm petrel (Hydrobates pelagicus). *Progress in Oceanography, 117*, 118-129. doi: 10.1016/j.pocean.2013.06.011

Send, U., Regier, L., & Jones, B. (2013). Use of Underwater Gliders for Acoustic Data Retrieval from Subsurface Oceanographic Instrumentation and Bidirectional Communication in the Deep Ocean. *Journal of Atmospheric and Oceanic Technology, 30*(5), 984-998. doi: 10.1175/jtech-d-11-00169.1

Sharples, J. (2008). Potential impacts of the spring-neap tidal cycle on shelf-sea primary production. *Journal of Plankton Research, 30*(2), 183-197. doi: 10.1093/plankt/fbm088

Sharples, J., Ross, O. N., Scott, B. E., Greenstreet, S. P. R., & Fraser, H. (2006). Inter-annual variability in the timing of stratification and the spring bloom in the North-western North Sea. *Continental Shelf Research, 26*(6), 733-751. doi: 10.1016/j.csr.2006.01.011

Sharples, J., Scott, B. E., & Inall, M. E. (2013). From physics to fishing over a shelf-sea bank Preface. *Progress in Oceanography, 117*, 1-8. doi: 10.1016/j.pocean.2013.06.015

Simpson, J. H. (1977). Fronts on the continental shelf. *Transactions-American Geophysical Union, 58*(9), 887-887.

Simpson, J. H. (1981). The shelf-sea fronts- Implications of their existence and behavior. *Philosophical Transactions of the Royal Society of London Series a-Mathematical Physical and Engineering Sciences, 302*(1472), 531-&.

Simpson, J. H., & Bowers, D. (1981). Models of stratification and frontal movement in shelf-seas. *Deep-Sea Research Part a-Oceanographic Research Papers, 28*(7), 727-738. doi: 10.1016/0198-0149(81)90132-1

Simpson, J. H., & Hunter, J. R. (1974). Fronts in the Irish Sea. *Nature, 250*(5465), 404-406. doi: 10.1038/250404a0

Simpson, J. H., & Sharples, J. (2012). *Introduction to the physical and biological oceanography of shelf-seas*: Cambridge University Press.

Simpson, J. H., Tett, P. B., Argoteespinoza, M. L., Edwards, A., Jones, K. J., & Savidge, G. (1982). Mixing and phytoplankton growth around an island in a stratified sea. *Continental Shelf Research, 1*(1), 15-31. doi: 10.1016/0278-4343(82)90030-9

Sims, D. W., & Quayle, V. A. (1998). Selective foraging behaviour of basking sharks on zooplankton in a small-scale front. *Nature, 393*(6684), 460-464.

Sims, D. W., & Southall, E. J. (2002). Occurrence of ocean sunfish, Mola mola near fronts in the western English Channel. *Journal of the Marine Biological Association of the United Kingdom, 82*(5), 927-928. doi: 10.1017/s0025315402006409

Skov, H., Humphreys, E., Garthe, S., Geitner, K., Gremillet, D., Hamer, K. C., Hennicke, J., Parner, H., & Wanless, S. (2008). Application of habitat suitability modelling to tracking data of marine animals as a means of analyzing their feeding habitats. *Ecological Modelling, 212*(3-4), 504-512. doi: 10.1016/j.ecolmodel.2007.11.006

Sournia, A. (1994). Pelagic biogeography and fronts. *Progress in Oceanography, 34*(2-3), 109-120.

Sournia, A., Birrien, J. L., Camus, P., Daniel, J. Y., Jacq, E., Koutsikopoulos, C., Lecorre, P., Lecoz, J. R., Lesaos, J. P., Mariette, V., Martinjezequel, V., Moal, J., Morin, P., Poulet, S. A., Prieur, D., Samain, J. F., Slawyk, G., & Videau, C. (1988). A physical, chemical and biological charaterization of the Ushant tidal front. *Internationale Revue Der Gesamten Hydrobiologie, 73*(5), 511-536.

Stegmann, P. M., & Ullman, D. S. (2004). Variability in chlorophyll and sea surface temperature fronts in the Long Island Sound outflow region from satellite observations. *Journal of Geophysical Research, 109*(C7), 12 pp.-12 pp. doi: 10.1029/2003jc001984

Suryan, R. M., Santora, J. A., & Sydeman, W. J. (2012). New approach for using remotely sensed chlorophyll a to identify seabird hotspots. *Marine Ecology-Progress Series, 451*, 213-225. doi: 10.3354/meps09597

Sveegaard, S., Nabe-Nielsen, J., Staehr, K. J., Jensen, T. F., Mouritsen, K. N., & Teilmann, J. (2012). Spatial interactions between marine predators and their prey: herring abundance as a driver for the distributions of mackerel and harbour porpoise. *Marine Ecology Progress Series, 468*, 245-253. doi: 10.3354/meps09959

Temperoni, B., Vinas, M. D., Martos, P., & Marrari, M. (2014). Spatial patterns of copepod biodiversity in relation to a tidal front system in the main spawning and nursery area of the Argentine hake Merluccius hubbsi. *Journal of Marine Systems, 139*, 433-445. doi: 10.1016/j.jmarsys.2014.08.015

Thompson, A. F. (2008). The atmospheric ocean: eddies and jets in the Antarctic Circumpolar Current. *Philosophical Transactions of the Royal Society of London A: Mathematical, Physical and Engineering Sciences, 366*(1885), 4529-4541.

Ting, M. C., Mujeebu, M. A., Abdullah, M. Z., & Arshad, M. R. (2012). Numerical Study on Hydrodynamic Performance of Shallow Underwater Glider Platform. *Indian Journal of Geo-Marine Sciences, 41*(2), 124-133.

Todd, R. E., Gawarkiewicz, G. G., & Owens, W. B. (2013). Horizontal Scales of Variability over the Middle Atlantic Bight Shelf Break and Continental Rise from Finescale Observations. *Journal of Physical Oceanography, 43*(1), 222-230. doi: 10.1175/jpo-d-12-099.1

Tomita, T., Nonaka, M., & Yamaura, T. (2010). Interannual variability in the subseasonal northward excursion of the Baiu front. *International Journal of Climatology, 30*(14), 2205-2216. doi: 10.1002/joc.2040

Tremblay, Y., Bertrand, S., Henry, R. W., Kappes, M. A., Costa, D. P., & Shaffer, S. A. (2009). Analytical approaches to investigating seabird-environment interactions: a review. *Marine Ecology-Progress Series, 391*, 153-163. doi: 10.3354/meps08146

Ullman, D. S., Cornillon, P. C., & Shan, Z. (2007). On the characteristics of subtropical fronts in the North Atlantic. *Journal of Geophysical Research-Oceans, 112*(C1). doi: C0101010.1029/2006jc003601

Ullman, D. S., Dale, A. C., Hebert, D., & Barth, J. A. (2003). The front on the Northern Flank of Georges Bank in spring: 2. Cross-frontal fluxes and mixing. *Journal of Geophysical Research-Oceans, 108*(C11). doi: 801010.1029/2002jc001328

Urick, R. (1983). *Principles of underwater sound* (3rd ed.): McGraw-Hill.

Van Waerebeek, K., Baker, A. N., Félix, F., Gedamke, J., Iñiguez, M., Sanino, G. P., Secchi, E., Sutaria, D., van Helden, A., & Wang, Y. (2007). Vessel collisions with small cetaceans worldwide and with large whales in the Southern Hemisphere, an initial assessment. *Latin American Journal of Aquatic Mammals, 6*(1), 43-69.

Villadsgaard, A., Wahlberg, M., & Tougaard, J. (2007). Echolocation signals of wild harbour porpoises, Phocoena phocoena. *Journal of Experimental Biology, 210*(1), 56-64. doi: 10.1242/jeb.02618

Votier, S. C., Bicknell, A., Cox, S. L., Scales, K. L., & Patrick, S. C. (2013). A Bird's Eye View of Discard Reforms: Bird-Borne Cameras Reveal Seabird/Fishery Interactions. *Plos One, 8*(3). doi: 10.1371/journal.pone.0057376

Vrana, B., & Schuurmann, G. (2002). Calibrating the uptake kinetics of semipermeable membrane devices in water: Impact of hydrodynamics. *Environmental Science & Technology, 36*(2), 290-296. doi: 10.1021/es0100625

Wang, D. P., Chen, D., & Sherwin, T. J. (1990). COUPLING BETWEEN MIXING AND ADVECTION IN A SHALLOW SEA FRONT. *Continental Shelf Research, 10*(2), 123-136. doi: 10.1016/0278-4343(90)90026-i

Warner, A. J., & Hays, G. C. (1994). Sampling by the Continuous Plankton Recorder Survey. *Progress in Oceanography, 34*(2-3), 237-256. doi: 10.1016/0079-6611(94)90011-6

Watkins, J. L., & Brierley, A. S. (1996). A post-processing technique to remove background noise from echo integration data. *Ices Journal of Marine Science, 53*(2), 339-344. doi: 10.1006/jmsc.1996.0046

Webb, D. C., Simonetti, P. J., & Jones, C. P. (2001). SLOCUM: An underwater glider propelled by environmental energy. *Ieee Journal of Oceanic Engineering, 26*(4), 447-452. doi: 10.1109/48.972077

Weeks, S. J., Magno-Canto, M. M., Jaine, F. R. A., Brodie, J., & Richardson, A. J. (2015). Unique Sequence of Events Triggers Manta Ray Feeding Frenzy in the Southern Great Barrier Reef, Australia. *Remote Sensing, 7*(3), 3138-3152. doi: 10.3390/rs70303138

Weidberg, N., Lobon, C., Lopez, E., Florez, L. G., Rueda, M. D. F., Largier, J. L., & Acuna, J. L. (2014). Effect of nearshore surface slicks on meroplankton distribution: role of larval behaviour. *Marine Ecology Progress Series, 506*, 15-30. doi: 10.3354/meps10777

Weilgart, L. S. (2007). The impacts of anthropogenic ocean noise on cetaceans and implications for management. *Canadian Journal of Zoology, 85*(11), 1091-1116.

Westgate, A. J., Read, A. J., Berggren, P., Koopman, H. N., & Gaskin, D. E. (1995). DIVING BEHAVIOR OF HARBOR PORPOISES, PHOCOENA-PHOCOENA. *Canadian Journal of Fisheries and Aquatic Sciences, 52*(5), 1064-1073. doi: 10.1139/f95-104

Weston, K., Fernand, L., Mills, D. K., Delahunty, R., & Brown, J. (2005). Primary production in the deep chlorophyll maximum of the central North Sea. *Journal of Plankton Research, 27*(9), 909-922. doi: 10.1093/plankt/fbi064

Willcox, J. S., Bellingham, J. G., Zhang, Y., & Baggeroer, A. B. (2001). Performance metrics for oceanographic surveys with autonomous underwater vehicles. *Oceanic Engineering, IEEE Journal of, 26*(4), 711-725.

Wilson, R. J., Speirs, D. C., & Heath, M. R. (2015). On the surprising lack of differences between two congeneric calanoid copepod species, Calanus finmarchicus and C. helgolandicus. *Progress in Oceanography, 134*, 413-431. doi: 10.1016/j.pocean.2014.12.008

Wishner, K. F., Outram, D. M., & Ullman, D. S. (2006). Zooplankton distributions and transport across the northeastern tidal front of Georges Bank. *Deep-Sea Research Part Ii-Topical Studies in Oceanography, 53*(23-24), 2570-2596. doi: 10.1016/j.dsr2.2006.06.003

Wood, S. N. (2006). Generalized Additive Models: An Introduction with R. *Chapman and Hall/CRC.*

Woodson, C. B., & Litvin, S. Y. (2015). Ocean fronts drive marine fishery production and biogeochemical cycling. *Proceedings of the National Academy of Sciences of the United States of America, 112*(6), 1710-1715. doi: 10.1073/pnas.1417143112

Worm, B., Sandow, M., Oschlies, A., Lotze, H. K., & Myers, R. A. (2005). Global patterns of predator diversity in the open oceans. *Science, 309*(5739), 1365-1369. doi: 10.1126/science.1113399

Young, E. F., Brown, J., Aldridge, J. N., Horsburgh, K. J., & Fernand, L. (2004). Development and application of a three-dimensional baroclinic model to the study of the seasonal circulation in the Celtic Sea. *Continental Shelf Research, 24*(1), 13-36. doi: 10.1016/j.csr.2003.09.003

Young, J. W., Hunt, B. P. V., Cook, T. R., Llopiz, J. K., Hazen, E. L., Pethybridge, H. R., Ceccarelli, D., Lorrain, A., Olson, R. J., Allain, V., Menkes, C., Patterson, T., Nicol, S., Lehodey, P., Kloser, R. J., Arrizabalaga, H., & Choy, C. A. (2015). The trophodynamics of marine top predators: Current knowledge, recent advances and challenges. *Deep-Sea Research Part Ii-Topical Studies in Oceanography, 113*, 170-187.

Yu, Y. Y., & Emery, W. J. (1996). Satellite-derived sea surface temperature variability in the Western Tropical Pacific Ocean, 1992-1993. *Remote Sensing of Environment, 58*(3), 299-310. doi: 10.1016/s0034-4257(96)00074-0

Zamon, J. E., Phillips, E. M., & Guy, T. J. (2014). Marine bird aggregations associated with the tidally-driven plume and plume fronts of the Columbia River. *Deep-Sea Research Part Ii-Topical Studies in Oceanography, 107*, 85-95. doi: 10.1016/j.dsr2.2013.03.031

Zeger, S. L., & Liang, K. Y. (1986). LONGITUDINAL DATA-ANALYSIS FOR DISCRETE AND CONTINUOUS OUTCOMES. *Biometrics, 42*(1), 121-130. doi: 10.2307/2531248

Zuur, A. F., Ieno, E. N., Walker, N. J., Saveliev, A. A., Smith, G. M., & . (2009). *Mixed Effects Models and Extensions in Ecology with R*. New York.

9 APPENDIX

9.1 Peer-reviewed publications:

Chapter 5 ‘Assessing the potential of autonomous submarine gliders for ecosystem monitoring across multiple trophic levels (plankton to cetaceans) and pollutants in shallow shelf-seas’ was published under the same title in a special issue on underwater robotics in Methods in Oceanography 10 (2014).

Methods in Oceanography 10 (2014) 70–89

Contents lists available at ScienceDirect

Methods in Oceanography

journal homepage: www.elsevier.com/locate/mio

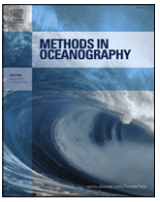

Full length article

Assessing the potential of autonomous submarine gliders for ecosystem monitoring across multiple trophic levels (plankton to cetaceans) and pollutants in shallow shelf seas

Lavinia Suberg [a,*], Russell B. Wynn [a], Jeroen van der Kooij [b], Liam Fernand [b], Sophie Fielding [c], Damien Guihen [c], Douglas Gillespie [d], Mark Johnson [d], Kalliopi C. Gkikopoulou [d], Ian J. Allan [e], Branislav Vrana [f], Peter I. Miller [g], David Smeed [a], Alice R. Jones [a,h]

[a] *National Oceanography Centre Southampton (NOCS), European Way, Southampton SO14 3ZH, UK*

[b] *Centre for Environment, Fisheries and Aquaculture Science (CEFAS), Pakefield Road, Lowestoft, Suffolk NR33 0HT, UK*

[c] *British Antarctic Survey, High Cross, Madingley Road, Cambridge CB3 0ET, UK*

[d] *Scottish Oceans Institute, East Sands, University of St Andrews, St Andrews, Fife, KY16 8LB, UK*

[e] *Norwegian Institute of Water Research, Oslo Centre Interdisciplinary Environmental & Social Research, Gaustadalléen 21, NO-0349 Oslo, Norway*

[f] *Masaryk University, Research Centre for Toxic Compounds in the Environment (RECETOX), Kamenice 753/5, 62500 Brno, Czech Republic*

[g] *Remote Sensing Group, Plymouth Marine Laboratory, Prospect Place, Plymouth PL1 3DH, UK*

[h] *The Environment Institute & School of Ocean and Earth Sciences, University of Adelaide, South Australia 5005, Australia*

ARTICLE INFO

Article history:
Received 7 March 2014
Received in revised form
13 June 2014
Accepted 17 June 2014
Available online 22 July 2014

ABSTRACT

A combination of scientific, economic, technological and policy drivers is behind a recent upsurge in the use of marine autonomous systems (and accompanying miniaturized sensors) for environmental mapping and monitoring. Increased spatial–temporal resolution and coverage of data, at reduced cost, is particularly vital for effective spatial management of highly dynamic and heterogeneous shelf environments. This proof-of-concept study involves

* Corresponding author. Tel.: +44 0 2380 596544.
E-mail addresses: lavinia.suberg@noc.soton.ac.uk, lavinia-suberg@gmx.de (L. Suberg).

http://dx.doi.org/10.1016/j.mio.2014.06.002

Keywords:
Autonomous underwater vehicles
Submarine glider
Slocum
Ecosystem monitoring
Multiple trophic levels

integration of a novel combination of sensors onto buoyancy-driven submarine gliders, in order to assess their suitability for ecosystem monitoring in shelf waters at a variety of trophic levels. Two shallow-water *Slocum* gliders were equipped with CTD and fluorometer to measure physical properties and chlorophyll, respectively. One glider was also equipped with a single-frequency echosounder to collect information on zooplankton and fish distribution. The other glider carried a Passive Acoustic Monitoring system to detect and record cetacean vocalizations, and a passive sampler to detect chemical contaminants in the water column. The two gliders were deployed together off southwest UK in autumn 2013, and targeted a known tidal-mixing front west of the Isles of Scilly. The gliders' mission took about 40 days, with each glider travelling distances of >1000 km and undertaking >2500 dives to depths of up to 100 m. Controlling glider flight and alignment of the two glider trajectories proved to be particularly challenging due to strong tidal flows. However, the gliders continued to collect data in poor weather when an accompanying research vessel was unable to operate. In addition, all glider sensors generated useful data, with particularly interesting initial results relating to subsurface chlorophyll maxima and numerous fish/cetacean detections within the water column. The broader implications of this study for marine ecosystem monitoring with submarine gliders are discussed.

1. Introduction

Shelf and adjacent coastal seas host highly productive ecosystems and are shared by an increasing variety of stakeholders utilizing limited space, e.g. shipping, fishing, aquaculture, recreation, hydrocarbon and aggregate extraction, and renewable energy (Collie and Adamowicz et al., 2013; Sharples and Ellis et al., 2013). These potentially conflicting demands require appropriate management, e.g. through Marine Spatial Planning, a complex task that is dependent upon high quality data and evidence (Gilman, 2002; Douvere and Ehler, 2011).

In addition to the management of multiple stakeholders to ensure that ecosystem health and services are maintained, additional data from shelf seas are required to meet international statutory obligations such as establishment of Marine Protected Areas (MPAs) and implementation of the EU Marine Strategy Framework Directive (MSFD) (European Union, 2008; Brennan and Fitzsimmons et al., 2013). However, marine mapping and monitoring using dedicated research and survey vessels is expensive, and offshore operations can be hindered due to weather constraints (Schofield and Glenn et al., 2013). In addition, the spatial and temporal resolution of vessel-based data are often insufficient to fully capture ecosystem dynamics, including the linkage of physical and biological processes, predator–prey interactions, community structure, and the spatio-temporal variability of different ecosystem components (Day, 2008). Satellite remote sensing of the oceans can provide useful supporting data at large spatial scales, but is restricted to the uppermost layers of the sea surface. Fixed moorings and profiling floats may provide long time series, but the former only collects data at a single point and the latter are difficult to spatially control (L'Heveder and Mortier et al., 2013).

Submarine (buoyancy-driven) gliders are a type of Autonomous Underwater Vehicle (AUV) that oscillates through the water column and can remain unattended at sea for several weeks to months (Rudnick and Crowley et al., 2012). Gliders carrying appropriate sensors can simultaneously monitor a range of physical and biological parameters, and regular surface communications with satellite allow their movement to be controlled and data to be uploaded in near real-time. However, gliders

are relatively slow moving (20–40 cm/s horizontally), making them prone to drift in areas of strong currents (Leonard et al., 2007; Davis and Leonard et al., 2009). Their sensor load is limited and each mission necessitates a balance between battery life, mission duration, sampling frequency, and data quality (Willcox and Bellingham et al., 2001). Despite these limitations, the scientific research community is increasingly focusing on gliders as a tool for monitoring of features at the meso- and sub-mesoscale, including highly variable and dynamic phenomena such as oceanic fronts, eddies and upwelling regions (Davis and Ohman et al., 2008).

Traditionally, gliders have been deployed with a basic set of sensors that enable measurement of physical oceanographic parameters such as temperature, salinity or currents (e.g. Perry and Sackmann et al., 2008; Ruiz and Pascual et al., 2009; Bouffard and Pascual et al., 2010; Merckelbach and Smeed et al., 2010; Todd and Gawarkiewicz et al., 2013) and lower trophic levels of the ecosystem (i.e. phytoplankton and zooplankton, e.g. Baumgartner and Fratantoni, 2008; Niewiadomska and Claustre et al., 2008; Fox and Gower et al., 2009; Frajka-Williams and Rhines et al., 2009; Guihen et al., 2014). More recently, new sensors have been integrated onto gliders that can measure abundance of higher trophic level organisms, e.g. fish and cetaceans (e.g. Baumgartner and Fratantoni, 2008; Ferguson and Lo et al., 2010; Klinck and Mellinger et al., 2012; Meyer-Gutbrod and Greene et al., 2012; Baumgartner and Fratantoni et al., 2013; Send and Regier et al., 2013). In addition, glider 'fleets' are increasingly used to establish ocean monitoring networks rather than single platform deployments (e.g. English and Chuanmin et al., 2009; Alvarez and Mourre, 2012; Bouffard and Renault et al., 2012; Alvarez and Chiggiato et al., 2013). However, until now, there has been limited effort devoted to the simultaneous measurement of physical parameters and multiple biological components of the ecosystem using gliders.

This contribution describes a deployment of gliders carrying sensor loads capable of simultaneously monitoring multiple marine ecosystem components, from physical parameters and chlorophyll *a* fluorescence (CTD and fluorometer) to zooplankton and fish (echosounder), and cetaceans (hydrophone). This 'proof-of-concept' study involved the deployment of two shallow-water gliders off southwest UK in autumn 2013, targeting a known tidal-mixing front in a productive inner-shelf environment. By targeting a frontal area, the gliders were expected to encounter steep vertical and horizontal gradients in physical parameters and potentially elevated levels of biomass. In addition, fronts in UK shelf waters are considered as potential targets for spatial protection measures (e.g. MPAs; (Miller and Christodoulou, 2014)) and are therefore a particular target for multi-trophic-level monitoring.

The aims of the paper are therefore to: (1) describe the various sensors that were deployed on the gliders, (2) provide an overview of glider and sensor operations during the autumn 2013 deployment, (3) present some initial scientific results and examples of collected data, and (4) discuss some of the benefits and issues that arose from the glider missions. The intention is that this study will aid future assessment of submarine gliders as a suitable platform for cost-effective, long-term monitoring of shelf sea ecosystems.

2. Survey area

The survey was conducted west of the Isles of Scilly, off southwest UK (Fig. 1), where shelf waters are $<$100 m deep. Here, tidal flows to the northeast and southwest peak at $\sim$75 cm/s during spring tides, and are weakest towards the northwest and southeast. Residual currents flow northwest and northwards with speeds of up to 5 cm/s (Pingree and Lecann, 1989). Shelf waters to the west of the Isles of Scilly are seasonally stratified (typically from late spring to late autumn), whereas inshore waters around the islands themselves remain mixed as a result of tidal–topographic interactions; a series of seasonal bottom and surface tidal-mixing fronts occur at the boundary between these stratified and mixed water masses (Simpson, 1981). Frontal dynamics lead to cooler, nutrient-rich waters being transferred into the photic zone and thus enhancing primary production (Pingree and Holligan et al., 1976; Simpson and Tett et al., 1982), which can in turn lead to fronts (including the Isles of Scilly fronts) becoming hotspots for higher trophic levels such as marine mammals (Beaumont and Austen et al., 2007; Leeney and Witt et al., 2012). The recognition of a wide variety of important marine habitats around the Isles of Scilly has led to the designation of the Isles of Scilly Marine Conservation Zone

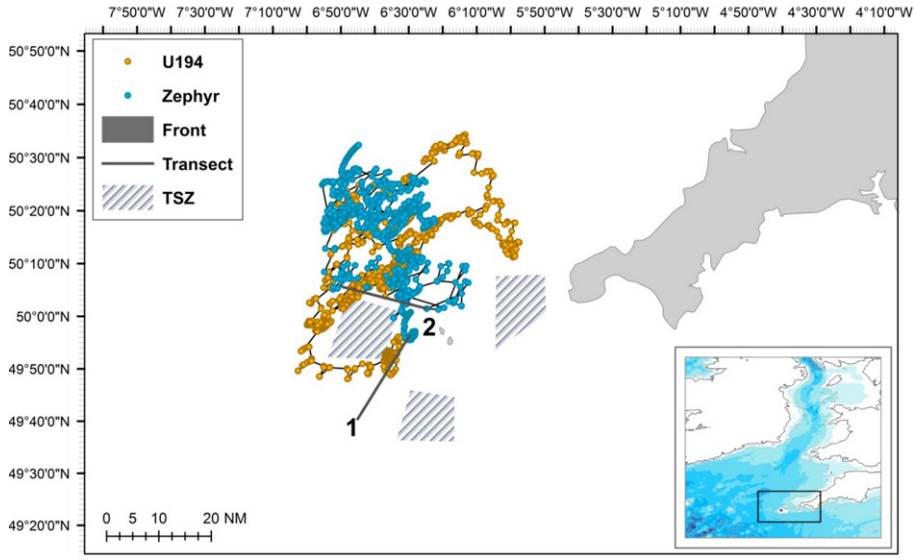

Fig. 1. Map of survey area and glider positions. Inset shows geographic overview of the survey area and depth contours (dark blue = deeper water; white = land). Enlarged map shows land in grey (Isles of Scilly and west Cornwall). Dots represent glider GPS positions (blue: *Zephyr*; orange: *U194*); thin black lines indicate glider tracks between positions, based on linear interpolation. Large grey arrows indicate the approximate location of the Isles of Scilly tidal mixing front determined by remote sensing Fig. A.1. Numbered dark grey lines indicate the initial (1) and revised (2) transects. Shaded areas represent traffic separation zones (TSZ). Note that *U194* locations are only based upon GPS fixes received following re-deployment on 04 October 2013 (*cf.* Table 1 and Fig. 2). (For interpretation of the references to colour in this figure legend, the reader is referred to the web version of this article.)

Table 1
Key events in chronological order.

Date	Event
12/09/2013	Deployment
14/09/2013	*Zephyr* d-tag memory card full (no data stored hereafter) until re-deployment
17/09/2013	*U194* "beached"
21/09–03/10/2013	Recovery and repairs *U194*
04/10/2013	Re-deployment *U194*; exchange *Zephyr* d-tag
10/10/2013	*Zephyr* d-tag stops recording: no power supply due to damaged cable
21/10/2013	Retrieval of *Zephyr*
13/11/2013	Retrieval of *U194*

(MCZ) in 2013 (Defra, 2013). In addition, the waters around the Isles of Scilly are valuable for marine recreation and tourism (Beaumont and Austen et al., 2007). There is also significant commercial fishing activity in the area, including a nearshore industry for shellfish and crustaceans (Beaumont and Austen et al., 2007). There are three traffic separation zones (TSZ) surrounding the islands due to high levels of shipping traffic (Fig. 1).

3. Methods

3.1. Gliders

We used two shallow-water *Slocum* gliders, *Zephyr* and *U194* (Fig. 2), developed by Teledyne Webb Research Corporation, which are specifically designed for shallow-water operations (<200 m). A detailed description of the glider can be found in Webb and Simonetti et al. (2001), but here we

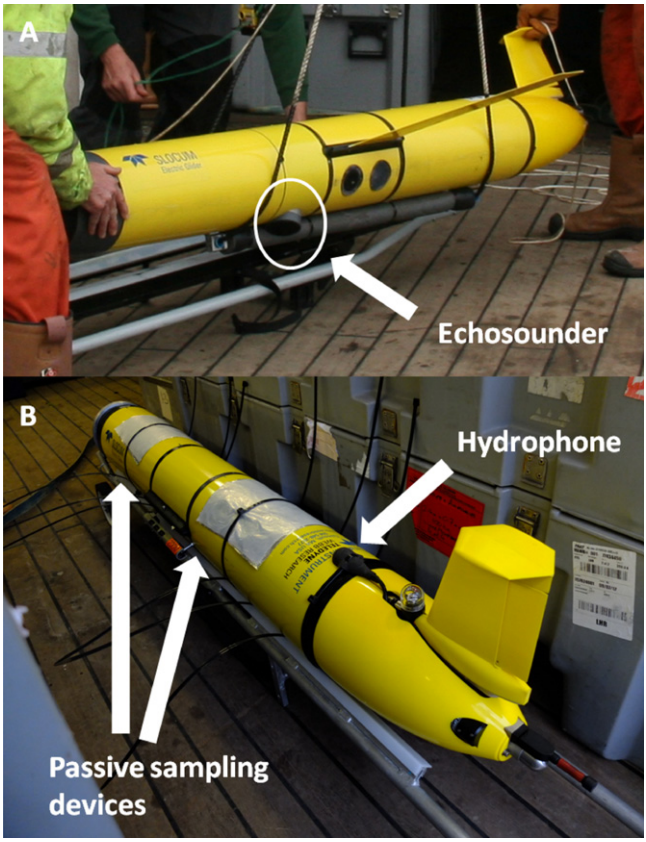

Fig. 2. (A) Picture of *U194* showing ES853 echosounder on the underside of the glider and (B) picture of *Zephyr* (wings not yet attached), showing the d-tag hydrophone and silicone rubber passive sampling sheets attached to the glider body.

focus on aspects relevant to this paper. *Slocums* move through the water column in a saw-tooth motion induced by changes in their buoyancy. A pump transfers seawater in and out of a holding chamber, which results in a change to the vehicle's density; this leads to a sequence of sinking and rising, which is translated into a forward motion by the attached wings. The average horizontal speed is 20–40 cm/s and vertical motion is 10–20 cm/s. Dive depth can be regulated by either a pressure sensor or an altimeter. Due to the shallow depth and varying bathymetry, we used the altimeter with an inflexion height of 10 m above the bottom to maximize dive depth. Forward and backward shifting of the battery packs controls dive angle; a rudder in the tail fin controls the yaw. When at the surface for communication, an air bladder at the tail is filled for additional buoyancy. Two-way communication is via Iridium satellite connection, allowing for near real-time transfer of subsets of data and manipulation of mission settings. Navigation is by Global Positioning System (GPS) when the vehicle is at the surface, and via dead reckoning during dives.

3.2. Glider sensors

3.2.1. Oceanographic sensors

Both gliders were equipped with the standard *Slocum* science package, which includes a non-pumped, low-drag, continuous profile Sea-bird SBE-41 CTD (temperature, conductivity and pressure) and WET Labs ECO pucks (BB2FLS, *Zephyr*; FlbbCD-SLK, *U194*), providing combined measurements of

chlorophyll *a* fluorescence, coloured dissolved organic matter (CDOM), and backscatter. The excitation wavelengths were 470, 370 and 700 nm, the emission wavelengths 695, 460 nm. The ECO pucks were mounted in the science bay, facing downwards. Also included are an Aanderaa Oxygen Optode 4835 and an altimeter. CDOM and backscatter provide information on organic and inorganic material in the water-column, which would be useful for an in-depth examination on ecosystem dynamics along a tidal mixing front. However, in this study, only temperature and chlorophyll *a* fluorescence measurements are considered for demonstration purposes, which were obtained on a 1 Hz sampling frequency. All acquired data were stored internally and a subset transmitted via Iridium each time the glider surfaced.

Ensuring data quality from autonomous vehicles is an important, but potentially difficult task. The issues can be reduced by using stable instruments (such as ship-borne CTD rosettes) with calibrations pre- and post-deployment. Therefore, we used two ship-based CTD casts, one taken directly after *Zephyr* retrieval (21st October 2013) and one taken at day 38 (19th October 2013) of the *U194* mission to correct the glider data (temperature and chlorophyll a) where necessary. Due to the problems of "in-mission" calibration (e.g. aligning the ship and glider position), we were unable to take CTD casts at the same time and location as *U194*. Therefore, we present the ship-based profile with the nearest spatio-temporal *U194* match (Δ time: 27 min; distance: 7.65 km). Additional water samples at surface and bottom were taken for chlorophyll *a* measurement verification. A subset of oceanographic data was stored on the National Oceanography Centre (NOC) sftp server and made available to the Met Office via the British Oceanographic Data Centre (BODC), for inclusion in their Forecasting Ocean Assimilation Models (FOAM).

3.2.2. Echosounder

In addition to the standard science payload, glider *U194* was equipped with an Imagenex ES853: a self-contained, single-beam 120 kHz echosounder (Fig. 2A). The ES853 was mounted in a science bay, aligned centrally along the short axis of the glider and at an angle of 64° from the long axis (towards the nose). This ensured that when the glider was in a downward glide (typical dive angle of −26°), the transducer pointed directly downwards, analogous with the downward-looking orientation of a ship's echosounder. The echosounder operates with a pulse length of 100 μs, beam angle of 10°, range of 100 m, configurable gain of either 20 or 40 dB, and measures mean volume backscattering (S_v, dB re 1 m^{-1}) per range bin interval of 0.5 m. It requires power of 0.25 W, drawn from a 24 V DC supply, and can output values to a PC or record data to internal storage. The ES853 has a dynamic range of 120 dB and records signals as integer values, thus the resolution in signal strength is reduced compared with typical floating-point recording of larger, ship-based echosounders.

The glider-integrated ES853 was controlled via serial port and polled at a frequency of 0.25 Hz, with data stored on the glider's internal memory. Upon retrieval of the glider the data were downloaded and processed following Guihen et al. (2014), where raw echo-intensity data were converted to mean volume backscattering strength (S_v), using the active version of the SONAR equation (Urick, 1983) and calibration and manufacturers' constants for echosounder receiving response and source level. Glider position data are used to locate individual pings in time, depth and aspect. These data were then processed using Myriax Echoview software (version 4.80), including subtraction of time-varied gain amplified background noise (after Watkins and Brierley, 1996), and accounting for variability in aspect of the transducer (after Dunford, 2005) and depth of the echosounder. Due to operational difficulties, the ES853 was not calibrated using standard sphere methods (Foote et al., 1987), so data shown here are relative. However, Guihen et al. (2014) showed that a calibrated ES853, mounted on a glider, provided quantitative estimates of zooplankton distribution comparable to a ship-borne echosounder, providing a suitable sampling strategy is employed. As a result we are confident that the ES853 data provide a relative index of zooplankton distribution.

3.2.3. Passive acoustic monitoring

Glider *Zephyr* was equipped with a Passive Acoustic Monitoring (PAM) system based on a modified d-tag sensor (Johnson and Tyack, 2003). The d-tag was mounted in the glider's aft wet space close to the buoyancy bladder, with the hydrophone on top of the glider just in front of the rudder (Fig. 2B).

Power was taken from the glider's main batteries. The sensor was configured to sample at 480 kHz, and an automatic detector was implemented to detect the narrow-band high-frequency clicks of harbour porpoise *Phocoena phocoena* (Villadsgaard et al., 2007). A 2 ms waveform clip of detected clicks was stored to flash memory. Recordings were also made of acoustic data decimated to a sample rate of 96 kHz for offline detection of other cetacean species and the measurement of noise. Although recordings were made using a lossless compression format which typically gives a compression ratio of 4:1 (Johnson et al., 2013), continuous recording would have filled available storage in approximately two weeks. The recorder was therefore programmed to operate for 10 out of every 40 s and only at water depths >40 m.

Recovered data were processed offline with PAMGuard software (Gillespie et al., 2008) to detect cetacean clicks and whistles and to measure noise in third octave bands between 22 Hz and 45 kHz. An operator (KG) viewed all detections manually, viewing click waveforms and whistle time frequency contours, and listening to sections of data to confirm detections and classify groups of transient sounds as either 'cetacean clicks' or as 'pump noise'.

3.2.4. Passive sampling devices for trace organic contaminant monitoring

Passive sampling devices made of a thin layer of polymer were deployed on *Zephyr* (Fig. 2B). These polymer sheets are made of AlteSil® silicone rubber (24 cm × 28 cm × 0.5 mm thick), and were Soxhlet extracted with ethyl acetate before further soaking in methanol. Performance reference compounds (PRC; perdeuterated polycyclic aromatic hydrocarbons and fluorinated polychlorinated biphenyls) were then uniformly spiked into the batch of samplers according to a method similar to that described by Booij et al. (2002). Samplers were kept in closed containers at −20 °C until deployment. Control samplers were used to assess possible contamination during transport, deployment and retrieval operations, and to measure initial PRC concentrations. Two sampling sheets were placed on top of the glider and fastened using cable ties (Fig. 2B). A thin sheet of aluminium foil (muffle furnaced prior to exposure) was placed between the samplers and the glider body to minimize possible contamination of the samplers by direct diffusion from the glider hull itself.

After retrieval, the surface of the samplers was thoroughly cleaned in the laboratory to remove any bio-fouling before static batch extraction with pentane (three times 300 mL over 72 h). Extracts were combined and reduced in volume. The solvent was changed to dichloromethane before clean-up by gel permeation chromatography. The extracts were then reduced in volume and analysed by gas chromatography–mass spectrometry for polycyclic aromatic hydrocarbons (PAHs), polychlorinated biphenyls (PCBs) and other chlorinated organic compounds. Field and laboratory procedures have been described elsewhere in more detail (e.g. Allan et al., 2010, 2013).

3.3. Glider mission

Both gliders were deployed southwest of the Isles of Scilly from the RV*CEFAS Endeavour* on 12 September 2013, in order to conduct repeated transects over the targeted tidal-mixing front (Fig. 1, 'transect 1'). The approximate location of the front was monitored prior to the survey via satellite-derived front maps (Miller, 2009). A ship-based pre-deployment transect was performed in order to ensure the area was free of static fishing gear (which is common in this area and represents a potential hazard to any glider) and to take repeated CTD and water samples to affirm the transect was located over the target front. A ship-based transect was performed on 21 October 2013 along the glider survey line (Fig. 1, 'transect 2'), in order to (1) compare the ES853 echosounder data with those collected using the calibrated multi-frequency (38, 120 and 200 kHz) split-beam Simrad EK60 on the RV *CEFAS Endeavour*, and (2) to collect CTD and water samples for *U194* calibration purposes. Due to glider control problems encountered during the mission, the initial glider transect (Fig. 1, 'transect 1') was shifted to the north of the Isles of Scilly on 24 September 2013 (Fig. 1, 'transect 2'). *Zephyr* was recovered from the RV *CEFAS Endeavour* on 21 October 2013 and on this occasion, a CTD cast was conducted for glider-sensor calibration. Due to quickly deteriorating weather, retrieval of *U194* had to be abandoned and the glider was picked up via fast-boat three weeks later on 13 November 2013.

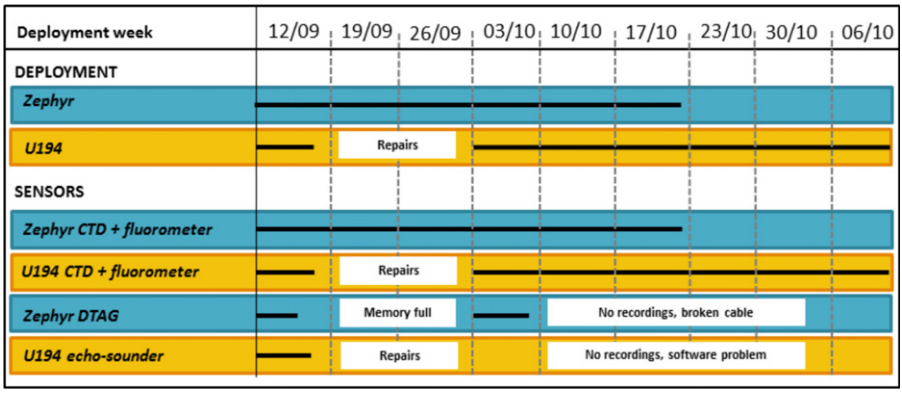

Fig. 3. Timeline glider deployments (blue shading: *Zephyr*; yellow: *U194*) and sensor activity, represented by black lines. Dates indicate the beginning of each week of the deployment, white boxes provide information on sensor malfunctions. (For interpretation of the references to colour in this figure legend, the reader is referred to the web version of this article.)

4. Results

4.1. Mission summary

Strong tidal flows and northwards density currents deflected both gliders to the northwest of the Isles of Scilly soon after deployment on 12 September 2013 (Hill et al., 2008). Unable to counteract these currents, *U194* was pushed into very shallow waters West of the islands on 17 September 2013, where manoeuvring was impossible and the glider needed to be recovered. Emergency recovery and subsequent repairs were carried out between 20 September and 04 October 2013 (Table 1).

U194 was redeployed on 04 October 2013 via fast-boat northwest of the Isles of Scilly. This also provided an opportunity to update faulty software on the *Zephyr* d-tag; both gliders then resumed their mission. The planned glider transect was repositioned to the north of the western TSZ (Fig. 1), where tidal flows and currents were weaker and where *Zephyr* had been located for most of the previous three weeks. Using a more dynamic piloting approach (e.g. regularly adjusting waypoints according to tidal flows, changing current correction setting), control of the flight path of *U194* was much improved. In contrast, piloting of *Zephyr* became increasingly challenging following redeployment, possibly due to the hydrocarbon sensor sheets loosening and adding extra drag to the vehicle (making it more susceptible to current drift). Nevertheless, both gliders executed the mission without any further problems until retrieval. A summary of key events and a timeline of sensor activity is given in Table 1 and Fig. 3, respectively.

Over the six-week deployment, the two gliders performed a total of 5474 dives (each dive comprising one up and downcast, based on dives of $\geq$10 m) to a maximum depth of 101 m (*Zephyr*) and 104 m (*U194*) (Table 2). The total horizontal distance covered was 2389 km, with an average distance of $\sim$0.9 km between GPS fixes.

4.2. Physical environment

Fig. 4 shows the glider data is in good agreement with measurements obtained from ship-based CTD-casts. However, *U194* chlorophyll *a* displayed a significant offset (Fig. A.2) and data shown here are corrected based on the vessel-profile by applying an ordinary linear model and adjusting the *U194* chlorophyll *a* data by the slope and offset ($U194_{corrected} = U194_{raw} \times 1.33 + 0.084$). Although there is a slight offset between Zephyr and ship chlorophyll *a*, no correction was applied, because the water samples suggest that the glider fluorometer gives a better reflection of the true chlorophyll than the vessel data. No correction of temperature measurements was necessary.

Glider *Zephyr* predominantly sampled thermally stratified waters during its mission, although it crossed the targeted tidal-mixing front several times in the first 500 h (Fig. 5A, Fig. A.3). A strong

Table 2
Mission statistics. Statistics only considers dives of ≥10 m (to exclude non-mission dives) and GPS fixes of ≥100 m apart. *U194* statistics based on post-redeployment dives only.

Statistic	*Zephyr*	*U194*
Total deployment days	38	39
Total number of dives	2654	2821
Total horizontal distance (km)	1080	1309
Mean horizontal distance b/w GPS fixes (km)	0.9	0.85
Max distance b/w GPS fixes (km)	13.7	10.3
Mean dive depth (m)	44.55	40
Max dive depth (m)	101.49	103.89

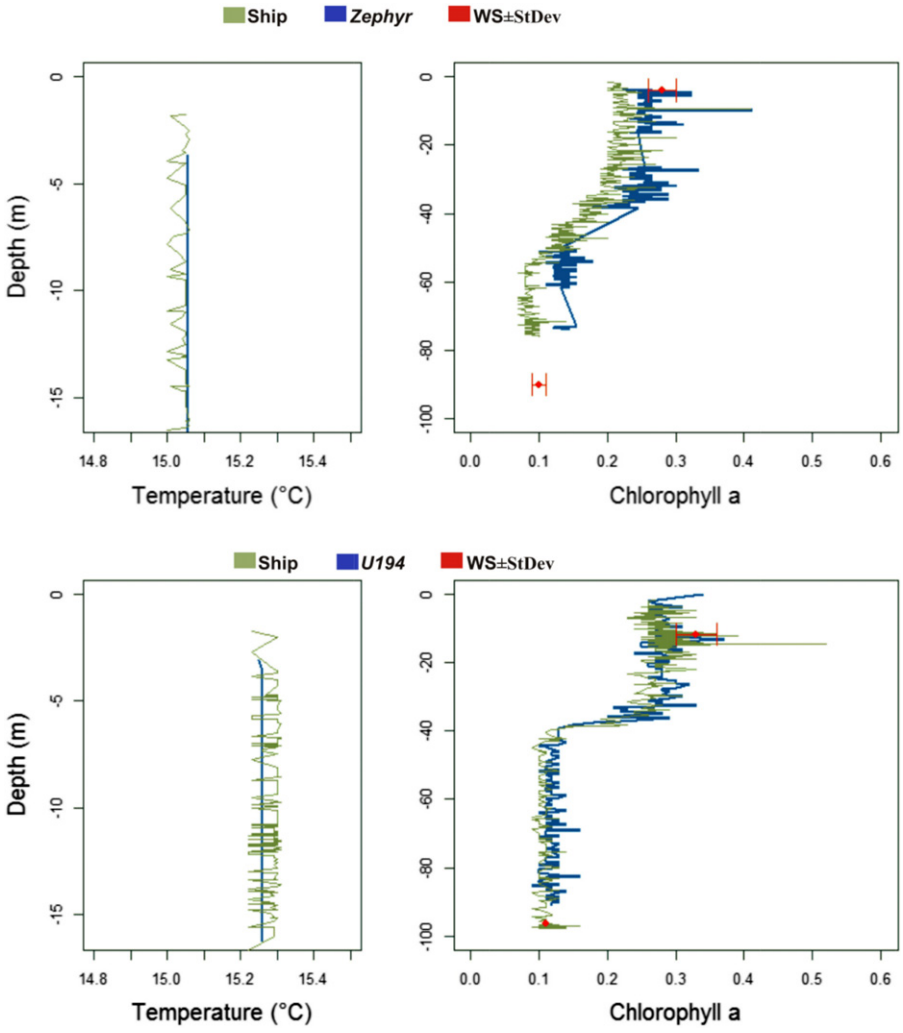

Fig. 4. Comparison between ship and glider derived temperature and chlorophyll for *Zephyr* (upper panel) and *U194* (lower panel). Green: Ship; blue: glider; red points show chlorophyll *a* from water samples ± standard deviation ($N = 3$). (For interpretation of the references to colour in this figure legend, the reader is referred to the web version of this article.)

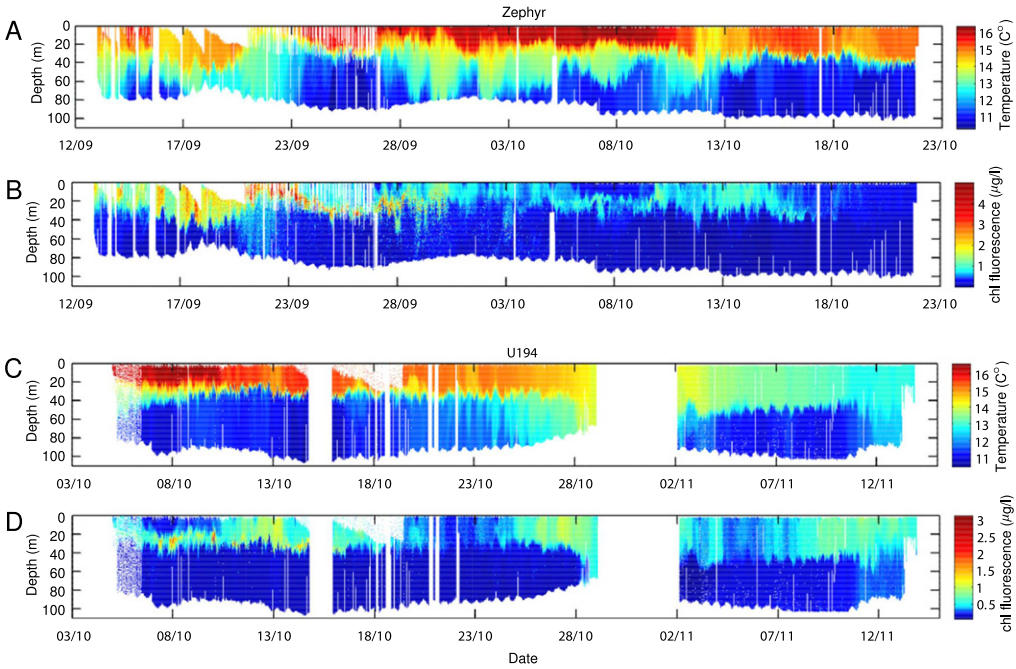

Fig. 5. Time series plots of temperature and chlorophyll concentration of both gliders against depth (panels A–B, *Zephyr*; panels C–D, *U194*). Time refers to hours since the mission start on 12 September 2013 at 1200 h. Note shifted time axis for *U194*, which only considers data since re-deployment from 04 October 2013.

thermocline at 20–40 m depth is particularly evident after ∼500 h (Fig. 5A). Elevated levels of chlorophyll *a* fluorescence are visible in the water column towards the base of the thermocline, particularly around 300 h (Fig. 5B). Fluorescence increases notably where the thermocline crops towards the surface in the frontal region, e.g. during a frontal crossing at ∼200 h (Fig. 5B). High levels of chlorophyll *a* fluorescence remain visible even after the equinox (21 September 2013; ∼200 h), which is usually taken as the end of the primary production period elsewhere on the UK shelf (Weston et al., 2005).

Glider *U194* also predominantly sampled thermally stratified waters throughout its mission, but spent less time in frontal regions (Figs. 1 and 5C). Subsurface chlorophyll maxima at ∼30 m depth, associated with the thermocline, are clearly visible in *U194* profiles until ∼800 h into the mission (Fig. 5D). The deployment of *U194* was substantially longer than that of *Zephyr* (Fig. 3), and included a major storm event on 27 October 2013 (1080 h into the mission, Fig. 5C). Interestingly, the water mass remained stratified (although much weaker) after this storm event, although surface waters had cooled significantly and the thermocline depth increased to ∼50 m (Fig. 5C).

An interesting feature visible on the *Zephyr* temperature profile is the lack of an obvious relationship between bottom temperature gradients and surface gradients, particularly around 400-600 h (Fig. 5A). Consistently high surface temperatures were experienced throughout this period (>15 °C), whereas the bottom temperature alternated between ∼11–13 °C. In general, the transition zone along the bottom appears wider than at the surface (Fig. 5A, Fig. A.3). In addition, clear bottom front crossings occurred on nine occasions, whereas the surface front was intersected six times only (Fig. 5A, Fig. A.3).

4.3. Echosounder

The ES853 120 kHz echosounder, integrated onto *U194* (Fig. 2A), successfully recorded acoustic data from the water column during the first five-day deployment (Figs. 3 and 6). Unfortunately,

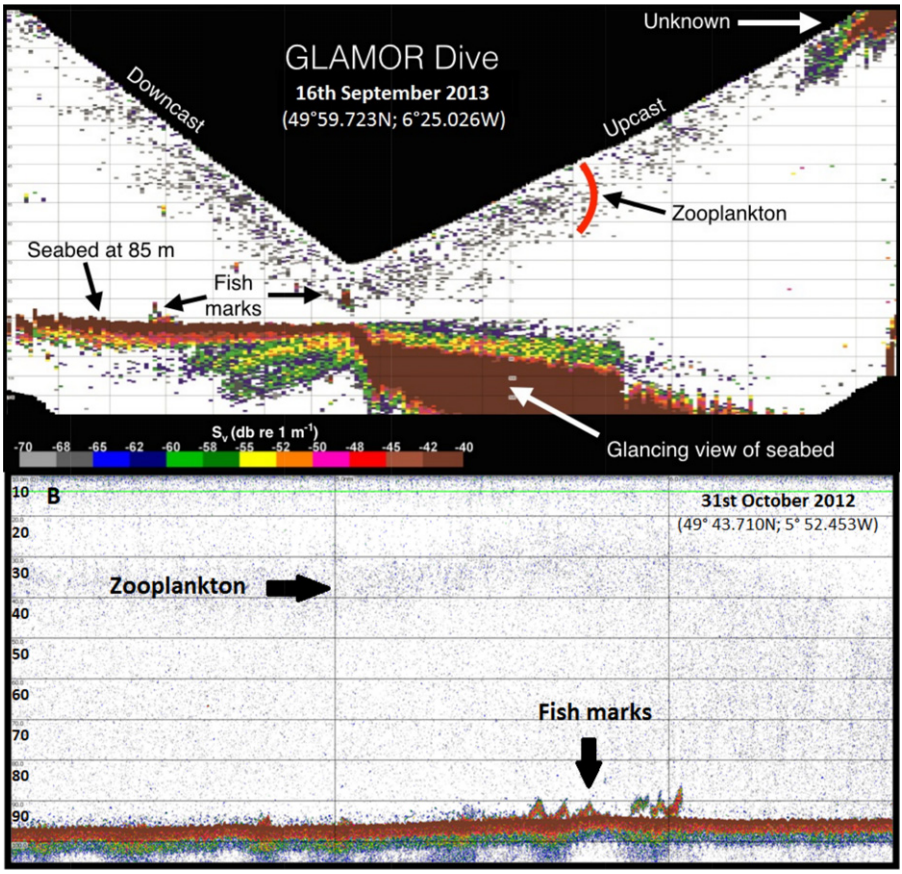

Fig. 6. Echograms of glider-integrated ES853 at 120 kHz (A) and equivalent vessel based EK60 120 kHz (B). Distance between the two sites 43.3 km. Features such as the seabed, fish shoals and zooplankton scattering have been indicated. Gain thresholds for both echograms were set to −70 dB.

after redeployment a technical error prevented communication between the echosounder and the glider and, as a consequence, acoustic data for the rest of the mission were not stored on the internal memory of glider and echosounder. Focusing on the downcast, when the echosounder is vertically orientated and most comparable to a ship-based echosounder, typical features observed in echograms include the seabed and fish shoals (Fig. 6A). Similar acoustic features were observed in an echogram derived from the ship-based echosounder in the same area at the same time of year (Fig. 6B).

A band of scattered targets, consistently present within 20–25 m of the glider echosounder during both down- and up-casts (Fig. 6A), was interpreted to represent small organisms such as zooplankton. The vessel-based echogram at 120 kHz revealed similar scattered targets throughout the water column, with some evidence for elevated concentrations at ∼30–40 m depth associated with the thermocline (Fig. 6B). Due to the reduced signal-to-noise ratio of the glider echosounder, these small targets were only observed within a limited range of the transducer. In contrast, the stronger water column targets related to fish shoals were recorded throughout the water column on glider data (Fig. 6A). These targets appeared similar to those recorded from RV *CEFAS Endeavour* during its annual pelagic fish survey in the area (Fig. 6B), and were thought to consist of boarfish (*Capros aper*). Due to differing ping rates (4 vs 0.25 s^{-1}) and vehicle speeds (5 ms^{-1} vs. 0.3 ms^{-1}), the horizontal resolution of acoustic data obtained from the glider was nearly twice as high compared to the vessel (1.2 m vs.

2.5 m per ping), which suggests that the fish shoals imaged on the glider echogram are possibly small examples of these boarfish shoals.

A noticeable feature on glider acoustic profiles is the presence of high backscatter patches in the uppermost water column, observed down to ~20 m water depth during upcasts (Fig. 6A). Adverse weather conditions, with large waves or swell, are known to introduce bubbles into surface waters; however, weather conditions were favourable during the period that these features were observed so this cause is doubtful. Technical issues, such as side-lobe detection of the sea surface, are also thought to be unlikely as these patches were not always present, absent during previous trial deployments, and no changes had been applied to the echosounder settings. Vessel-derived echograms did not show the same features, although the transducer depth of the vessel-based echosounders was 8.2 m below the surface and so did not cover the surface layer. It is therefore possible that these high backscatter patches have a biological origin, representing organisms restricted to surface layers. However, their unusually high backscatter, widespread occurrence, and consistent appearance throughout the deployment, also make this an unlikely source. Therefore, further investigation is required to determine the true origin.

4.4. Passive acoustic monitoring

The power cable to the d-tag acoustic sensor was damaged during or soon after installation, so PAM data were only collected between 04 and 10 October (Fig. 3). These data included 2413 10s recordings over 291 separate dive cycles, with an average of eight recordings per dive. Harbour porpoise clicks were detected during two separate dives, although one of these consisted of only a single click. Dolphin clicks and whistles were detected during 194 dives: 145 of these were clicks only, 49 whistles only, and 42 both (for map of locations of recordings see Fig. A.4). Fig. 7 shows the waveforms and power spectra of a typical dolphin and porpoise click. No other obvious noise sources, such as the pitch battery motor were apparent in the data.

Noise attributable to the glider pump was recorded on 169 occasions. The times of these noises corresponded to the times when the pump was 'on' in the glider log files, typically occurring for only a few seconds at the bottom of each dive. Fig. 8 shows the distribution of noise in third octave bands with the pump on and the pump off. Median noise levels with the pump off are generally low indicating that the system can be used to make accurate measurements of ambient noise. Noise levels at all frequencies are considerably higher when the pump is in operation. However since the duration of these noisy periods is relatively short, it will have little effect on overall survey effort.

4.5. Passive sampling devices

Recovered silicone rubber sample sheets were visually inspected for bio-fouling before analysis (as this can affect the uptake of contaminants into passive samplers); bio-fouling levels were found to be very low compared to static exposures. Significant dissipation of performance reference compounds (PRC) was observed from sample sheets. PRC dissipation was used to estimate sampling rates using a published procedure (Booij and Smedes, 2010). These rates were in the range of 3–7 L d^{-1} depending on the chemical. Sampling rates were normalized to a standard surface area (Huckins et al., 1993) and compared with those observed during static or other mobile deployments of passive samplers e.g. Booij et al., 2007; Allan and Harman, 2011; Lohmann et al., 2012); Table 3). Sampling rates for the glider-mounted passive samplers used here are in a similar range to those commonly observed for static deployments, whereas mobile exposures with high velocities tend to achieve high sampling rates (Table 3). The PRC data from this passive sampler exposure (i.e. 50% dissipation for d_{10}-phenanthrene) indicate that sampling was time-integrative for substances with octanol–water partition coefficient (log K_{ow}) above 4.5. Since gliders are launched for periods of weeks to months, these exposures can still detect polycyclic aromatic hydrocarbons (PAH) and polychlorinated biphenyls (PCB) in the low pg L^{-1} range, i.e. levels at which these compounds typically occur in oceanic waters.

Freely dissolved concentrations of PAHs ranged from just over 1 ng L^{-1} for phenanthrene down to below 10 pg L^{-1} for higher molecular weight PAHs. Polychlorinated biphenyls (PCBs) were found

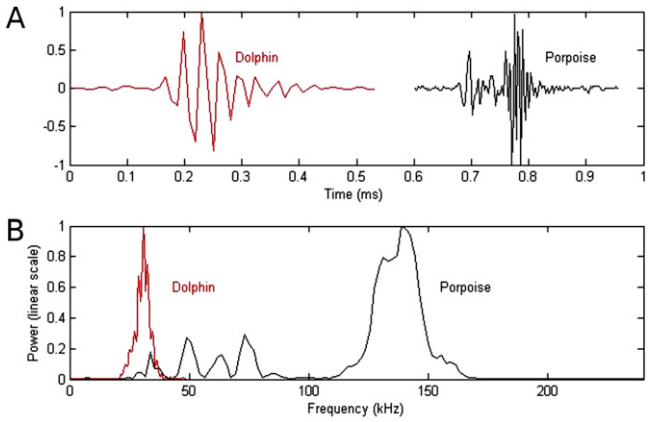

Fig. 7. (A) waveforms and (B) power spectra of detected dolphin and porpoise clicks using the d-tag hydrophone on *Zephyr*.

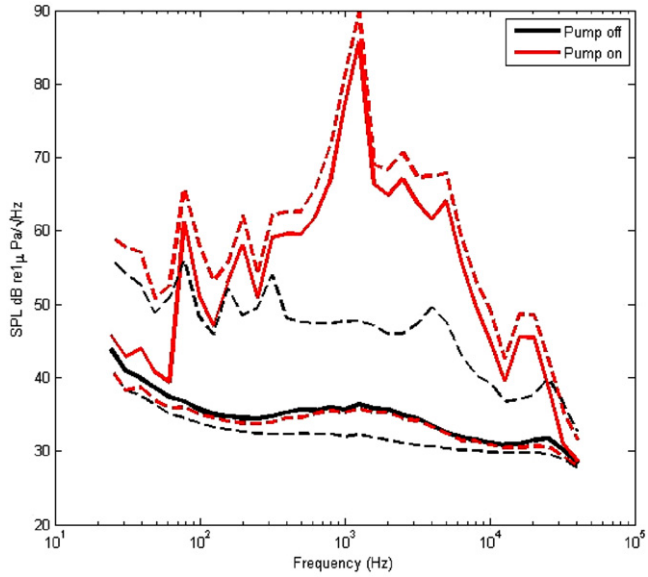

Fig. 8. Spectrum-level noise measurements at third octave intervals for times when the Zephyr pump was on and when the pump was off. The three lines for each situation represent the median values and the lower and upper 90% intervals.

at levels below 10 pg L^{-1} (except for PCB congener 28 with a concentration of 32 pg L^{-1}). The freely dissolved concentration of hexachlorobenzene was 45 pg L^{-1}. These concentrations were not corrected for temperature or salinity, but are generally in the range of those measured in open waters of the North Atlantic.

5. Discussion

In this 'proof-of-concept' study, two submarine gliders were equipped with sensors capable of simultaneously measuring physical properties of the water column and multiple trophic levels, in order to test their potential for ecosystem monitoring. The results highlight the advantages and current limitations of utilizing gliders as autonomous platforms for the outlined purpose. The key

Table 3
Passive sampling rates, typical exposure times, and limits of detection for various passive sampler deployment modes.

Deployment mode	Sampling R_s ($L\ d^{-1}$)[a]	Exposure time	Limits of detection ($pg\ L^{-1}$)[b]	Refs.
Static	1–20	0.5–3 months	0.3–30	(Vrana and Schuurmann, 2002; Allan et al., 2010; Prokes et al., 2012; Allan et al., 2013)
Mobile[c]	18–27	4–6 days	3.0–7.0	(Booij et al., 2007)
Mobile[d]	70–200	5 h and 48 h	1.0–30	(Allan and Harman, 2011; Allan et al., 2011; Lohmann et al., 2012)
Calibration[e]	60–200	15 days	0.2–0.6	(Booij et al., 2003)
Glider[f]	3–7[g]	39 days	2.0–4.0	Present study

[a] For a standard semipermeable membrane device sampling surface area of 460 cm^2.
[b] Limits of detection in water for PAHs/PCBs in the linear phase of uptake ($C_{w,lim} = m_{lim}/[R_s t]$) with a arbitrarily set m_{lim} of 0.5 ng per sample.
[c] Ship-based measurement using the ship's continuous water supply (water velocity in the pipe of 15 cm s^{-1}).
[d] Samplers towed behind a benthic trawl net (1.2–1.4 knot); towed behind a research vessel.
[e] During sampler calibration with water velocity of 90 cm s^{-1} and water temperature of 30 °C.
[f] Average glider velocity through water of 20–40 cm s^{-1} (horizontal velocity).
[g] Sampling rates corrected to a surface area of 460 cm^2.

outcomes relate to operational aspects, current sensor technology, instrument calibration and data validation.

5.1. Glider operations

The two gliders successfully completed their missions, which lasted for just under 40 days and which each comprised >2500 dives to depths of up to 100 m over total horizontal travel distances of 1000–1300 km. The gliders continued to collect data in weather conditions that stopped research vessel activity in the region, including a particularly severe storm on 27 October 2013 (Fig. 5C).

The two major operational challenges were flight control and alignment of the two glider trajectories in space and time. Although previous deployments have demonstrated that gliders are capable of following a proposed transect in areas of strong tidal flow (e.g. Leonard et al., 2007), this proved extremely challenging in the present study (Fig. 1). This is likely due to the combination of strong tidal and non-tidal residuals acting on the vehicles together. In order to fully understand the effect of hydrodynamics on our gliders, a detailed analysis is required including currents, tides and meteorological forcing in relation to the glider tracks and flight settings, which is beyond the scope of this paper.

The flight of *U194* was significantly improved by applying a more dynamic piloting approach, including e.g. increased monitoring, modifying dive angle and current correction settings, and adjusting waypoints depending on currents and tidal state. Hybrid *Slocums* equipped with a thruster are also now commercially available (Jones, 2012), which should further aid future deployments in tidally dominated environments. Furthermore, ongoing modelling and simulation research, dealing with optimal path planning and influences on glider trajectories, can be used to aid the survey design (e.g. Fernandez-Perdomo and Hernandez-Sosa et al., 2011; Ting and Mujeebu et al., 2012).

Aligning the flight of multiple gliders is a key requirement in whole-ecosystem monitoring, as the sensors required to simultaneously measure multiple ecosystem components cannot currently be integrated onto a single vehicle due to limited payload capacity and energy constraints. In addition, certain instruments need to go onto different platforms due to acoustic interference problems (e.g. active echosounder and passive hydrophone). In order to obtain meaningful data on multiple parameters simultaneously, the vehicles should be aligned in time and space; ideally the maximum distance between the vehicles should not exceed the scale on which the variables change. This is a challenging task, because gliders equipped with different sensors will display specific flight behaviours, e.g. due to different ballasting and external sensor configurations. For example, the hydrocarbon sheets used on *Zephyr* in this study are likely to have added extra drag to the vehicle resulting in different flight behaviour compared to *U194* (*cf.* Fig. 1). If time and budget allow, extended

trials focusing on simultaneous flight prior to a mission could improve piloting for individual gliders and, therefore, trajectory alignment.

5.2. Sensors

Throughout the mission, CTD and fluorometer sensors on both gliders provided water-column data at a spatio-temporal resolution and frequency not attainable through ship-based surveys or satellite imagery. For example, *Zephyr* crossed the Isles of Scilly tidal-mixing front several times (Fig. 5A), with collected data highlighting the spatial offset of the surface and bottom fronts (Fig. 5) as well as chlorophyll maxima associated with the thermocline (Fig. 5B); these features would not be detected using remote sensing data. Glider *U194* dominantly sampled stratified waters, and monitored change in the water column from seasonally stratified to mixed over a period of six weeks (Fig. 5C); within this period the glider continued collecting data during the severe storm event on 27 October 2013. Despite the high resolution and amount of information collected, file sizes were small enough for a subset of data to be transmitted via Iridium during the mission.

The newly integrated ES853 echosounder and d-tag passive acoustic monitoring system provided promising data on the spatial distribution of higher trophic-level organisms. The hydrophone recorded numerous cetacean clicks and whistles from different species during the six days of operation (Figs. 7 and A.4). The echosounder was capable of detecting targets, including fish and zooplankton, similar to targets detected by vessel-based data echosounders (Fig. 6).

The novel hydrocarbon sheets trialed here can easily be attached to gliders and AUVs, and collect supplementary information on water quality. This has particular application for regulatory monitoring, e.g. in response to European legislation such as the Water Framework Directive and the Marine Strategy Framework Directive. The sampling scheme can be extended from hydrophobic compounds (as used in this study) to samplers specifically designed to sample hydrophilic substances and metals.

Limitations of glider-integrated instrumentation include the need for data calibration and validation, particularly over long-term surveys. CTD and fluorometer calibration procedures are generally undertaken during glider deployment and retrieval using calibrated ship-based CTDs and by taking water samples. However, depending on survey area and season, a considerable amount of bio-fouling can affect the glider-integrated instruments; this causes sensor drift in a non-linear fashion, which is difficult to account for with calibration procedures at the beginning and end of a mission. In addition, collection of water samples remains essential for phytoplankton biomass estimations or species identification.

Although the echosounder and PAM system are capable of collecting data on the distribution of higher trophic level organisms over large spatio-temporal scales, they are significantly harder to calibrate compared with the physical sensors. Single-beam single-frequency echosounders provide a limited capability for target identification, which are normally undertaken using multi-frequency discrimination methods (e.g. Korneliussen and Ona, 2003). However, these instruments are currently too large and powerful to be integrated into underwater gliders. To establish fish species with absolute certainty, verification via net sampling also remains essential. Size–length relationships needed for target strength model parameterization for conversion to biomass and information on age-class distribution are additional parameters that can only be acquired with dedicated net sampling from vessel-based surveys. There has been some success at classifying cetacean whistles collected by PAM systems to species level (Gillespie et al., 2013), although considerable problems remain in estimating absolute animal abundance from glider-based data. Critical data for the estimation of abundance are the range at which animals are detected and either the rate of vocalization or the ability to isolate and count individuals (Marques et al., 2013). Gliders are too slow moving to use target motion analysis to localize animals in the water columns, as is commonly done for sperm whales (e.g. Lewis et al., 2007) and vocalization rate is poorly known for most species. Finally, echosounder and PAM system development should focus on methods for summarizing the complex data to enable transmission of a subset of collected data, rather than after retrieval. This would enable the glider to target, on the fly, hotspots of animals.

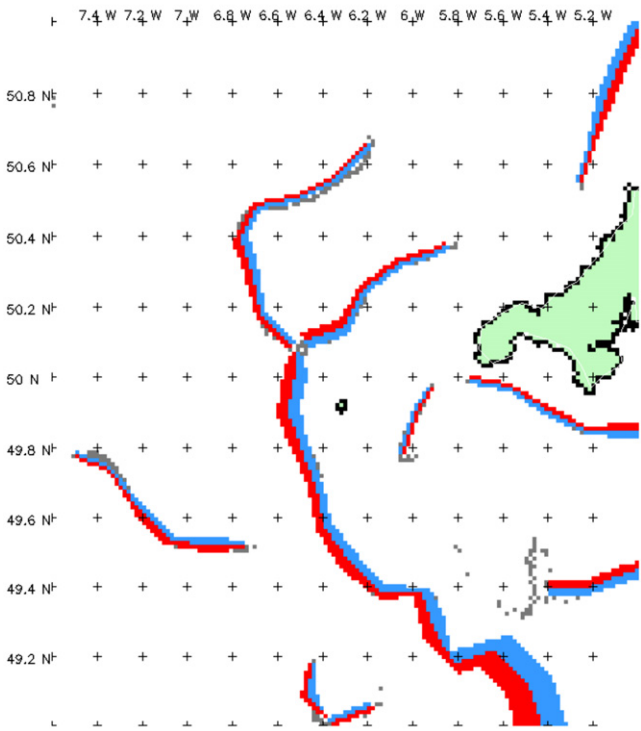

Fig. A.1. Composite satellite-derived front map of the survey area off southwest UK, based on data from 12 September–17 October 2013. Red indicates warm-water (stratified) side of tidal-mixing fronts, blue the cold-water (mixed) side. Line thickness equates to the strength of the front (the thicker the line, the stronger the front). Note the strong tidal-mixing front west of the Isles of Scilly, separating stratified waters to the west from tidally mixed waters to the east (*cf.* Fig. 1). (For interpretation of the references to colour in this figure legend, the reader is referred to the web version of this article.)

6. Conclusions and recommendations

This proof-of-concept study has highlighted some of the advantages and current limitations of utilizing submarine gliders for the purpose of ecosystem monitoring. Advantages include cost efficiency, capability of working in adverse weather, and collection of 3D water-column data at high spatio-temporal resolution over periods of weeks to months. This is not achievable with other single platforms, but is essential in order to detect change and its effect on an ecosystem, e.g. breakdown of seasonal stratification, impact of short-duration storm events. All of the novel glider-integrated sensors used in this study delivered useable data, although they could only provide information on distribution of biological indicators rather than accurate estimates of abundance or biomass. More broadly, glider sensor calibration and data validation remain challenging and dependent upon supporting infrastructure (ships, moorings), so acquired data are often only suitable for qualitative analysis. In addition, for the purpose of multi-vehicle surveys, aligning glider trajectories and flight control are significant issues that require further improvement (especially in dynamic tidally-dominated environments). Nevertheless, the promising results achieved in this study have led to a further deployment targeting oceanic fronts off southwest UK (planned for autumn 2014) using unmanned surface vehicles (USVs) as an in addition to submarine gliders.

For effective whole-ecosystem monitoring in the future, a range of autonomous platforms will need to be deployed within a marine monitoring network, including USVs, AUVs and gliders. Successful implementation of an autonomous monitoring network has already been demonstrated in the

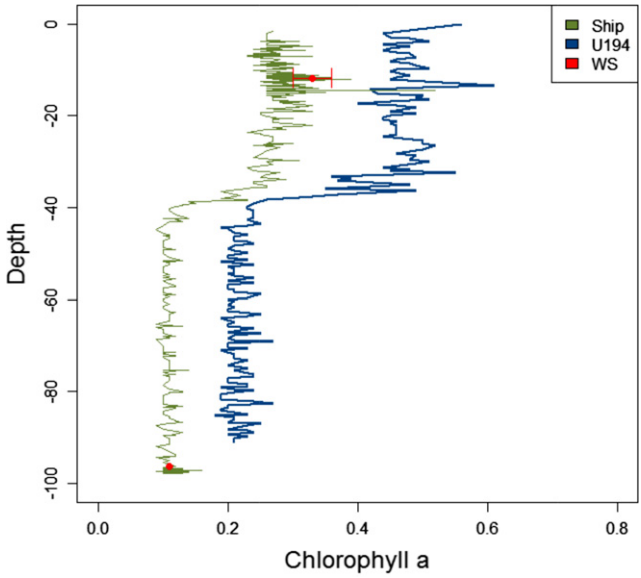

Fig. A.2. Calibration profiles between ship (green) and U194 (blue), showing uncorrected chlorophyll *a* data. Red points show values from water samples ± standard deviation ($N = 3$). (For interpretation of the references to colour in this figure legend, the reader is referred to the web version of this article.)

California Current Ecosystem, where satellite imagery, vessel surveys, gliders, floats and moorings are used in combination to provide compatible data on ecosystem dynamics at various spatio-temporal scales (Ohman et al., 2013). Satellite remote sensing provides information on large-scale surface processes, which is supplemented by submarine gliders measuring water column properties. Moorings and targeted vessel surveys utilize more powerful sensors working at high frequency, and are used to calibrate satellite and glider data; vessels are also used to run structured experimental surveys, which require ship-based equipment. Together, the sampling network efficiently provides a synoptic view of an ecosystem at multiple scales, which can significantly advance our understanding of marine ecosystem functioning and drivers of change.

Acknowledgements

This project would not have been possible without the hard work and professionalism of the Marine Autonomous and Robotic Systems (MARS) staff at NOC, particularly David White, James Burris and Sam Ward. We also thank to the ship staff of the RV *CEFAS Endeavour* and the Scilly Inshore Fisheries and Conservation Authority for their support in glider deployment, recovery and calibration activities.

The Gliders and AUVs for Marine Observation and Research (GLAMOR) project was primarily funded by UK Department for the Environment, Food and Rural Affairs (Defra), through their Strategic Evidence and Partnerships Fund. Damien Guihen was funded by Natural Environment Research Council (NERC) grant NE/H014756/1. Additional financial support came through Defra project MF1112 (POSEIDON). Ian Allan (NIVA) and Branislav Vrana (RECETOX) acknowledge funding from the European Union Seventh Framework Programme (FP7/2007–2013) under grant agreement no. 262584, JERICO (TNA project GLISS). Passive sampler analyses were also carried out through the JERICO project (Work Package 10). We thank James Bowcott (PML) for providing the satellite front bulletins throughout the cruise.

The authors thank the two anonymous reviewers and guest editor Gwyn Griffiths for their detailed and helpful comments, which substantially improved the manuscript.

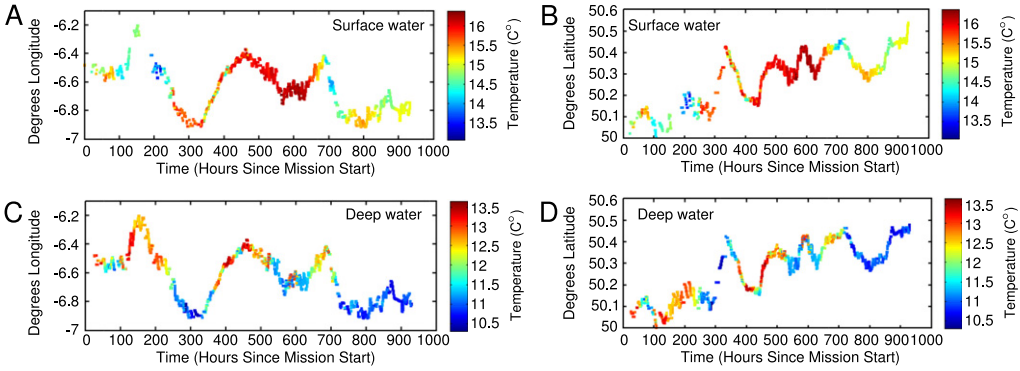

Fig. A.3. Temperature of surface waters (A and B, between 5–10 m depth) and deeper waters (C and D, between 60–70 m depth) as a function of time and longitude (A and C) and latitude (B and D).

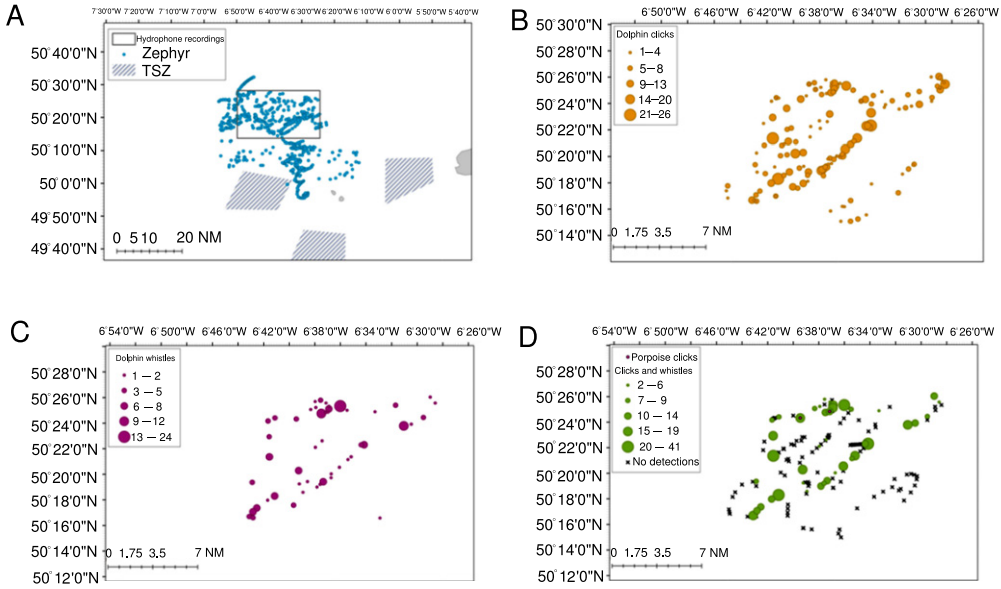

Fig. A.4. Maps showing the area where the d-tag hydrophone on *Zephyr* was active (A) and recorded dolphin clicks (B), whistles (C), and dives with both and porpoise clicks (D). Black crosses refer to locations of dives without recordings.

Appendix

See Figs. A.1–A.4.

References

Allan, I.J., Harman, C., 2011. Global aquatic passive sampling: maximizing available resources using a novel exposure procedure. Environ. Sci. Technol. 45 (15), 6233–6234.

Allan, I.J., Harman, C., et al., 2010. Effect of sampler material on the uptake of PAHs into passive sampling devices. Chemosphere 79 (4), 470–475.

Allan, I.J., Harman, C., et al., 2013. Passive sampling for target and nontarget analyses of moderately polar and nonpolar substances in water. Environ. Toxicol. Chem. 32 (8), 1718–1726.

Allan, I.J., Nilsson, H.C., et al., 2011. Mobile passive samplers: Concept for a novel mode of exposure. Environ. Pollut. 159 (10), 2393–2397.

Alvarez, A., Mourre, B., 2012. Oceanographic Field Estimates from Remote Sensing and Glider Fleets. J. Atmos. Ocean. Technol. 29 (11), 1657–1662.
Alvarez, A., Chiggiato, J., et al., 2013. Mapping sub-surface geostrophic currents from altimetry and a fleet of gliders. Deep-Sea Res. Oceanogr. Res. Papers 74, 115–129.
Baumgartner, M.F., Fratantoni, D.M., 2008. Diel periodicity in both sei whale vocalization rates and the vertical migration of their copepod prey observed from ocean gliders. Limnol. Oceanogr. 53 (5), 2197–2209.
Baumgartner, M.F., Fratantoni, D.M., et al., 2013. Real-time reporting of baleen whale passive acoustic detections from ocean gliders. J. Acoust. Soc. Am. 134 (3), 1814–1823.
Beaumont, N.J., Austen, M.C., et al., 2007. Identification, definition and quantification of goods and services provided by marine biodiversity: Implications for the ecosystem approach. Mar. Pollut. Bull. 54 (3), 253–265.
Booij, K., Hofmans, H.E., et al., 2003. Temperature-dependent uptake rates of nonpolar organic compounds by semipermeable membrane devices and low-density polyethylene membranes. Environ. Sci. Technol. 37 (2), 361–366.
Booij, K., Smedes, F., 2010. An Improved Method for Estimating in Situ Sampling Rates of Nonpolar Passive Samplers. Environ. Sci. Technol. 44 (17), 6789–6794.
Booij, K., Smedes, F., et al., 2002. Spiking of performance reference compounds in low density polyethylene and silicone passive water samplers. Chemosphere 46 (8), 1157–1161.
Booij, K., van Bommel, R., et al., 2007. Air-water distribution of hexachlorobenzene and 4,4'-DDE along a North-South Atlantic transect. Mar. Pollut. Bull. 54 (6), 814–819.
Bouffard, J., Pascual, A., et al., 2010. Coastal and mesoscale dynamics characterization using altimetry and gliders: A case study in the Balearic Sea. J. Geophys. Res.-Oceans 115.
Bouffard, J., Renault, L., et al., 2012. Sub-surface small-scale eddy dynamics from multi-sensor observations and modeling. Prog. Oceanogr. 106, 62–79.
Brennan, J., Fitzsimmons, C., et al., 2013. EU marine strategy framework directive (MSFD) and marine spatial planning (MSP): Which is the more dominant and practicable contributor to maritime policy in the UK? Marine Policy 43, 359–366.
Collie, J.S., Adamowicz, W.L., et al., 2013. Marine spatial planning in practice. Estuar. Coastal Shelf Sci. 117, 1–11.
Davis, R.E., Leonard, N.E., et al., 2009. Routing strategies for underwater gliders. Deep-Sea Res. Topical Stud. Oceanogr. 56 (3–5), 173–187.
Davis, R.E., Ohman, M.D., et al., 2008. Glider surveillance of physics and biology in the southern California Current System. Limnol. Oceanogr. 53 (5), 2151–2168.
Day, J., 2008. The need and practice of monitoring, evaluating and adapting marine planning and management - lessons from the Great Barrier Reef. Marine Policy 32 (5), 823–831.
Defra,, (2013). The Isles of Scilly Marine Conservation Zones Designation Order 2013. Ministerial Order. No 10, London: Department of Environment, Food and Rural Affairs.
Douvere, F., Ehler, C.N., 2011. The importance of monitoring and evaluation in adaptive maritime spatial planning. J. Coastal Conserv. 15 (2), 305–311.
Dunford, A.J., 2005. Correcting echo-integration data for transducer motion (L). J. Acoust. Soc. Am. 118 (4), 2121–2123.
English, D., Chuanmin, H., et al., 2009. Observing the 3-dimensional distribution of bio-optical properties of West Florida Shelf waters using gliders and autonomous platforms. Oceans 7.
European Union, 2008. Directive 2008/56/EC of the European Parliament and the Council of 17 June 2008. Establishing a framework for community action in the field of marine environmental policy (Marine Strategy Framework Directive). Official J. Eur. Union L164, 19–40.
Ferguson, B.G., Lo, K.W., et al., 2010. Sensing the underwater acoustic environment with a single hydrophone onboard an undersea glider. Oceans.
Fernandez-Perdomo, E., Hernandez-Sosa, D., et al., 2011. Single and multiple glider path planning using an optimization-based approach. Oceans.
Foote, K., Knudsen, H., et al., 1987. Calibration of acoustic instruments for fish density estimation: a practical guide. ICES Cooperative Research Report 144, 69.
Fox, R.D., Gower, J.F.R., et al., 2009. Slocum glider observations during the spring bloom in the Strait of Georgia. Oceans 9.
Frajka-Williams, E., Rhines, P.B., et al., 2009. Physical controls and mesoscale variability in the Labrador Sea spring phytoplankton bloom observed by Seaglider. Deep-Sea Research Part I-Oceanographic Research Papers 56 (12), 2144–2161.
Gillespie, D., Caillat, M., et al., 2013. Automatic detection and classification of odontocete whistles. J. Acoust. Soc. Am. 134 (3), 2427–2437.
Gillespie, D., Mellinger, D., et al., 2008. PAMGUARD: semiautomated, open source software for real-time acoustic detection and localisation of cetaceans. J. Acoust. Soc. Am. 30 (5), 54–62.
Gilman, E., 2002. Guidelines for coastal and marine site-planning and examples of planning and management intervention tools. Ocean & Coastal Manag. 45 (6–7), 377–404.
Guihen, D., Fielding, S., et al., 2014. An assessment of the use of ocean gliders to undertake acoustic measurements of zooplankton: the distribution and density of Antarctic krill (*Euphausia superba*) in the Weddell Sea. Limnol. Oceanogr.-Methods 12.
Hill, A.E., Brown, J., et al., 2008. Thermohaline circulation of shallow tidal seas. Geophys. Res. Lett. 35 (11).
Huckins, J.N., Manuweera, G.K., et al., 1993. Lipid-containing semipermeable-membrane devices for monitoring organic contaminants in water. Environ. Sci. Technol. 27 (12), 2489–2496.
Johnson, M., Partan, J., et al., 2013. Low complexity lossless compression of underwater sound recordings. J. Acoust. Soc. Am. 133 (3), 1387–1398.
Johnson, M.P., Tyack, P.L., 2003. A digital acoustic recording tag for measuring the response of wild marine mammals to sound. IEEE J. Ocean. Eng. 28 (1), 3–12.
Jones, C.P., 2012. Slocum glider: persistent oceanography. 2012 IEEE/OES Autonomous Underwater Vehicles (AUV 2012) 6.
Klinck, H., Mellinger, D.K., et al., 2012. Near-Real-Time Acoustic Monitoring of Beaked Whales and Other Cetaceans Using a Seaglider (TM). Plos One 7 (5).
Korneliussen, R.J., Ona, E., 2003. Synthetic echograms generated from the relative frequency response. ICES J. Marine Sci. J. Conseil 60 (3), 636–640.

Leeney, R.H., Witt, M.J., et al., 2012. Marine megavertebrates of Cornwall and the Isles of Scilly: relative abundance and distribution. J. Marine Biol. Assoc. United Kingdom 92 (08), 1823–1833.
Leonard, N.E., Paley, D.A., et al., 2007. Collective motion, sensor networks, and ocean sampling. Proc. IEEE 95 (1), 48–74.
Lewis, T., Gillespie, D., et al., 2007. Sperm whale abundance estimates from acoustic surveys of the Ionian Sea and Straits of Sicily in 2003. Journal of the Marine Biological Association of the United Kingdom 87 (1), 353–357.
L'Heveder, B., Mortier, L., et al., 2013. A Glider network design study for a synoptic view of the oceanic mesoscale variability. J. Atmos. Ocean. Technol. 30 (7), 1472–1493.
Lohmann, R., Klanova, J., et al., 2012. PCBs and OCPs on a east-to-west transect: the importance of major currents and net volatilization for PCBs in the Atlantic Ocean. Environ. Sci. Technol. 46 (19), 10471–10479.
Marques, T.A., Thomas, L., et al., 2013. Estimating animal population density using passive acoustics. Biol. Rev. 88 (2), 287–309.
Merckelbach, L., Smeed, D., et al., 2010. Vertical water velocities from underwater gliders. J. Atmos. Ocean. Technol. 27 (3), 547–563.
Meyer-Gutbrod, E., Greene, C., et al., 2012. Long term autonomous fisheries survey utilizing active acoustics. Oceans.
Miller, P., 2009. Composite front maps for improved visibility of dynamic sea-surface features on cloudy SeaWiFS and AVHRR data. J. Mar. Syst. 78 (3), 327–336.
Miller, P.I., Christodoulou, S., 2014. Frequent locations of ocean fronts as an indicator of pelagic diversity: application to marine protected areas and renewables. Marine Policy 45, 318–329.
Niewiadomska, K., Claustre, H., et al., 2008. Submesoscale physical-biogeochemical coupling across the Ligurian Current (northwestern Mediterranean) using a bio-optical glider. Limnol. Oceanogr. 53 (5), 2210–2225.
Ohman, M.D., Rudnick, D.L., et al., 2013. Autonomous ocean measurements in the California Current Ecosystem. Oceanography 26 (3), 18–25.
Perry, M.J., Sackmann, B.S., et al., 2008. Seaglider observations of blooms and subsurface chlorophyll maxima off the Washington coast. Limnol. Oceanogr. 53 (5), 2169–2179.
Pingree, R.D., Holligan, P.M., et al., 1976. Influence of physical stability on spring, summer and autumn phytoplankton blooms in the Celtic Sea. Journal of the Marine Biological Association of the United Kingdom 56 (4), 845–873.
Pingree, R.D., Lecann, B., 1989. Celtic and Armorican slope and shelf residual currents. Prog. Oceanogr. 23 (4), 303–338.
Prokes, R., Vrana, B., et al., 2012. Levels and distribution of dissolved hydrophobic organic contaminants in the Morava river in Zlin district, Czech Republic as derived from their accumulation in silicone rubber passive samplers. Environ. Pollut. 166, 157–166.
Rudnick, D.L., Crowley, M., et al., 2012. A National Glider Network for Sustained Observation of the Coastal Ocean. IEEE, New York.
Ruiz, S., Pascual, A., et al., 2009. Mesoscale dynamics of the Balearic Front, integrating glider, ship and satellite data. Journal of Marine Systems 78, S3–S16.
Schofield, O., Glenn, S., et al., 2013. The Robot Ocean Network. Am. Sci. 101 (6), 434–441.
Send, U., Regier, L., et al., 2013. Use of underwater gliders for acoustic data retrieval from subsurface oceanographic instrumentation and bidirectional communication in the deep ocean. J. Atmos. Ocean. Technol. 30 (5), 984–998.
Sharples, J., Ellis, J.R., et al., 2013. Fishing and the oceanography of a stratified shelf sea. Prog. Oceanogr. 117, 130–139.
Simpson, J.H., 1981. The shelf-sea fronts- Implications of their existence and behavior. Phil. Trans. R. Soc. Lond. Ser. A Math. Phys. Eng. Sci. 302 (1472), 531.
Simpson, J.H., Tett, P.B., et al., 1982. Mixing and phytoplankton growth around an island in a stratified sea. Cont. Shelf Res. 1 (1), 15–31.
Ting, M.C., Mujeebu, M.A., et al., 2012. Numerical Study on Hydrodynamic Performance of Shallow Underwater Glider Platform. Indian J. Geo-Mar. Sci. 41 (2), 124–133.
Todd, R.E., Gawarkiewicz, G.G., et al., 2013. Horizontal Scales of variability over the middle Atlantic bight shelf break and continental rise from finescale observations. J. Phys. Oceanogr. 43 (1), 222–230.
Urick, R., 1983. Principles of Underwater Sound. McGraw-Hill.
Villadsgaard, A., Wahlberg, M., et al., 2007. Echolocation signals of wild harbour porpoises, Phocoena phocoena. J. Exp. Biol. 210 (1), 56–64.
Vrana, B., Schuurmann, G., 2002. Calibrating the uptake kinetics of semipermeable membrane devices in water: Impact of hydrodynamics. Environ. Sci. Technol. 36 (2), 290–296.
Watkins, J.L., Brierley, A.S., 1996. A post-processing technique to remove background noise from echo integration data. ICES J. Mar. Sci. 53 (2), 339–344.
Webb, D.C., Simonetti, P.J., et al., 2001. SLOCUM: an underwater glider propelled by environmental energy. IEEE J. Ocean. Eng. 26 (4), 447–452.
Weston, K., Fernand, L., et al., 2005. Primary production in the deep chlorophyll maximum of the central North Sea. J. Plankton Res. 27 (9), 909–922.
Willcox, J.S., Bellingham, J.G., et al., 2001. Performance metrics for oceanographic surveys with autonomous underwater vehicles. IEEE J. Ocean. Eng. 26 (4), 711–725.